



Science and
Technology
Facilities Council

Central Laser Facility

Annual Report

2023–2024



Central Laser Facility

Science & Technology Facilities Council
Rutherford Appleton Laboratory
Harwell Campus
Didcot
Oxfordshire
OX11 0QX

T: +44 (0)1235 445647

E: clfannrep@stfc.ac.uk

W: clf.stfc.ac.uk

The production team for this Annual Report was as follows:

Editor:

Raoul Trines

Production:

Tracey Burge and Raoul Trines

Section Editors:

Hamad Ahmed, Nicolas Bourgeois, David Carroll, Dave Clarke, Rob Clarke, James Green, Greg Greetham, Robert Lees, Rajan Mistry, Pedro Oliveira, Rajeev Pattathil, Alex Robinson, Igor Sazanovich, Christopher Spindloe, Emma Springate, Dan Symes, Steph Tomlinson, Christopher Tynan, Tiffany Walmsley

This report is available on the CLF website at clf.stfc.ac.uk

Design, layout and production:

STFC's Digital Creative Services: Dominic Read

Thanks to all of the above for their contribution towards producing this report and, of course, to all of the authors for their submissions.

Front cover image:

Scientist working in the Artemis Laser Lab
Credit: Helen Towrie, CLF, STFC

Contents

Foreword	4
Overview of the Central Laser Facility (CLF)	6
Industry Partnerships and Innovation	12
Communications and Outreach Activities	14
Introducing the Harwell Heritage Project	24
High Energy Density and High Intensity Physics	28
Laser Science and Development	41
Theory and Computation	64
Plasma Diagnostics	65
Imaging and Dynamics for Physical and Life Sciences	68
Operational Statistics	92
Publications	106
Panel Membership and CLF Structure	120
Author Index	126

Foreword

At the start of this year, the Central Laser Facility underwent its 10-year review. These reviews aim to identify and recommend future improvements such that STFC facilities continue to be of world-leading quality. They are conducted by specifically-convened, external Panels who review key documentation and interview users and staff to provide an independent peer perspective.



Pulling together the report and presentations for the Panel was no small task. Over the last 10 years, a lot has been going on at the CLF! The review broadly looked at research, innovation, industrial engagement, skills development and expertise, and our strategic direction. As you can imagine, there was a lot to capture: user programmes, international activity, strategic partnerships, facility and technology development, innovations, training and support, communications and outreach, and sustainability, to name but a few. Each claim we made had to be—and was—backed up by robust evidence.

Over an intense two days, the Panel attended presentations, interviewed users and staff, and asked a lot of questions. It was a very thorough review, but ultimately rewarding.

The Panel commended the CLF for providing an outstanding capability for the UK research community, highlighting clear excellence in delivering and supporting world-leading research that is underpinned by exceptional technical capabilities. Moreover, the entrepreneurial culture of the CLF was cited as a key strength, with the DiPOLE laser programme and the target fabrication facility highlighted as examples of world-leading activities and great success stories.

These findings are fully in line with our own mission statement, “To be, and be seen as, a global exemplar of the best science, skills, innovation and driver of prosperity using lasers”.

The recommendations that came out of the review also aligned with our future plans. In over 45 years of operation, we have consistently responded to new opportunities, embraced technological breakthroughs and found new funding streams that have allowed us to become a globally leading hub for laser research. The CLF continues to work to enable and sustain the development of skilled people and the application of laser technologies, ably supporting the UK academic community, industry and other government departments, and connecting researchers across the world. Through the ongoing EPAC, Vulcan 20-20 and HiLUX projects, we're developing a new generation of laser facilities that will continue to inspire and serve scientists and engineers alike. Alongside outstanding engineering support, we offer scientific staff assistance, in-house target fabrication, and theoretical and computing work to our user community, helping to increase the productive output of research.

This annual report offers an insight into some of the incredible scientific and technical research that has been carried out by CLF users and staff over the financial year 2023/24. The research spans a broad range of science areas, and supports wide-reaching efforts to help solve major scientific, economic, and societal challenges.

I am delighted to see the impact we are having, and the difference we are making. I do hope that you enjoy reading this selection of abstracts, and feel inspired by the achievements of all those involved and motivated to explore the capabilities and services on offer through the CLF.

Professor John Collier FLSW

Director, Central Laser Facility

A handwritten signature in black ink, appearing to read 'John Collier', positioned to the right of the text identifying the Professor.

Overview of the Central Laser Facility (CLF)

Cristina Hernandez-Gomez

Associate Director, Head of High Power Lasers

Introduction

The CLF is a world-leading centre for research using lasers in a wide range of scientific disciplines. This section provides an overview of the capabilities offered to our international academic and industrial community.

Vulcan

Vulcan is a versatile high power laser system composed of Nd:glass amplifier chains capable of delivering up to 2.6 kJ of laser energy in long pulses (nanosecond duration) and up to 1 PW peak power in a short pulse (500 fs duration) at 1053 nm. It can deliver up to eight beam lines. Two of these beam lines can operate in either short pulse mode or long pulse mode, while the remaining six normally operate in a long pulse mode. The short-pulse can be directed to two different target areas, enabling sophisticated interaction and probing experiments, with all eight beamlines available to one target area (TAW).

In this configuration, the facility delivered four full academic experiments and one commercial experiment.

Following these, the Vulcan facility was decommissioned in advance of the start of the demolition and building work needed for the Vulcan 20-20 project. Decommissioning work began in October 2023 and was completed in February 2024.

The upgrade agreed will see the power of Vulcan increased by a factor of 20, to 20 PW, and its focused intensity increased by a factor of 100.

Gemini

Gemini is a dual-beam petawatt-class Ti:Sapphire laser system that provides unique capabilities for relativistic laser-matter interactions and secondary source production. With 30 J on target in two beams, an intensity greater than 10^{21} Wcm^{-2} and a repetition rate of three shots per minute, the extreme concentration of energy possible with Gemini makes it one of the most intense lasers in the world.

Gemini Target Area 3 (TA3) is the main target area with access to both Gemini beams (15 J, 35 fs) that can be focussed using f/20 or f/2 parabolic mirrors at a rate of one shot per 20 seconds. Plasma mirrors are optional in one beamline. The maximum intensity is of order $2 \times 10^{21} \text{ Wcm}^{-2}$.

During 2023/24, TA2 was closed for user operations to set it up for EPAC prototyping and testing. TA2 is being setup for a mock-up electron beamline at 5 Hz, which will de-risk much of the development for the EPAC laser wakefield area.

Target Fabrication

The Target Fabrication (TF) group works closely with the user community to provide delivery, characterisation and support of high specification micro-targets.

During 2023/24, the TF group made the majority of the solid targets shot on the CLF's high-power lasers, and also supported target design for the academic access on the Orion Facility at AWE.

The TF group has also supported the Lasers for Science Facility (LSF) with microfabrication capabilities to enable their experimental campaigns, and provided support for the wider STFC community with micro-fabrication. Commercial access to target fabrication capabilities was available to external laboratories and companies via the spinout company Scitech Precision Ltd.

In addition to this work, the Group has remained focused on delivery of target solutions for day one operations in EPAC. Further experiments were carried out on the tape drive system, further increasing confidence in the system ahead of EPAC installation. In collaboration with the SCAPA team at the University of Strathclyde, work continued to increase the shot rates and to add triggers to synchronise the system to the laser. The TF group is procuring a coating plant to integrate the tape roller system, which will enable the coating of tapes up to 50 m in length in one operation: this capability is key for high-repetition-rate (HRR) operations.

Liquid targets will also be essential for EPAC operations, and the TF group has designed and built a system to provide thin liquid sheets. A delivery system, nozzle and catcher system were installed in EPAC, and the target was run out of vacuum to test imaging and characterisation set ups.

The TF group continues to develop robotic target assembly. This capability is used as standard for HRR experiments.

Theory and Modelling

The Plasma Physics Group (PPG) supports scheduled experiments throughout the design, analysis and interpretation phases, as well as users who need theoretical support in matters relating to CLF science. In the 2023-24 period, the Group continued to base its support model around: direct collaborative support; code development; code hosting; and high performance computing (HPC) provision.

Direct collaborative support is greatly enhanced by the computational resources, externally sourced codes, and in-house codes available to the PPG. As well as maintaining a suite of in-house codes that are used by PhD students and in user support projects, PPG is working to expand the code portfolio.

The PPG continued to provide the PRISM computational suite to five different user groups, as well as access to the HYADES and h2D codes.

Alongside the core mission of the PPG, the group continues to engage with the academic community to contribute to Laser fusion research.

Artemis (Research Complex at Harwell)

Artemis is an ultrafast XUV science facility, using high harmonics to investigate electron dynamics in condensed matter and gas-phase molecules, and for lensless imaging.

The oscillator for the 100 kHz laser system, which is now used for all condensed matter experiments, was replaced and is now working well. At 100 kHz, condensed matter experiments continue to benefit from the smaller XUV spot sizes and better energy and angular resolution achievable with this higher repetition rate. The gas-phase experiments on the 1 kHz system continue to work well, with increased XUV flux and a new effusive gas source, and the user community is expanding.

This was an intense year for Artemis, with the start of the HiLUX upgrade project managed alongside operations. The HiLUX project is set to transform the CLF's ultrafast spectroscopy capability and increase accessibility, with upgrades to both the Ultra and Artemis facilities that will increase in average laser power and repetition rate and data rate, unlocking new science applications and greatly reducing timescales to results.

The HiLUX project has completed its first year, and the design of the new laser system within Artemis is complete. It will consist of three synchronised 200 W Yb:KGW lasers operating at 100 kHz: the output of one laser will be compressed to 1.5 mJ in 50 fs and used for high harmonic generation; a second will drive OPAs, providing short pulses from the UV to the MIR; and a third will provide longer, 0.8 mJ pulses for molecular alignment experiments. The concept design for the new materials science end-station has also been completed and will provide a UHV chamber with a momentum microscope, a more advanced hemispherical analyser, and a six-axis manipulator.

Ultra (Research Complex at Harwell)

The structural dynamics facilities at Ultra explore molecular structure during changes, such as chemical reactions or dynamics in complex environments, such as heterogeneous catalysts. Ultra's unique combination of multiple laser amplifiers provides light across UV to IR for electronic and vibrational spectroscopies and measures dynamics across femtoseconds to seconds, to address a diverse portfolio of scientific challenges. The scientific themes span studies of drug binding and protein folding to observation of battery charging and structural changes through catalytic cycles. The available techniques provide sensitive time-resolved vibrational and electronic absorption spectroscopies and Kerr-gated Raman spectroscopy to observe weak signals obscured by strong sample emission.

The whole Ultra team has also been engaged in the HiLUX project. The Ultra A system has been decommissioned and the labs cleared ready for renovation. The design of the new facilities has been completed and will be able to accommodate the new laser systems consisting of five synchronised ytterbium amplifiers, which will pump an unprecedented array of optical parametric amplifiers to support five end-stations servicing time-resolved spectroscopy experiments from the few femtosecond to second, UV to IR.

Octopus (Research Complex at Harwell)

In the imaging area, the Octopus cluster offers a range of microscopy stations linked to a central core of pulsed and CW lasers, offering “tailor-made” illumination for imaging. Optical resolution techniques offered include total internal reflection (TIRF) and multi-wavelength single-molecule imaging, confocal microscopy (including multiphoton), fluorescence energy transfer (FRET), fluorescence lifetime imaging (FLIM), and Light Sheet Microscopy. Super-resolution techniques are also available: 2D and 3D Stochastic Optical Reconstruction Microscopy (STORM), Photo-activated Localization Microscopy (PALM), Structured Illumination Microscopy (SIM), gated 3D Stimulated Emission Depletion Microscopy (STED), 3D MINFLUX, and super-resolution cryo-microscopy. Laser tweezers are available for combined manipulation/trapping and imaging with other Octopus stations, and can also be used to study Raman spectra and pico-Newton forces between particles in solution for bioscience and environmental research. Two cryo focused ion beam scanning electron microscope (FIB-SEM) systems are also available. One is dedicated to 3D volume electron imaging, and the other, currently being commissioned, is dedicated to the preparation of lamellas and lift-out to prepare samples for cryo electron tomography. This latter system forms part of a correlative light and electron microscopy (CLEM) workflow currently under development.

Chemistry, biology, and spectroscopy laboratories support the laser facilities, and the CLF offers access to a multidisciplinary team providing advice to users on all aspects of imaging and spectroscopy, including specialised biological sample preparation, data acquisition, and advanced data analysis techniques. Access is also available to shared facilities in the Research Complex, including cell culture, scanning and transmission electron microscopy, NMR, and x-ray diffraction.

The portfolio of environmentally based research continues to advance, with studies in a wide range of areas including determining aerosol properties relevant to the atmosphere, super-resolution imaging of butterfly wings that relates colour and structure, and plant studies on ultra weak photoemission and endomembrane interaction with organelles. Materials imaging of catalyst structure has used the FIB-SEM technique, in collaboration the UK Catalysis Hub, to follow the compositional evolution of individual nanoparticles.

Regarding facility development, 3D MINFLUX is now established and attracting users, and the development of cryoCLEM facilities has continued. This has extended the CLF’s EPIC collaboration with India into biomedical imaging and will accelerate cryoCLEM developments in Octopus. A novel super-resolution technique based on radial fluctuation microscopy has also undergone preliminary development.

Engineering Services

Engineering is fundamental to all the operations and developments in the CLF. The engineering division operates across all of the CLF's facilities. Mechanical, electrical and software support is provided to deliver the experimental programmes, and the research and development activities. Support can range from making small-scale modifications to existing equipment to improve its performance, through to carrying out larger scale projects, such as the design and development of commercial projects. In addition, there are active engineering collaborations with regional and international partners such as, HiLASE (Prague, Czech Republic), the European XFEL (Hamburg, Germany) and TIFR (Hyderabad, India).

The CLF Engineering and Technology Centre (ETC) is now fully operational and has allowed the Engineering Division to develop capability not previously possible due to space constraints.

The CLF's Mechanical Workshop has taken custodianship of a diamond turn lathe, previously owned by RAL Space PDF department who used it to support the CLF's Target Fabrication Facility. This new capability, in addition to the CNC and wire eroding machines purchased last year, continues to expand the capabilities of the division. The focus has been to develop and upskill staff on this new technology and push the boundaries of target fabrication.

In 2023/24, the Engineering Team took the novel decision to install equipment that would enable production of nitrogen gas from air. The nitrogen generating plant has been successfully commissioned and is now providing the majority of the CLF's nitrogen gas supply.

The Centre for Advanced Laser Technology and Applications (CALTA)

CALTA aims to deliver societal, scientific and economic impact from developments in the CLF.

CALTA continues to support the EPAC Project, which will be driven by a 10 Hz petawatt-class laser enabled by STFC's proprietary DiPOLE laser technology. The next generation of 100 Hz DiPOLE lasers was developed as part of a Widespread teaming project, and was shipped to the ELI Beamlines Facility in autumn 2023.

Commissioning of the D-100X laser system at the European XFEL has been completed, and it exceeded all expectations on its first experiment in spring 2023. While not operating at its full energy and repetition rate quite yet, the D-100X laser delivered up to 40 J of energy per pulse at up to 1 Hz in the green, generating highly reproducible data at a rate not previously possible.

The Extreme Photonics Applications Centre (EPAC)

EPAC, a new facility at the CLF, has been designed to further the development and application of laser-driven accelerators in academic, industrial, medical and defence spheres.

EPAC will initially deliver a petawatt laser operating at 10 Hz to two dedicated experimental areas housed in a stand-alone building. In order to achieve this high peak power and repetition rate, DiPOLE technology will be used to pump a high energy titanium sapphire amplifier operating at 10 Hz.

The first experimental area (EA1) will be especially designed for laser wakefield acceleration (LWFA), where multi-GeV electron beams and synchrotron-like x-ray beams can be generated. The second experimental area (EA2) will be a very versatile area for fundamental science and applications with flexible focusing geometries.

The EPAC project continues to make good progress, with installation, design work and commissioning all now running in parallel.

Access to Facilities

The CLF operates “free at the point of access” and is available to any UK academic or industrial group engaged in open scientific research, subject to external peer review. European collaboration is fully open for the high power lasers, whilst European and international collaborations are also encouraged across the CLF suite for significant fractions of the time. Dedicated access to CLF facilities is awarded to European researchers via the Laserlab-Europe initiative (www.laserlab-europe.net) funded by the European Commission.

Hiring of the facilities and access to CLF expertise is also available on a commercial basis for proprietary or urgent industrial research and development.

Industrial access and partnerships

The Impact, Partnerships and Innovation (IPI) Group has been responsible for the delivery of the industrial access and establishing new collaborations with industry. The IPI group ensures that the interactions delivered are strategically aligned to the CLF and of the highest economic and societal impact to the UK. This year, industry contract-access projects has continued across all CLF facilities.

The CLF remains a strong department for innovation. Internationally, the CLF has driven forward its innovation policy and the growth of industry liaison offices, through shared learning and knowledge exchange across EU laser facilities. The CLF was a project partner organisation on the European Horizon 2020 IMPULSE project (completed January 2024).

Please visit clf.stfc.ac.uk for more details on all aspects of the CLF.

Industry Partnerships and Innovation

Sneha Banerjee

Industrial Liaison Scientist

Claire Pizzey

Group Leader, Impact, Partnerships and Innovation

Over the past year, the CLF has remained an essential hub for scientific collaboration and discovery. Between April 2023 and March 2024, the CLF worked alongside industrial partners and launched several innovative projects. These initiatives reflect the facility's ongoing commitment to advancing research, driving technological progress, and nurturing valuable partnerships.

In recent years, industry engagement at the CLF has grown significantly. This year alone, approximately 14 weeks of access to industry users has been provided across the Lasers for Science (LSF) and the High Power Laser (HPL) facilities. The Industry Partnerships and Innovation (IPI) group has engaged with a wide array of stakeholders, spanning sectors such as life sciences, net-zero projects, and healthcare. The CLF remains dedicated to strengthening collaborations and building meaningful partnerships with both academic and industrial sectors. In particular, this year, there has been an increase in the number of SMEs accessing CLF, many taking advantage of exciting innovation funding calls supported by UKRI.

Ongoing collaborations with both academia and industry have led to notable breakthroughs. Professor Jim Thomas, along with his spin-out company MetalloBio, has focused his research on unravelling the mechanisms of various antimicrobial complexes. This work is advancing our understanding of antimicrobial resistance and contributing to the development of a new generation of drugs. Professor Thomas had accessed the facility as an academic in previous years; he has now received funding via the STFC Industry Impact Fund (I2F), enabling his spinout to access the facility in the FY 2024-25.

The I2F funding scheme has played a key role in facilitating industry access to the CLF, with two additional companies gaining access via the scheme this year. One of these companies, MetaGuideX, has used both the STED (Stimulated Emission Depletion) microscope and the ONI microscope to investigate surface proteins present in extracellular vesicles. This research is aimed at improving the sensitivity of cancer assays, potentially enabling more accurate detection of cancer at earlier stages.

Phytoceutical, in partnership with the University of Surrey, has been researching their new micellar retinol formulations, using Fluorescence Microscopy to examine how retinol is converted in the skin. This research is focused on understanding the dynamics of retinol conversion, which is essential for its effectiveness in skincare. This year, they were awarded funding via two key calls, I2F and the BBSRC-STFC Facilities Access scheme, to advance their studies of chemical and biological processes at the molecular level. With this financial support, they plan to investigate the performance of their formulations and assess their potential for promoting wound healing. The aim is to understand the efficiency of the formulations in both skincare and therapeutic applications. This collaboration highlights the promising overlap between cosmetic innovation and medical science.

If you have a project that you would like to explore, please do get in touch, the IPI group would be very happy to hear from you. You can reach us via e-mail at **CLFindustry@stfc.ac.uk** or on LinkedIn.

Communications and Outreach Activities

Helen Towrie

CLF Impact and Engagement Officer

The CLF's communication strategies

The role of the CLF's Impact and Engagement Team is to promote CLF science and technology to some of our key audiences, with a view to sharing what we are capable of, engaging with our community, and recruiting new people. Different audiences require different types of interaction, and we are continually working to develop and harness the tools needed to communicate with each effectively.

As a Team, we are responsible for internal and external engagement functions, including: the CLF website and social media for our general science audience, staff and user community; talks, tours and activities for our general and 'next-gen' audiences; and a fortnightly newsletter for CLF staff.

CLF Website

Between 1 April 2023 and 31 March 2024:



Our website had
32,000 active users



Most users found our website via
organic searches
(such as Google)



People around the world

viewed our website—the highest numbers of users were based in the UK, USA, India, China, Germany and France



“Facilities”, “News” and “Vulcan”
were the most visited pages after landing on the homepage



Over 4,000 people

viewed the website during the month of October—around the time of the **Vulcan 20–20 announcement**

Social media

We maintain a social media presence to create and sustain connections with the science community, primarily users, industry and stakeholders. Our primary audience are CLF users and potential new recruits.

We have had consistently high engagement rates on both platforms, with Twitter reaching over four-times, and LinkedIn over two-and-a-half-times, the standard engagement rate.

Due to ownership and platform changes on Twitter, it has been harder to track analytics and gain followers. Whilst our follower count has had some growth this year, this was largely seen between April and August 2023. Around this time, Twitter's major rebrand to X was rolled out, which included several unpopular changes to the platform. Despite this, we have maintained a strong interaction with our intended communities.

As for LinkedIn, the platform continues to grow steadily, attracting our target demographics.

Twitter in 2023–24

1,456
followers

132,887
people saw our posts

4.3%
engagement rate

LinkedIn in 2023–24

664
followers

1,868
people saw our posts

4.88%
engagement rate
(good engagement rate is 2%)

Top follower demographics on LinkedIn 2023–24*

1. Research
2. Engineering
3. Education
4. Operations
5. Business Development



*Data was collected from Q3–4 of 2023–24

Connecting to wider audiences

We keep in close contact with the STFC Social Media team, through whom we can reach a more general public audience. Additionally, we regularly touch base with Social Media teams from the other STFC department to share new ideas, campaigns and best practices.

Engaging the public

As part of our goal to engage with the next-gen audience, we often host visits to our facilities. These visits, organised through RAL Public Engagement, have allowed us to engage a key demographic: 8 to 14-year-olds. This is the age at which children are starting to think about their future careers, and is also around the age when many young girls unfortunately decide that science and engineering is not for them.



Overall, in Financial Year 2023–2024, we engaged with 1,271 people in 119 visits hosted by our facility:



Looking more closely at next-gen public engagement efforts...

A total of

48 events

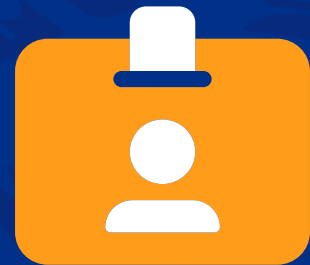
(including an Engineering Experience Programme project, which actually comprised multiple interactions (about 10 sessions), but counted as one here)



were supported by

18 CLF staff

including work experience supervisors



reaching a total of

1,789 people

(counting both visits to the CLF, and CLF events and activities conducted elsewhere)



49% of which were from

Wonder Areas

(Index of Multiple Deprivation 1–4)



“ I cannot express how much my pupils loved the trip. By the end of it everyone was giddy with excitement. All of us felt like kids in a toy shop, or geeks and nerds at a ComiCon or Sci-Fi Convention. Thank you so much for the experience. ”

– Feedback from one group who visited facilities at RAL site, including the CLF

Attracting a wider audience

Communication this year has begun to look a little more like how we operated before the COVID-19 pandemic, although things may never fully return to the way they were. For example, many audiences are now far more comfortable with online engagement, and this means that we can reach people without the constraints of distance and capacity.

We have completed an array of projects to help make the CLF more appealing to a wide range of audiences. Several of these projects have already been mentioned in this summary, and a few more are highlighted below

Daresbury Open Week 2023

One of the most memorable events of 2023 was taking part in the Open Week at Daresbury Laboratory, with over 5,000 people visiting the site on 15 July. The dedicated school days that took place in the days before saw 1,300 pupils from 50 schools across the region visit for curriculum-related activities, encouraging engagement with STEM.

Led by the CLF's Impact and Engagement Officer Helen Towrie, the Open Day team consisted of the CLF's communications Industrial Placement student Kaylyn Snelgrove, Mechanical Design Engineer Cameron Taylor, and Graduate Mechanical Design Engineer Churk Chung. After spending hours setting up on the night before and the morning of the event, the team of four dove headfirst into engaging with the public about the wonders of scientific lasers, how they work and what we can do with them.

The popularity of our exhibition could be seen thanks to the numerous families walking around with their "laser lanterns", and the total depletion of CLF-themed postcards by noon. Additionally, feedback from our location (which included all exhibits in the DL Visitor Centre) was overwhelmingly positive.





“ There were just four volunteers from the CLF in my area at the Open Day, but they somehow kept a constant stream of children interested in science all day. I’m still not sure how!

The paper lanterns activity was very popular, and it was fantastic to see the children hanging onto the volunteer’s every word and concentrating hard despite all the other exciting distractions in the area.

And who doesn’t love a good laser demo? Especially when it’s been created in-house for such events. ”

— Mark Leese, Senior Network Engineer and Area Manager for the Visitor Centre on the Open Day



The CLF was just one of over 250 meticulously designed activities, and we were pleased to have been given the opportunity represent laser science on the first Open Day in nearly a decade.

Engaging the next generation

International Day of Light

In May, we celebrated International Day of Light 2023. Around 200 secondary school pupils found out how to create supernovae with lasers, and saw the Vulcan Control Room and future EPAC facility up close. This was an excellent opportunity to share the excitement of laser science with students who are just beginning to think about their future careers, and indeed many of these young people seemed invested in the talk with several thought-provoking questions being asked. This event also prompted the 'What's your favourite thing about lasers?' board, which was filled with ideas from staff who were encouraged to think about the work and technology that inspires them. These ideas were shared with the visiting students, giving them an insight into the exciting world of scientific research through the varied responses from the team.

Visit from the Lightyear Foundation

In October, the CLF welcomed a group of post-16 education students with the Lightyear Foundation, who encourage young disabled people to consider careers in STEM. Part of the day was hosted in the CLF Visitor Centre, featuring its interactive activities and an experiment with vacuums and marshmallows. The feedback was incredibly positive and reflected that the students enjoyed the visit and were more likely to think about a job that includes physics as a result.

But, there's another problem!!

- Now the pulse is so powerful that it's going to start burning the air around it!
- We fix this by directing the beam into a vacuum, where there is no air to burn.
- If we are using Vulcan's Petawatt target area, this is the final step before the pulse hits the target and creates the mini supernova.



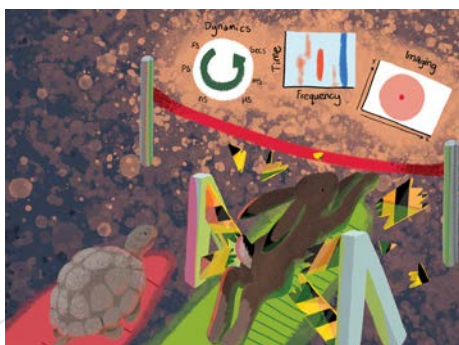
Now into 2024, RAL has recently held its annual Stargazing event, featuring activities across campus. The CLF Visitor Centre was opened up with all its demonstrations, in an excellent display of how different technologies and sciences can come together in exciting fields such as space research. Over 600 people attended and gave an average rating of 4.7/5—a great success.



Engaging through artwork

Over the past few years, the CLF has increasingly used illustration as a tool to attract and engage different audiences. Illustrations have a way reaching across the invisible boundary between STEM and the public, elevating CLF science within the scientific community, and creating a unique identifiable image for the CLF.

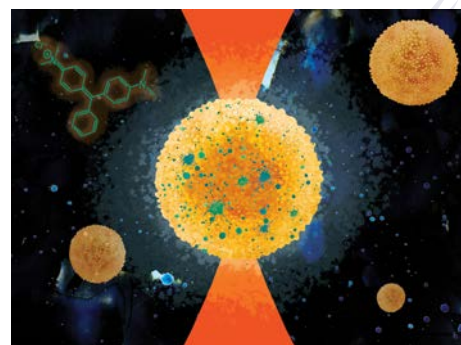
This year, we have been especially focused on using art to help push CLF papers to the forefront. Two front cover submissions and one article front cover have been accepted by peer-reviewed scientific journals, giving the associated papers the best chance possible of being noticed.



Chemical Science



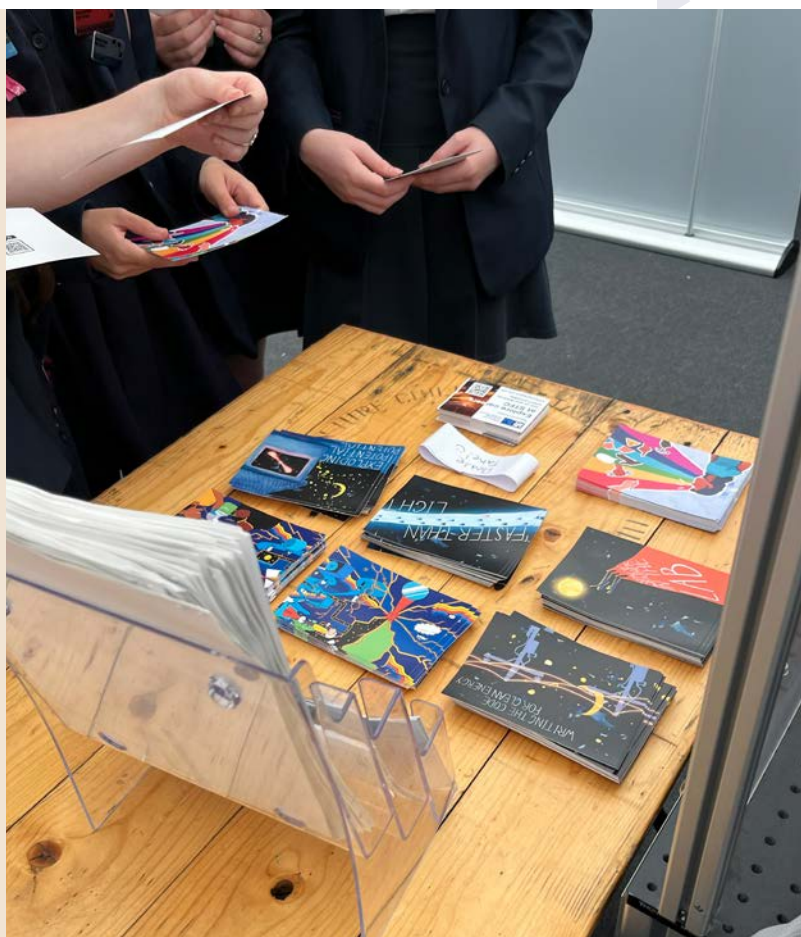
Accounts of Chemical Research



Materials Advances

Additionally, we used an in-house illustration to accompany a major press release on identifying COVID-19 counterfeit vaccines.

Finally, we have continued to reuse existing illustrations, most notably for Daresbury Open Week 2023, where the CLF mural was used on roller banner posters, and a fresh batch of CLF-themed postcards were printed as freebies.



Vulcan 20-20 publicity and celebration

The announcement of Vulcan 20-20, the CLF's plan to build the most powerful laser in the world, was huge – not just for the CLF, but for the UK government as a whole. Our team spent considerable time and energy preparing for and supporting this announcement and in helping to develop the ensuing short- and long-term publicity for all audiences.

The Vulcan Celebration Event welcomed senior scientists, staff and long-term Vulcan users to walk through the doors of Target Area Petawatt for one last time. The day included a selection of talks from impactful members of the High-Power Laser community and a gallery of images recalling the last 40 years of Vulcan. Over 100 people attended the event to reminisce over the CLF's flagship laser.

On a very different note, we also took inspiration from SunSpaceArt's activity at Daresbury Open Week and worked with them to create a new CLF craft activity for KS2 (7-11) based on Vulcan. Named "Space in a Box", the activity will be trialled for the first time at a local Primary School in the next few weeks.



Harwell Open Week 2024

In July 2024, Harwell Campus will open its doors for the first time since 2015 to welcome thousands of families to learn about all the different types of science we do. Preparations are already well underway for this mammoth event, and we expect it to be our focus until after July.

Introducing the Harwell Heritage Project

Victoria Marshall

Senior Software Engineer and Harwell Heritage Project

Although the Central Laser Facility was not founded until the late 1970s, some twenty years after the Rutherford High Energy Laboratory was established at Harwell, the CLF fully supports the work that is underway to uncover archive material located near to its facilities and to find out more about the site's heritage.

In April 2022, STFC Executive Board agreed that Campus heritage, and RAL heritage in particular, was worth preserving, and approved the setting up of a small project team to develop the idea further. The Arts and Humanities Research Council (AHRC) has since awarded a grant for a professional archivist to make an initial assessment of the campus archives. These archives encompass the Chilton Computing Collection created by Professor Bob Hopgood, the Ditton Park and Appleton Laboratory Collections created by Matthew Wild and RAL Space, the “stuff in the dungeon” inherited from RAL Library, AERE Harwell memorabilia owned by the Nuclear Decommissioning Authority (NDA) in the shell of the DIDO reactor, and an ever-increasing list of material held by retired and nearly-retired staff either on site or in various spare rooms, home offices and sheds.

Assessment of the various archives is just the beginning of the process; it will take years to produce a full, detailed catalogue. The initial aim is simply to find out what there is. The second aim is to figure out what to do next, and what to do with all the material.

Getting started on the Project

The Harwell Campus has seen a great number of technological and scientific achievements over its near 80-year history. The AERE Harwell story – with its 14 reactors leading Britain's early atomic energy development – is fairly well known. What is less well known is that Harwell also built 12 accelerators of various designs that were key not only to the formation of the Rutherford High Energy Laboratory (RHEL) next door, but also to the development of accelerators at CERN.

A decade younger, the early part of the Rutherford Laboratory story is also a mystery to many. Information is scant and scattered; people who were there are no longer here, and we are in danger of losing our institutional memory.

A year or so ago, what used to be the Laboratory Archives were (re)discovered in what used to be the NIMROD (“National Institute Machine Radiating On [the] Downs” or “National Institute Machine for Research On the Downs”) Motor Alternator Hall Basement.

The basement measures 37 x 15 m and is divided into eight secure cages, of which the Library Archives is one of the largest. This cage contains six rolling stacks holding five tons of material on 1.5 km of shelving. As can be seen in the photograph, this was nothing like a standard office environment. Explorations began...

Over the last year or so, much original material has been rediscovered from the early days of the laboratory in the 1950s until the 1980s, when use of the cage ceased for archival purposes. Much of this has been scanned and is available in the "Rutherford Laboratory" and "AERE Harwell" sections of the **Chilton Computing** website.

The timeline overleaf includes a few of the photographs that have been found so far, which provide a fascinating insight into RAL's early history. More information on the photographs, papers and other material uncovered by the project can be found in the online version of this report.



The basement archives in October 2022. The first challenge was to push the door open and clamber round an over-loaded trolley. Happily, the cage is now considerably tidier and far more accessible.

A journey through time

Rutherford High Energy Laboratory (1957)

Both John Cockcroft and Edward Appleton (at the time Secretary of the Department of Scientific and Industrial Research (DSIR)) were instrumental in naming the new national accelerator facility Rutherford High Energy Laboratory, in honour of their PhD advisor at Cambridge, Nobel Prize-winner Sir Ernest Rutherford.



Aerial view of Rutherford Laboratory looking east. In the foreground is the green mound of Nimrod; the star shape of the R22 Restaurant is eastwards centre, with the houses of Frome Road in the distance (1963).

Rutherford Laboratory (1975)

The “High Energy” part of RHEL’s name was dropped in 1975 to reflect the wider scientific interests of the Laboratory and its recent merger with the Atlas Computer Laboratory.

Radio Research Station (1924) and Appleton Laboratory (1973)

In 1924 the DSIR formed the Radio Research Station (RRS) at Ditton Park, near Slough, to research radio science and to continue Edward Appleton’s ionospheric work which he began in the 1920s.

The Station was renamed the Radio and Space Research Station (RSRS) in 1965 to better reflect their wider work and facilities, which now included an 85-foot (26 m) radio telescope capable of following earth satellites, and artificial satellites, known as Topside Sounders, to explore the ionosphere from above.

RSRS was renamed yet again on 7 November 1973 to Appleton Laboratory in honour of Nobel Prize-winner Edward Appleton.

Central Laser Facility (1977)

In 1975, the government gave approval for the Science Research Council (SRC) to provide at RL a high-power laser for use by academia. The Central Laser Facility was formally inaugurated in 1977, and its Neodymium Glass Laser began operations. This laser is now known as Vulcan (Versicolor Ultima Lux Cohaerens pro Academica Nostra or The latest multi-coloured coherent light for our academics).



Components of the Vulcan laser being delivered to the west end of R1 (25 September 1976).

Rutherford Appleton Laboratory (1979)

Appleton Laboratory was closed in 1979 and many of the staff transferred to Rutherford Laboratory, whereupon it was briefly known as The Rutherford and Appleton Laboratories before simplification to the modern-day, and more digestible, Rutherford Appleton Laboratory.



Three Directors all in a row: John Houghton, Godfrey Stafford and Geoff Manning. In the background is the IRAS project's 12-metre Transportable Ground Station (aka The Dish) built on behalf of NASA in the 1960s. (September 1979).



Aerial view of Rutherford Laboratory looking north. The NASA/IRAS satellite dish is in the right foreground with the R22 Restaurant further to the north. The hill covered in dried grass is Nimrod/ISIS spoil (this photo was taken in July); the accelerator mound itself is the green(ish) circle northwards (1984).

High Energy Density and High Intensity Physics

Low divergence electron beams from a gas cell

We report on the generation of electron beams with unusually low divergences. The beams were produced by laser wakefield acceleration in a gas cell, which typically produces high quality beams, but with a large divergence due to the strong focusing fields present in the plasma. By using a gas cell with a shaped exit aperture, the transition between the plasma and the vacuum was smoothed, resulting in improved transverse beam properties. Measurements from the electron spectrometer indicate divergences of approximately 0.2 mrad, while higher resolution measurements made using image plate suggest that the true resolution was lower than this, reaching a minimum of 0.04 mrad. These results are of interest for many potential applications where transverse beam quality is paramount, such as for light sources and for staged acceleration.

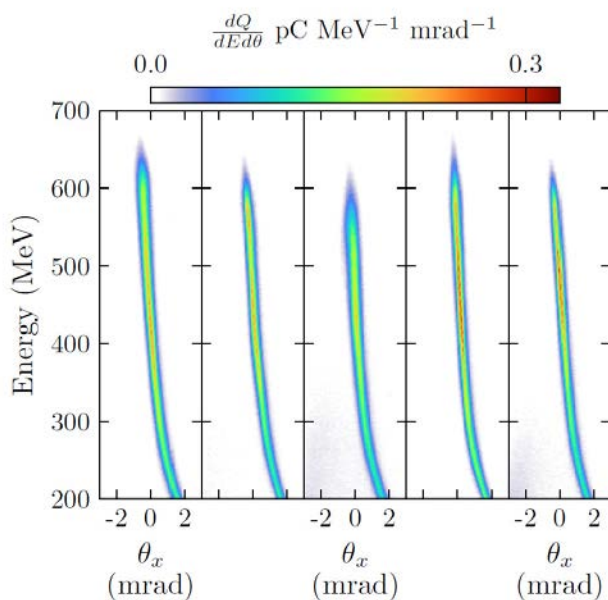


Figure 1: Sequential electron beam spectra highlighting the low divergence of the beams.

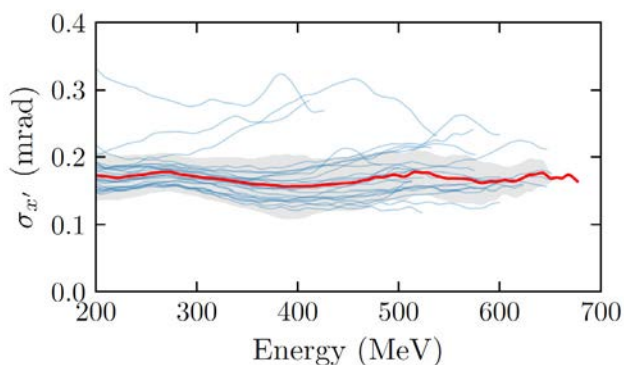



Figure 2: Energy resolved divergence measurements. The blue lines are the measurements for each spectrum in the data set, the red line is the median, and the shaded region is the standard deviation.

Authors: M.P. Backhouse , R. Luo, J. Hills, L. Kennedy, C. Cobo, E. Los, Z. Najmudin, N. Lopes, E. Gerstmayr, J. Sarma, N. Bourgeois, D. Bloemers, A. Thomas, S. Hawkes, S. Dann

Beam driven electron acceleration to 4 GeV at Gemini

We present measurements of electrons accelerated to high energies using both arms of the Gemini laser system. The experiment used a pair of gas cells, where the first cell acted as an injector stage, producing electron beams with peak energies of approximately 1 GeV, and the second cell provided a secondary energy boost. The boost could be large enough to approach the measurement limit of the magnetic spectrometer used, at 4.0 GeV. The modulation of the spectrum due to the plasma in the second cell is consistent with beam driven acceleration, making this experimental setup an example of the LWFA-PWFA hybrid accelerator concept. These results have implications for future implementations of LWFA seeded beam driven plasma accelerators.

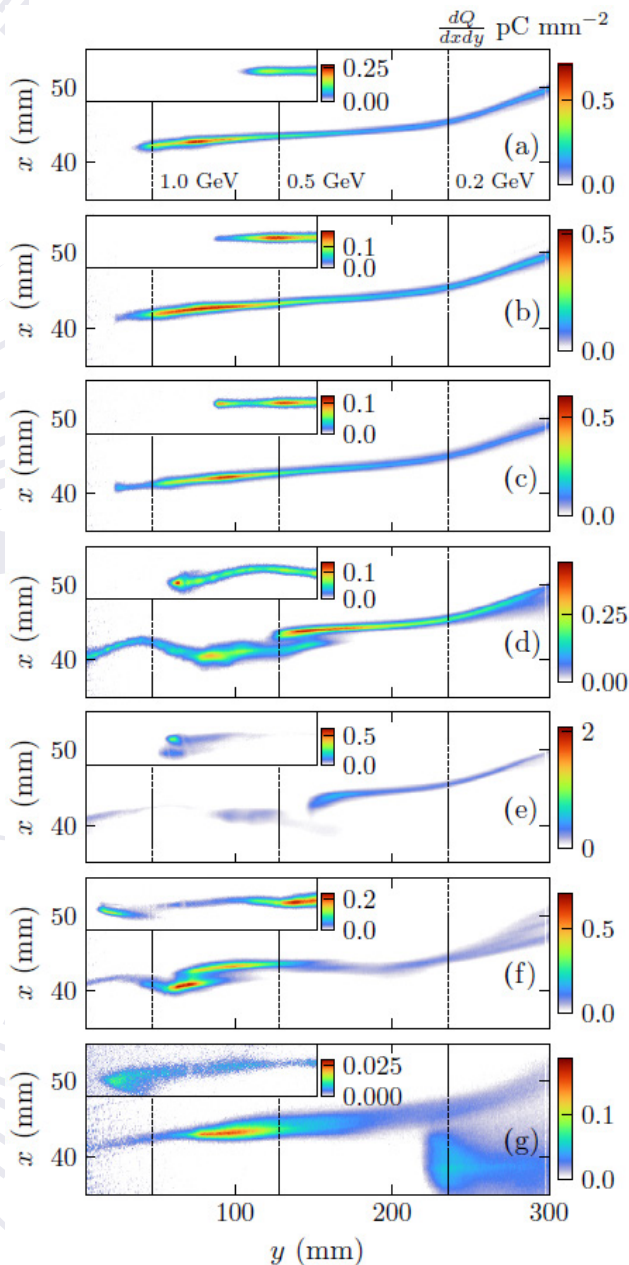


Figure 1 (left): Example images from the electron spectrometer screens. The main panels show images from the lower energy screen while the inset shows the measurements from the higher energy screen. Panels (a-c) show electron spectra after generation in cell 1. Subplots (d-g) show beams after propagating through the plasma in the second cell, resulting in an energy boost for some electrons and transverse modulations of the beam.

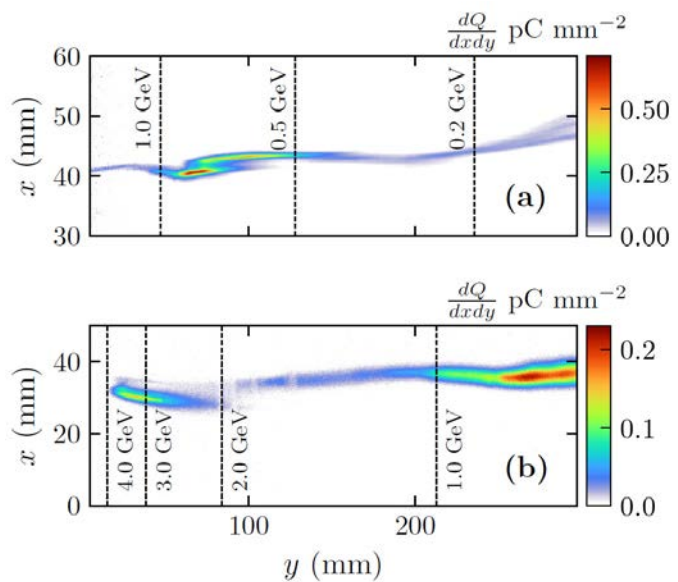
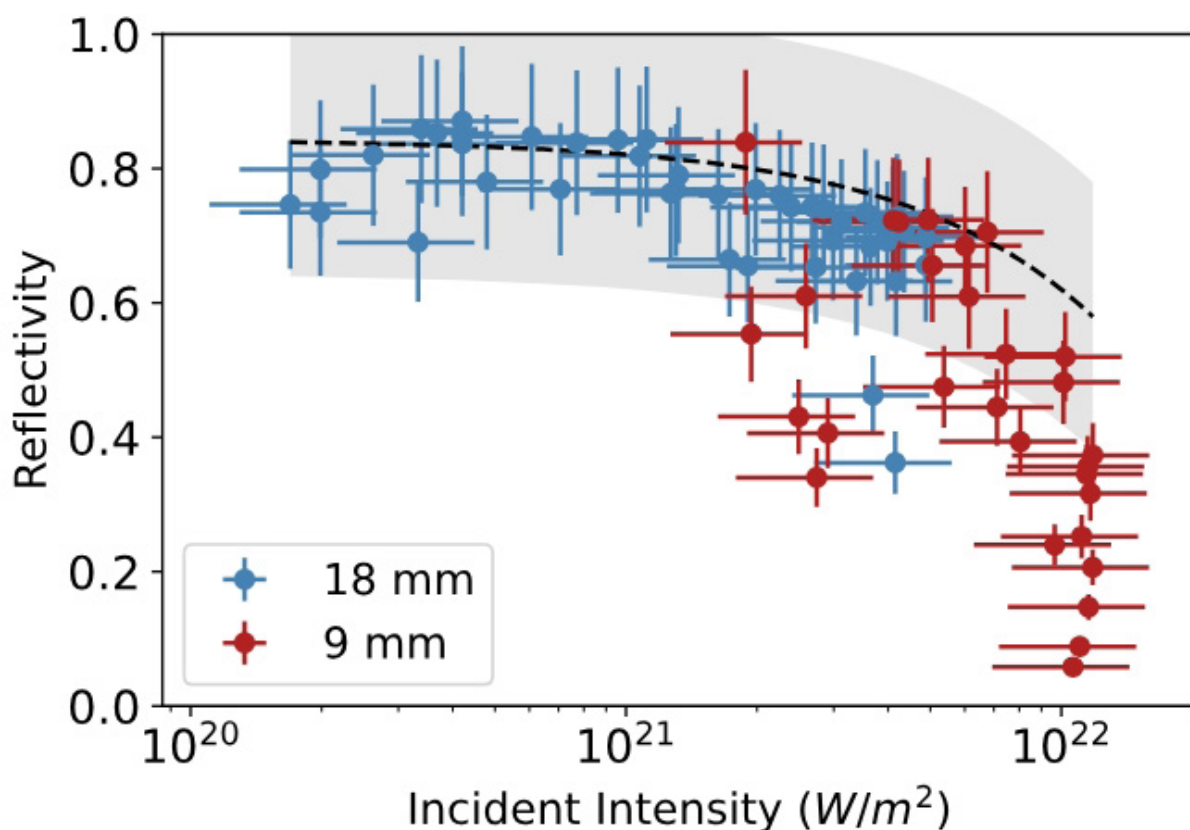


Figure 2 (above): Electron spectrometer images with overlaid energy contours from a shot where a large gain of energy was observed due to the second cell.

Authors: M.P. Backhouse ✉, R. Luo, J. Hills, L. Kennedy, C. Cobo, E. Los, Z. Najmudin, N. Lopes, E. Gerstmayr, J. Sarma, G. Sarri, P. Blum, R.J. Shalloo, N. Bourgeois

Plasma mirror operation at high intensity: Reflectivity and beam profile

Reflectivity and reflected beam profile from a plasma mirror at high incident intensities (on the order of $10^{19} - 10^{21} \text{ Wm}^{-2}$) was characterised for the Gemini North beam incident on 125 μm thick Kapton tape. Post-reflection pointing was characterised with an additional pointing variation of $\theta_{\text{av}} = 2.6 \text{ mrad}$ generated by the formation of the plasma mirror. Adjusting focal spot area on the tape and pulse energy allowed for on-tape intensity variation. A maximum reflectivity above 70% was observed with a drop off for intensities nearing $3 \times 10^{21} \text{ Wm}^{-2}$. Focusing further from the tape resulted in a lower quality of reflected spot at comparable intensities, with less energy contained within the FWHM (20% compared to 10% at 10^{21} Wm^{-2}). The results presented highlight important areas for development and optimal operation regimes of plasma mirrors for future staging applications.

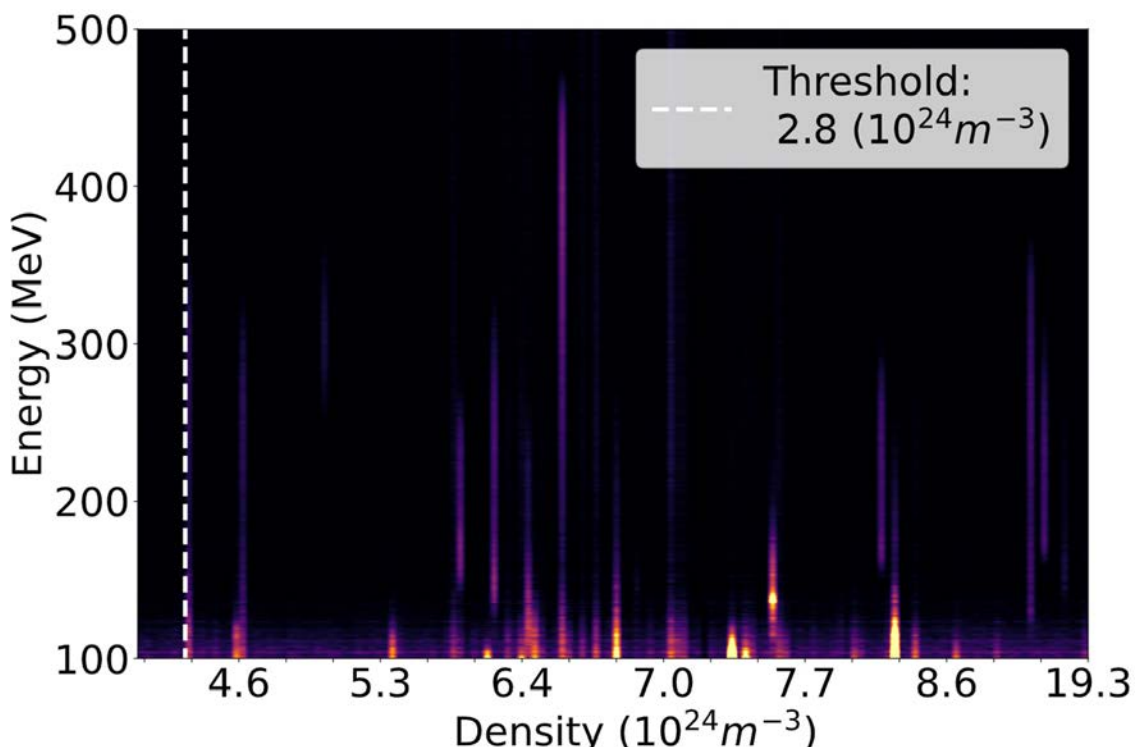


Decreasing reflectivity across incident intensities with a sharp reduction towards 10^{22} Wm^{-2} . The distances of 9 mm and 18 mm refer to the position of the tape relative to the laser focus.

Authors: J. Hills ✉, M.P. Backhouse, R. Luo, L. Kennedy, C. Cobo, E. Los, Z. Najmudin, E. Gerstmayr, J. Sarma, P. Blum, N. Lopes, N. Bourgeois, D. Bloemers, A. Thomas, S. Hawkes, S. Dann

Wakefield accelerator driven to ionisation injection using a laser reflected off a plasma mirror at high intensities

We report on a laser wakefield accelerator driven to ionisation injection using a laser pulse reflected from a thin-film plasma mirror operating at high intensities. Reflected pulses containing a maximum total energy of 3.2 ± 0.9 J were used to demonstrate a guided central spot at densities exceeding $0.5 \times 10^{24} \text{ m}^{-3}$. Entire blue shifting of the transmitted pulse was observed between $0.5 \times 10^{24} \text{ m}^{-3}$ and $2 \times 10^{24} \text{ m}^{-3}$. Ionisation injection was demonstrated with spots containing up to 0.4 ± 0.1 J in their FWHM at densities exceeding $2.7 \pm 0.4 \times 10^{24} \text{ m}^{-3}$. Electrons were accelerated in a cell of $6.7 \pm 0.8 \times 10^{24} \text{ m}^{-3}$ to energies up to 455 ± 28 MeV using the reflected pulse. The results presented here support the utility of a tape-based plasma mirror for driving the accelerating stage of a wakefield accelerator.

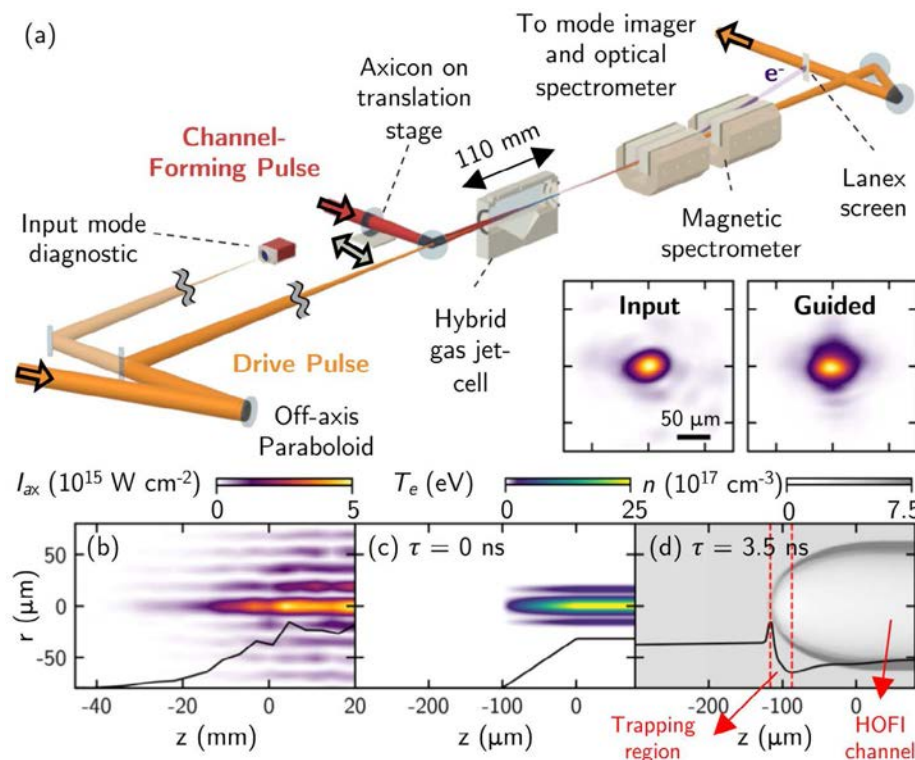


Density scan of electron spectra at different cell densities with a 10 mm long cell. Densities here are arranged in ascending order but have large uncertainties.

Authors: J. Hills ✉, M.P. Backhouse, R. Luo, L. Kennedy, C. Cobo, E. Los, Z. Najmudin, E. Gerstmayr, J. Sarma, P. Blum, N. Lopes, N. Bourgeois

All-optical GeV electron bunch generation in a laser-plasma accelerator via truncated-channel injection

We describe a simple scheme, truncated-channel injection, to inject electrons directly into the wakefield driven by a high-intensity laser pulse guided in an all-optical plasma channel. We use this approach to generate dark-current-free 1.2 GeV, 4.5% relative energy spread electron bunches with 120 TW laser pulses guided in a 110 mm-long hydrodynamic optical-field-ionized plasma channel. Our experiments and particle-in-cell simulations show that high-quality electron bunches were only obtained when the drive pulse was closely aligned with the channel axis, and was focused close to the density down ramp formed at the channel entrance. Start-to-end simulations of the channel formation, and electron injection and acceleration show that increasing the channel length to 410 mm would yield 3.65 GeV bunches, with a slice energy spread $\sim 5 \times 10^{-4}$.



Schematic of truncated-channel injection scheme. (a) Setup: channel-forming (red) and drive (orange) beams were coupled into the gas target. The input mode, output mode, optical, and electron spectra were measured on every shot. Inset: measured transverse fluence profiles of the drive laser at focus and at the exit of the HOFI channel. (b) Measured axicon longitudinal intensity profile, (c) calculated initial electron temperature profile, and (d) calculated density profile of the truncated HOFI plasma channel 3.5 ns after arrival of the channel-forming pulse. In each panel, the black curve shows the relative magnitude of each variable along the optical axis.

Reproduced from A. Picksley et al. Phys. Rev. Lett. 131, 245001 (2023), under the terms of the **CC-BY-4.0 license**. doi: 10.1103/PhysRevLett.131.245001

Authors: A. Picksley, J. Chappell, E. Archer, N. Bourgeois, J. Cowley, D.R. Emerson, L. Feder, X.J. Gu, O. Jakobsson, A.J. Ross, W. Wang, R. Walczak, **S.M. Hooker** ✉

Measurement of the decay of laser-driven linear plasma wakefields

We present measurements of the temporal decay rate of one-dimensional (1D), linear Langmuir waves excited by an ultrashort laser pulse. Langmuir waves with relative amplitudes of approximately 6% were driven by 1.7 J, 50 fs laser pulses in hydrogen and deuterium plasmas of density $n_{e0} = 8.4 \times 10^{17} \text{ cm}^{-3}$. The wakefield lifetimes were measured to be $\tau_{\text{wf}}^{\text{H}_2} = (9 \pm 2) \text{ ps}$ and $\tau_{\text{wf}}^{\text{D}_2} = (16 \pm 8) \text{ ps}$, respectively, for hydrogen and deuterium. The experimental results were found to be in good agreement with 2D particle-in-cell simulations. In addition to being of fundamental interest, these results are particularly relevant to the development of laser wakefield accelerators and wakefield acceleration schemes using multiple pulses, such as multipulse laser wakefield accelerators.

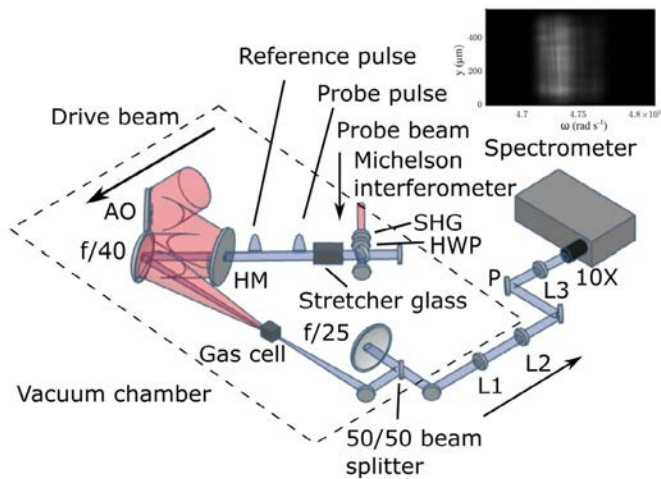


Figure 1: Schematic of the experimental layout inside the target vacuum chamber. Both beams of the Gemini TA3 laser were used: one as the drive beam, one as the diagnostic probe beam. The 800 nm beams are shown in red, and the 400 nm diagnostic beam in blue. After leaving the gas cell, the diagnostic beam was transported to a 400 nm spectrometer located outside the vacuum chamber.

Inset: example recording of a wakefield in a spectral interferogram, as captured by the spectrometer camera.

AO: Adaptive optic; HM: Holed mirror; HWP: Half-wave plate; L1: $f=500 \text{ mm}$ lens; L2: $f=-100 \text{ mm}$ lens; L3: $f=300 \text{ mm}$ lens; P: polariser; 10X: microscope objective; SHG: second harmonic generating crystal.

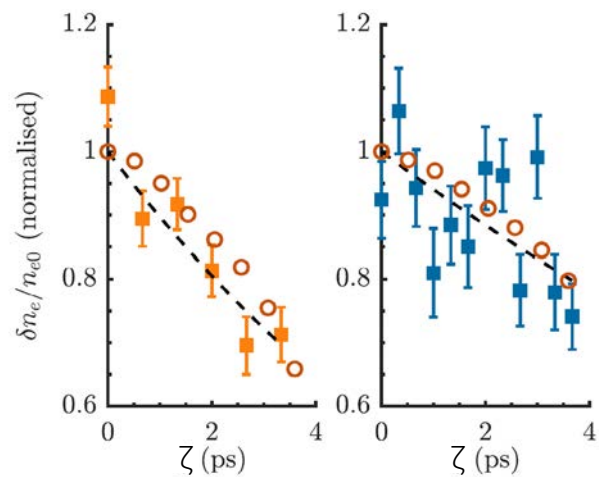


Figure 2: Measured normalized relative wakefield amplitude calculated using the TESS technique (see referenced paper) as a function of delay for: (a) hydrogen; (b) deuterium, recorded with a backing pressure $P_{\text{cell}}=(17.0 \pm 1.2) \text{ mbar}$. For each delay are shown the uncertainty-weighted average wakefield amplitude ($\delta n_e(\zeta)/n_{e0}$) and the standard error. The uncertainty was calculated using the background noise in the Fourier-transformed interferograms. The wakefield amplitude calculated from the PIC simulations are shown as open circles. Also shown are fits of the exponential function to the data as black lines.

Reproduced from J. Jonnerby et al. Phys. Rev. E 108, 055211 (2023), under the terms of the **CC-BY-4.0 license**. doi: 10.1103/PhysRevE.108.055211

Authors: J. Jonnerby, A. von Boetticher, J. Holloway, L. Corner, A. Picksley, A.J. Ross, R.J. Shalloo, C. Thornton, N. Bourgeois, R. Walczak, **S.M. Hooker** ✉

CFD modelling of gas cell target for laser wakefield accelerators

We performed 2D and 3D simulations of a gas cell target designed for laser wakefield acceleration. These are among the first full 3D simulations conducted for such a target. The simulations show that it takes a few hundred milliseconds for the density inside the cell to plateau. The cell is capable of providing density uniformity below 1%, which is a crucial factor in reducing shot-to-shot instability and improving beam quality.

The equilibrium time, based on the 3D fluid simulations, can be used to estimate the minimal delay required for the initiation of gas flow to achieve a uniform target density. The results also suggest that, for a 10 Hz LWFA, a gas cell operating in continuous mode might provide a more uniform density profile.

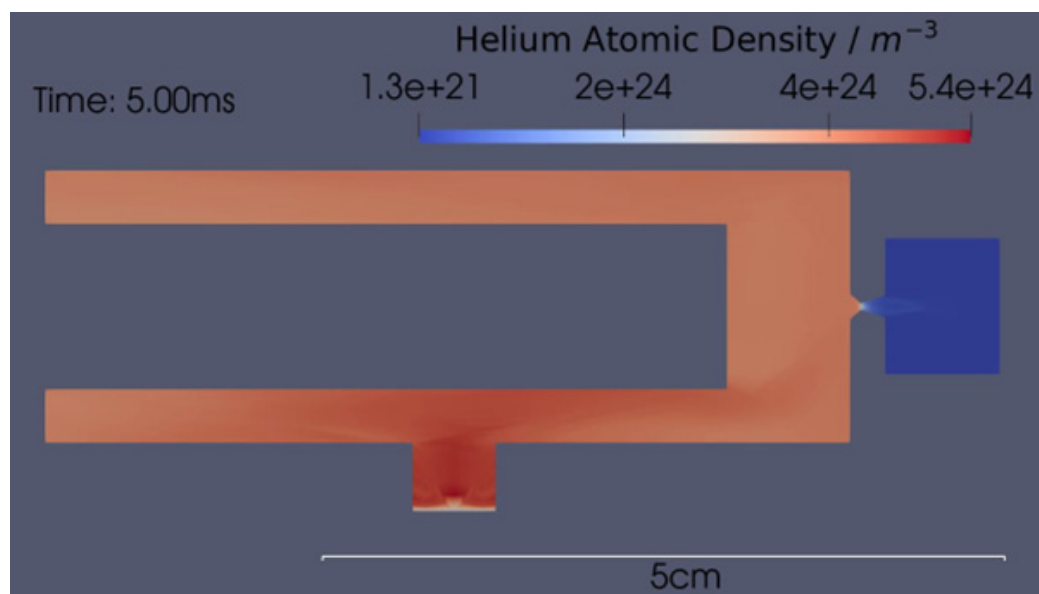


Figure 1: A transverse slice of the density distribution at 5 ms for the 3D simulation.

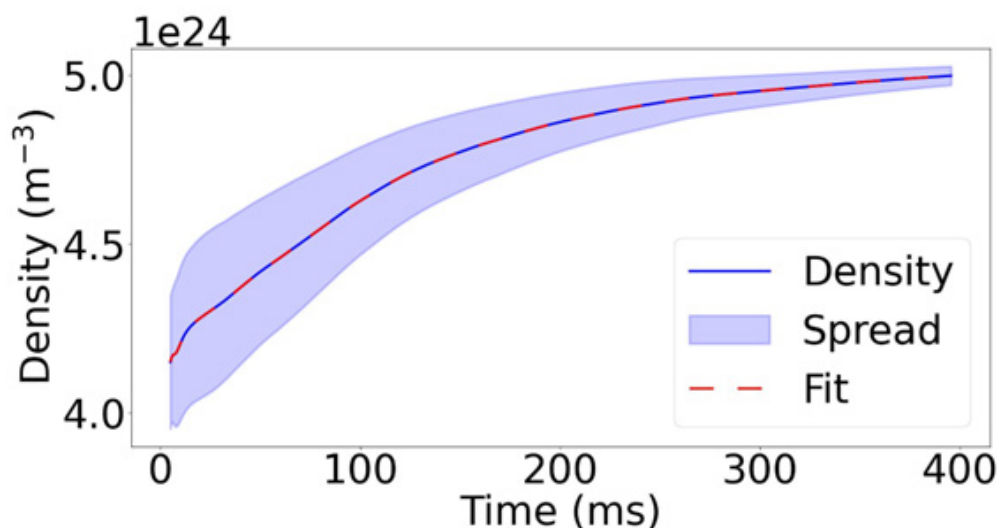

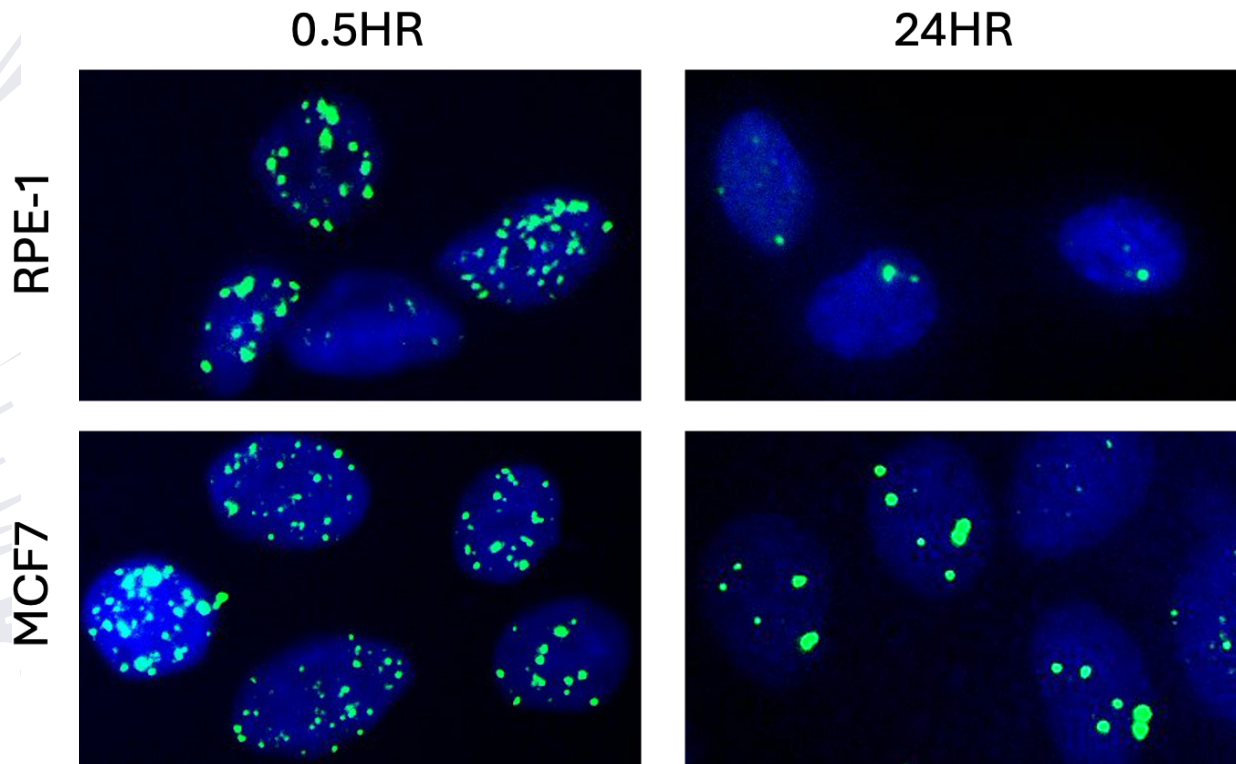


Figure 2: Mean helium atomic density evolution for in the cell for the 3D simulation.

Authors: R. Luo , G. Christian, J. Hills, C. Cobo, E. Los, L. Kennedy, M.P. Backhouse, Z. Najmudin, N. Lopes, P. Blum, R.J. Shalloo, E. Gerstmayr, J. Sarma, G. Sarri, N. Bourgeois

Cellular response to femtosecond-scale radiation at dose-rates exceeding 10^{13} Gy/s

We report on the characterisation of a laser driven, very high energy electron source for radiobiological applications. Here, nanocoulomb scale electron beams were generated by a laser wakefield accelerator, allowing for dose deposition up to 3 Gy per pulse. The electron beam duration is approximated to be 25 femtoseconds, equating to unprecedented single shot dose-rates in excess of 10^{13} Gy/s. The source is characterised and compared to Monte Carlo simulations, with the applications to biological research discussed.

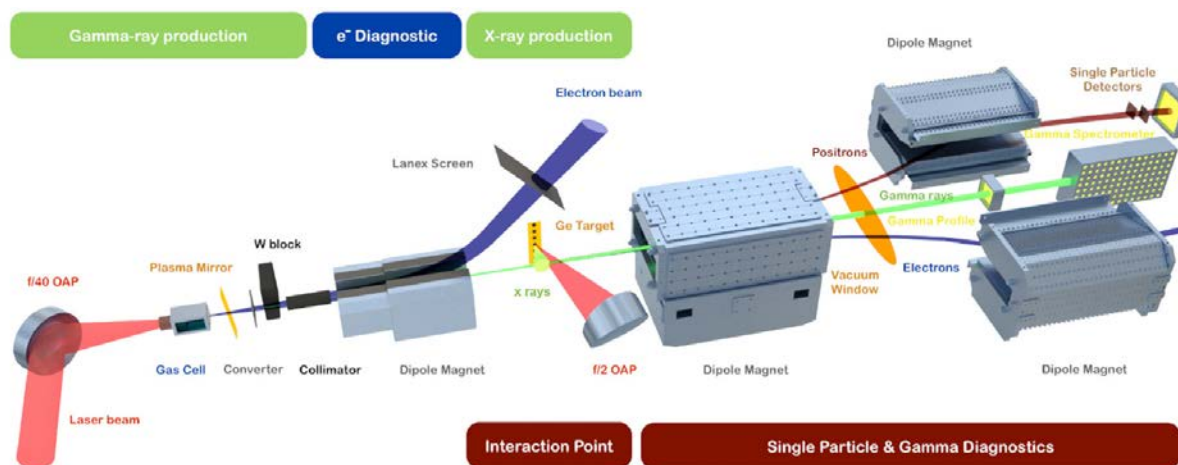


53BP1 foci formation, a DNA double strand break marker, as a function of time (0.5hr and 24hr after irradiation) for RPE-1, a healthy cell line, and MCF7, a cancerous cell line. Shown are merged channel images of 53BP1 DNA DSB marker (green) and DAPI nuclear stain (blue).

Authors: H. Maguire ✉, C.A. McAnespie, E. Gerstmayr, L. Calvin, J. Sarma, G. Sarri, C. McDonnell, S.J. McMahon, K.M. Prise, P. Chaudhary, G. Schettino, S.W. Botchway, S. Needham, O.J. Finlay

Monte Carlo modeling of the linear Breit-Wheeler process within the GEANT4 framework

A linear Breit-Wheeler module for the code GEANT4 has been developed. This allows signal-to-noise ratio calculations of linear Breit-Wheeler detection experiments to be performed within a single framework. The interaction between two photon sources is modelled by treating one as a static field, then photons from the second source are sampled and tracked through the field. To increase the efficiency of the module, we have used a Gaussian process regression, which can lead to an increase in the calculation rate by a factor of up to 1000. To demonstrate the capabilities of this module, we use it to perform a parameter scan, modelling an experiment based on that recently reported by Kettle et al. [New J. Phys. 23, 115006 (2021)]. We show that colliding 50-fs duration γ rays, produced through bremsstrahlung emission of a 100 pC, 2-GeV laser wakefield accelerator beam, with a 50-ps x-ray field, generated by a germanium burn-through foil heated to temperatures >150 eV, this experiment is capable of producing >1 Breit-Wheeler pair per shot.



Schematic of Gemini linear Breit-Wheeler (BW) detection experiment. Starting from the left: a LWFA generates an electron beam which is converted into a gamma ray beam through bremsstrahlung emission in a thin bismuth converter foil. A tungsten collimator and block are placed in the beam path to remove highly divergent gamma rays and those directed toward the x-ray foil, respectively. A large number of Bethe-Heitler (BH) pairs are produced in the converter foil, collimator, and block. These are removed with an on-axis magnet before the interaction zone. The gamma rays interact with an x-ray field, generated by a laser heated germanium foil, producing BW pairs. The residual gamma rays continue on axis to a spectrometer. The BW pairs pass through a magnetic chicane to single particle detectors, situated behind lead shielding (not shown). Diagram provided by Gerstmayr.

Reproduced from S.P.D. Mangles et al. Phys. Rev. Accel. Beams 26, 054601 (2023), under the terms of the **CC-BY-4.0 license**. doi: 10.1103/PhysRevAccelBeams.26.054601

Authors: R.A. Watt, S.J. Rose, B. Kettle, S.P.D. Mangles ✉

Narrow bandwidth, low-emittance positron beams from a laser-wakefield accelerator

The rapid progress that plasma wakefield accelerators are experiencing is now posing the question as to whether they could be included in the design of the next generation of high-energy electron positron colliders. However, the typical structure of the accelerating wakefields presents challenging complications for positron acceleration. Despite seminal proof-of-principle experiments and theoretical proposals, experimental research in plasma-based acceleration of positrons is currently limited by the scarcity of positron beams suitable to seed a plasma accelerator. Here, we report on the first experimental demonstration of a laser-driven source of ultra-relativistic positrons with sufficient spectral and spatial quality to be injected in a plasma accelerator. Our results indicate, in agreement with numerical simulations, selection and transport of positron beamlets containing $N_{e^+} \geq 10^5$ positrons in a 5% bandwidth around 600 MeV, with femtosecond-scale duration and micron-scale normalised emittance. Particle-in-cell simulations show that positron beams of this kind can be guided and accelerated in a laser-driven plasma accelerator, with favourable scalings to further increase overall charge and energy using PW-scale lasers. The results presented here demonstrate the possibility of performing experimental studies of positron acceleration in a laser-driven wakefield accelerator.

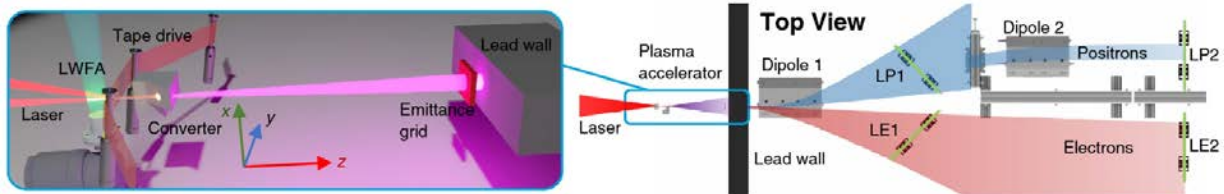


Figure 1: Illustration of the experimental setup, showing the electron plasma accelerator, the converter, the emittance mask, scintillators for electrons (LE1 and LE2) and positrons (LP1 and LP2). Electron (red) and positron (blue) trajectories are also shown to guide the eye.

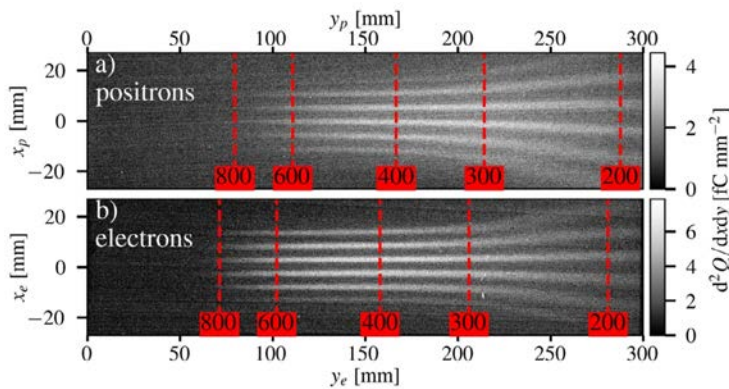


Figure 2: Raw images of energy-resolved beam profiles with the emittance mask. Example modulated (a) positron and (b) electron spatial charge density as a function of position on the screens (x_p , y_p , x_e , y_e) for a single shot with a converter thickness of 8.0 mm and the emittance mask in the beam-line. Vertical red dashed lines indicate positions corresponding to the given particle energies in MeV. The difference between electron and positron raw data is due to the slightly different position of the scintillator screens (see published paper).

Reproduced from M.J.V. Streeter, C. Colgan, J. Carderelli et al. Narrow bandwidth, low-emittance positron beams from a laser-wakefield accelerator. Sci Rep 14, 6001 (2024), under the terms of the **CC-BY-4.0 license**. doi: 10.1038/s41598-024-56281-1

Authors: M.J.V. Streeter, C. Colgan, J. Carderelli, Y. Ma, N. Cavanagh, E.E. Los, H. Ahmed, A.F. Antoine, T. Audet, M.D. Balcazar, L. Calvin, B. Kettle, S.P.D. Mangles, Z. Najmudin, P.P. Rajeev, D.R. Symes, A.G.R. Thomas, **G. Sarri** ✉

Measurement of magnetic cavitation driven by heat flow in a plasma

Experiments at Vulcan TAW led to direct measurements of the dynamics of magnetic fields driven by heat flow in a plasma. In ideal plasma, field lines are considered to be locked to the bulk motion ('frozen in flow'), but we measured that the magnetic field was instead expelled from a hot plasma much faster than the plasma could move. This Nernst advection is driven by electron heat conduction occurring on the timescale of a few 100s ps, whereas bulk plasma motion is limited by heavier ions, which take longer to respond.

By making these measurements of magnetic field advection we demonstrated a new way of studying heat flow in hot magnetised plasmas. We showed that while the hydrodynamic motion is insufficient to explain the magnetic field dynamics, extended MHD simulations do a surprisingly good job of modelling the advection process because the magnetic field effectively localises the heat flow.

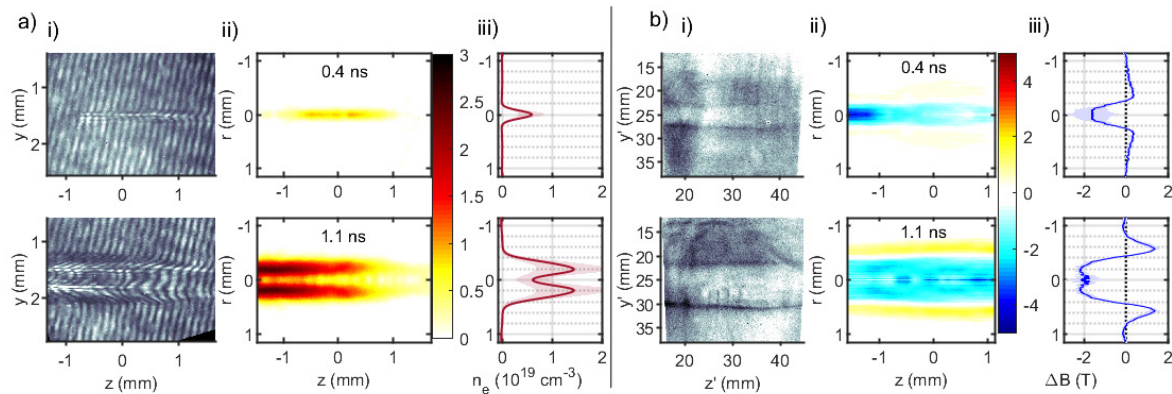


Figure 1 (from doi: 10.1103/PhysRevLett.131.015101): Results from a) optical interferometry, measuring electron density and b) proton radiography, measuring change in the magnetic field. (i) Raw data for two different shots taken under the same conditions, one 0.4 ns after the start of the heater beam and one 1.1 ns after the start. (ii) The plasma column and cavity in the magnetic field both expand over time, with the longitudinally averaged profiles (iii) showing how the cavity remains larger than the plasma column throughout.

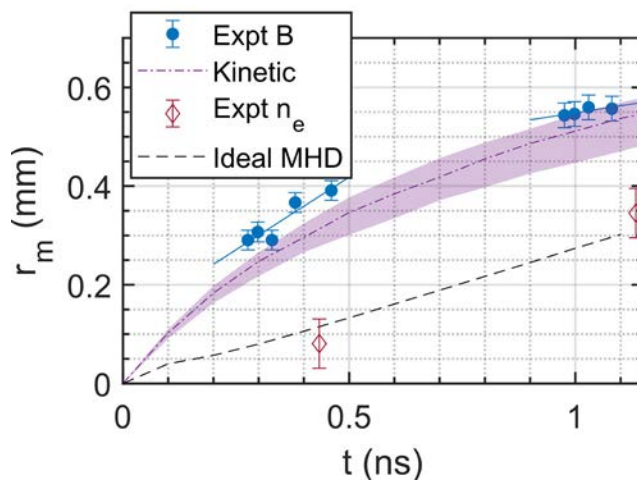

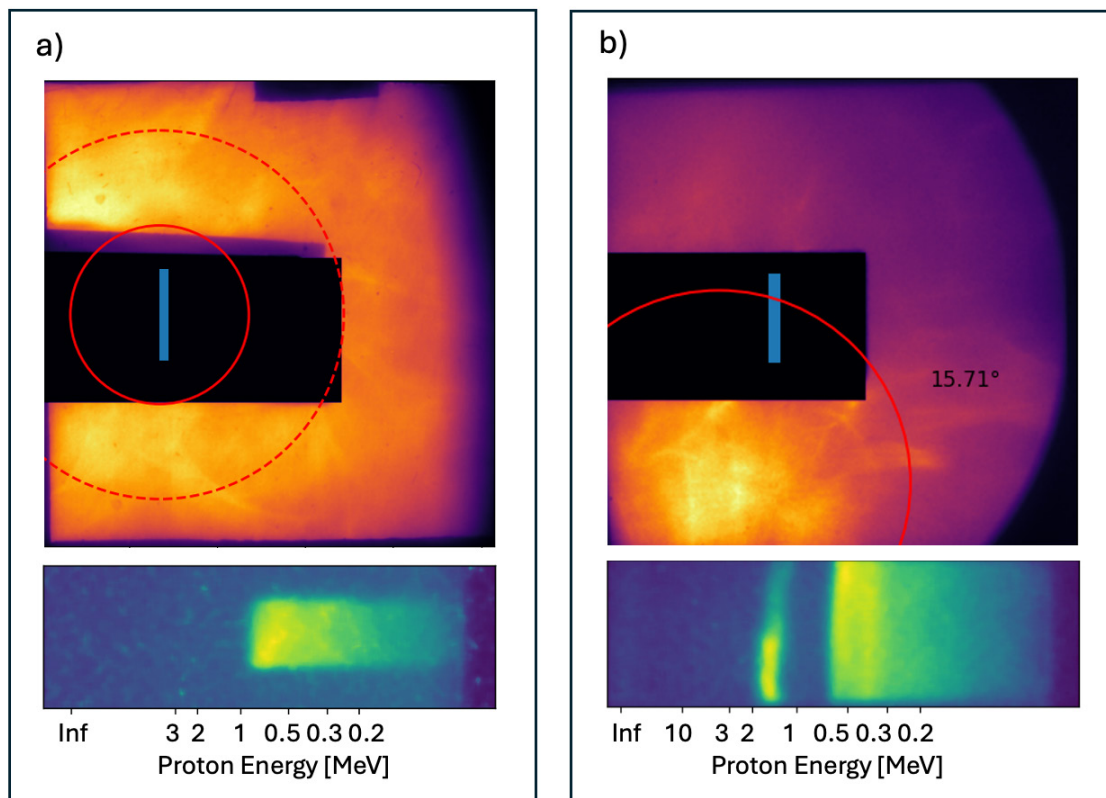


Figure 2: The position of the peak in the magnetic field over time (blue circles), compared with the position of the HWHM of the plasma density (red open diamonds). Overlaid are the positions predicted from simulations, showing how kinetic simulations (dash-dotted) do a good job of predicting the magnetic field dynamics, whereas ideal MHD predicts much slower advection tied to the motion of the plasma (frozen-in-flow).

Authors: C. Arran , P. Bradford, A. Dearling, G.S. Hicks, S. Al-Atabi, L. Antonelli, O.C. Ettlinger, M. Khan, M.P. Read, K. Glize, M. Notley, C.A. Walsh, R.J. Kingham, Z. Najmudin, C.P. Ridgers, N.C. Woolsey

Proton beam divergence measurements from radiation pressure driven shock acceleration

Laser-plasma ion acceleration is a fast-developing field of research, yielding ion sources capable of generating high energy, high current, short ion beams. These characteristics make them ideally suited to many applications, including hadron radiation therapy and nuclear physics. We performed a radiation driven, front surface ion acceleration experiment using a long wavelength CO₂ laser to irradiate gas targets. We devised and fielded a proton spatial diagnostic which enabled us to make novel measurements of ion beam divergence. By comparison with shadowgraphy, we observed a relationship between the emission angle of the energetic ions and the electrons generated in the laser plasma interaction. We also observed spatial and spectral modulations of the proton beam on our ion diagnostics.

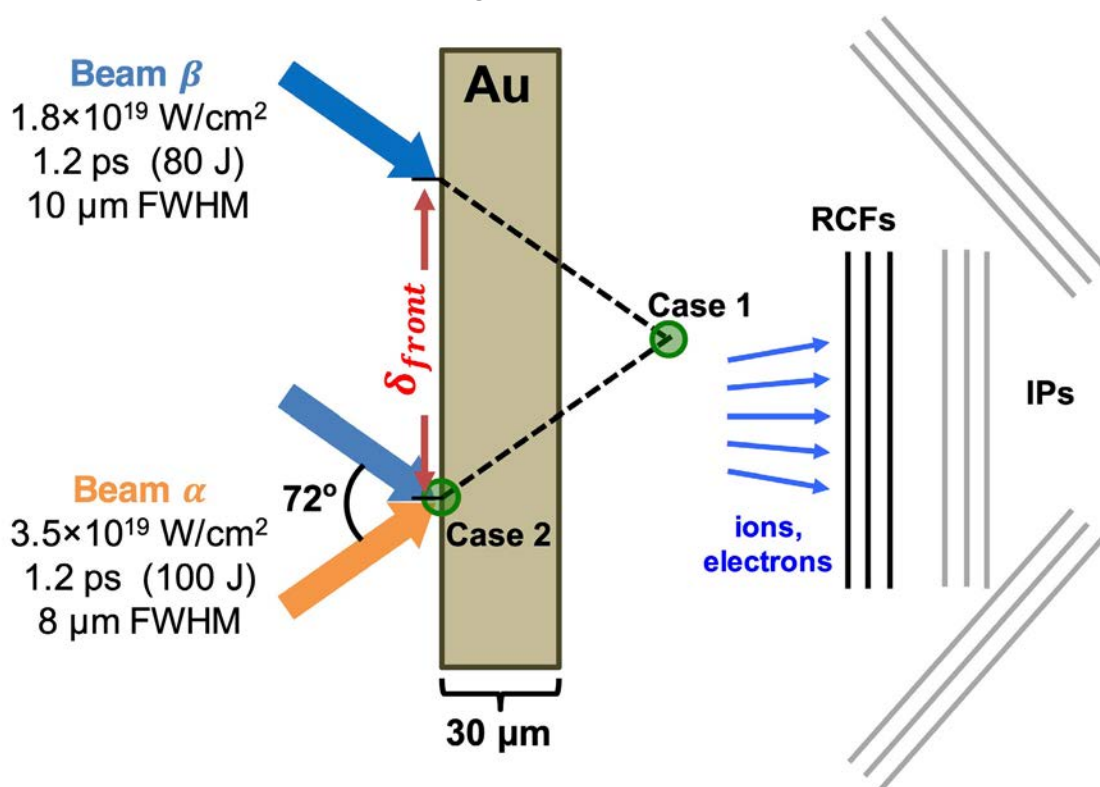


Representative proton spatial (top) and Thompson spectrometer data (bottom) for two different acceleration modes. The blue region on both scintillator images shows where the Thompson parabola's slit is located spatially. The red circles in a) show the 10° and 20° beam divergence boundaries, in b) the red circle shows the FWHM of the ion beam obtained by fitting Gaussians. Laser energies were 5 J for both shots, the pre-pulse was 5 mJ in a) and 40 mJ in b).

Authors: G. Casati , N.P. Dover, O.C. Ettlinger, C.A.J. Palmer, I. Pogorelsky, M. Polyanskiy, N. Xu, W. Li, M. Babzien, Z. Najmudin


Optimizing laser coupling, matter heating, and particle acceleration from solids using multiplexed ultra-intense lasers

This paper uses laboratory experiments and detailed numerical simulations to investigate how to optimise the coupling of multi-petawatt (PW) class lasers onto solid targets. We show, in brief, that stacking beams side-by-side to irradiate a target in a mirror-like configuration gives rise to an enhanced absorption and injection of fast electrons in the target. This is due to magnetic reconnection taking place between the magnetic fields induced by each laser, which thus generates an electric field that boosts the generation of electrons. Further, we show that this induces a virtuous cascade, because the enhanced electron injection can benefit from self-induced enhanced transport through the target. Thus, we show that physics can be advantageously exploited to improve particle acceleration compared to the mere addition of several lasers onto a target.



Schematic of the experiment, using two intense laser beams irradiating a solid gold target with opposite incidence angles and a variable separation distance between the laser spots on the target front surface. In all cases, the focus of the laser beams coincides with the target surface. The outgoing hot electrons are diagnosed by image plate (IP) stacks, located along each laser beam axis, as well as in the target normal direction. The accelerated ions are characterized by a radiochromic film (RCF) stack located in the target normal direction.

Further details can be found in W. Yao et al., Matter Radiat. Extremes 9, 047202 (2024). doi: 10.1063/5.0184919

Authors: W. Yao , M. Nakatsutsumi, S. Buffechoux, P. Antici, M. Borghesi, A. Ciardi, S. Chen, E. d'Humières, L. Gremillet, R. Heathcote, V. Horný, P. McKenna, M. Quinn, L. Romagnani, R. Royle, G. Sarri, Y. Sentoku, H.-P. Schlenvoigt, T. Toncian, O. Tresca, L. Vassura, O. Willi, J. Fuchs

Laser Science and Development

Improved stability second harmonic conversion of a diode-pumped Yb:YAG laser at the 0.5 kW level

We report on the efficient and stable, type-I phase-matched second harmonic conversion of a nanosecond high-energy, diode-pumped, Yb:YAG laser. With a frequency-doubling crystal in an enclosed temperature controller with optical windows, 0.5% energy stability was achieved for approximately half an hour. This resulted in 48.9 J pulses at 10 Hz (489 W) and a conversion efficiency of 73.8%. These results are particularly important for stable and reliable operation of high-energy, frequency-doubled lasers.

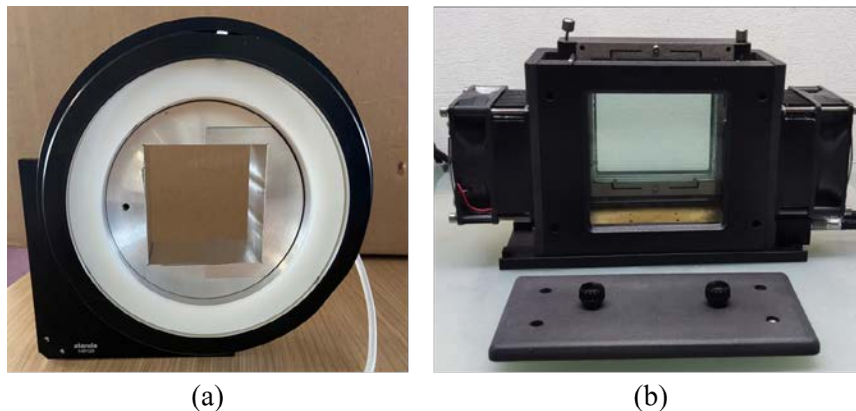


Figure 1: LBO crystal temperature-controllers (a) TC1 and (b) TC2, enclosed with optical windows (Applied Mezo Systems).

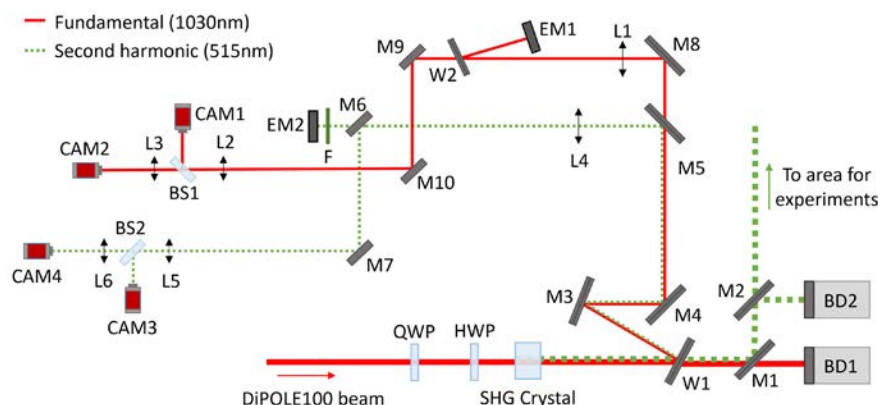



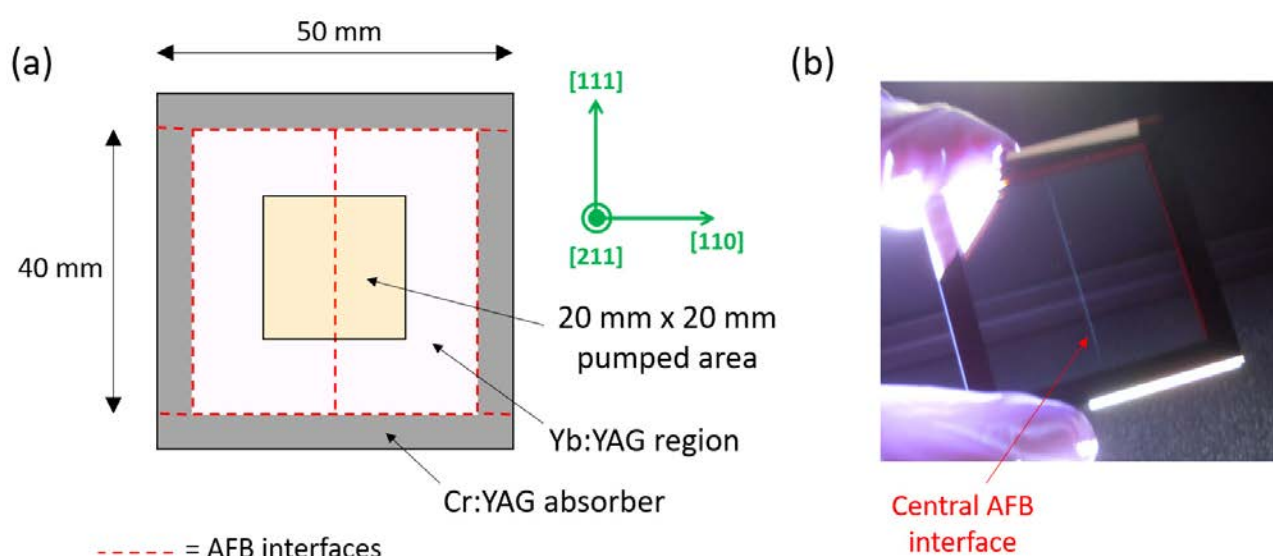
Figure 2: Schematic of the SHG experimental setup.

Reproduced from D.L. Clarke et al., "Improved stability second harmonic conversion of a diode-pumped Yb:YAG laser at the 0.5 kW level," Opt. Lett. 48, 6320-6323 (2023), published by Optica Publishing Group under the terms of the **CC-BY-4.0 license**. doi: 10.1364/OL.497181

Authors: D.L. Clarke , P.J. Phillips, M. Divoky, J. Pilar, P. Navratil, M. Hanus, P. Severova, O. Denk, T. Paliesek, M. Smrz, P.D. Mason, T.J. Butcher, C.B. Edwards, J.L. Collier, T. Mocek

High energy, high pulse rate laser operation using crystalline adhesive-free bonded Yb:YAG slabs

We report on the successful amplification of 10 ns pulses to 10 J energy at 10 Hz in a DiPOLE laser amplifier using crystalline Yb:YAG/Cr:YAG composite slabs manufactured using adhesive-free bonding (AFB) technology. We demonstrate that bonded slabs are suitable for operation in high energy cryogenic laser amplifiers. We also report on frequency doubling of the beam amplified in the bonded slabs. When the pulse energy of the output infrared beam is set to 5 J, a pulse energy of 3.9 J is achieved in the green (corresponding to 78% conversion efficiency). Results demonstrate that AFB technology is suitable for producing large-sized gain material slabs and can overcome current limitations in the manufacture of large-aperture gain material pieces. We believe this work will facilitate energy scaling of high energy lasers where aperture scaling of optical elements is not achievable via conventional manufacturing techniques.



(a) Drawing showing composite slab geometry, position of AFB interfaces (red dotted lines) and area exposed to laser irradiation (yellow area). The green arrows indicate the crystal orientation.

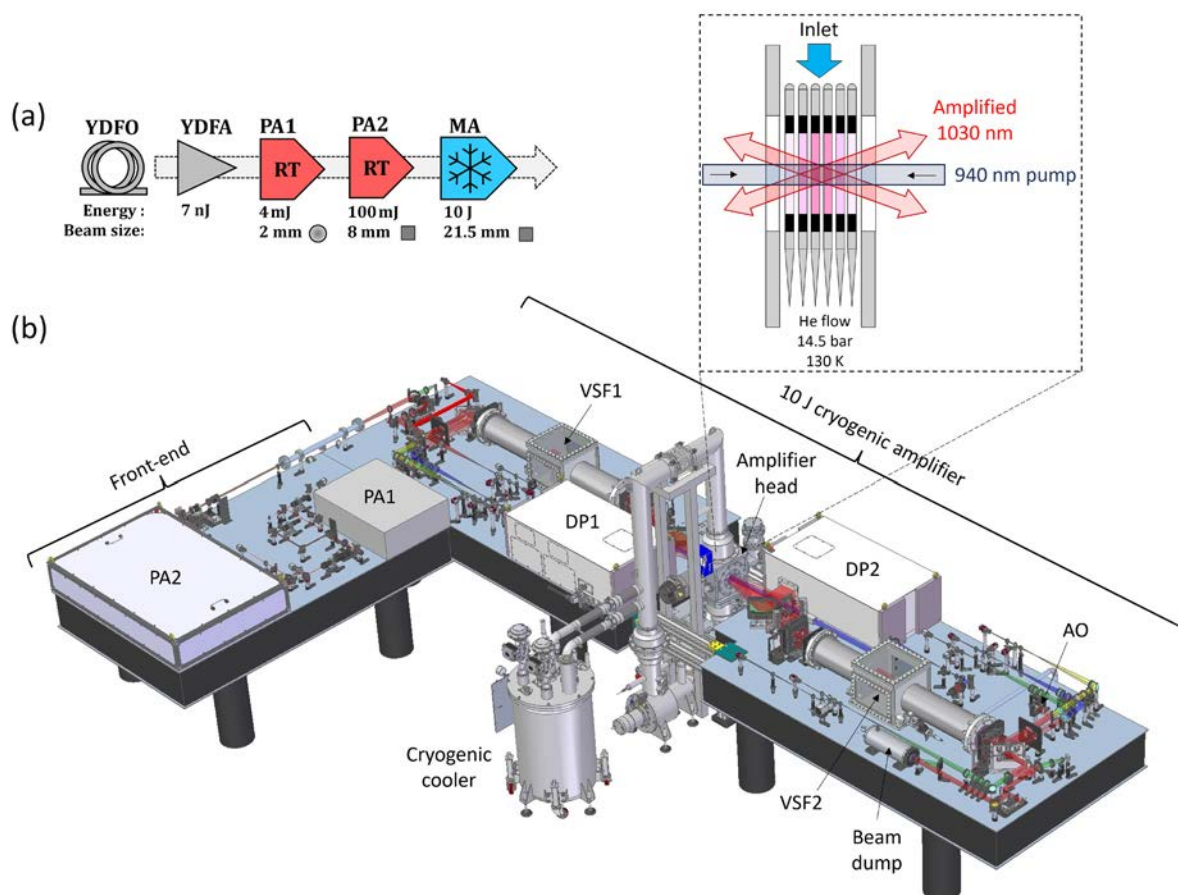
(b) Photo of one of the bonded slabs under bright white light illumination. The bonding interface is visible at the centre of the slab.

Reproduced from M. De Vido et al., "High energy, high pulse rate laser operation using crystalline adhesive-free bonded Yb:YAG slabs," Opt. Express 31, 28101-28111 (2023), published by Optica Publishing Group under the terms of the **CC-BY-4.0 license**. doi: 10.1364/OE.497948

Authors: M. De Vido ✉, P.J. Phillips, D. Meissner, S. Meissner, G. Quinn, S. Banerjee, M. Divoky, P.D. Mason

Demonstration of stable, long-term operation of a nanosecond pulsed DPSSL at 10 J, 100 Hz

We report on the stable, long-term operation of a diode-pumped solid-state laser (DPSSL) amplifying 15 ns pulses at 1029.5 nm wavelength to 10 J energy at 100 Hz pulse rate, corresponding to 1 kW average power, with 25.4% optical-to-optical efficiency. The laser was operated at this level for over 45 minutes ($\sim 3 \times 10^5$ shots) in two separate runs with a rms energy stability of 1%. The laser was also operated at 7 J, 100 Hz for four hours (1.44×10^6 shots) with a rms long-term energy stability of 1% and no need for user intervention. To the best of our knowledge, this is the first time that long-term reliable amplification of a kW-class high energy nanosecond pulsed DPSSL at 100 Hz has been demonstrated.



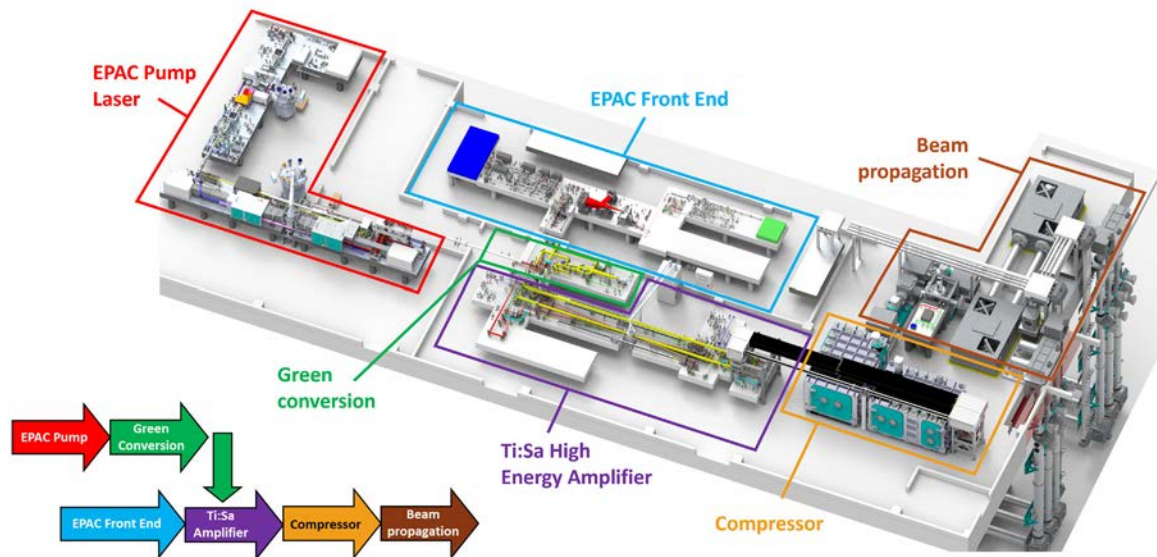
(a) Schematic of the DiPOLE-100Hz laser chain showing typical output performance after each stage: YDFO / YDFA = Yb-silica fiber oscillator / amplifier; PA = room-temperature pre-amplifier (1 = Yb:YAG regenerative, 2 = Yb:YAG multi-pass); MA = main cryogenic amplifier (Yb:YAG multi-slab). (b) 3D rendering of the DiPOLE 100 Hz system: DP = diode pump; VSF = vacuum spatial filter; AO = adaptive optic mirror. Inset: Schematic of main cryogenic amplifier head, showing pump and extraction geometry.

Reproduced from M. De Vido et al., "Demonstration of stable, long-term operation of a nanosecond pulsed DPSSL at 10 J, 100 Hz," Opt. Express 32, 11907-11915 (2024), published by Optica Publishing Group under the terms of the **CC-BY-4.0 license**. doi: 10.1364/OE.521049

Authors: M. De Vido ✉, G. Quinn, D.L. Clarke, L. McHugh, P.D. Mason, J.L. Spear, J.M. Smith, M. Divoky, J. Pilar, O. Denk, T.J. Butcher, C.B. Edwards, T. Mocek, J.L. Collier

Progress on Laser Development at the Extreme Photonics Applications Centre

The Extreme Photonics Applications Centre (EPAC) is a new state-of-the-art laser facility being built at the Central Laser Facility (CLF) to study applications of laser-driven sources in industry, medicine, and security. The first laser system to be built in the facility is a petawatt laser delivering 30 J, 30 fs pulses at 10 Hz pulse rate that will be used to drive plasma accelerators. This petawatt laser will be housed on the second floor of a new dedicated building that was completed in April 2022.



Layout and schematic of the EPAC 30 J, 30 fs, 10 Hz petawatt laser.

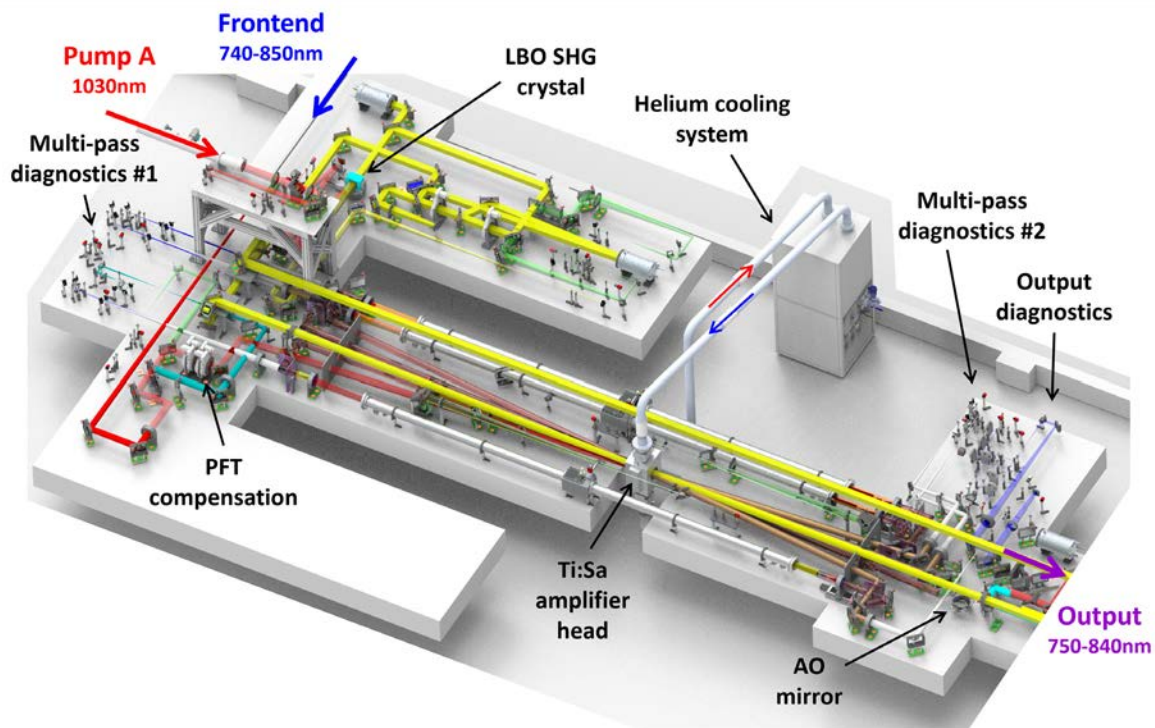
Presented at Conference on Lasers and Electro-Optics/Europe (CLEO/Europe 2023) and European Quantum Electronics Conference (EQEC 2023), Technical Digest Series (Optica Publishing Group, 2023), paper ca_8_2.

https://opg.optica.org/abstract.cfm?URI=CLEO_Europe-2023-ca_8_2

Authors: P.D. Mason ✉, N.H. Stuart, P.J. Phillips, R. Heathcote, S. Buck, A. Wojtusiak, M. Galimberti, T. de Faria Pinto, S. Hawkes, S. Tomlinson, R. Pattathil, T.J. Butcher, C. Hernandez-Gomez, J.L. Collier


Design of a High Energy Ti:Sapphire Amplifier for the Extreme Photonics Applications Centre

This paper presents details of a high energy Ti:Sapphire amplifier, capable of delivering up to 50 J broadband pulses at 10 Hz for a state-of-the-art petawatt laser-driver at the Extreme Photonics Applications Centre (EPAC).



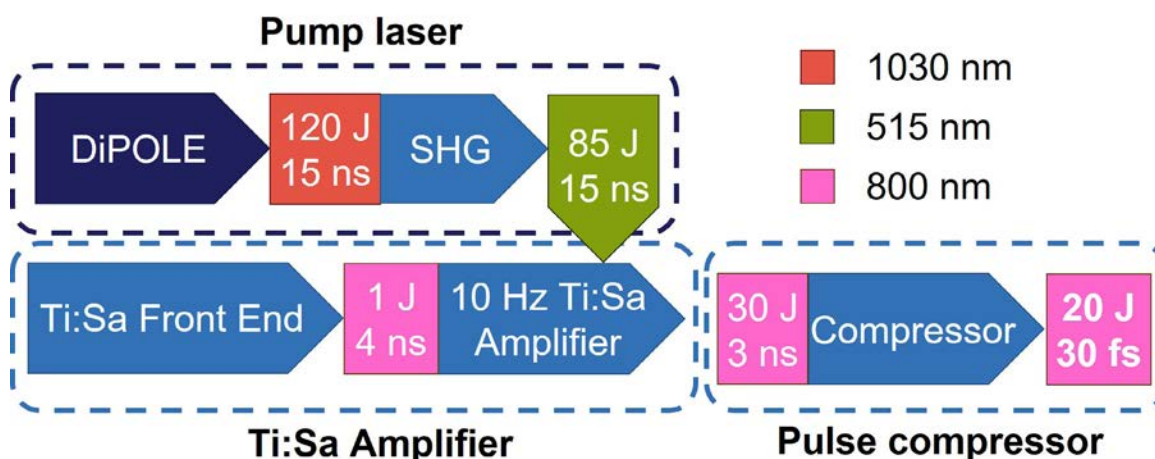
Layout of EPAC high energy Ti:Sa amplifier, highlighting key system components.

Presented at the 12th Advanced Lasers and Photon Sources Conference (ALPS2023), Japan, 18 - 21 April 2023

Authors: P.D. Mason , R. Heathcote, P.J. Phillips, T. de Faria Pinto, O. Chekhlov, Y. Tang, H. Schmitz, M. Harman, A. Wojtusiak, S. Hawkes, S. Tomlinson, T.J. Butcher, C. Hernandez-Gomes, J.L. Collier

Modelling the energetics of a potential new-look 10 Hz, 100 J class DiPOLE amplifier

This paper describes an investigation to identify possible modifications of the existing 100 J DiPOLE amplifier design, looking ahead to future systems with a particular focus on the second EPAC Pump Laser that will be used to pump a high energy Ti:Sa amplifier. Standard amplifier design rules are reviewed, and a 1D energetics model is used in tandem with previous experimental results to investigate the impact of relaxing previous design constraints.



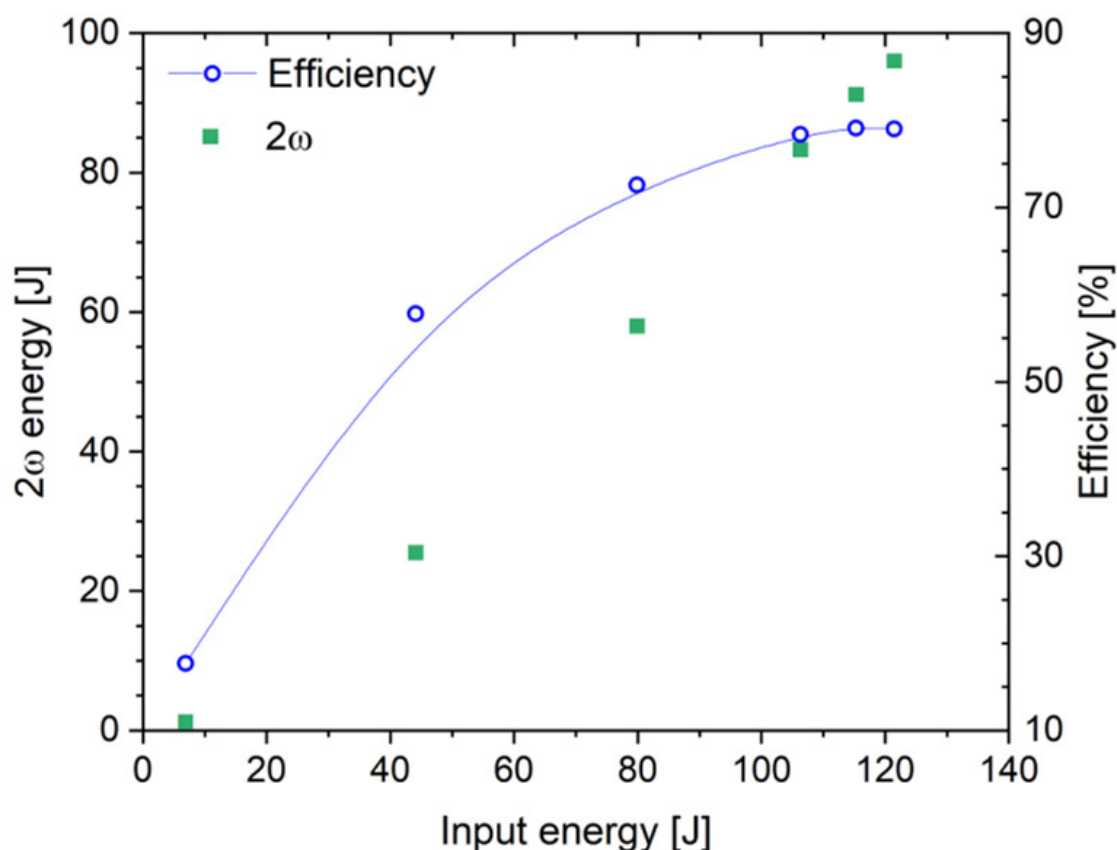
A simplified version of the 10 Hz Petawatt laser currently under construction in EPAC. A second DiPOLE100 system will be added in parallel to nearly double the available green pump energy and enable petawatt (30 J, 30 fs) operation.

Presented at Laser Congress 2023 (ASSL, LAC), Technical Digest Series (Optica Publishing Group, 2023), paper JM4A.5. doi: 10.1364/ASSL.2023.JM4A.5

Authors: L. McHugh , P.D. Mason, P.J. Phillips, T.J. Butcher, C. Hernandez-Gomez

Kilowatt-class high-energy frequency conversion to 95 J at 10 Hz at 515 nm

We report on frequency doubling of high-energy, high repetition rate nanosecond pulses from a cryogenically gas cooled multi-slab ytterbium-doped yttrium aluminium garnet laser system, Bivoj/DiPOLE, using a type-I phase matched lithium triborate crystal. We achieved conversion to 515 nm with energy of 95 J at repetition rate of 10 Hz and conversion efficiency of 79%. High conversion efficiency was achieved due to successful depolarization compensation of the fundamental input beam.



Dependence of the second harmonic frequency output energy and conversion efficiency on the input energy during the energy ramp at the beginning of the experiment.

Reproduced from M. Divoky et al. (2023) 'Kilowatt-class high-energy frequency conversion to 95 J at 10 Hz at 515 nm', High Power Laser Science and Engineering, 11, p. e65, published by Cambridge University Press in association with Chinese Laser Press under the terms of the **CC-BY-4.0 license**. doi:10.1017/hpl.2023.60.

Authors: M. Divoky, P.J. Phillips, J. Pilar, M. Hanus, P. Navratil, O. Denk, T. Paliesek, P. Severova, **D. Clarke** ✉, M. Smrz, T.J. Butcher, C.B. Edwards, J.L. Collier, T. Mocek

Pathway for experiments for a DiPOLE D100-X 100 J amplifier synchronised to the European XFEL

A 100 J DiPOLE amplifier, with the capability to have arbitrary pulse shaping, has been successful installed at the European XFEL in Hamburg for High Energy Density Physics.

We have demonstrated 70 J at 1 Hz, which has been delivered to the target chamber for an experiment using frequency doubled energy at 60% efficiency. During the experimental period, the system was run for 24 hours over a period of seven days.

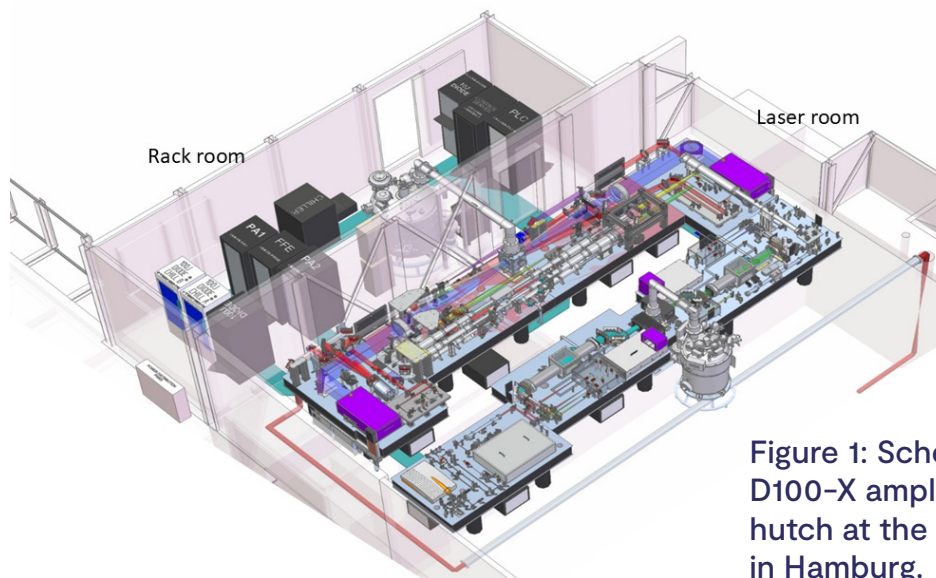


Figure 1: Schematic of the D100-X amplifier in the laser hutch at the European XFEL in Hamburg.

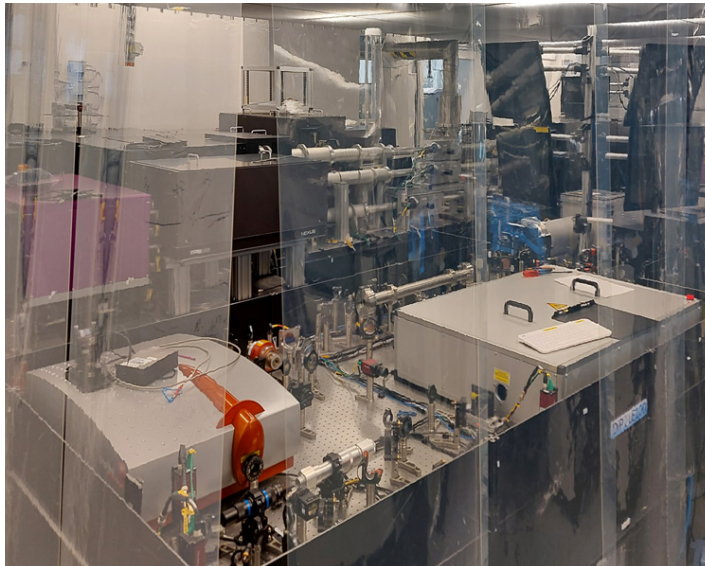


Figure 2: Image of the system installed in the Laser Hutch at the European XFEL.

Presented at Photonics West 2024: P.J. Phillips et al., "Pathway for experiments for a DiPOLE D100-X 100 J Amplifier synchronized to the European XFEL," Proc. SPIE PC12864, Solid State Lasers XXXIII: Technology and Devices, PC128640C (13 March 2024). doi: 10.1117/12.3005649.

Authors: P.J. Phillips, P.D. Mason, **J.L. Spear** ✉, J. Smith, S. Banerjee, A. Shepperd, T.J. Butcher, C.B. Edwards, R. Harding, E. Brambrink, T. Zata, S.D. Cafiso, M. Toncian, M. Masruri, H. Hoepfner, K. Knoefel, J-P. Shwinkendorf, T. Toncian, T. Cowan, C. Hernandez-Gomez, J.L. Collier

Overview of optical characterisation capabilities for assessing suitability of optics for high-energy, high repetition rate lasers

We present an overview of the optical characterisation capabilities available at the Central Laser Facility and describe how they are used to assess the suitability of optics and coatings for high-energy, high repetition rate laser.

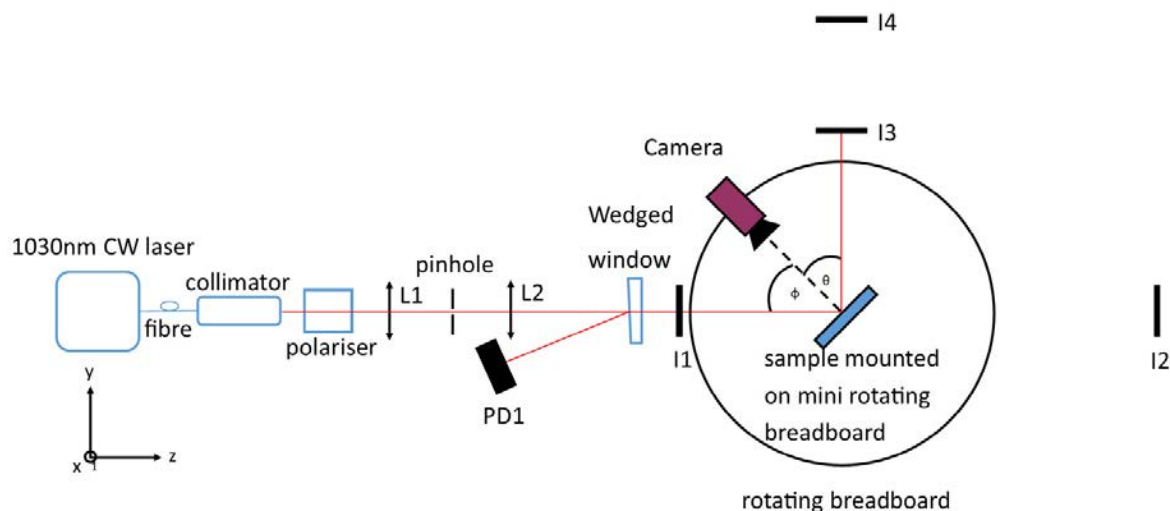


Figure 1: Layout of the setup used for measuring the transmittance and reflection of optical coatings over a range of angles.

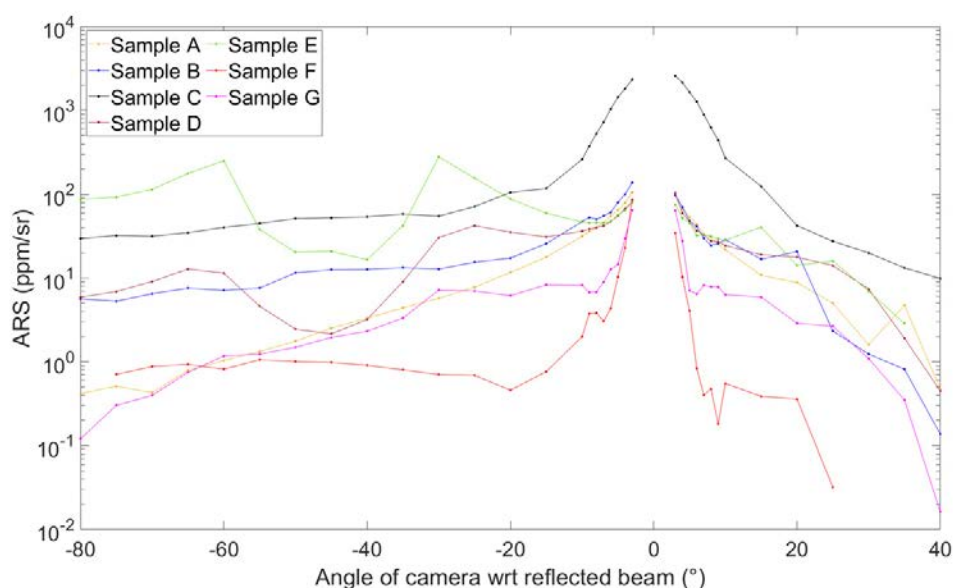


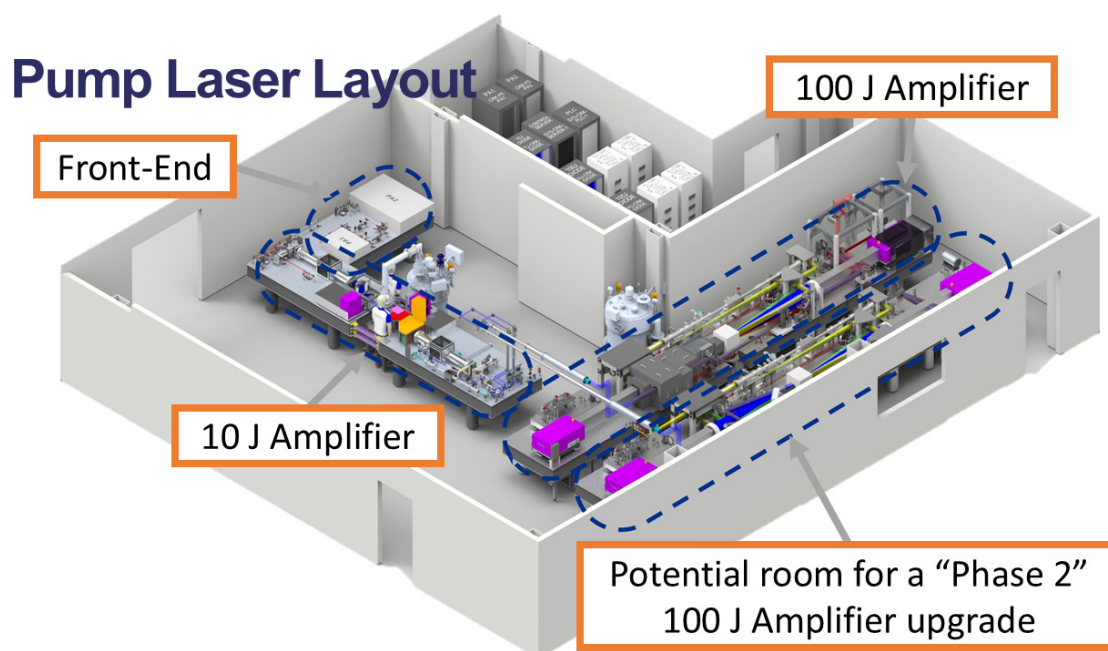
Figure 2: Experimental results of the angle-resolved scatter (ARS) from a number of HR mirror samples from different suppliers, with reflection optimised for 45°.

Presented at Laser Congress 2023 (ASSL, LAC), Technical Digest Series (Optica Publishing Group, 2023), paper JM4A.3. doi: 10.1364/ASSL.2023.JM4A.3.

Authors: G. Quinn , D.L. Clarke, M. De Vido

Pump laser for the EPAC petawatt amplifier

The Extreme Photonics Applications Centre (EPAC) is a world-class research facility currently under development at the STFC Rutherford Appleton Laboratory in the United Kingdom. It will house a titanium-doped sapphire (Ti:Sa) amplifier, which will be capable of delivering petawatt-level pulses at an unprecedented repetition rate of 10 Hz. Such combination of high peak power and repetition rate will be achieved by pumping the Ti:Sa amplifier with a Diode-Pumped Solid State Laser (DPSSL) based on the Central Laser Facility's DiPOLE technology.



Schematic of the EPAC pump amplifier.

Presented at Photonics West 2024: A. Wojtusiak et al., "Pump laser for the EPAC petawatt amplifier," Proc. SPIE PC12864, Solid State Lasers XXXIII: Technology and Devices, PC128640D (13 March 2024). doi: 10.1117/12.3005639

Authors: A. Wojtusiak ✉, P.J. Phillips, J. Smith, P.D. Mason, M. De Vido, T.J. Butcher, C. Hernandez-Gomez, J.L. Collier

Design of an electron energy spectrometer and energy selector for laser-plasma driven beams at EPAC

The Extreme Photonics Applications Centre (EPAC) is a new national facility currently under construction at the Rutherford Appleton Laboratory, UK. EPAC is designed to enable a wide variety of user experiments with a state-of-the-art petawatt-class laser system. It is anticipated that early experiments will include laser-plasma acceleration of electrons to energies ranging from 100 MeV to 5 GeV or higher, with later experiments using these electrons as a beam once stable generation is achieved. EPAC is designed to be flexible, allowing users to select the relevant central electron energy for their experiment. To achieve this goal, EPAC and the Accelerator Science and Technology Centre (ASTeC) at STFC Daresbury Laboratory have developed a beamline design to capture laser-plasma driven electrons with broad energy spread, measure their energy spectrum, perform selection of specific energies if necessary, and deliver these electrons to a user interaction point. We present here the conceptual design of the proposed spectrometer and energy selection system.

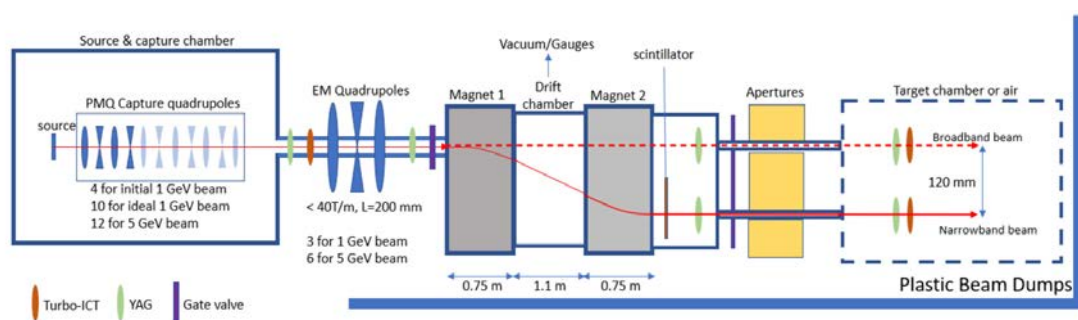


Figure 1: Overview of the basic layout of the proposed energy spectrometer chicane and energy selector, showing the spectrometer concept, energy selection, and proposed surrounding components. (Dimensions not to scale.)

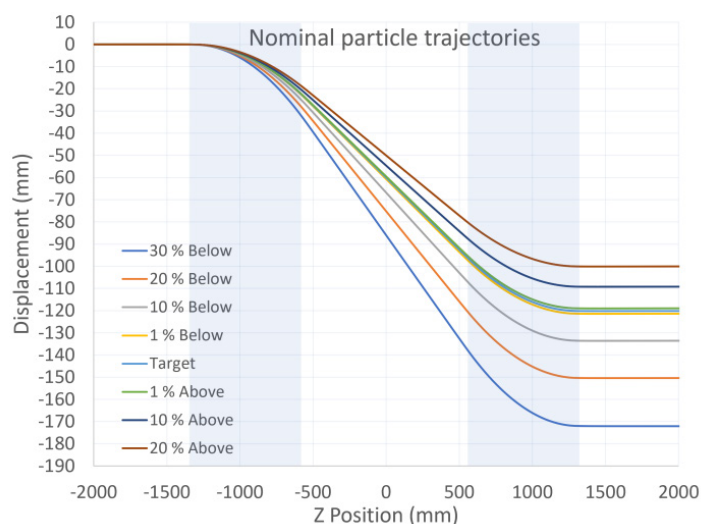


Figure 2: Simulated electron trajectories through the dipoles (shaded) showing the relation between electrons of the target energy and electrons of certain percentages above and below the target, assuming the field is chosen such that the central energy is displaced by 120 mm.

Reproduced from A.R. Bainbridge et al. Design of an electron energy spectrometer and energy selector for laser-plasma driven beams at EPAC, in Proc. 14th Int. Particle Accelerator Conf. (IPAC'23), paper THPL063, pp 4568-4571, under the terms of the **CC-BY-4.0 license**. doi: 10.18429/JACoW-IPAC2023-THPL063

Authors: A.R. Bainbridge ✉, J. Crone, J.K. Jones, B.D. Muratori, H.L. Owen, T.H. Pacey, B.J.A. Shepherd, D. Angal-Kalinin, D.R. Symes, N. Bourgeois

The EPAC electron transport beamline—physics considerations and design

The Extreme Photonics Applications Centre (EPAC) is a planned UK national facility, intended to use a 1 PW, 1 Hz laser system to drive laser-plasma acceleration with output energies ranging from 100 MeV up to at least 5 GeV. A design is presented in this paper for the capture and transport of the initially very divergent plasma-source electrons. We propose a unique, modular beam capture optics based on a FODO channel of Halbach permanent-magnet quadrupoles, which flexibly allows different-energy electron bunches to be captured and conditioned for experimental use. We show an engineering concept for the beamline that incorporates diagnostics and drive laser removal, and describe the effect of field errors and misalignments and their mitigation.

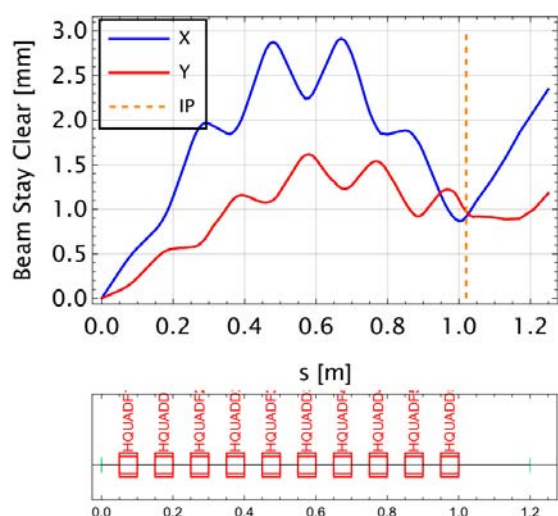


Figure 1: Beam stay clear as a function of distance in both planes for the 1 GeV permanent-magnet quadrupole (PMQ) array. IP position (orange) at ~ 1 m.

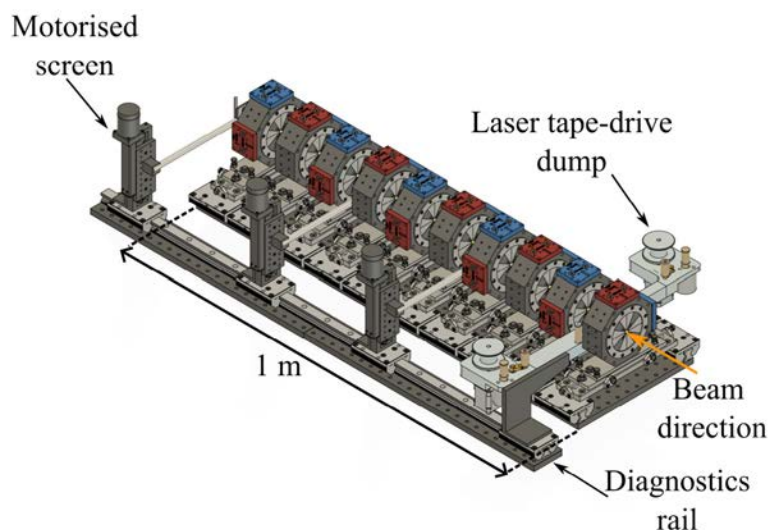


Figure 2: Engineering illustration of a 10 quadrupole capture array that may bring a 1 GeV electron bunch to a focus within around 1 m distance. Individual quadrupoles will be pre-aligned to around $50 \mu\text{m}$ relative accuracy (to the plasma source and to each other). One possible location for the tape drive beam dump is shown (between the first and second PMQs); also shown are the separately-mounted diagnostic screens and mounting mechanisms.

Reproduced from B.D. Muratori et al. The EPAC electron transport beamline – physics considerations and design, in Proc. 14th Int. Particle Accelerator Conf. (IPAC'23), paper TUPA105, pp 1553-1556, under the terms of the **CC-BY-4.0 license**. doi: 10.18429/JACoW-IPAC2023-TUPA105

Authors: B.D. Muratori ✉, A.R. Bainbridge, J. Crone, J.K. Jones, H.L. Owen, T.H. Pacey, D.R. Symes, N. Bourgeois

Upgrade to the Astra amplifier 3 optical pumping scheme

This report details an upgrade to the Gemini Astra amplifier 3 optical pumping scheme, which resulted in a doubling of the available pump energy from 3.5 J to 7 J and a smoother pump beam profile. This will be followed in the future by the installation of a larger-aperture Ti:Sa crystal, which will allow Astra amplifier 3 to double its output from 1 J to 2 J at 10 Hz.

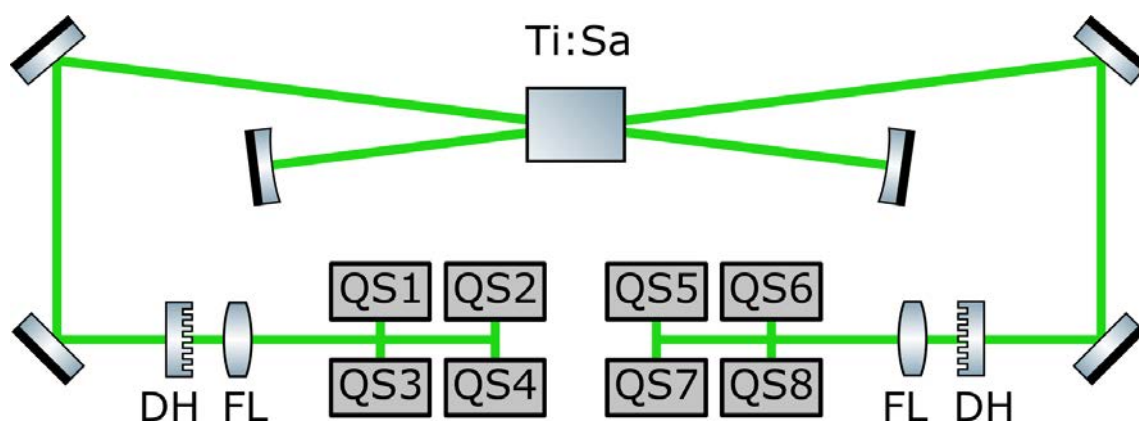


Figure 1: Astra amplifier 3 optical pumping layout. DH: diffractive homogeniser; FL: field lens.

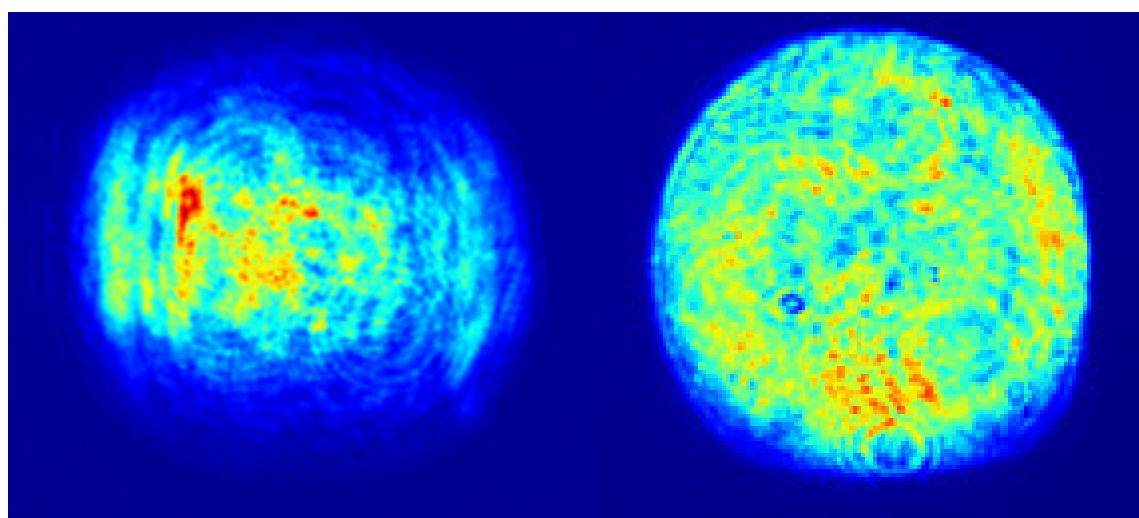


Figure 2: Left: Typical TA2 input near-field when pumped with Spectra Physics Quanta-Ray lasers. Right: Typical TA2 near-field when pumped with Lumibird Q-Smart HE 1500 lasers. Pulse energy of 1 J in both cases.

Neutral gas interferometry in Gemini TA1

An important step to achieving stable, controlled laser wakefield acceleration is thorough design and characterisation of the gas targetry used. This is the remit of the EPAC gas target development programme, which includes fluid simulation, manufacturing and experimental testing of targets. An interferometry rig has been established in Gemini TA1 for experimental measurement of neutral gas density profiles generated by targets. An overview of the setup and the developments made in the last year are presented here.

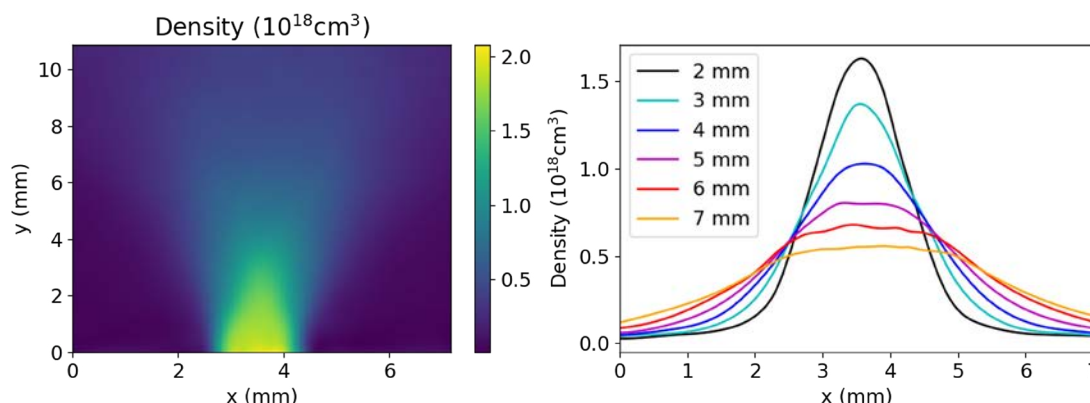


Figure 1: 2D density profile of the nozzle in the end-on geometry (left) and line outs at a number of heights above the nozzle (right).

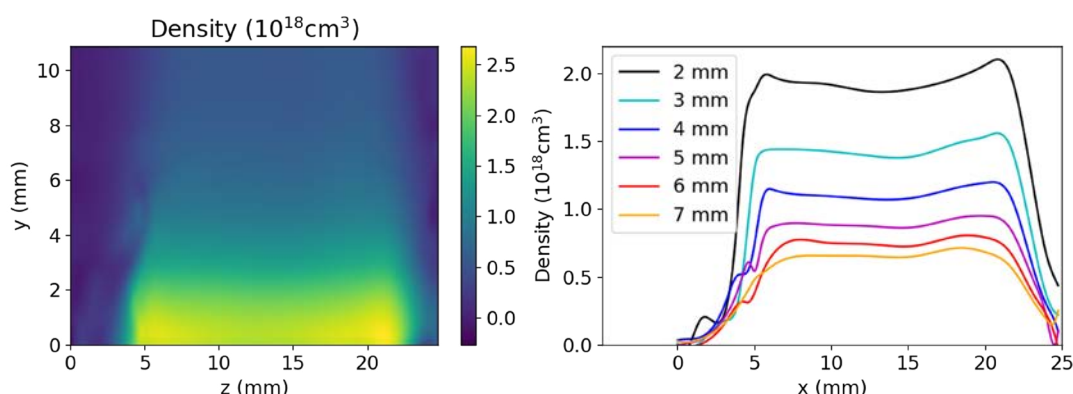


Figure 2: 2D density profile of the nozzle in the side-on geometry (left) and line outs at a number of heights above the nozzle (right).

Development of an optical probe for a laser wakefield accelerator in Gemini Target Area 2

A high repetition rate laser-wakefield accelerator will be established in Gemini TA2. This will allow for testing of optimisation, automation and stabilisation techniques that will be implemented at the Extreme Photonics Applications Centre (EPAC). This report details the commissioning of the optical probe that will allow us to monitor the plasma formed during accelerator operation.

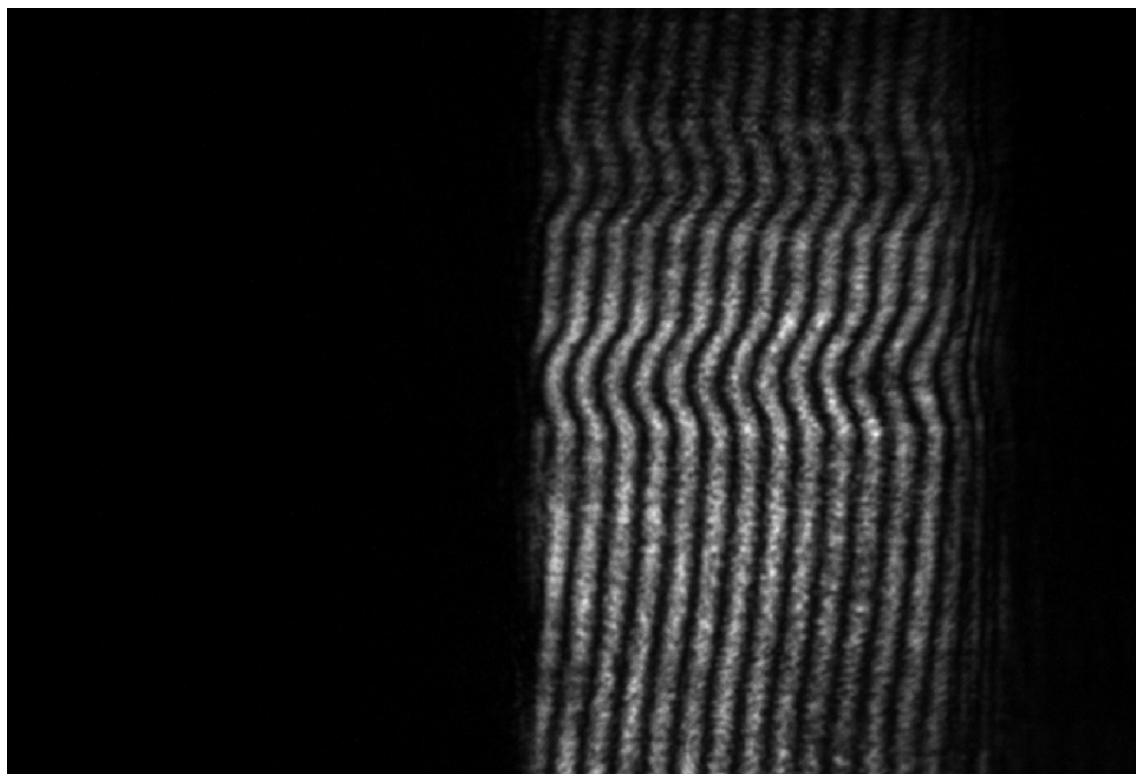


Figure 1: An interferometry image captured by the probe diagnostics showing a phase shift caused by the plasma during laser wakefield operation.

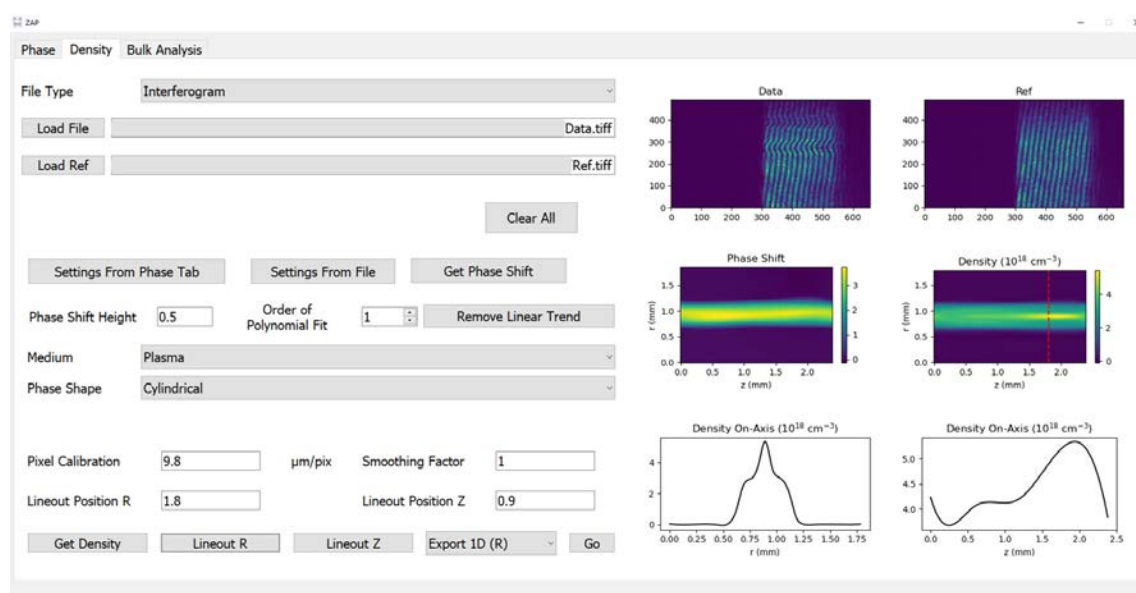


Figure 2: A screenshot of the phase and density retrieval software performing analysis on the data shown in Figure 1.

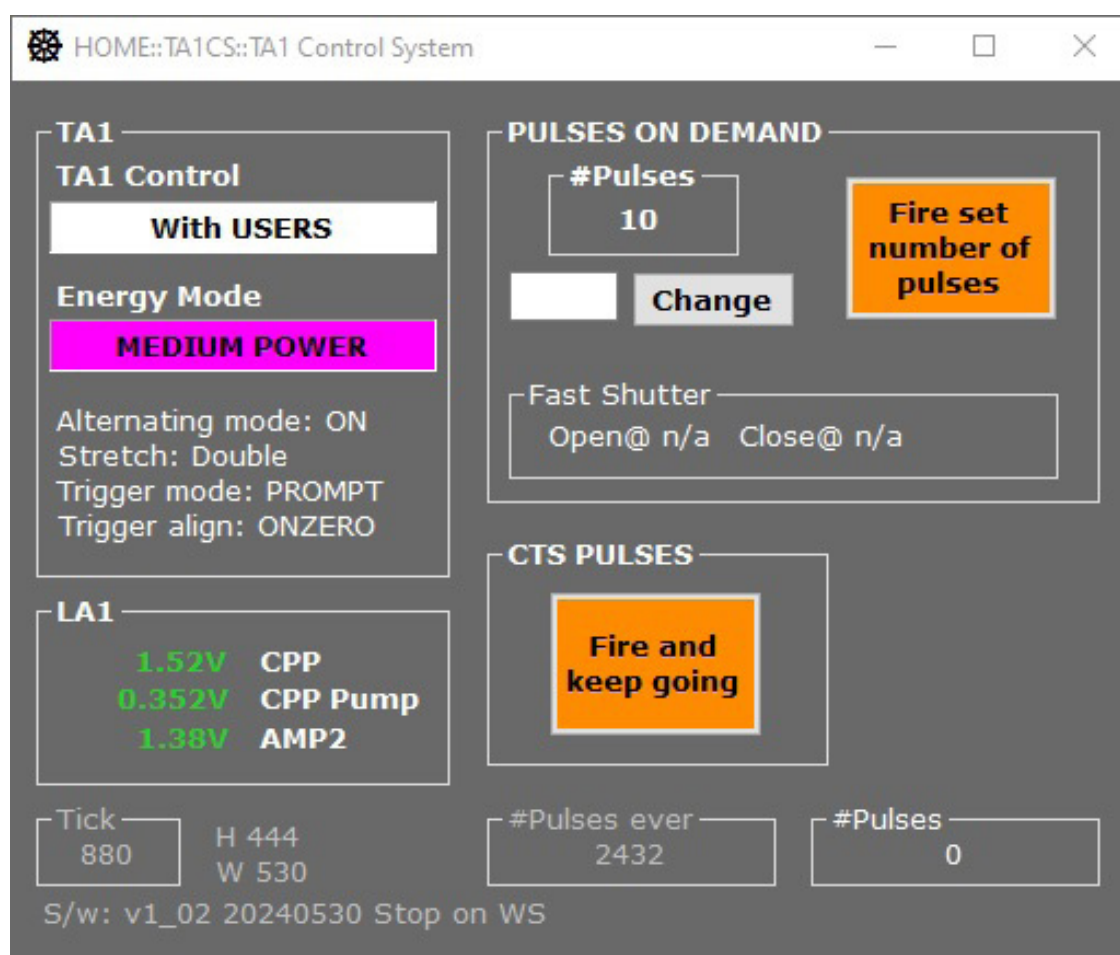
Authors: Z. Athawes-Phelps, T. Dzelzainis, K. Fedorov, O. Finlay ✉, D. Symes

Software developments in Gemini

Part of the commissioning process for the EPAC (Extreme Photonics Applications Centre) laser facility requires the development and testing of new laser diagnostics and characterisation of various optics to test their resilience to laser-induced damage. It is desirable to be able to do this with a laser operating at a repetition rate close to that of EPAC and as independently as possible from the rest of the facility so that long testing runs do not interfere with on-going experiments and other development work.

The original Astra laser Target Area, next to what is now Gemini TA2, was ideally suited for this purpose and so was brought back into service as TA1 (Target Area 1).

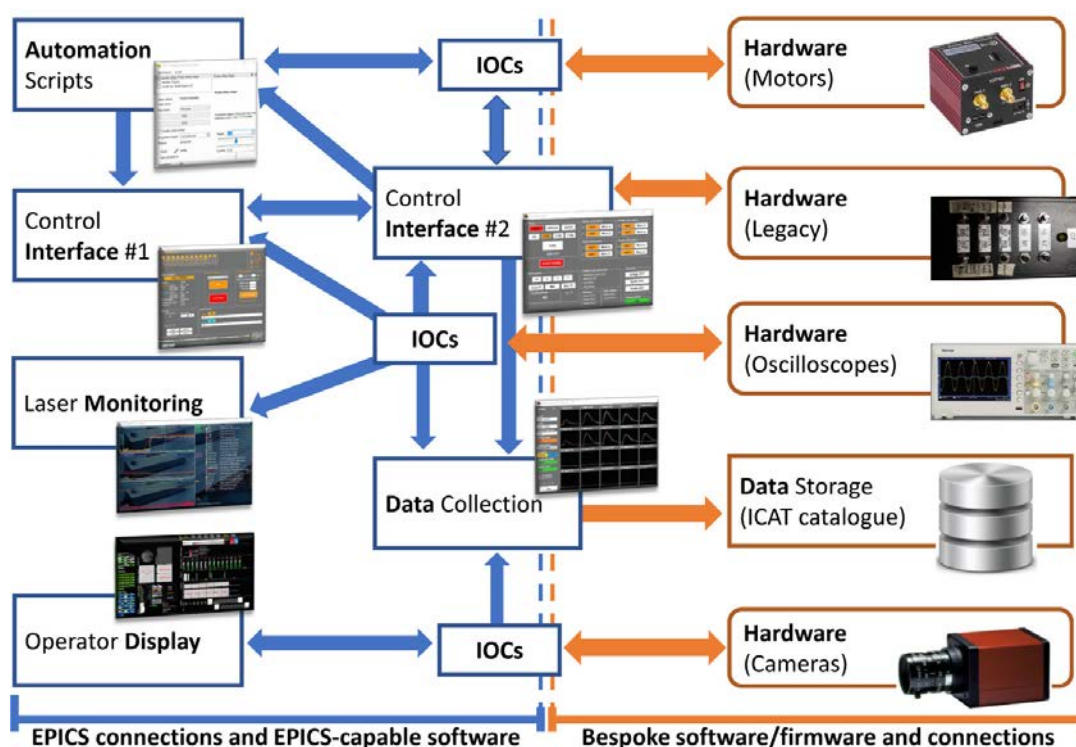
Various adjustments were made to the fabric of the room, including reopening the wall shutter between TA1 and the laser area, re-routing part of the beam through it, installing cabling for the laser network and updating the safety interlock system. A new TA1 Control System was also developed (see figure) and integrated with the existing main Gemini Control System.



Screenshot of TA1 control system.

Control systems and data management for high-power laser facilities

The next generation of high-power lasers enables repetition of experiments at orders of magnitude higher frequency than what was possible using the prior generation. Facilities requiring human intervention between laser repetitions need to adapt in order to keep pace with the new laser technology. A distributed networked control system can enable laboratory-wide automation and feedback control loops. These higher-repetition-rate experiments will create enormous quantities of data. A consistent approach to managing data can increase data accessibility, reduce repetitive data-software development and mitigate poorly organized metadata. An opportunity arises to share knowledge of improvements to control and data infrastructure currently being undertaken. We compare platforms and approaches to state-of-the-art control systems and data management at high-power laser facilities, and we illustrate these topics with case studies from our community.



Architecture of the Gemini Control System. EPICS input/output controllers (IOCs) are software + hardware layers providing an abstraction between low-level device hardware and high-level control system software. Legacy hardware is connected into the system through a legacy interface, Control Interface #2. A differentiation is made between EPICS-interfacing components and connections (in blue) and bespoke components and connections (in orange). Clients for device data include human control interfaces, informational laboratory displays, automation software and archival data collectors.

Reproduced from S. Feister et al. (2023) 'Control systems and data management for high-power laser facilities', High Power Laser Science and Engineering, 11, p. e56, published by Cambridge University Press in association with Chinese Laser Press under the terms of the **CC-BY-4.0 license**. doi: 10.1017/hpl.2023.49

Authors: S. Feister ✉, K. Cassou, S.J.D. Dann, A. Döpp, P. Gauron, A.J. Gonsalves, A. Joglekar, V. Marshall, O. Neveu, H.-P. Schlenvoigt, M.J.V. Streeter, **C.A.J. Palmer** ✉

Super-resolution radial fluctuations microscopy for optimal resolution and fidelity

Fluorescence fluctuations super-resolution microscopy (FF-SRM) has emerged as a promising method for fast, low-cost and uncomplicated imaging of biological specimens beyond the diffraction limit. Amongst the FF-SRM techniques, super-resolution radial fluctuations (SRRF) microscopy is a popular technique, but is prone to artefacts, resulting in low fidelity, especially under conditions of high-density fluorophores.

In this paper, we developed a novel combinatory computational super-resolution microscopy method, namely VeSRRF, that demonstrated superior performance in SRRF microscopy. VeSRRF combined intensity and gradient variance reweighted radial fluctuations (VRRF) and enhanced-SRRF (eSRRF) algorithms, leveraging the enhanced resolution achieved through intensity and gradient variance analysis in VRRF and the improved fidelity obtained from the radial gradient convergence transform in eSRRF. Our method was validated using microtubules in mammalian cells as a standard biological model system. Our results demonstrated that VeSRRF consistently achieved the highest resolution and exceptional fidelity compared to those obtained from other algorithms in FF-SRM.

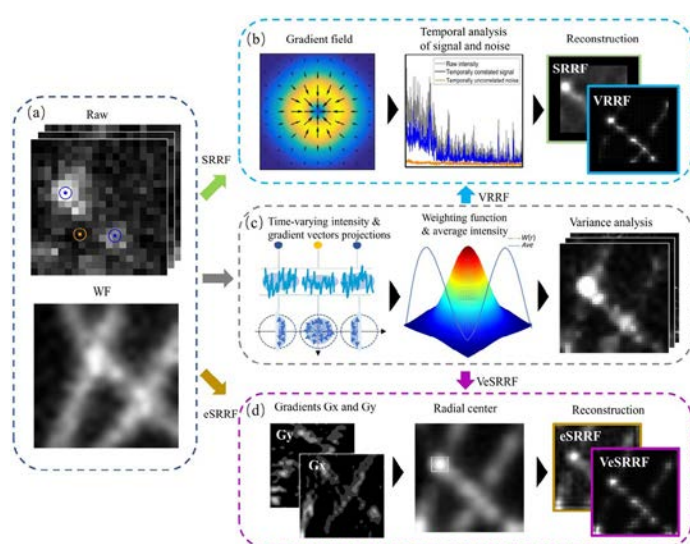


Figure 1: SRRF microscopy image reconstruction algorithm schematic. (a) Raw image sequence and wide-field image of microtubules. (b) SRRF reconstruction steps. (c) VRRF reconstruction steps. The reconstruction is then completed using the SRRF algorithm. (d) eSRRF reconstruction steps. The VeSRRF algorithm first processes the image sequence through VRRF, and then completes the image reconstruction using the eSRRF algorithm.

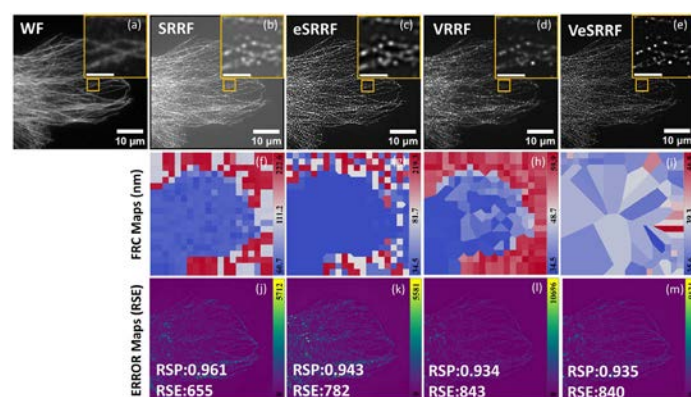


Figure 2: Comparison of the reconstructed images of Tubulin- AF488 in fixed COS7 cells. (a) Wide-field images. (b-e) Reconstructed images from the SRRF, eSRRF, VRRF, and VeSRRF algorithms. (f-i) Corresponding FRC maps. (j-m) Corresponding error maps. Scale bar in the enlarged image of the region indicated by the yellow border box: 2 μm .

Drift-free single molecule localization microscopy provides artefact-free super-resolution imaging

Single-molecule localization microscopy (SMLM) has the power to unravel intricate cellular structures and functions at the nanometre scale. However, the spatial resolution and image fidelity of SMLM may be hindered by the drift of samples during its long image acquisition. In this paper, we present SMLM based on innovative reinforced optical cage systems (ROCS) for proactively preventing sample drift. The ROCS features custom-designed optomechanical components and reinforced mechanical construction that uses tungsten steel rods to seamlessly connect and support optomechanical components holistically. We demonstrated that, owing to the implementation of ROCS, the sample drift was 29 nm over 30 minutes in SMLM, which has a negligible impact on the resolution. The ROCS offers a straightforward, inexpensive, open-source, and state-of-the-art solution that not only allows biomedical scientists to gain easy access to high-performance super-resolution microscopy, but also empowers the wider scientific community to achieve reliable precision instrumentation.

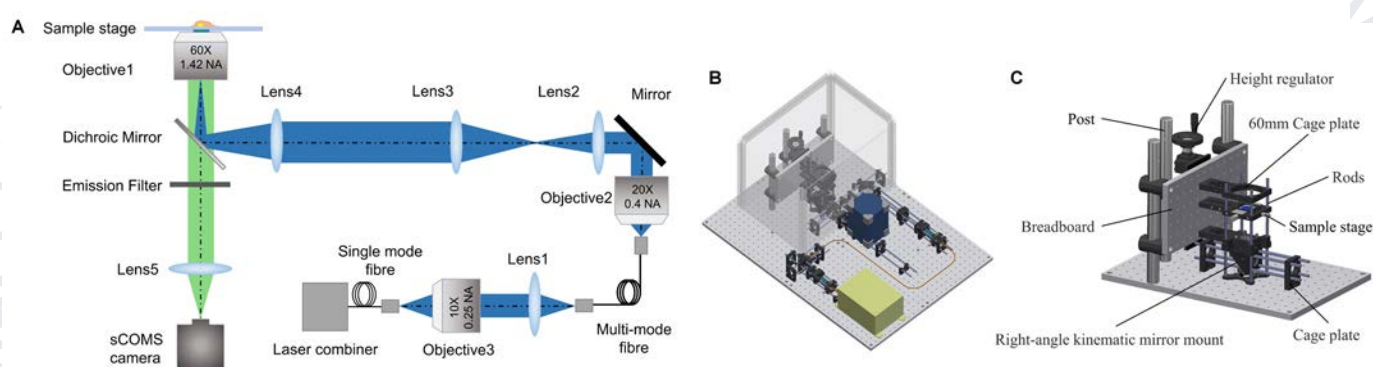
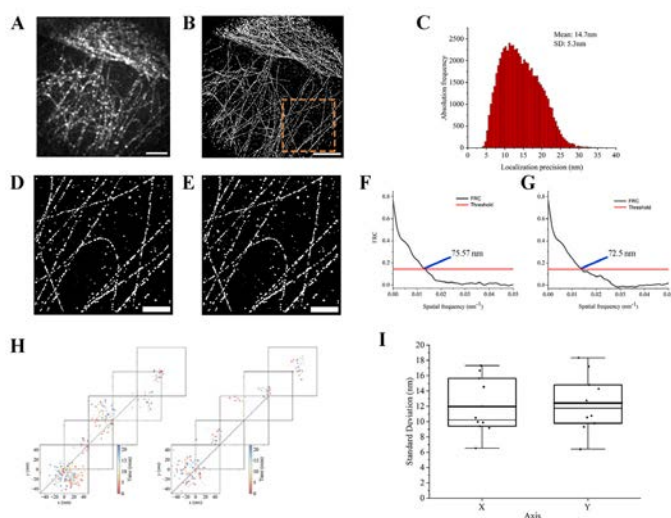


Figure 1 (above): (A) Schematic of the optical setup. (B) 3D CAD rendering of the microscope and (C) the sample stage sub-system.

Figure 2 (left): (A) Wide-field image of Alexa Fluor 647-labelled microtubules in COS-7 cells. (B) Super-resolution STORM image of the microtubules. Scale bar: 5 μm . (C) Localization precision histogram of the STORM image. (D) Enlarged image of the region enclosed by the orange box in (B). (E) Drift-corrected STORM image following cross-correlation drift correction of (D). Scale bar: 2 μm . (F) FRC curve of the region shown in (D); resolution 75.57 nm at a correlation threshold of 0.143. (G) FRC curve of the region shown in (E); resolution 72.5 nm at a correlation threshold of 0.143. (H) Scatterplots of the drift from 10 AF647 molecules in the STORM image sequence. (I) Box plot of the standard deviations of the drift of the AF647 molecules along the x- and y-axes.



Authors: H. Qiu, M.C. Tang, S.K. Roberts, L. Wang

Characterisation of tape-drive targets using X-Ray Fluorescence Spectroscopy

Tape-drive targets are commonly used in high-repetition rate experiments, as they provide a simple but robust method of delivering 2.5D laser targets to the interaction point of the laser, while remaining as close to the focal spot position as possible. This removes the time-costly need to refocus the laser on each shot. The demand for these targets is increasing to support the future demands of the Extreme Photonics Applications Centre (EPAC) facility, which will be operational by 2027, and it is critical to know the parameters of these targets, including any coatings that are applied.

We have investigated X-Ray Fluorescence Spectroscopy as a method to measure the coating thickness on the tapes, and the use of machine learning models to predict the thickness of the coating on the tape from the XRF data.



Figure 1: Hitachi FT110A XRF machine.

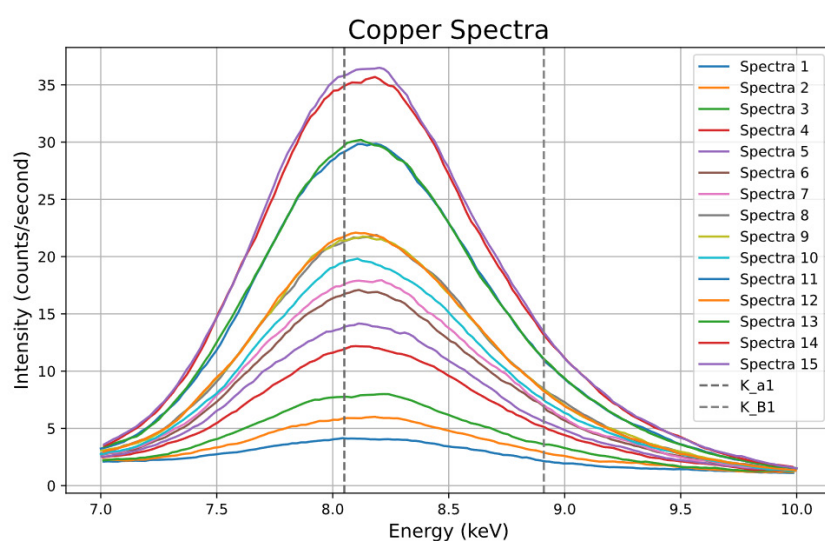




Figure 2: XRF spectra for copper samples.

Authors: J. Fields  , P. Ariyathilaka, S. Astbury, M. Tolley, C. Spindloe  , H. Edwards, R. Sarasola, G. Stenning, P. Hunyor

Development of experimental target platforms for Rayleigh-Taylor and jetting experiments at LLE

This report looks at the development of two examples of targets that Scitech Precision were tasked with delivering for high power laser experiments at The University of Rochester's Laboratory for Laser Energetics (LLE). LLE hosts the Omega laser facility and the Omega laser^[1] where the following targets were fielded over a period of two years. Working closely with the Target Fabrication group in the Central Laser Facility (CLF) and the target fabrication team at the University of Michigan, Scitech Precision were able to bring together expanded capabilities and technologies to fabricate ever increasing complex targets and to characterise them in the high detail required to benchmark them for the experimental campaigns.

^[1]lle.rochester.edu

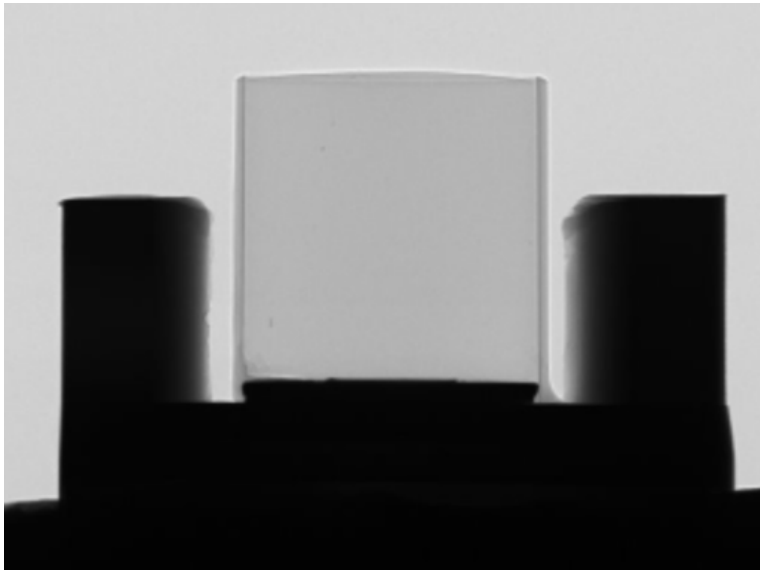


Figure 1: X-ray radiography showing the foam quality of a completed target.

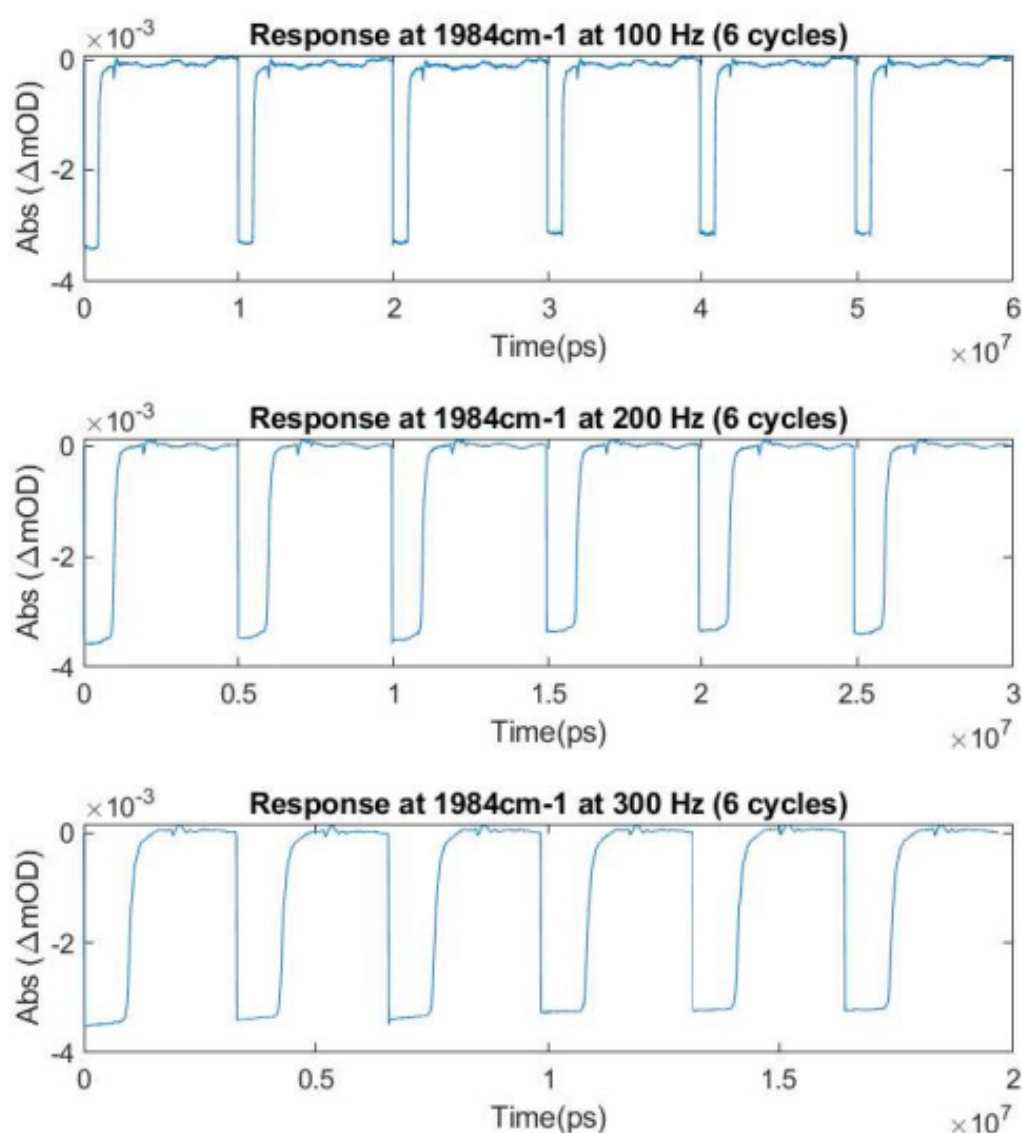


Figure 2: Optical image of the complete target

Authors: J. Robinson ✉, C. Spindloe, S. Klein, J. Schnell, S. Irving, D. Wyatt, C. Dobson, M. Harrs, P. Ariyathilaka, P.M. Nilson

A stop-flow sample delivery system for TRMPS experiments

Developing new sample delivery solutions, to keep up with the new technologies in time-resolved spectroscopy, is an essential part of enabling the spreading and ease of use of such technologies to the academic community. Since time-resolved spectroscopy averages many samples to improve the signal-to-noise in the data, there is a need for systems that can advance the sample in a controlled manner during analysis. We are presenting improvements on a stop-flow sample system, which uses custom designed electronics and microvalves attached to a microfluidic channel to move liquid samples in a step-like manner. This allows the synchronisation of the sample movement to a laser trigger, leading to a system that is easy to use and reliable.



Transient IR response at three valve opening frequencies, showing the signal dropping, in line with excitation by the pump pulse and creation of the water adduct, and staying at around -3mOD until the valves are open, where the signal recovers to zero, showing the full replacement of the sample. This behaviour is seen to be consistent across different frequencies.

Authors: S. Dragomir ✉, P. Malakar ✉

Multi-amplifier laser system for time-resolved spectroscopy at HiLUX-Ultra

HiLUX is a UKRI Infrastructure Fund project, to deliver the next generation of ultrafast laser spectroscopy facilities. The facility will provide a range of capabilities in ultrafast XUV – IR spectroscopy, photoelectron and photoion spectroscopy, and non-linear spectroscopies. The facilities will be accessible to academia and industry in the UK and internationally.

We present an outline of the HiLUX-Ultra laser system, currently under construction. It will supply a broad range of multi-kilohertz, femtosecond to picosecond pulsed laser outputs, in a multi-amplifier format, enabling pump-probe spectroscopy measurements across femtoseconds to seconds timescales.

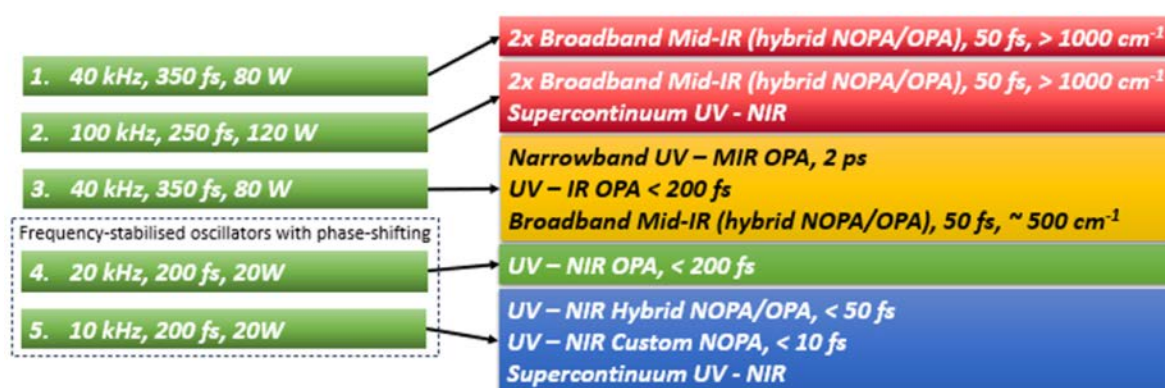


Figure 1: Schematic of the HiLUX-Ultra laser system.

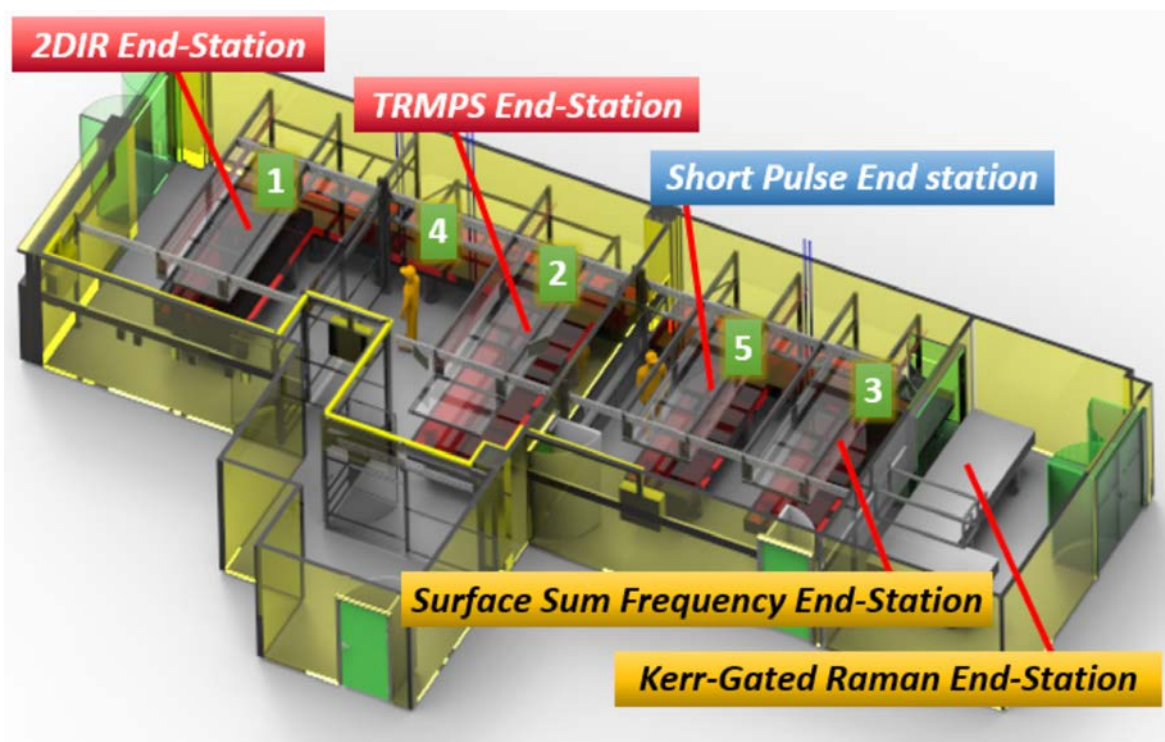
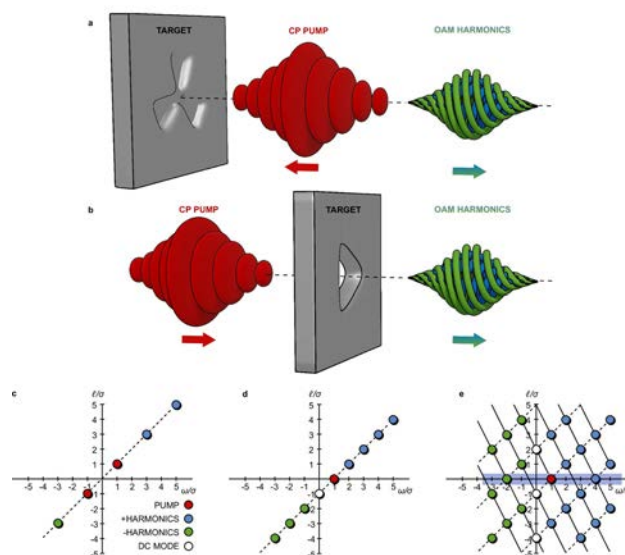


Figure 2: The HiLUX-Ultra laser laboratory, under construction. End-stations are labelled with the associated laser systems.

Theory and Computation

Laser harmonic generation with independent control of frequency and orbital angular momentum

The non-linear optical process of laser harmonic generation (HG) enables the creation of high-quality pulses of UV or even X-ray radiation, which have many potential uses at the frontiers of experimental science, ranging from lensless microscopy to ultrafast metrology and chiral science. Although many of the promising applications are enabled by generating harmonic modes with orbital angular momentum (OAM), independent control of the harmonic frequency and OAM level remains elusive. Here we show, through a theoretical approach, validated with 3D simulations, how unique 2-D harmonic progressions can be obtained, with both frequency and OAM level tuned independently, from tailored structured targets in both reflective and transmissive configurations. Through preferential selection of a subset of harmonic modes with a specific OAM value, a controlled frequency comb of circularly polarised harmonics can be produced. Our approach to describe HG, which simplifies both the theoretical predictions and the analysis of the harmonic spectrum, is directly applicable across the full range of HG mechanisms and can be readily applied to investigations of OAM harmonics in other processes, such as OAM cascades in Raman amplification, or the analysis of harmonic progressions in nonlinear optics.



Schematic illustrating the generation of higher-order harmonics: shown are the LCP ($\sigma=1$, blue) and RCP ($\sigma=-1$, green) harmonics of an incoming CP pump pulse (red) in a reflection and b transmissive configurations, from a threefold structured target. c–e Expected 2D harmonic spectrum from: c a flat target driven by an LP pump pulse with $\ell=1$; d a circular aperture or dent target driven by a CP pump pulse of $\ell=0$; and, e a threefold reflective or transmissive target with a CP pump pulse of $\ell=0$. The blue shaded area indicates the potential for a frequency comb at $\ell=0$.

Reproduced from R. Trines, H. Schmitz, M. King, et al. Laser harmonic generation with independent control of frequency and orbital angular momentum. Nat Commun 15, 6878 (2024), published by Springer Nature under the terms of the **CC-BY-4.0 license**. doi: 10.1038/s41467-024-51311-y

Authors: R. Trines , H. Schmitz, M. King, P. McKenna, R. Bingham

Plasma Diagnostics

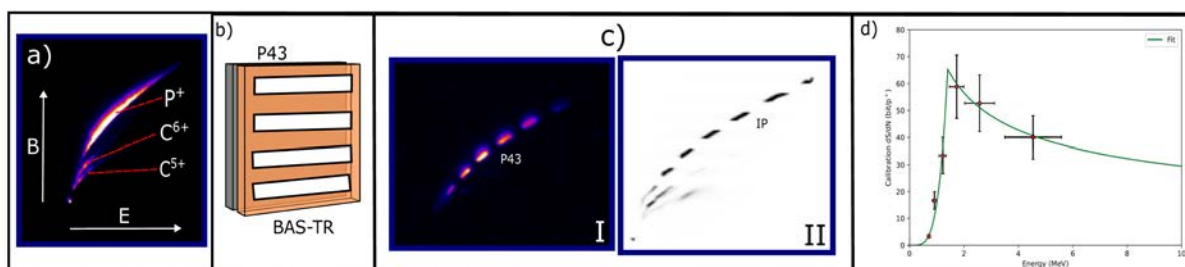
An active ion spectrometer for laser-driven ion beams

We present the development of an active Thomson parabola spectrometer capable of operation at a high repetition rate.



The response of different scintillating screens, such as phosphor screen (P43), glass scintillators (LYSO) and plastic scintillators (EJ260 and BC430), to multi-species ion beams driven by intense lasers, has been studied.

Two optical setups were compared, involving direct imaging of the scintillating screen and transporting the light via a fibre bundle, to reveal their efficiencies when transporting light from the detector to the camera. Experimental data showed that Gadox-based phosphor P43 was the brightest image for a given proton energy, compared to other scintillating materials, allowing a more distinguishable detection of other species present in the laser-driven ion beams.

The response of P43 was calibrated against a BAS-TR image plate (IP) to determine the absolute particle number for the proton and carbon ion beams produced. The cut-off energy found for the P43 proton trace was 21.9 MeV, a value close to the figure of 22 ± 1 MeV from BAS-TR, making it a potential alternative, with the advantage of its capability to operate laser-driven ion beams at rates commensurate with the upcoming petawatt-class lasers, including EPAC.



a) Raw image of the ion traces seen when using a P43 detector. The direction of the magnetic (B) and electric (E) fields are shown, and the proton, C^{6+} and C^{5+} ion beams have been successfully distinguished. b) Schematic of the setup used to calibrate P43 scintillating screens against the image plate (IP). c) Raw image for P43 (I) with a slotted IP placed in front of it and the image plate scan (II). d) The calibration curve applied over P43 proton trace spectra.

Authors: M.J. Cook , T. Hall, C. Armstrong, C. Baird, D. Carroll, R. Clarke, J. Green, H. Ahmed , P. Martin, C. Fegan, A. McCay, D. Molloy, O. Cavanagh, S. Kar, M. Borghesi

Implementation of an optical probe with anamorphic imaging in Gemini TA3

Optical probing diagnostics are key for laser plasma experiments to determine fundamental plasma properties and to characterise the interaction. In laser wakefield acceleration experiments with petawatt class lasers, the plasma channel can be greater than a centimetre in length, yet $\sim 100\text{ }\mu\text{m}$ in radius. This extreme aspect ratio means that imaging transversely with sufficient field of view (in the drive laser direction) and spatial resolution (in the plasma radial direction) is challenging with spherical imaging optics. With higher power laser facilities such as EPAC coming online, this aspect ratio will only increase. Here, a 3:1 anamorphic imaging system has been demonstrated on Gemini.

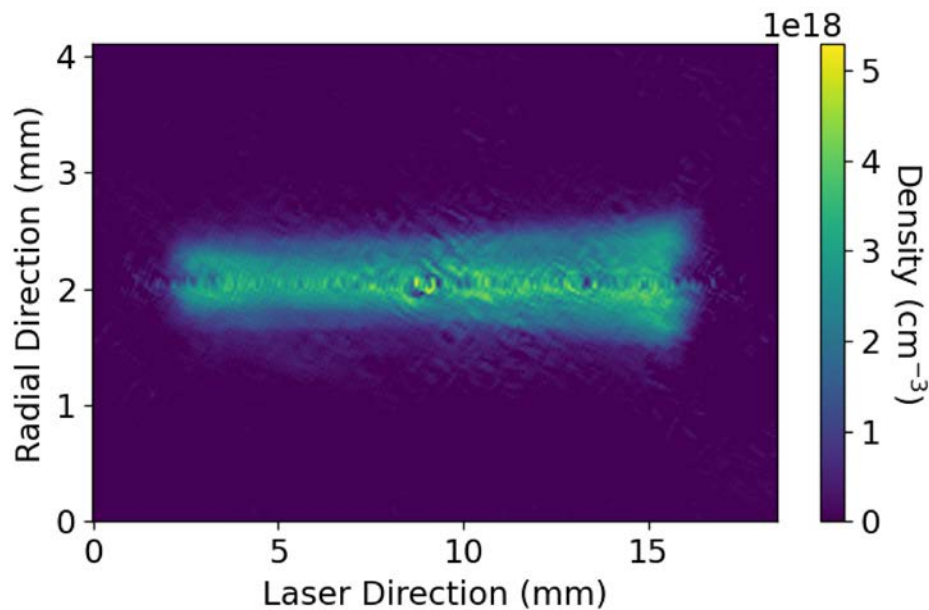


Figure 1: Measured plasma density assuming cylindrical symmetry of the plasma channel.

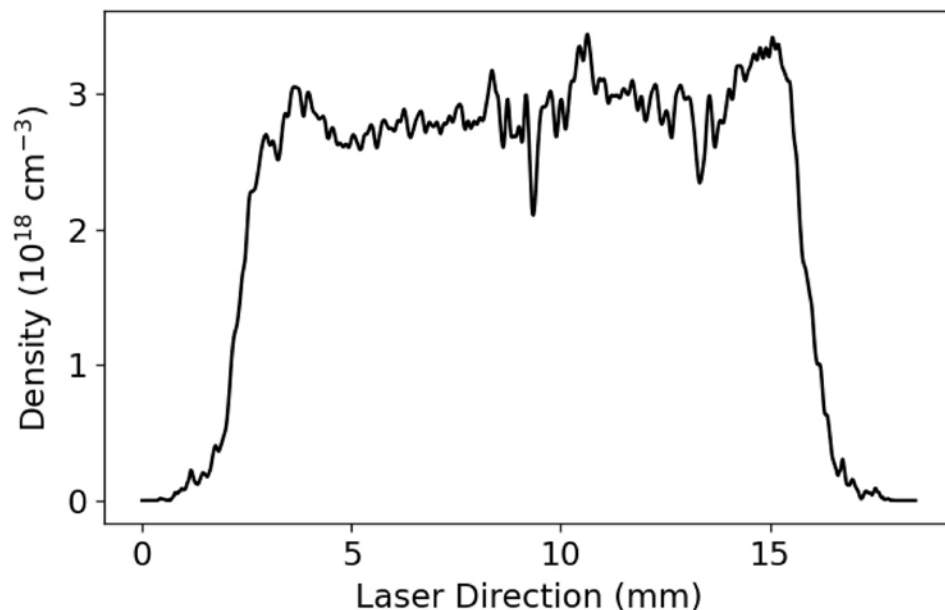
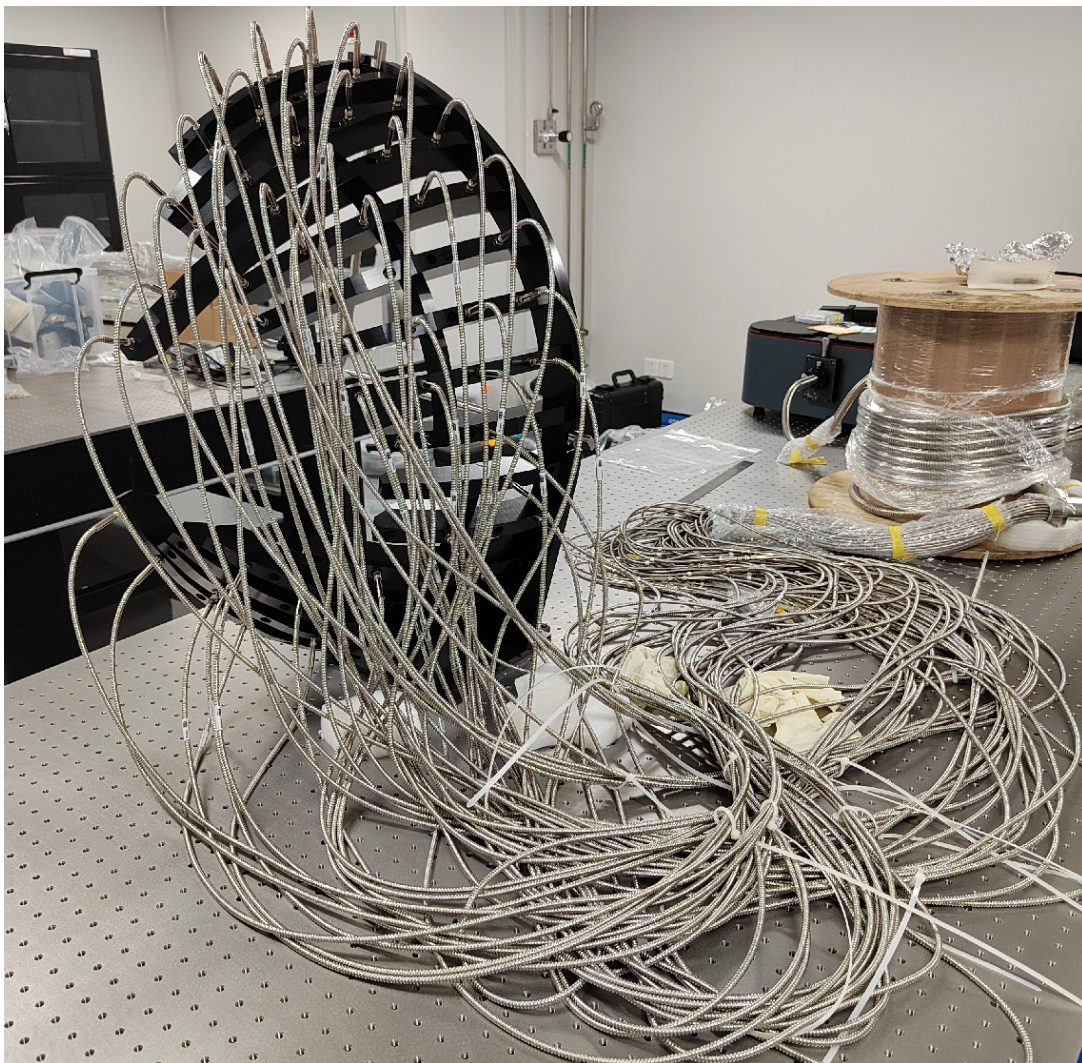


Figure 2: On-axis plasma density seen by the drive laser.

Authors: O. Finlay , Z. Athawes-Phelps, C. McAnespie, M. Streeter

A high-angular-coverage optical diagnostic to measure scattered light directionality on Vulcan Target Area West

Direct-drive approach to Inertial Confinement Fusion is prone to several laser-plasma instabilities (LPI). Recently, stimulated Raman side-scattering (SRSS) predominance was observed on several experiments. However, due to its particular geometry, this instability leads to a complex emission over a very large range of directions. Therefore, experimental characterisation has been quite limited, and assessing the total energy loss driven by SRSS is not achievable with current diagnostic methods. A dedicated diagnostic has been developed to answer these limitations, by collecting the light emitted from the plasma over a large solid angle. This fibre-based diagnostic collects the light emitted in 55 directions over a π surface and provides a spectral and energy measurement resolved in angle. This enables reconstruction of the SRSS emission profile and estimation of the total reflectivity.



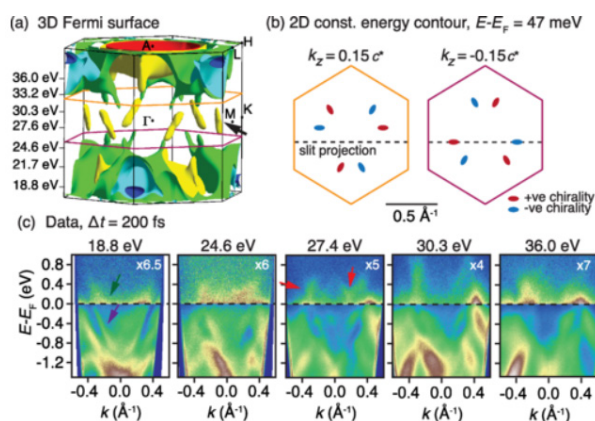
The High Angular Coverage Side-scattering Station or HACSS. At the front is the 400 mm radius aluminium structure holding 55 fibres while maintaining clear aperture for the incident laser beams. The fibres are multiplexed in a single line bundle, with a total length of 14m, and coupled to an imaging spectrometer visible at the back.

Authors: K. Glize ✉, X. Zhao, X.H. Yuan, J. Zhang, Y.H. Zhang, Y.F. Dong, Y.Y. Wang, B. Fisher, M. Khan, N.C. Woolsey, E. Hume, G. Cristoforetti, P. Koester, L. Gizzi, S. Zaehner

Imaging and Dynamics for Physical and Life Sciences

Ultrafast carrier dynamics throughout the three-dimensional Brillouin zone of the Weyl semimetal PtBi₂

Using time- and angle-resolved photoemission spectroscopy, we examine the unoccupied electronic structure and electron dynamics of the type-I Weyl semimetal PtBi₂. Using the ability to change the probe photon energy over a wide range, we identify the predicted Weyl points in the unoccupied three-dimensional band structure and we discuss the effect of k_{\perp} broadening in the normally unoccupied states. We characterise the electron dynamics close to the Weyl point and in other parts of three-dimensional Brillouin zone using k -means, an unsupervised machine learning technique. This reveals distinct differences—in particular, dynamics that are faster in the parts of the Brillouin zone that host most of the bulk Fermi surface than in parts close to the Weyl points.



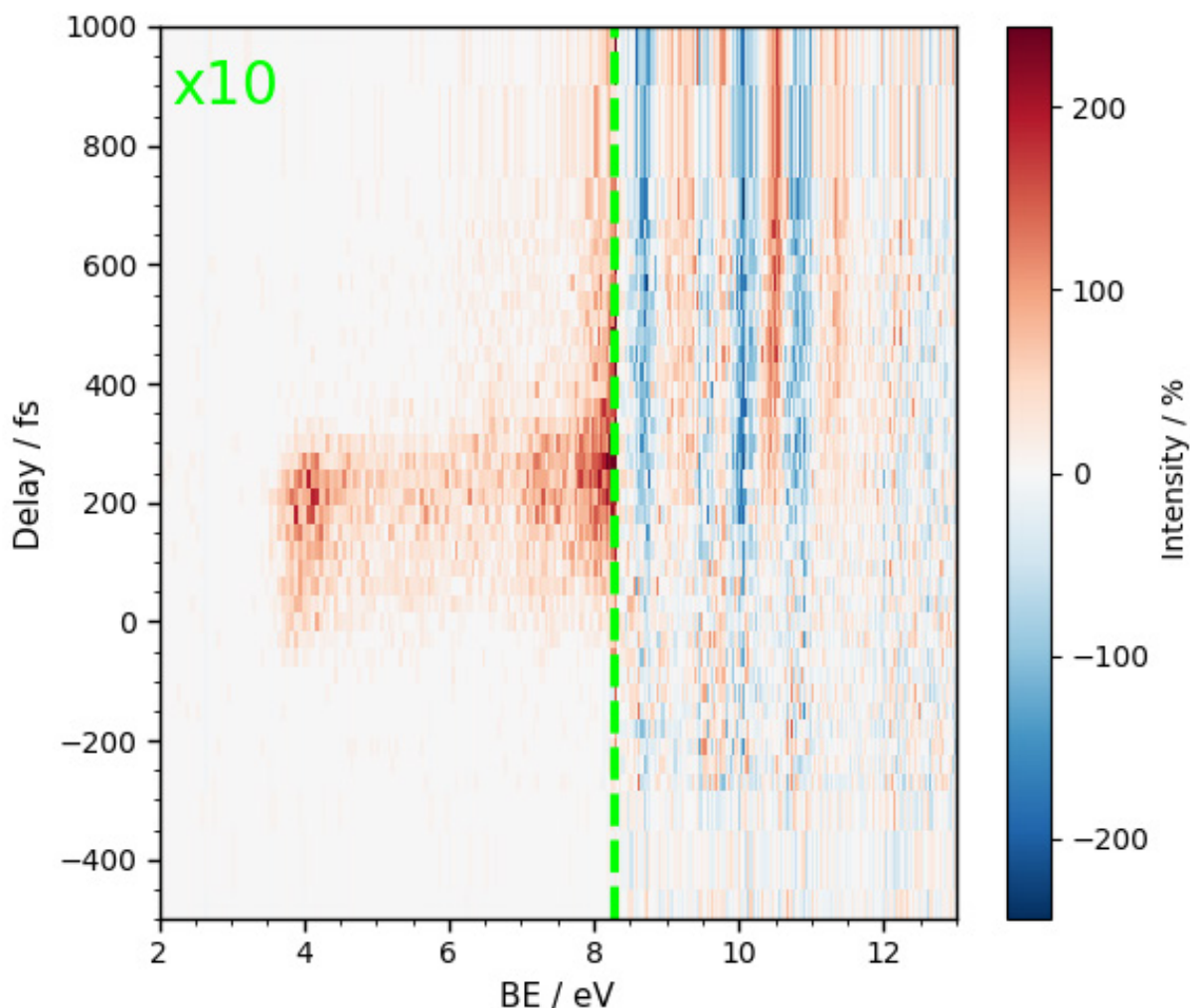
(a) Bulk Brillouin zone and Fermi surface of PtBi₂. The k_z values for the photon energies in our experiment are marked, as well as the planes containing the Weyl points. (b) Two-dimensional cuts through the Brillouin zone at k_z indicated by the corresponding colours in panel (a). The dashed line shows the approximate location of the reported ARPES measurements. The markers represent the location of the Weyl points and the colour their chirality. (c) Dispersion along this dashed line in panel (b) for different probe photon energies following pumping by a 1.46 eV laser pulse at peak excitation. A different grey scale is chosen for the states below and above the Fermi energy, as indicated by insets. Teal (purple) arrows point to the metallic bulk (surface) states.

Subsequently published by the American Physical Society in Machine-learning approach to understanding ultrafast carrier dynamics in the three-dimensional Brillouin zone of PtBi₂, Phys. Rev. Research 7, 013025 (2025) under the terms of the **CC-BY-4.0 license**. doi: 10.1103/PhysRevResearch.7.013025

Authors: P. Majchrzak, C. Sanders, Y. Zhang, A. Kuibarov, O. Suvorov, E. Springate, I. Kovalchuk, S. Aswartham, G. Shipunov, B. Büchner, A. Yaresko, S. Borisenko, **P. Hofmann** ✉

Time-resolved photoelectron spectroscopy study of halothiophene photochemistry

Halothiophenes are heterocyclic rings containing a sulphur (S) atom, with a penderal halogen attached. The photochemistry is highly dependent on the character of both the halogen attached, and the character of the initially excited state. We have compared the photochemistry of bromo and iodothiophene at two pump wavelengths and see wavelength and halogen dependent changes in the photochemistry. In this article we report on the iodothiophene photochemistry occurring upon excitation of the $\pi\pi^*$ or $(n/\pi)\sigma^*$ states.

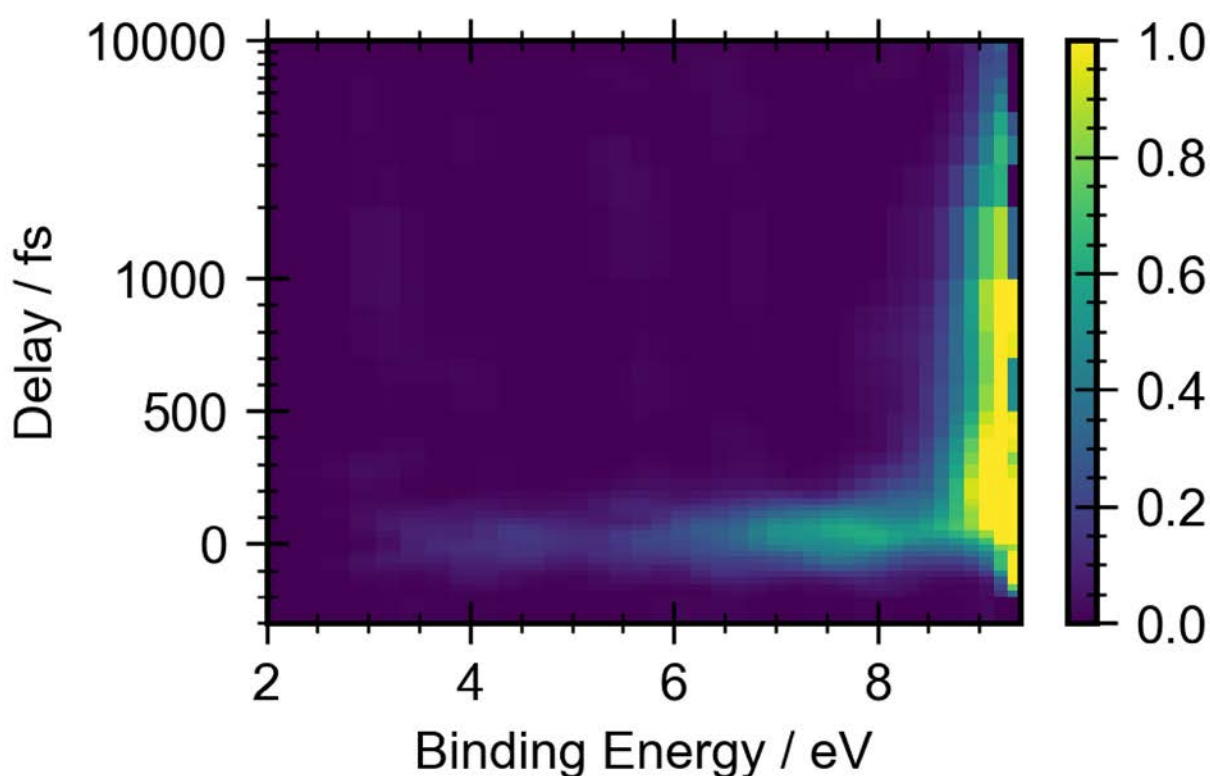


Time-resolved photoelectron spectra of UV (245 nm) pumped 2-iodothiophene. Structural changes are seen as shifts in binding energy as a function of time with iodine and thiophenyl radical product formation seen with a few hundred femtoseconds.

Authors: W.O. Razmus, H.J. Thompson, **R.S. Minns** ✉, M.A. Parkes, E. Springate, R.T. Chapman, Y. Zhang, J.O.F. Thompson

Ultrafast dynamics in the 1,2-dichloroethenes

Isomerisation is a crucial process that occurs following absorption of a photon, it is especially prevalent for C=C double bonds. Isomerisation around a carbon double bond being at the root of vision. It is therefore important to look at how different isomers of different molecules behave. Using a 200 nm pump and an XUV (22 eV probe) we looked at the time resolved photoelectron signals from *trans* and *cis*-1,2-dichloroethene. The position of the signals in the photoelectron spectrum indicates what products are being formed. We observe an ultrafast decay from the initially formed molecular excited state to the ground state. This decay is slower in the *trans* isomer compared to the *cis*. This shows the effect of the relative position of the chlorine atoms. Rapid formation of fragments was also observed on an ultrafast timescale, showing how quickly dissociation can occur.



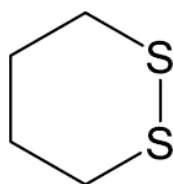
Pump-Probe photoelectron spectrum of *trans*-1,2-dichloroethene with 200 nm pump, 22 eV probe.

Subsequently published in Phys. Chem. Chem. Phys., 26, 28406 (2024) under the terms of the **CC-BY-3.0 license**. doi: 10.1039/d4cp02952f

Authors: H.G. McGhee, H.J. Thompson, J. Thompson, Y. Zhang, A.S. Wyatt, E. Springate, R.T. Chapman, D.A. Horke, R.S. Minns, R.A. Ingle, **M.A. Parkes** ✉

Ring-opening dynamics of a cyclic disulfide captured by time-resolved Coulomb explosion imaging

We used Coulomb explosion imaging, an ultrafast time resolved structure determination technique, to show how the molecular structure of 1,2-dithiane, a model cyclic disulfide, evolves when the disulfide bond is broken with ultraviolet light. Our preliminary analysis reveals that breaking the disulfide bond on the first excited state creates a vibrational wavepacket that represents a torsional motion of the molecular structure, oscillating between a closed and linear biradical structure on a period of approximately 400 femtoseconds. This is in direct agreement with quantum dynamics simulations and this vibrational wavepacket dynamics is observable in our experimental fragment ion yields. We rationalise our observation by calculating how the first, second and third ionisation potentials of 1,2-dithiane vary as the molecular geometry evolves along this vibrational motion. Our work shows how disulfide bonds respond to ultraviolet radiation. They provide an empirical validation of theoretical quantum dynamics calculations and demonstrate the suitability of 1,2-dithiane as a powerful benchmark molecule for ultrafast structural dynamics techniques.



1,2-dithiane ($C_4H_8S_2$)

Figure 1: The molecular structure of 1,2-dithiane.

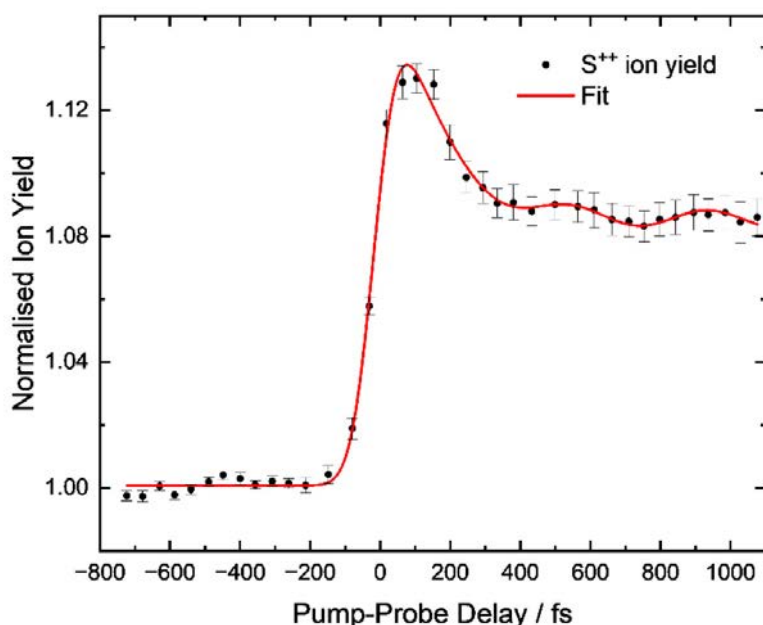



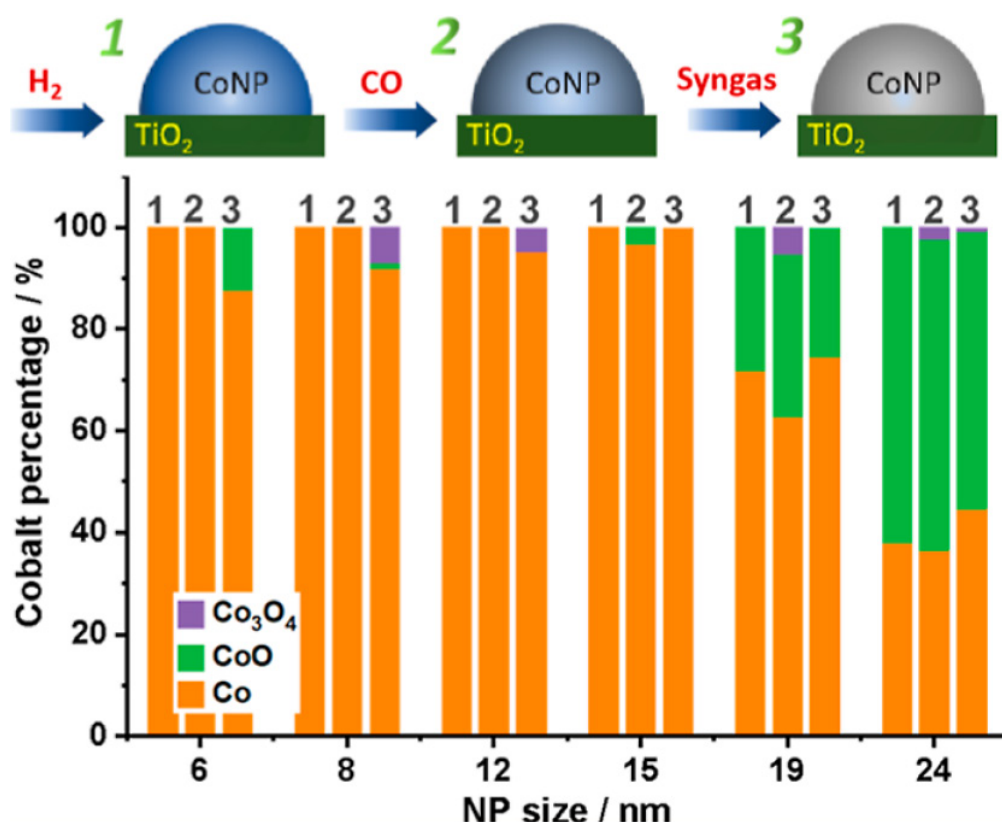
Figure 2: Time-dependent S^{++} ion yield from the Coulomb explosion of 1,2-dithiane following UV photoexcitation.

Subsequently published in Chemical Physical Letters, 871, 142095 (2025) under the terms of the **CC-BY-4.0 license**. doi: 10.1016/j.cplett.2025.142095

Authors: P.A. Robertson , J. Merrick, D. Heathcote, M.S. Robinson, A.A. Butler, J.F.P. Nunes, C. Rankine, Z. Liu, S. Arrowsmith, J.O.F. Thompson, N.M. Madugula, Y. Zhang, R. Chapman, E. Springate, Y. Biddick, E.A. Anderson, A. Kirrander, C. Vallance

Compositional evolution of individual CoNPs on Co/TiO₂ during CO and syngas treatment resolved through soft XAS/X-PEEM

The nanoparticle (NP) redox state is an important parameter in the performance of cobalt-based Fischer–Tropsch synthesis (FTS) catalysts. Here, the compositional evolution of individual CoNPs (6–24 nm) in terms of the oxide vs metallic state was investigated in situ during CO/syngas treatment using spatially resolved X-ray absorption spectroscopy (XAS)/X-ray photoemission electron microscopy (X-PEEM). It was observed that in the presence of CO, smaller CoNPs (i.e., ≤12 nm in size) remained in the metallic state, whereas NPs ≥ 15 nm became partially oxidized, suggesting that the latter were more readily able to dissociate CO. In contrast, in the presence of syngas, the oxide content of NPs ≥ 15 nm reduced, while it increased in quantity in the smaller NPs; this reoxidation that occurs primarily at the surface proved to be temporary, reforming the reduced state during subsequent UHV annealing. O K-edge measurements revealed that a key parameter mitigating the redox behaviour of the CoNPs were proximate oxygen vacancies (O_{vac}). These results demonstrate the differences in the reducibility and the reactivity of Co NP size on a Co/TiO₂ catalyst and the effect O_{vac} have on these properties, therefore yielding a better understanding of the physicochemical properties of this popular choice of FTS catalysts.



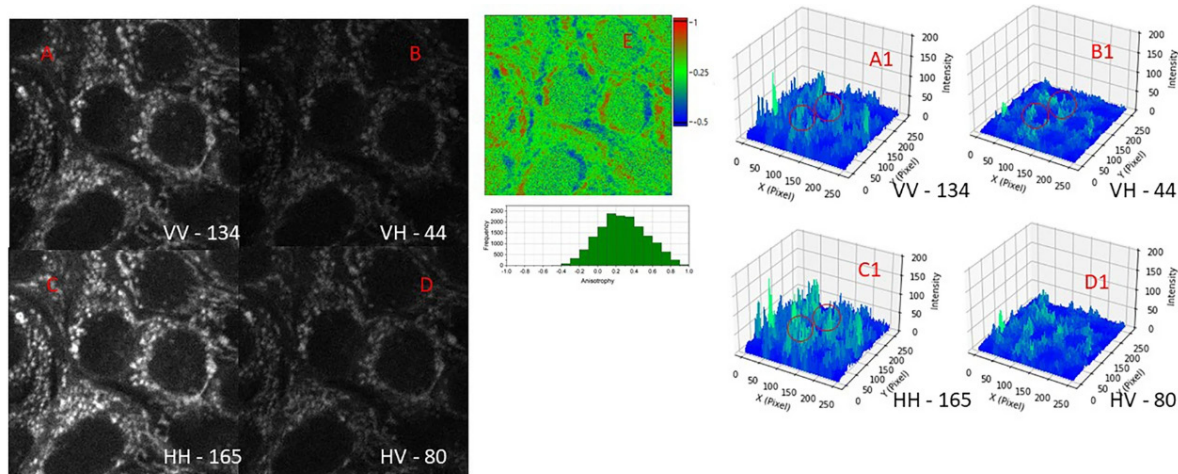
Reproduced from ACS Catal. 2023, 13, 15956-15966, under the terms of the CC-BY-4.0 license. doi: 10.1021/acscatal.3c03214

Authors: C. Qiu, Y. Odarchenko, Q. Meng, H. Dong, I. Lezcano Gonzalez, M. Panchal, P. Olalde-Velasco, F. Maccherozzi, L. Zanetti-Domingues, M.L. Martin-Fernandez, A.M. Beale ✉

The use of NADH anisotropy to investigate mitochondrial cristae alignment

Life may be expressed as the flow of electrons, protons, and other ions, resulting in large potential difference. It is also highly photo-sensitive, as a large proportion of the redox capable molecules it relies on are chromophoric. It is thus suggestive that a key organelle in eukaryotes, the mitochondrion, constantly adapt their morphology as part of the homeostatic process. Studying unstained in vivo nano-scale structure in live cells is technically very challenging.

One option is to study a central electron carrier in metabolism, reduced nicotinamide adenine dinucleotide (NADH), which is fluorescent and mostly located within mitochondria. The studies we describe present a novel avenue for exploring a possible fixed and ordered nature of NADH molecule particularly in mitochondria towards the beginning of understanding the other properties of the mitochondria, as well as the potential involvement of NADH in quantum biology.



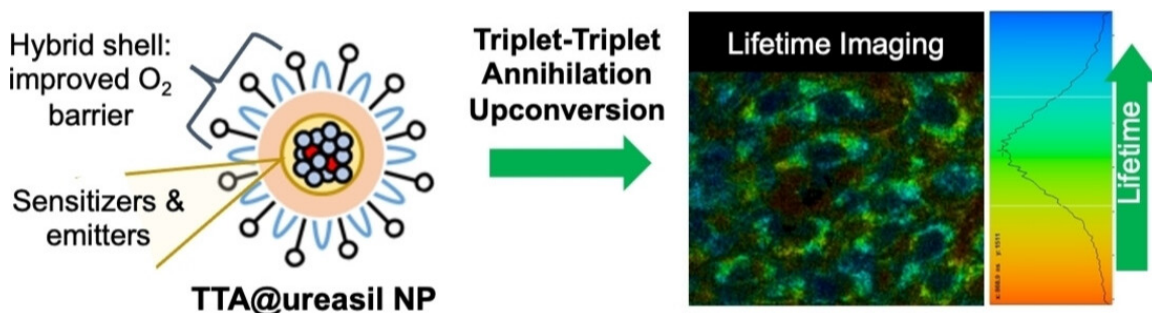
Two-photon fluorescence images of natural NADH in mitochondria from MCF7 cells. Time resolved decay profiles confirm NADH. Representative images from three repeat experiments. (A) is vertical excitation and vertical emission, (B) is vertical excitation, horizontal emission, (C) is horizontal excitation, vertical emission, (D) is horizontal excitation and horizontal emission. A1–D1 are the equivalent count profile plots where difference in intensities are reflected. Red circles also represent polarisation specific emissions, (E) is an anisotropy map of and pixel distributions. FoV 50 μm .

Taken from H.E. Smith, A.M. Mackenzie, C. Seddon, et al. The use of NADH anisotropy to investigate mitochondrial cristae alignment. Sci Rep 14, 5980 (2024) under the **CC-BY-4.0 license**. doi: 10.1038/s41598-024-55780-5

Authors: H.E. Smith, A.M. Mackenzie, C. Seddon, R. Mould, I. Kalampouka, P. Malakar, S.R. Needham, K. Beis, J.D. Bell, A. Nunn, **S.W. Botchway** ✉

Ultra-small air-stable triplet-triplet annihilation upconversion nanoparticles for anti-Stokes time-resolved imaging

Image contrast is often limited by background autofluorescence in steady-state bioimaging microscopy. Upconversion bioimaging can overcome this by shifting the emission lifetime and wavelength beyond the autofluorescence window. Here we demonstrate the first example of triplet-triplet annihilation upconversion (TTA-UC) based lifetime imaging microscopy. A new class of ultra-small nanoparticle (NP) probes based on TTA-UC chromophores encapsulated in an organic–inorganic host has been synthesised. The NPs exhibit bright UC emission (400–500 nm) in aerated aqueous media with a UC lifetime of $\approx 1\ \mu\text{s}$, excellent colloidal stability and little cytotoxicity. Proof-of-concept demonstration of TTA-UC lifetime imaging using these NPs shows that the long-lived anti-Stokes emission is easily discriminable from typical autofluorescence. Moreover, fluctuations in the UC lifetime can be used to map local oxygen diffusion across the subcellular structure. Our TTA-UC NPs are highly promising stains for lifetime imaging microscopy, affording excellent image contrast and potential for oxygen mapping that is ripe for further exploitation.



A new class of ultra-small nanoparticle (NP) probes based on triplet-triplet annihilation upconversion (TTA-UC) chromophores in an organic–inorganic ureasil host have been prepared and used to stain living cells as a proof-of-concept demonstration of TTA-UC lifetime imaging for the first time. Fluctuations of the UC lifetime in the stained cells indicate the NPs can be used to map local oxygen diffusion across the subcellular structure.

Reproduced from Angew. Chem. Int. Ed. 2023, 62, e202308602, under the terms of the **CC-BY-4.0 license**. doi:10.1002/anie.202308602

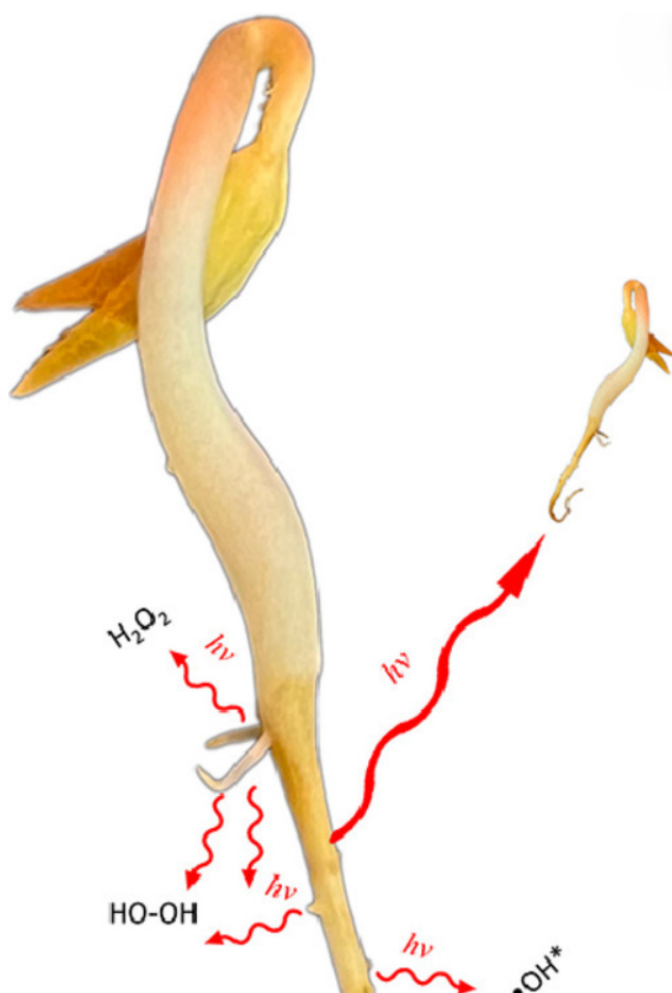
Authors: B. Zhang, K.D. Richards, B.E. Jones, A.R. Collins, R. Sanders, S.R. Needham, P. Qian, A. Mahadevegowda, C. Ducati, S.W. Botchway, **R.C. Evans** ✉

Rooting out ultraweak photon emission a-mung bean sprouts

It is well known that life has evolved to use and generate light, for instance, photosynthesis, vision and bioluminescence. What is less well known is that during normal metabolism, it can generate $1\text{--}100\text{ photons s}^{-1}\text{ cm}^{-2}$ known as ultra-weak photon emission (UPE), biophoton emission or biological autoluminescence.

We have established a highly sensitive experimental setup using opposing single photon detectors to study spontaneous and induced UPE in germinating mung beans, at stages from beans to leafy plants. Using this method, we observed a steady state photonic emission directly related to plant size, a temporary increase in emission in relation to dehydration and then rehydration, and an increase in photonic emission related to secondary root growth, possibly caused by increased cell division.

Our data therefore adds to the investigation of UPE which originates from the studies of the mitogenic effect first observed almost exactly a hundred years ago by Alexander Gurwitsch.

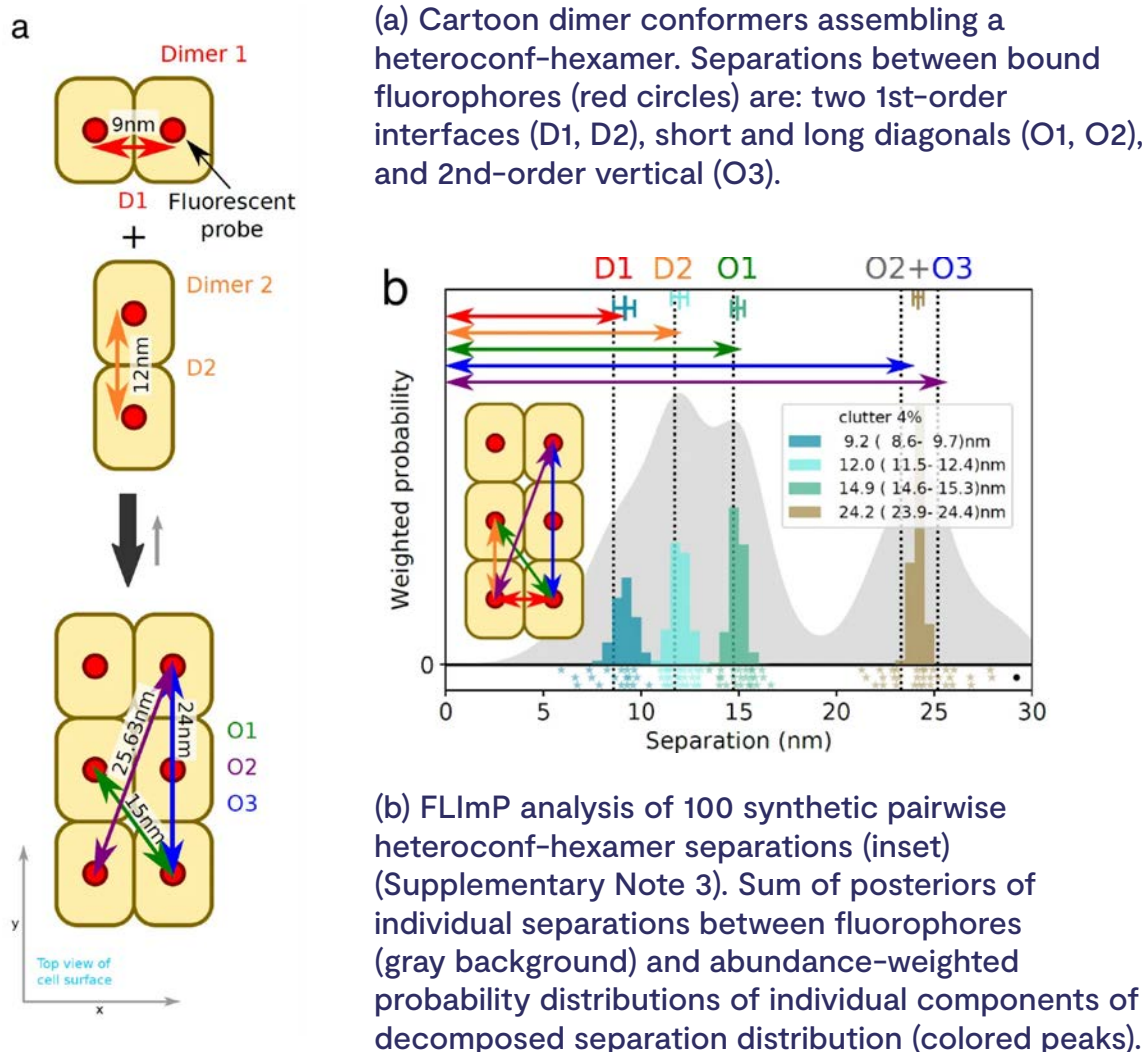


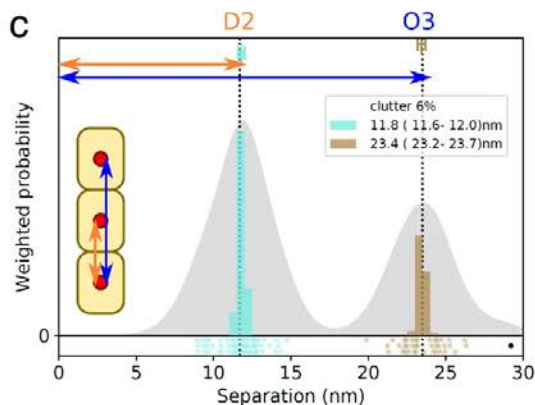
Taken from A.M. Mackenzie et al. Journal of Photochemistry and Photobiology 19 (2024) 100224 under the terms of the **CC-BY-4.0 license**. doi: 10.1016/j.jpap.2023.100224

Authors: A.M. Mackenzie ✉, H.E. Smith, R.R. Mould, J.D. Bell, A.V. Nunn, S.W. Botchway ✉

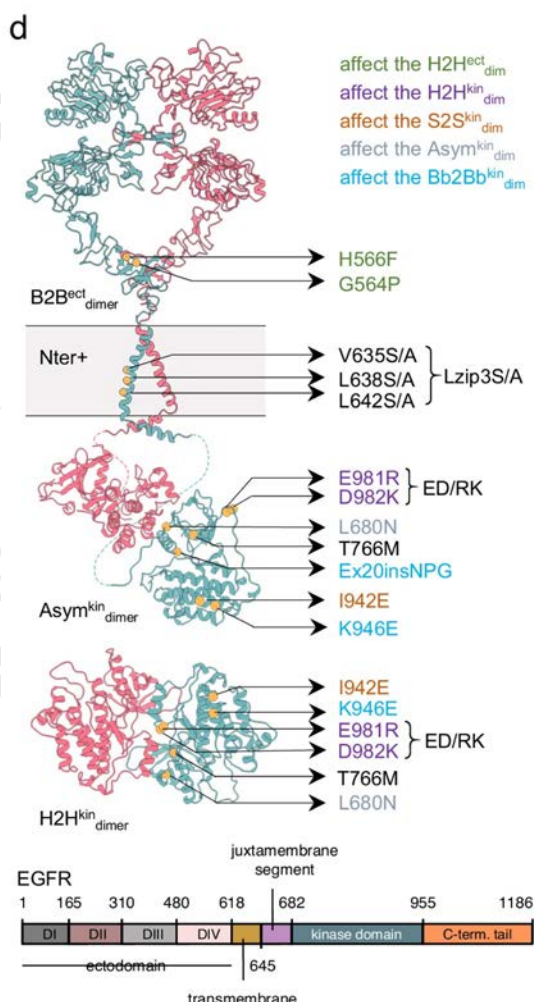
Drug-resistant EGFR mutations promote lung cancer by stabilizing interfaces in ligand-free kinase-active EGFR oligomers

The Epidermal Growth Factor Receptor (EGFR) is frequently found to be mutated in non-small cell lung cancer. Oncogenic EGFR has been successfully targeted by tyrosine kinase inhibitors, but acquired drug resistance eventually overcomes the efficacy of these treatments. Attempts to surmount this therapeutic challenge are hindered by a poor understanding of how and why cancer mutations specifically amplify ligand-independent EGFR auto-phosphorylation signals to enhance cell survival and how this amplification is related to ligand-dependent cell proliferation. Here we show that drug-resistant EGFR mutations manipulate the assembly of ligand-free, kinase-active oligomers to promote and stabilize the assembly of oligomer-obligate active dimer sub-units and circumvent the need for ligand binding. We reveal the structure and assembly mechanisms of these ligand-free, kinase-active oligomers, uncovering oncogenic functions for hitherto orphan transmembrane and kinase interfaces, and for the ectodomain tethered conformation of EGFR. Importantly, we find that the active dimer sub-units within ligand-free oligomers are the high affinity binding sites competent to bind physiological ligand concentrations and thus drive tumour growth, revealing a link with tumour proliferation. Our findings provide a framework for future drug discovery directed at tackling oncogenic EGFR mutations by disabling oligomer-assembling interactions.

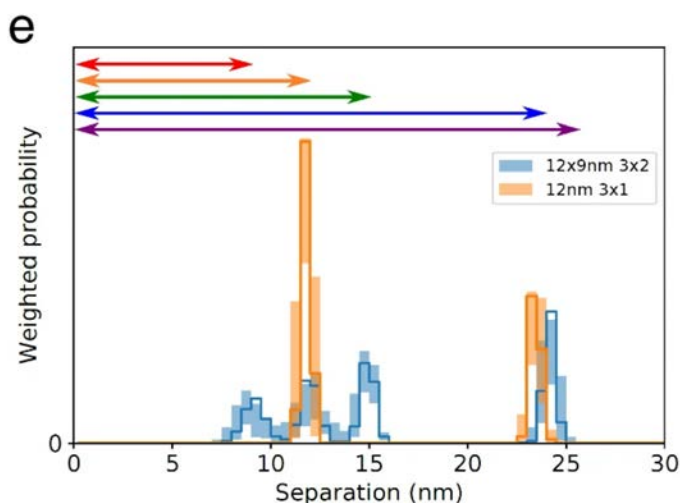




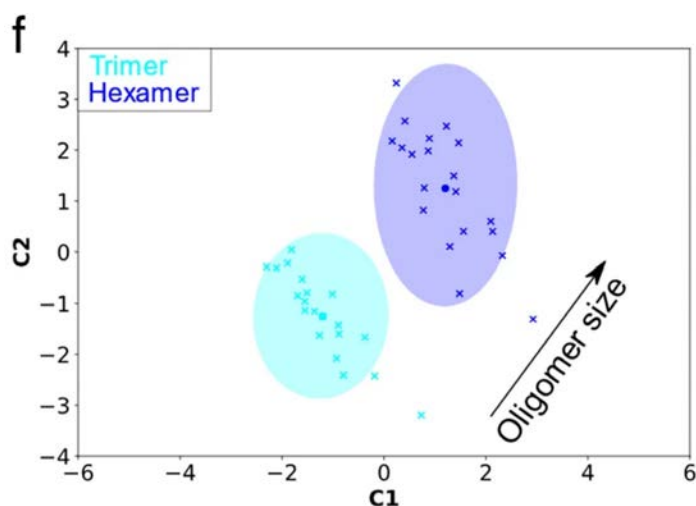
(c) As (b) for the homo-trimer formed by the Dimer 2 conformer.



(d) Top, map of mutations and treatments superimposed on the B2BectdimerCR8181, an Asymkindimer3, and H2Hkindimer54 sub-units. Mutations colored according to the different dimer conformers they inhibit or disrupt. Bottom, EGFR sequence diagram.



(e) Comparisons between decomposed separation probability distributions between datasets.



(f) Wasserstein MDS analysis of FLImP decompositions. This measures the work needed to convert a decomposed separation set into another, thereby estimating similarities and differences between whole FLImP separation decompositions.

Reproduced from R.S. Iyer, S.R. Needham, I. Galdadas et al. Drug-resistant EGFR mutations promote lung cancer by stabilizing interfaces in ligand-free kinase-active EGFR oligomers. Nat Commun 15, 2130 (2024) under the terms of the **CC-BY-4.0 license**. doi: 10.1038/s41467-024-46284-x

Authors: R.S. Iyer, S.R. Needham, I. Gladadas, B.M. Davis, S.K. Roberts, R.C.H. Man, L.C. Zanetti-Domingues, D.T. Clarke, G.O. Fruhwirth, P.J. Parker, **D.J. Rolfe** ✉, **F.L. Gervasio** ✉, **M.L. Martin-Fernandez** ✉

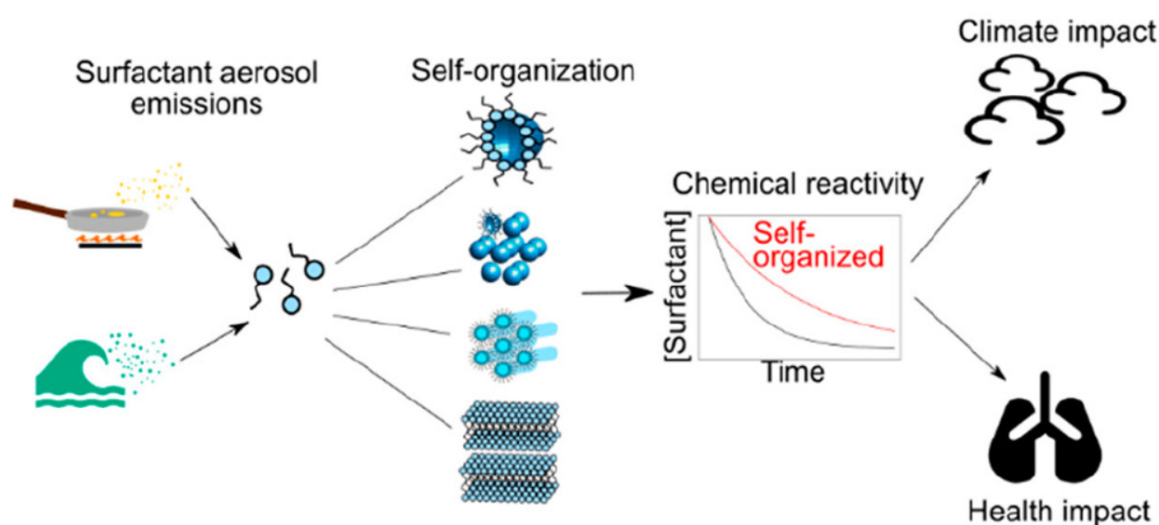
Molecular self-organization in surfactant atmospheric aerosol proxies

Aerosols are ubiquitous in the atmosphere, both outdoors and indoors. Surfactants make significant contributions to aerosol emissions, with sources ranging from cooking to sea spray. These molecules alter the cloud droplet formation potential by changing the surface tension of aqueous droplets and thus increasing their ability to grow. They can also coat solid surfaces such as windows (“window grime”) and dust particles.

A common cooking and marine emission, oleic acid, is known to self-organise into a range of 3-D nanostructures, which are highly viscous and as such can impact the kinetics of aerosol and film ageing.

Most literature studies on oleic acid oxidation have focused on pure liquid oleic acid in its native form either as particles, deposited films, or monolayers, occasionally mixed with cosurfactants. Our work represents a new avenue, focusing on how the surfactant itself is organised and how this self-organisation could impact the key aerosol processes of water uptake and chemical reaction outdoors and indoors.

We created a body of experimental and modelling work to study self-organised proxies as nanometre-to-micrometre films, levitated droplets, and bulk mixtures. Our findings suggest that hazardous, reactive materials may be protected in aerosol matrices underneath a highly viscous shell, thus extending the atmospheric residence times of otherwise short-lived species.

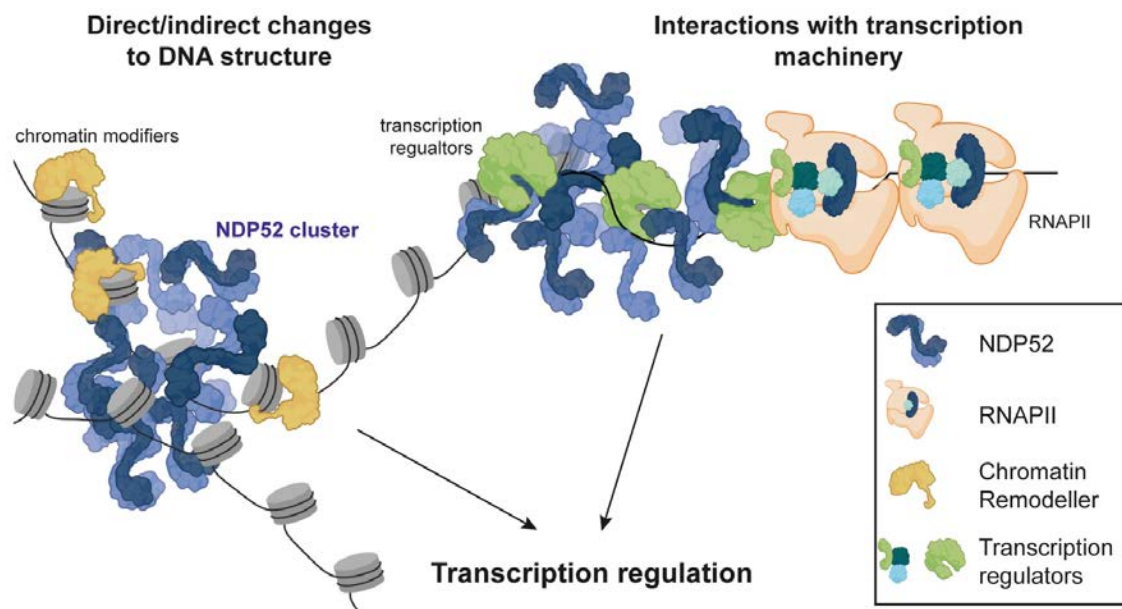


Taken from Acc. Chem. Res. 2023, 56, 19, 2555–2568 published by the American Chemical Society under the terms of the **CC-BY-4.0 license**. doi: 10.1021/acs.accounts.3c00194

Authors: A. Milsom, A.M. Squires, A.D. Ward, C. Pfrang ✉

Autophagy receptor NDP52 alters DNA conformation to modulate RNA polymerase II transcription

NDP52 is an autophagy receptor involved in the recognition and degradation of invading pathogens and damaged organelles. Although NDP52 was first identified in the nucleus and is expressed throughout the cell, to date, there is no clear nuclear functions for NDP52. Here, we use a multidisciplinary approach to characterise the biochemical properties and nuclear roles of NDP52. We find that NDP52 clusters with RNA Polymerase II (RNAPII) at transcription initiation sites and that its overexpression promotes the formation of additional transcriptional clusters. We also show that depletion of NDP52 impacts overall gene expression levels in two model mammalian cells, and that transcription inhibition affects the spatial organisation and molecular dynamics of NDP52 in the nucleus. This directly links NDP52 to a role in RNAPII-dependent transcription. Furthermore, we also show that NDP52 binds specifically and with high affinity to double-stranded DNA (dsDNA) and that this interaction leads to changes in DNA structure in vitro. This, together with our proteomics data indicating enrichment for interactions with nucleosome remodelling proteins and DNA structure regulators, suggests a possible function for NDP52 in chromatin regulation. Overall, here we uncover nuclear roles for NDP52 in gene expression and DNA structure regulation.



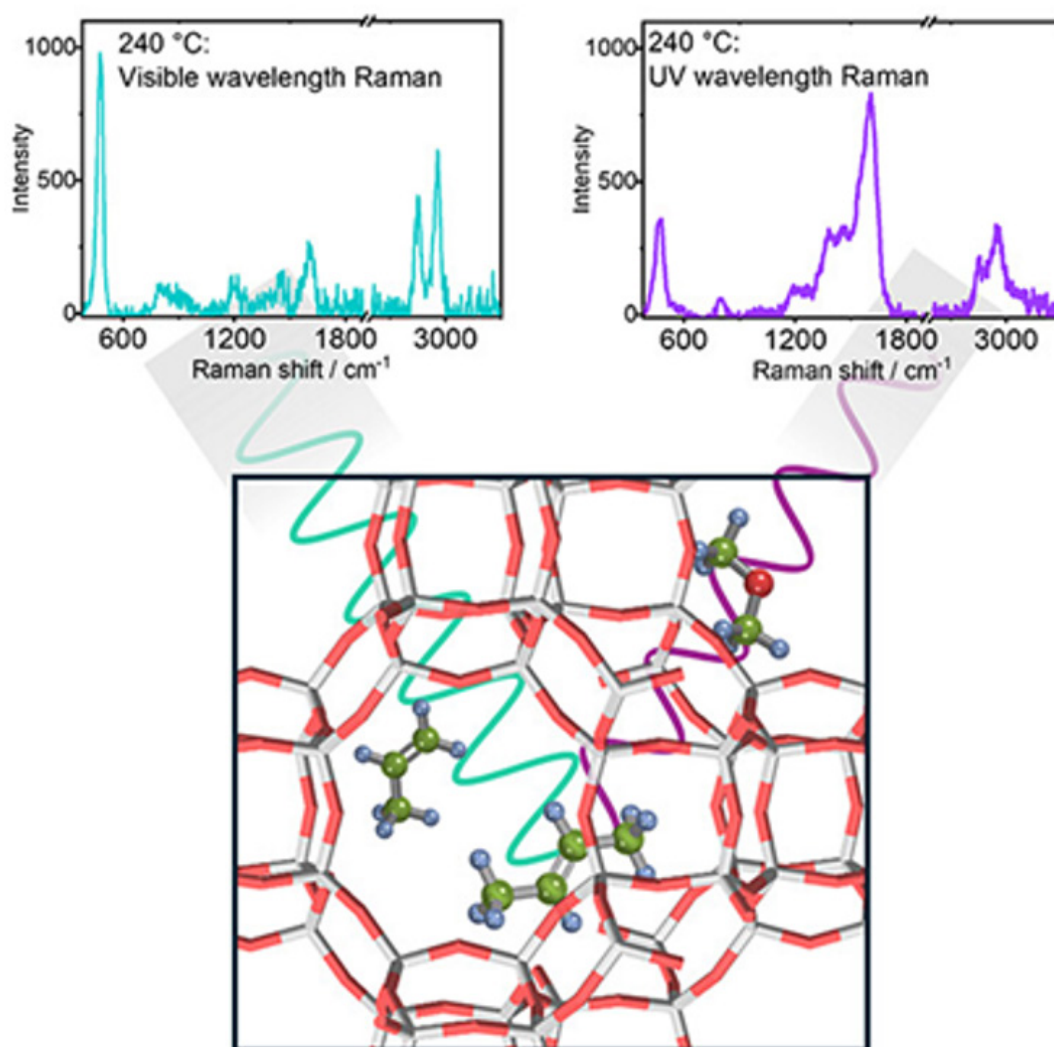
Model of possible mechanism for NDP52's activity in transcription. NDP52 could directly interact with DNA in the nucleus, or with chromatin modifiers (e.g. histone modifiers), to cause local changes to chromatin structure. Conversely, interactions with transcription factors/coactivators and transcription machinery could also modulate transcription activity of genes. Created with BioRender.com.

Reproduced from dos Á Santos, D.E. Rollins, Y. Hari-Gupta, et al. Autophagy receptor NDP52 alters DNA conformation to modulate RNA polymerase II transcription. Nat Commun 14, 2855 (2023) under the terms of the **CC-BY-4.0 license**. doi: 10.1038/s41467-023-38572-9

Authors: Á. dos Santos, D.E. Rollins, Y. Hari-Gupta, H. McArthur, M. Du, S. Yong Zi Ru, K. Pidlisna, A. Stranger, F. Lorgat, D. Lambert, I. Brown, K. Howland, J. Aaron, L. Wang, P.J.I. Ellis, T.-L. Chew, M. Martin-Fernandez, A.L.B. Pyne, **C.P. Toseland** ✉

Methanol-to-olefins studied by UV Raman spectroscopy as compared to visible wavelength: Capitalization on resonance enhancement

Resonance Raman spectroscopy can provide insights into complex reaction mechanisms by selectively enhancing the signals of specific molecular species. In this work, we demonstrate that, by changing the excitation wavelength, Raman bands of different intermediates in the methanol-to-hydrocarbons reactions can be identified. We show in particular how UV excitation enhances signals from short-chain olefins and cyclopentadienyl cations during the induction period, while visible excitation better detects later-stage aromatics. However, visible excitation is prone to fluorescence that can obscure Raman signals, and hence, we show how fast fluorescence rejection techniques like Kerr gating are necessary for extracting useful information from visible excitation measurements.

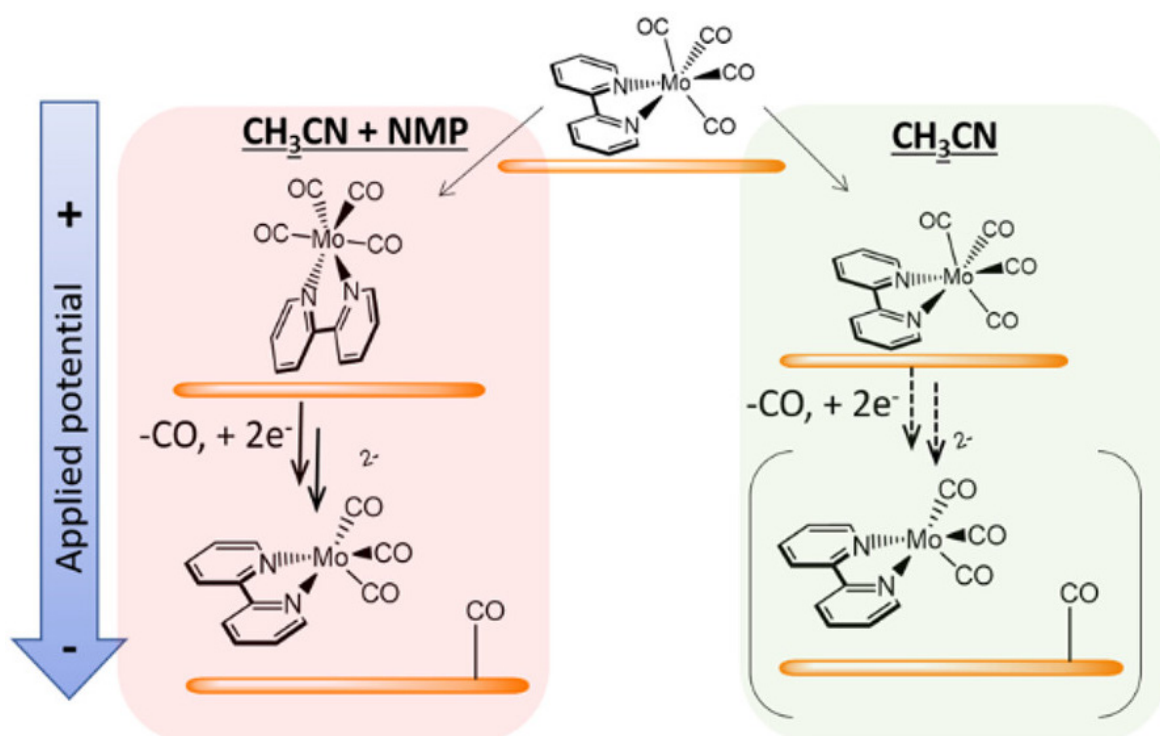


Reproduced from J. Phys. Chem. Lett. 2024, 15, 26, 6826–6834, published by the American Chemical Society under the terms of the **CC-BY-4.0 license**. doi: 10.1021/acs.jpcllett.4c00865

Authors: E. Campbell, I.V. Sazanovich, M. Towrie, M.J. Watson, I. Lezcano-Gonzalez ✉, A.M. Beale ✉

Potential dependent reorientation controlling activity of a molecular electrocatalyst

The activity of molecular electrocatalysts depends on the interplay of electrolyte composition near the electrode surface, the composition and morphology of the electrode surface, and the electric field at the electrode–electrolyte interface. This interplay is challenging to study and often overlooked when assessing molecular catalyst activity. Here, we use surface specific vibrational sum frequency generation (VSFG) spectroscopy to study the solvent and potential dependent activation of $\text{Mo}(\text{bpy})(\text{CO})_4$, a CO_2 reduction catalyst, at a polycrystalline Au electrode. We find that the parent complex undergoes potential dependent reorientation at the electrode surface when a small amount of *N*-methyl-2-pyrrolidone (NMP) is present. This preactivates the complex, resulting in greater yields at less negative potentials, of the active electrocatalyst for CO_2 reduction.



The large increase in electrocatalytic activity of $\text{Mo}(\text{bpy})(\text{CO})_4$ when a small (10% vol.) amount of NMP is added to an electrolyte solution is shown to be due to a potential dependent solvent restructuring of the double layer that leads to reorientation of $\text{Mo}(\text{bpy})(\text{CO})_4$ at the electrode surface.

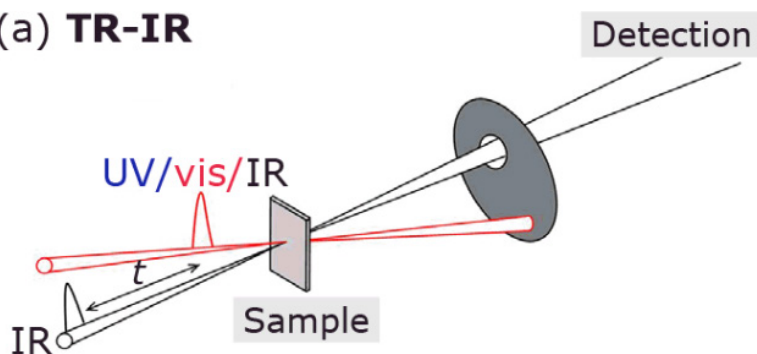
Reproduced from J. Am. Chem. Soc. 2024, 146, 11, 7130–7134 published by American Chemical Society under the terms of the **CC-BY-4.0 license**. doi: 10.1021/jacs.3c13076

Authors: A.M. Gardner, G. Neri, B. Siritanaratkul, H. Jang, K.H. Saeed, P.M. Donaldson, **A.J. Cowan** ✉

Ultrafast spectroscopy at the Central Laser Facility: Applications to the study of commercially relevant materials

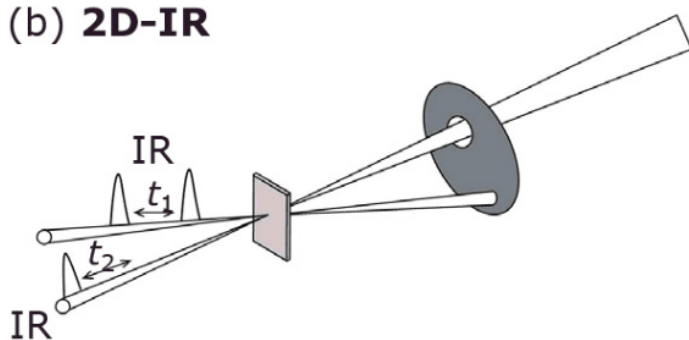
In this article, we will examine ultrafast spectroscopy techniques and applications, covering time-resolved infrared (TR-IR) spectroscopy, time resolved visible (TA) spectroscopy, two-dimensional infrared (2D-IR) spectroscopy, Kerr-gated Raman spectroscopy, time-resolved Raman and surface sum-frequency generation (SSFG) spectroscopy. In addition to introducing each technique, we will cover some basics, such as what kinds of lasers are used and discuss how these techniques are applied to study a diversity of chemical problems such as photocatalysis, photochemistry, electrocatalysis, battery electrode characterisation, zeolite characterisation and protein structural dynamics.

(a) TR-IR



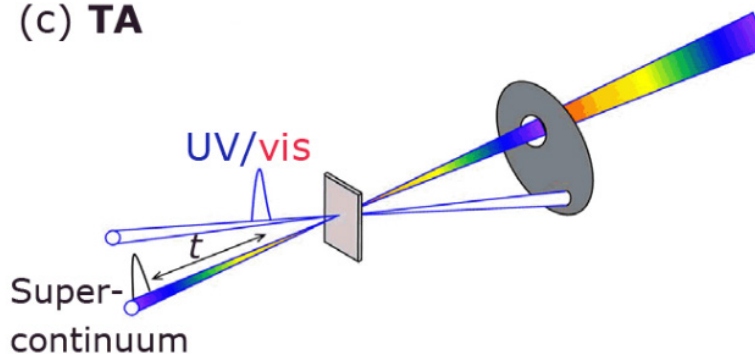
Example laser beam configurations for ultrafast spectroscopy: (a) TR-IR with UV-visible-IR pumping

(b) 2D-IR



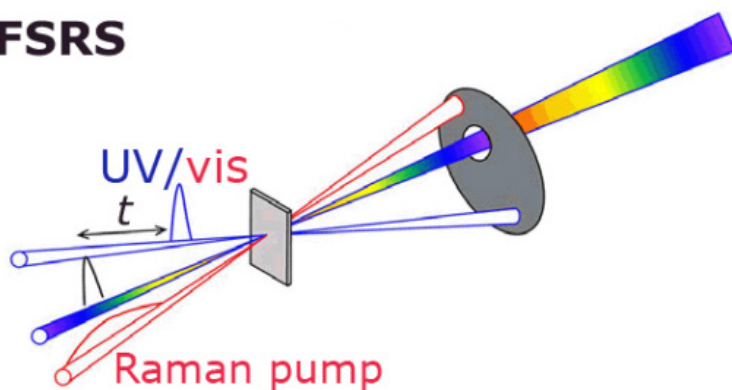
(b) 2D-IR

(c) TA



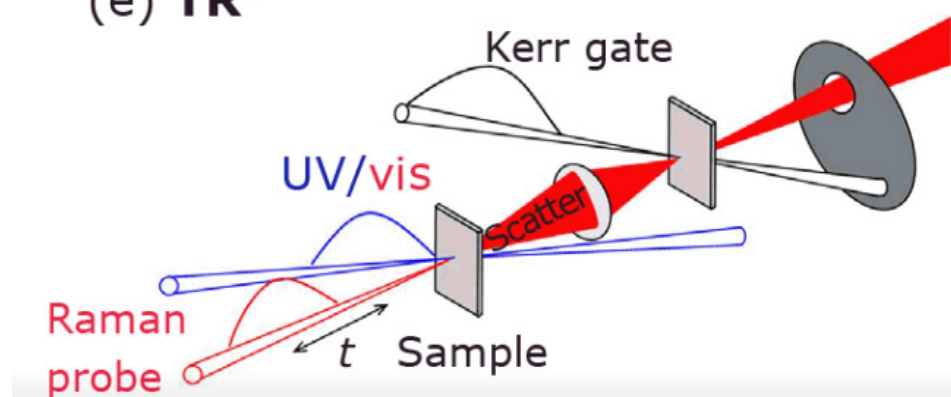
(c) TA (transient visible absorption spectroscopy)

(d) **FSRS**



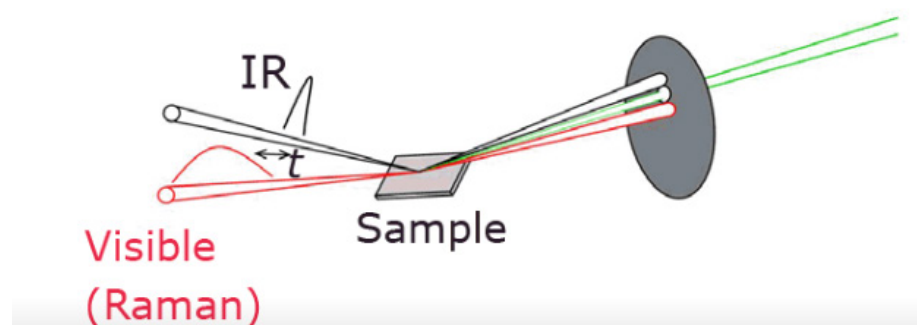
(d) FSRS

(e) **TR³**



(e) Kerr-gated TR3

(f) **IR-vis SSFG**



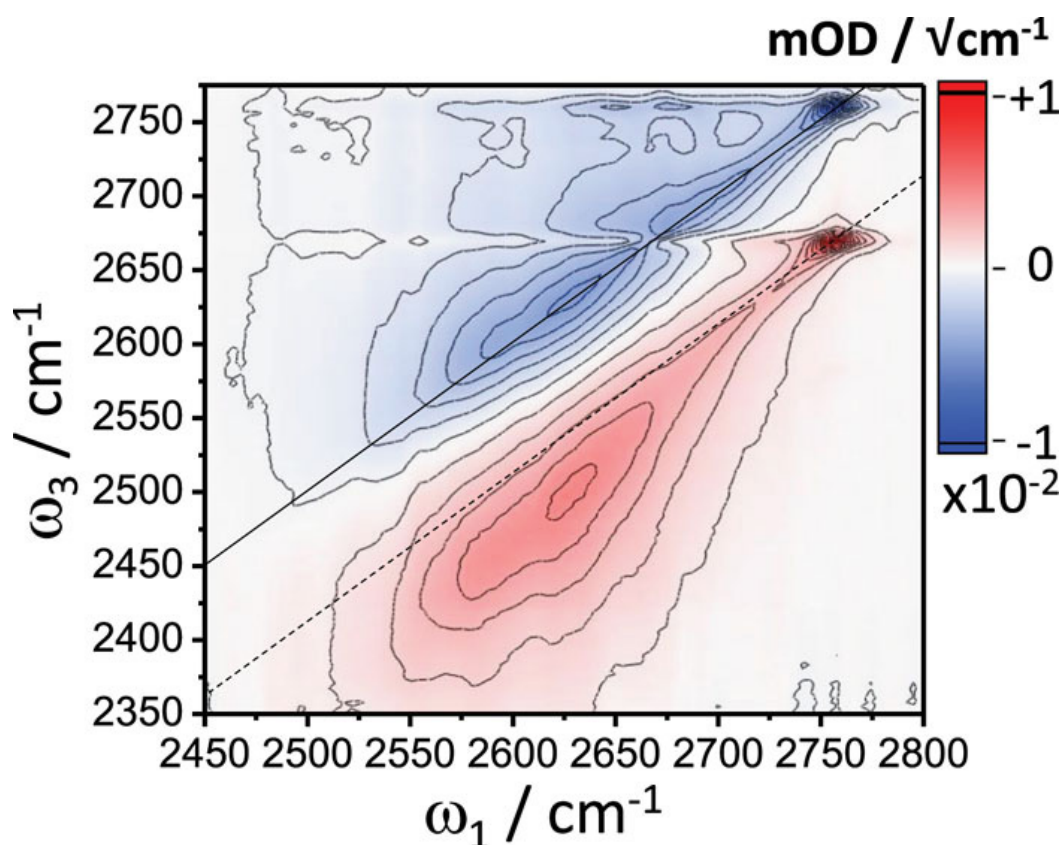
(f) IR-visible SSFG

Reproduced from Johnson Matthey Technol. Rev., 2024, 68, (4), 503–520, published by Johnson Matthey under the terms of the **CC-BY-4.0 license**. doi: 10.1595/205651324X17092043851525

Authors: P.M. Donaldson ✉, I.V. Sazanovich, P. Malakar, S. Maiti, M. Towrie, G.M. Greetham ✉

The 2D-IR spectrum of hydrogen-bonded silanol groups in pyrogenic silica

Pyrogenic silica is a form of amorphous silica with a high surface area and a heterogeneous distribution of silanol hydroxyl terminations and defects. In this work, the interesting and unusual form of the hydroxyl-stretch 2D-IR spectrum of pyrogenic silica is presented and explored in the deuterated (deuteroxyl) form. Transition dipole couplings between hydrogen-bonded and non-hydrogen-bonded silanol groups give a distinct cross-peak in the 2D-IR spectrum, displaying interstate coherence oscillations during the 2D-IR experimental waiting time. The strong asymmetry about the diagonal is proposed to be the result of both the relatively small transition dipole coupling strength and the extreme differences in the width of the hydrogen-bonded and non-hydrogen-bonded silanol bands. The resulting interference of negative and positive cross-peaks has minimal intensity in the below-diagonal $\omega_3 < \omega_1$ region of the spectrum. An additional strong positive cross-peak is observed at a position in the 2D-IR spectrum inconsistent with transition dipole coupling. An assignment as a fifth order effect is proposed.



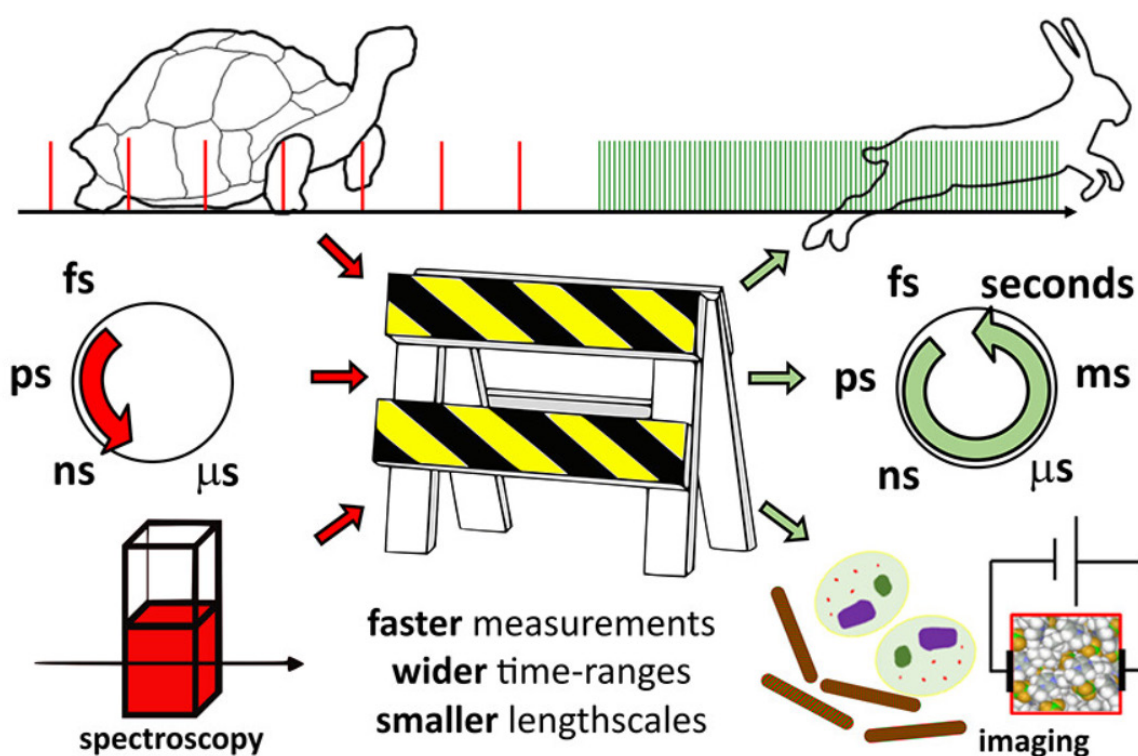
The 2D-IR spectrum of deuterated pyrogenic silica held at 175 °C. The diagonal of the spectrum is indicated by a solid black line. The dotted line parallel to the diagonal is offset by the non-hydrogen-bonded SiOD anharmonicity Δ_b , revealing the increase in anharmonicity with decreasing wavenumber. The waiting time (t_2) is 600 fs and polarization (XXYY). The first five contour lines reach an amplitude of $5 \times 10^{-3} \text{ mOD}/\sqrt{\text{cm}^{-1}}$.

Reproduced from J. Chem. Phys. 160, 104204 (2024) under the **CC-BY-4.0** license.
doi: 10.1063/5.0193551

Author: P.M. Donaldson ✉

Breaking barriers in ultrafast spectroscopy and imaging using 100 kHz amplified Yb-laser systems

There is now a technology shift occurring in ultrafast spectroscopy, made possible by new Yb-based lasers, that is opening exciting new experiments in the chemical and physical sciences. Amplified Yb-based lasers are not only more compact and efficient than their predecessors but also, most importantly, operate at many times the repetition rate with improved noise characteristics in comparison to the previous generation of Ti:sapphire amplifier technologies. Taken together, these attributes are enabling new experiments, generating improvements to long-standing techniques, and affording the transformation of spectroscopies to microscopies. This Account aims to show that the shift to 100 kHz lasers is a transformative step in nonlinear spectroscopy and imaging. We are convinced that Yb-based 100 kHz laser systems will soon become a standard of femtosecond laser technology, replacing many Ti:Sapphire lasers applications. Their improved parameters will not only make already existing experiments easier, better, and faster, but also allow for conceptually new experiments and lower barriers to starting an ultrafast spectroscopy laboratory.

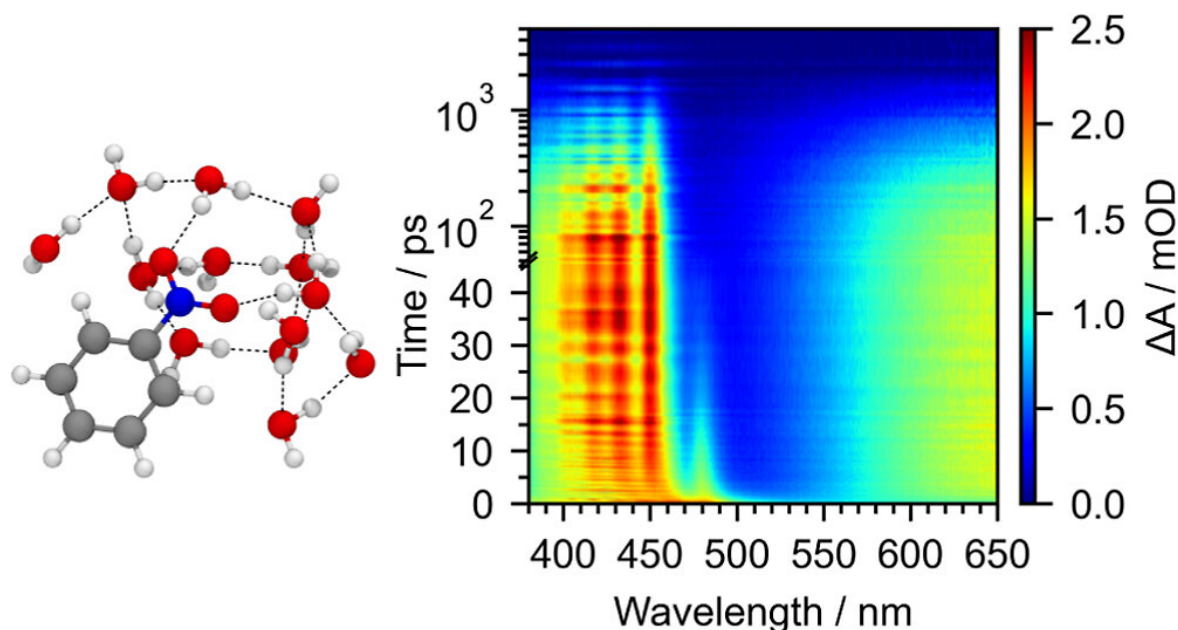


Taken from Acc. Chem. Res. 2023, 56, 15, 2062–2071, published by American Chemical Society under the terms of the **CC-BY-4.0 license**. doi: 10.1021/acs.accounts.3c00152

Authors: P.M. Donaldson ✉, G.M. Greetham, C.T. Middleton, B.M. Luther, M.T. Zanni, P. Hamm ✉, A.T. Krummel ✉

Unravelling the ultrafast photochemical dynamics of nitrobenzene in aqueous solution

Nitroaromatic compounds are major constituents of the brown carbon aerosol particles in the troposphere that absorb near-ultraviolet (UV) and visible solar radiation and have a profound effect on the Earth's climate. The primary sources of brown carbon include biomass burning, forest fires, and residential burning of biofuels, and an important secondary source is photochemistry in aqueous cloud and fog droplets. Nitrobenzene is the smallest nitroaromatic molecule and a model for the photochemical behavior of larger nitroaromatic compounds. Despite the obvious importance of its droplet photochemistry to the atmospheric environment, there have not been any detailed studies of the ultrafast photochemical dynamics of nitrobenzene in aqueous solution. Here, we combine femtosecond transient absorption spectroscopy, time-resolved infrared spectroscopy, and quantum chemistry calculations to investigate the primary steps following the near-UV ($\lambda \geq 340$ nm) photoexcitation of aqueous nitrobenzene. To understand the role of the surrounding water molecules in the photochemical dynamics of nitrobenzene, we compare the results of these investigations with analogous measurements in solutions of methanol, acetonitrile, and cyclohexane. We find that vibrational energy transfer to the aqueous environment quenches internal excitation, and therefore, unlike the gas phase, we do not observe any evidence for formation of photoproducts on timescales up to 500 ns. We also find that hydrogen bonding between nitrobenzene and surrounding water molecules slows the S_1/S_0 internal conversion process.



On the left: the calculated microsolvated structure of nitrobenzene in water environment. On the right: 2D-plot representation of the Transient Absorption data for nitrobenzene in water.

Reproduced from J. Am. Chem. Soc. 2024, 146, 15, 10407–10417, published by American Chemical Society under the terms of the **CC-BY-4.0 license**. doi: 10.1021/jacs.3c13826

Authors: N.A. Lau, D. Ghosh, S. Bourne-Worster, R. Kumar, W.A. Whitaker, J. Heitland, J.A. Davies, G. Karras, I.P. Clark, G.M. Greetham, G.A. Worth, A.J. Orr-Ewing, **H.H. Fielding** ✉

Background correction of time-resolved infrared spectroscopy data for the ‘tricky’ transcriptional regulator protein, B₁₂-dependent CarH

Time-resolved infrared (TRIR) spectroscopy is a powerful method providing information on excited state dynamics, conformational changes, intermolecular interactions and solvation. However, TRIR measurements on biological samples can be challenging, particularly when working close to the detection limit due to low sample concentration. This article will discuss how we correct for a delay-dependent step-like background pattern attributed to the detectors from the Central Laser Facilities LIFETIME instrument. TRIR data were collected for wildtype and variant chromophore binding domains of the photoreceptor protein B₁₂-dependent CarH, in addition to the full-length protein bound to DNA. This work may be of use to those who study challenging biological samples that are limited in quantity and/or produce low signals where background signal hinders a meaningful kinetic analysis. It also builds on our previous study, where we introduced a new method for handling/measuring light sensitive proteins in small volumes.

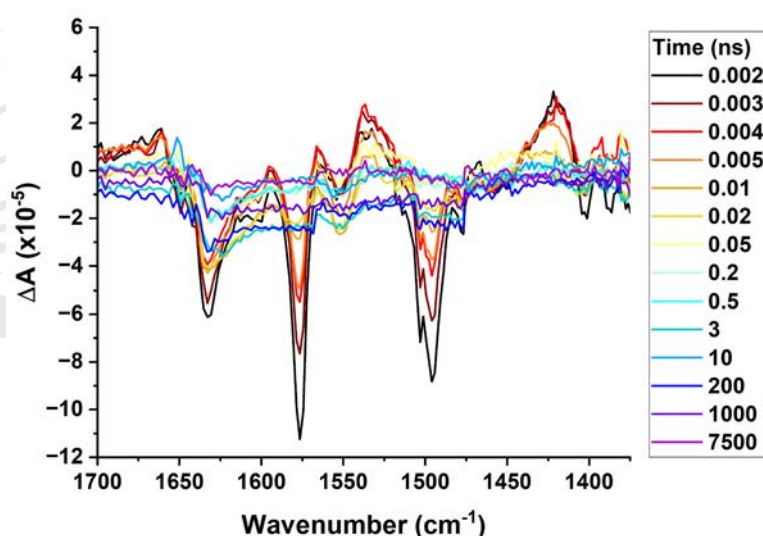


Figure 1: Raw TRIR difference spectra for T-WT CarH relative to the ground state between 2 ps–7.5 μ s following photoexcitation at 525 nm and averaged over five repeats. A block-like background pattern is evident, which originates from the detector and varies with delay time.

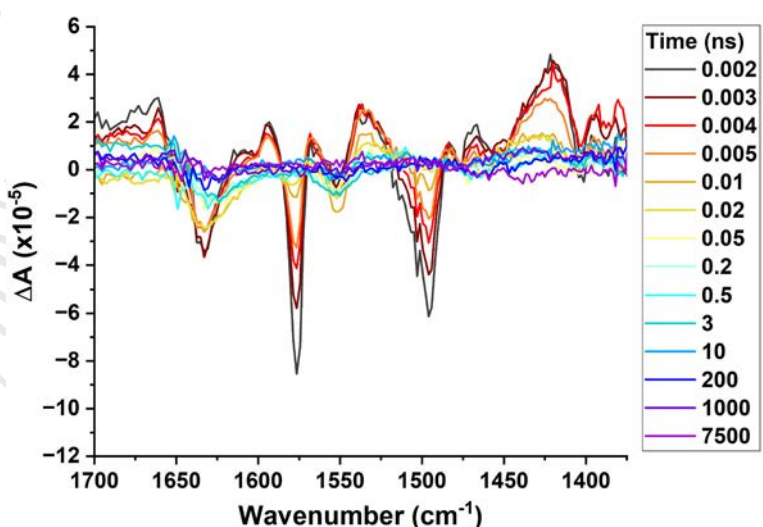
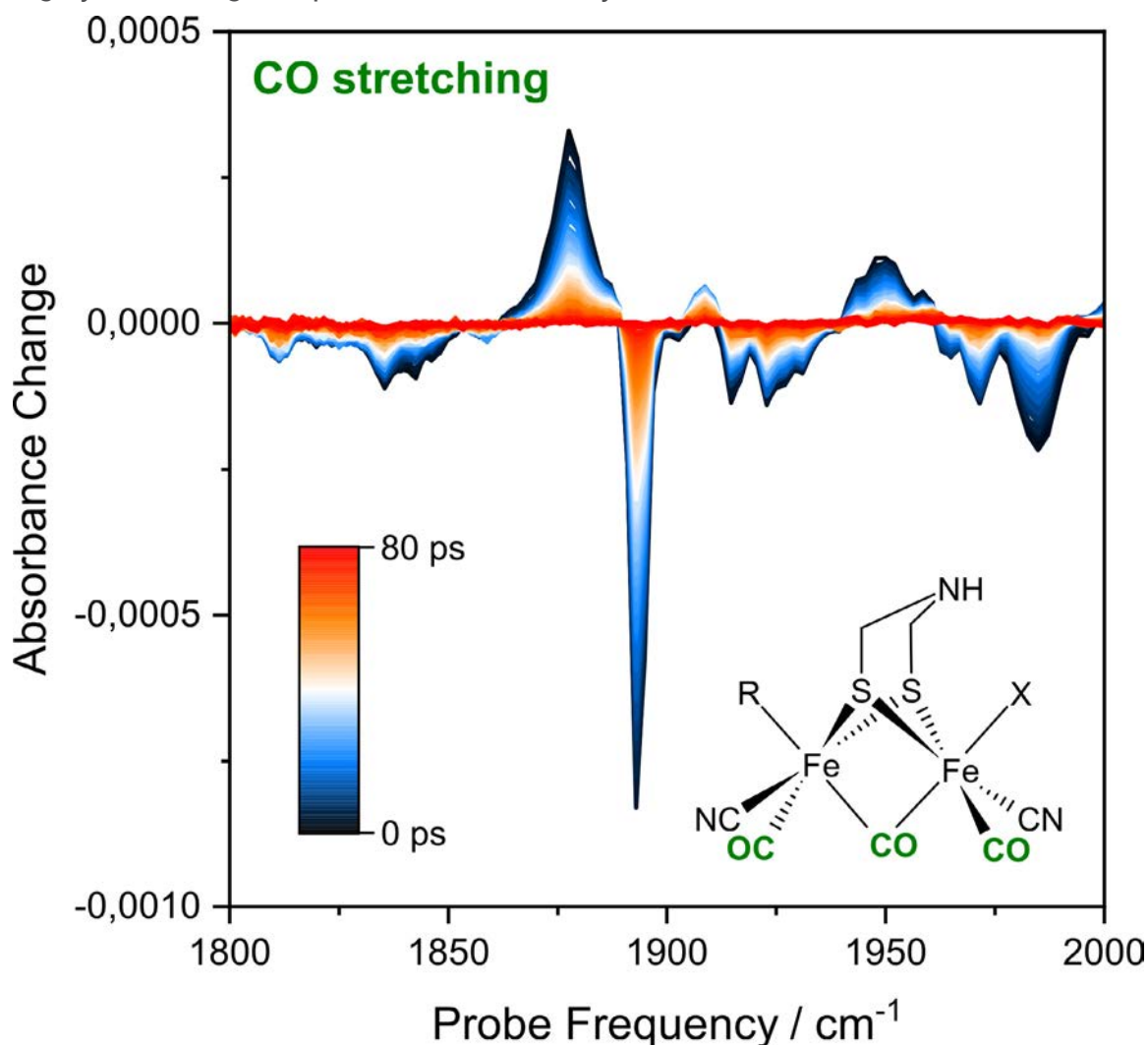


Figure 2: Corrected TRIR difference spectra for T-WT CarH relative to the ground state between 2 ps–7.5 μ s following photoexcitation at 525 nm and averaged over five repeats. The block-like background pattern evident in the raw data has been removed.


Authors: E. Wall, I.V. Sazanovich, M. Kurttila, I.S. Camacho, N.T. Hunt, A.R. Jones, S. Hay ✉

Progress in the 2D-IR characterisation of hydrogenases at Ultra

Hydrogenases are metalloenzymes that catalyse the cleavage and evolution of molecular hydrogen (H_2), a perfectly clean fuel. Due to the presence of biologically uncommon CO and CN⁻ ligands at the catalytic metal sites of hydrogenases, infrared (IR) spectroscopy is an ideal technique for studying these enzymes. 2D-IR and $IR_{\text{pump}}-IR_{\text{probe}}$ experiments performed at Ultra have previously gained detailed insights into the structure and dynamics of [NiFe] hydrogenases that cannot be obtained by linear IR absorption spectroscopy. Here we report on a twofold extension of this approach. On the one hand, we have obtained, for the first time, nonlinear IR spectra of more complex [FeFe] hydrogenases (see Figure). On the other hand, preliminary *in vivo* 2D-IR spectra of a [NiFe] hydrogenase within live cells were obtained by using an approach for probing highly scattering samples that was recently established at Ultra.

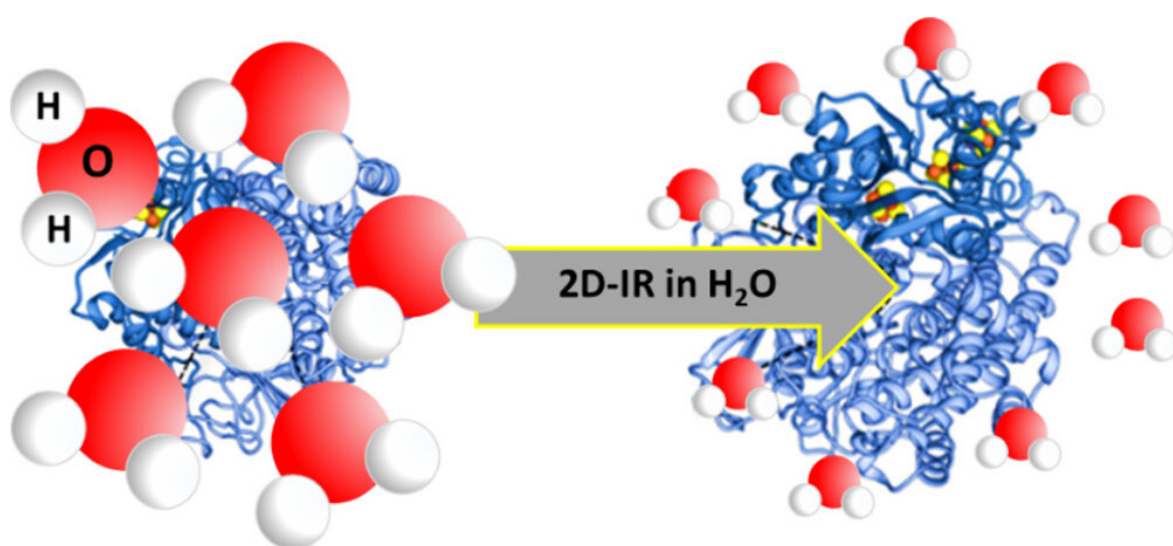


$IR_{\text{pump}}-IR_{\text{probe}}$ spectrum of reduced [FeFe] hydrogenase. Signals reflect stretching vibrations of CO ligands bound to the active site (see inset).

Authors: C.C.M. Bernitzky, M. Horch , D.M. Vaithyanathan, P. Donaldson, G.M. Greetham, I. Sazanovich, O. Lenz, J. Schoknecht, J.A. Birrell, P. Rodríguez Maciá

Using 2D-IR Spectroscopy to Measure the Structure, Dynamics, and Intermolecular Interactions of Proteins in H₂O

Infrared (IR) spectroscopy probes molecular structure at the level of the chemical bond or functional group. In this Account, a series of studies applying 2D-IR to study the spectroscopy and dynamics of proteins in H₂O-rich solvents is reviewed. A comparison of IR absorption spectroscopy and 2D-IR spectroscopy of protein-containing fluids is used to demonstrate the basis of the approach before a series of applications is presented. These range from measurements of fundamental protein biophysics to recent applications of machine learning to gain insight into protein–drug binding in complex mixtures. An outlook is presented, considering the potential for 2D-IR measurements to contribute to our understanding of protein behaviour under near-physiological conditions, along with an evaluation of the obstacles that still need to be overcome.



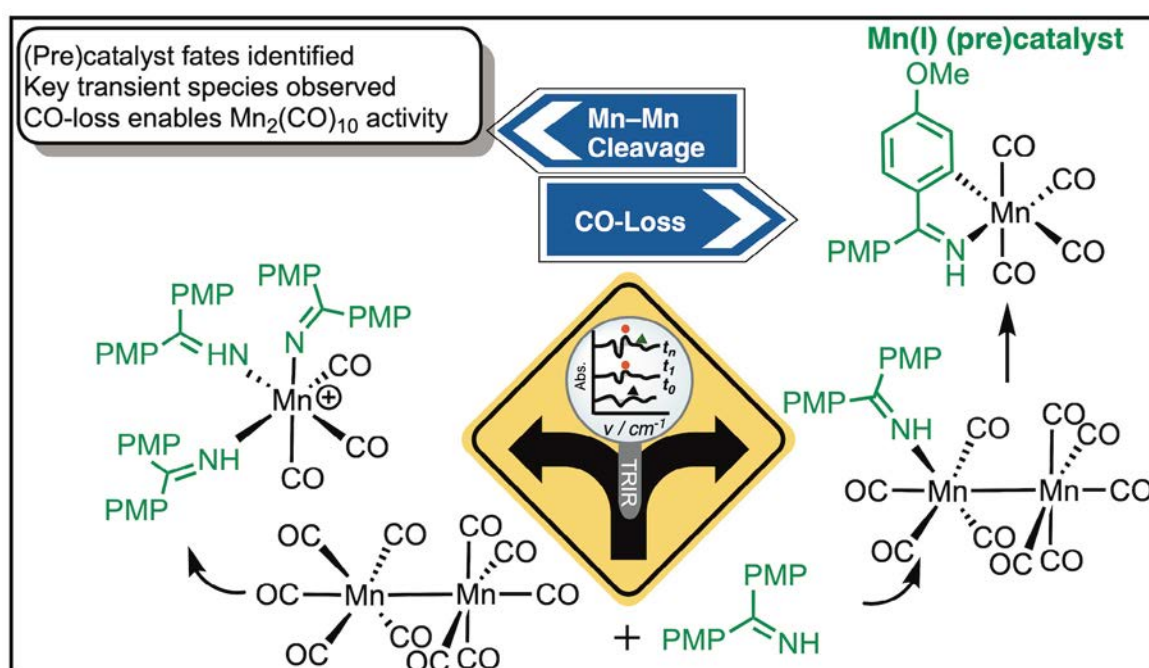
2D-IR spectroscopy can provide the ability to measure protein amide I spectra in H₂O-rich solutions without the need for isotopic substitution or complex data processing.

Taken from Acc. Chem. Res. 2024, 57, 5, 685–692 published by the American Chemical Society under the terms of the **CC-BY-4.0 license**. doi: 10.1021/acs.accounts.3c00682

Authors: N.T. Hunt ✉

The importance of understanding (pre)catalyst activation in versatile C–H bond functionalisations catalysed by $[\text{Mn}_2(\text{CO})_{10}]$

Mn-catalysed reactions offer great potential in synthetic organic and organometallic chemistry and the success of Mn carbonyl complexes as (pre) catalysts hinges on their stabilisation by strong field ligands enabling Mn(I)-based, redox neutral, catalytic cycles. The mechanistic processes underpinning the activation of the ubiquitous Mn(0) (pre)catalyst $[\text{Mn}_2(\text{CO})_{10}]$ in C–H bond functionalisation reactions is now reported for the first time. By combining time-resolved infra-red (TRIR) spectroscopy on a ps–ms timescale and *in operando* studies using *in situ* infra-red spectroscopy, insight into the microscopic bond activation processes which lead to the catalytic activity of $[\text{Mn}_2(\text{CO})_{10}]$ has been gained. Using an exemplar system, based on the annulation between an imine, 1, and Ph_2C_2 , 2, TRIR spectroscopy enabled the key intermediate $[\text{Mn}_2(\text{CO})_9(1)]$, formed by CO loss from $[\text{Mn}_2(\text{CO})_{10}]$, to be identified. *In operando* studies demonstrate that $[\text{Mn}_2(\text{CO})_9(1)]$ is also formed from $[\text{Mn}_2(\text{CO})_{10}]$ under the catalytic conditions and is converted into a mononuclear manganacycle, $[\text{Mn}(\text{CO})_4(\text{C}^*\text{N})]$ (C^*N = cyclometallated imine), a second molecule of 1 acts as the oxidant which is, in turn, reduced to an amine. As $[\text{Mn}(\text{CO})_4(\text{C}^*\text{N})]$ complexes are catalytically competent, a direct route from $[\text{Mn}_2(\text{CO})_{10}]$ into the Mn(I) catalytic reaction coordinate has been determined. Critically, the mechanistic differences between $[\text{Mn}_2(\text{CO})_{10}]$ and Mn(I) (pre)catalysts have been delineated, informing future catalyst screening studies.

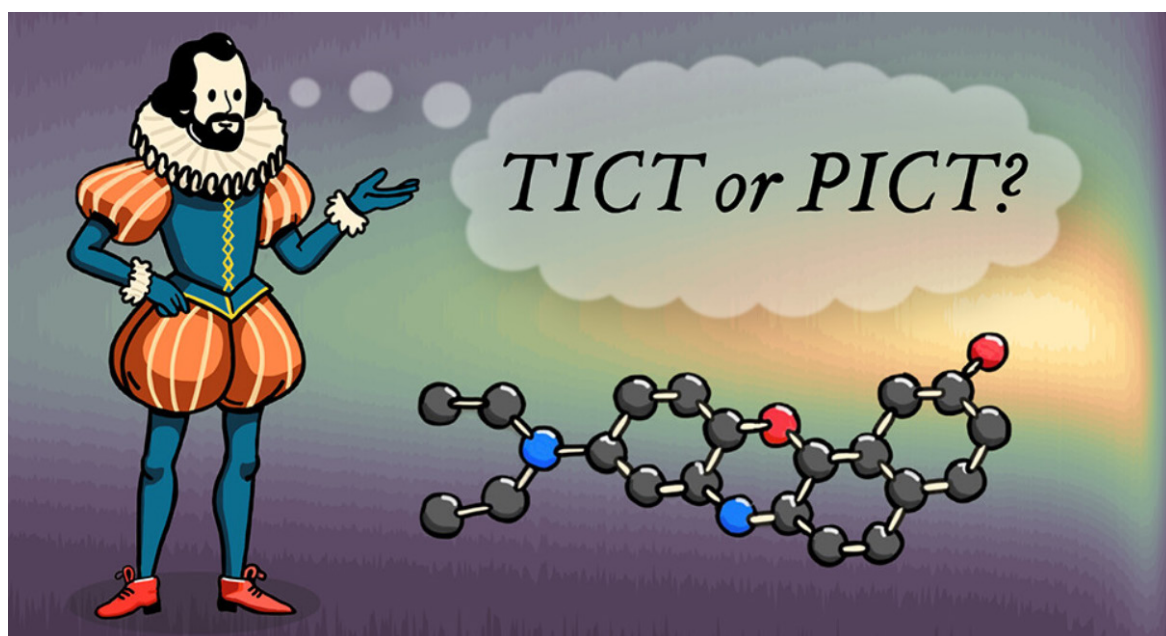


Reproduced from Chem. Sci., 2024, 15, 9183 published by the Royal Society of Chemistry under the terms of the **CC-BY-3.0 license**. doi: 10.1039/d4sc01215a

Authors: J.B. Eastwood, T.J. Burden, L. Anders Hammarback, C. Horbaczewski, T.F.N. Tanner, I.P. Clark, G.M. Greetham, M. Towrie, **I.J.S. Fairlamb** ✉, **J.M. Lynam** ✉

Nile Red fluorescence: Where's the twist?

Nile Red is a fluorescent dye used extensively in bioimaging due to its strong solvatochromism. The photophysics underpinning Nile Red's fluorescence has been disputed for decades, with some studies claiming that the dye fluoresces from two excited states and/or that the main emissive state is twisted and intramolecular charge-transfer (ICT) in character as opposed to planar ICT (PICT). To resolve these long-standing questions, a combined experimental and theoretical study was used to unravel the mechanism of Nile Red's fluorescence. Time-resolved fluorescence measurements indicated that Nile Red emission occurs from a single excited state. Theoretical calculations revealed no evidence for a low-lying TICT state, with the S_1 minimum corresponding to a PICT state. Ultrafast pump-probe spectroscopic data contained no signatures associated with an additional excited state involved in the fluorescence decay of Nile Red. Collectively, these data in polar and nonpolar solvents refute dual fluorescence in Nile Red and definitively demonstrate that emission occurs from a PICT state.



Reproduced from J. Phys. Chem. B 2024, 128, 47, 11768–11775, published by the American Chemical Society under the terms of the **CC-BY-4.0 license**. doi: 10.1021/acs.jpcb.4c06048

Authors: C. Gajo, D. Shchepanovska, J.F. Jones, G. Karras, P. Malakar, G.M. Greetham, O.A. Hawkins, C.J.C. Jordan, **B.F.E. Curchod** ✉, **T.A.A. Oliver** ✉

Operational Statistics

Gemini

During the reporting year, April 2023–April 2024, a total of six complete experiments were delivered in the Astra-Gemini Target Area. In total, 31 high power laser experimental weeks were delivered to the Gemini Target Area. The delivered Gemini schedule is presented in Table 1.

Table 1: Gemini 2023/24 operational schedule.

Week Commencing	Activity	Week Commencing	Activity
7 January	Hooker 2221009	7 July	N/A
14 January		14 July	N/A
21 January		21 July	N/A
28 January		28 July	Doria (EU) 22210024
4 February	Extension	4 August	
11 February	N/A	11 August	
18 February	Pump laser service	18 August	
25 February	Gas alarm replacement	25 August	N/A
3 March	N/A	1 September	
10 March	Kettle 22210012	8 September	
17 March		15 September	N/A
24 March		22 September	Christmas break
31 March		29 September	
7 April		6 October	N/A
14 April	N/A	13 October	
21 April	PoC experiment 23315000	20 October	
28 April		27 October	N/A
5 May	N/A	3 November	N/A
12 May	N/A	10 November	Sarri 23210006
19 May	Beamline set-up	17 November	
26 May		24 November	
2 June	Jaroszynski 22210025	1 December	
9 June		8 December	Configuration changes Beam stabilisation
16 June		15 December	
23 June		22 December	
30 June		29 December	
		5 January	

The availability of the Gemini laser system (delivery to the Gemini Target Area) was 85% during normal working hours, rising to 131% with time made up from running out of normal working hours. The reliability of the Gemini laser was 89%. An individual breakdown of the availability and reliability for the TA3 experiments conducted is presented in Figure 1.

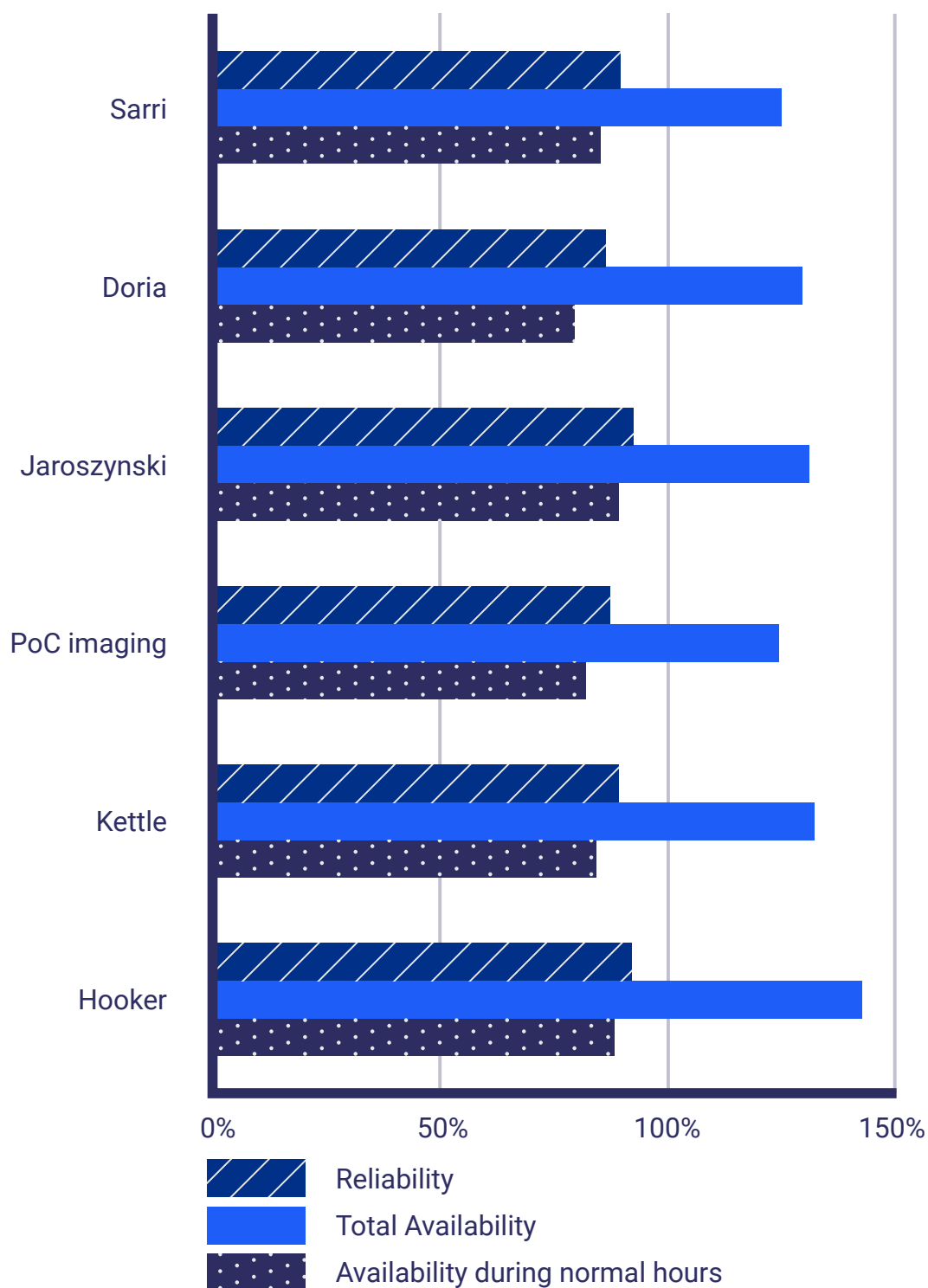


Figure 1: 2023/24 TA3 Operational statistics.

The high levels of total availability were made possible by the continued unique operational model employed on Gemini, which involves running the laser late into the evening. In addition, frequent weekend operational days were made available.

Lasers for Science Facility

Artemis facility

During this reporting period, the UK User Community applied for 74.5 weeks of peer-reviewed access to the Artemis facility, of which 29 weeks were awarded, representing an over-subscription ratio of 2.57. A total of five unique user groups performed six scheduled experiments. Figure 2 shows that atomic, molecular and optical were the most popular experiment subjects conducted.

4.08 weeks of downtime and 22.36 of additional weeks of access were reported for the scheduled experiments, corresponding to a total of 35.17 weeks access time delivered to the User Community. A total of two formal reviewed publications were recorded throughout the year.

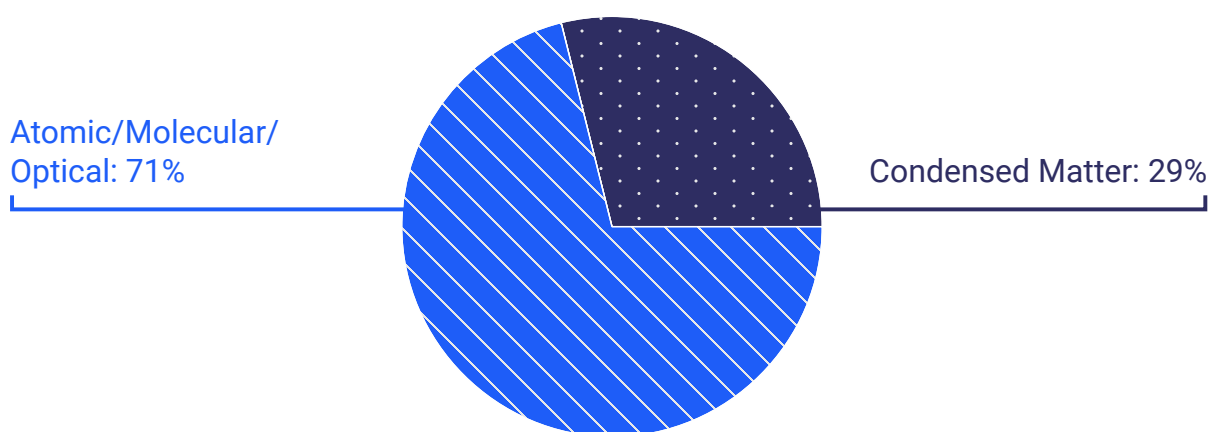


Figure 2: Artemis experiments by subject

Octopus facility

During this reporting period, the UK User Community applied for 167 weeks of peer-reviewed access to the Octopus facility, of which 90 weeks were awarded, representing an over-subscription ratio of 1.86. A total of 22 unique user groups performed 27 scheduled experiments. In addition, 16 days proof of concept experiments, 1 day of development and 49 days of commercial access were delivered. Figure 3 shows that Biology and Bio-materials were the most popular experiment subject conducted.

27 hours of downtime were reported. A total of 13 formal reviewed publications were recorded throughout the year.

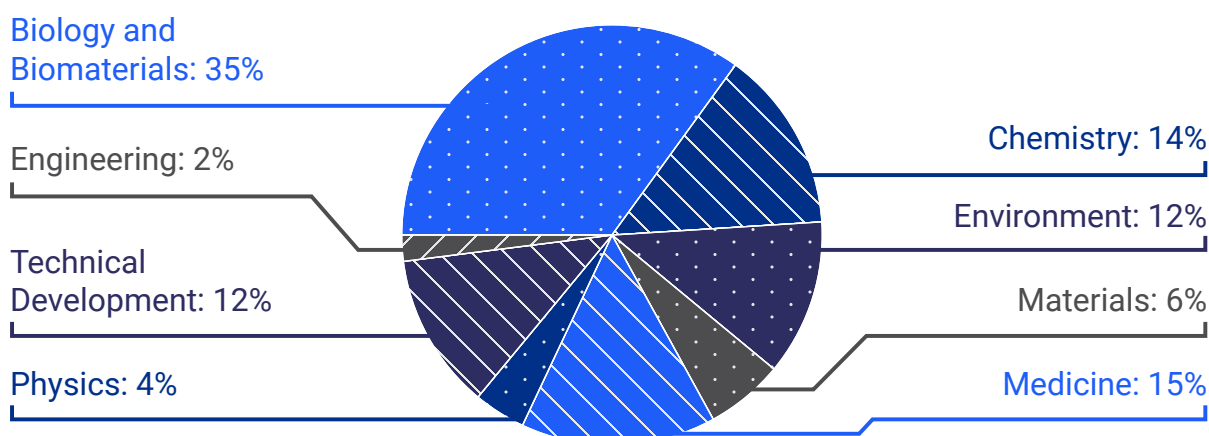


Figure 3: Octopus experiments by subject

Ultra facility

During this reporting period, the UK User Community applied for 76 weeks of peer-reviewed access to the Ultra facility, of which 50 weeks were awarded, representing an over-subscription ratio of 1.52. A total of 15 unique user groups performed 20 scheduled experiments. In addition, seven days proof of concept experiments and six weeks of commercial access were delivered. Figure 4 shows that Chemistry was the most popular experiment subject conducted.

145 hours of downtime and 587 additional hours of access were reported. A total of 22 formal reviewed publications were recorded throughout the year.

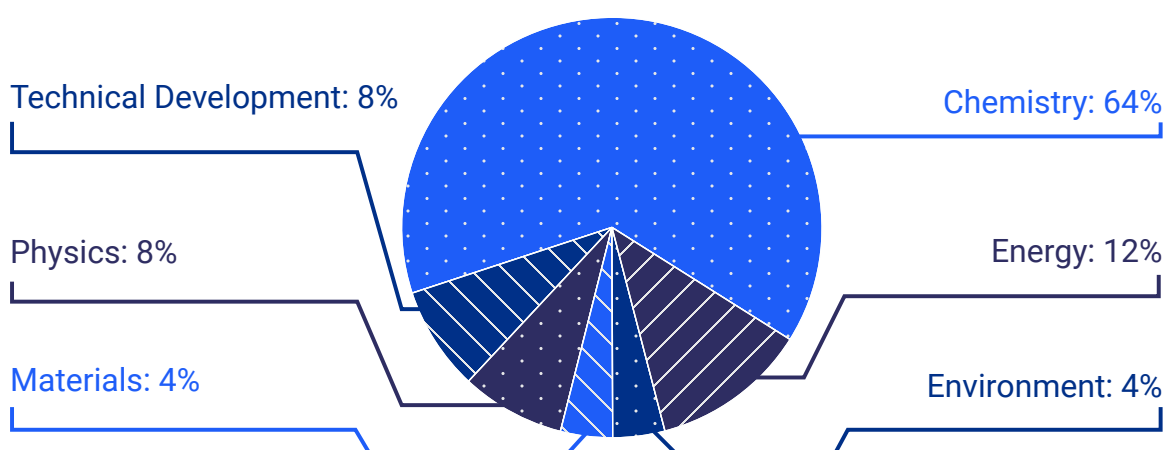


Figure 4: Ultra experiments by subject

User satisfaction feedback

Surveys completed by user groups after their experimental time indicate an average satisfaction rating of 91.6% over the five specified categories.

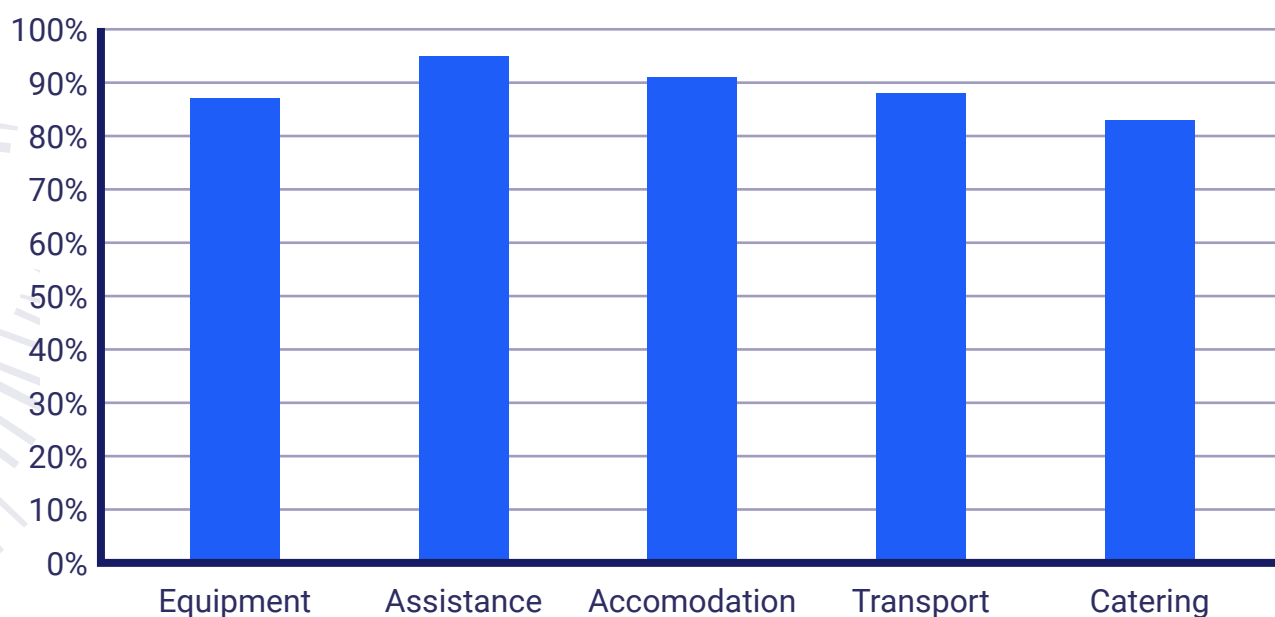


Figure 5: Average user satisfaction

Authors: B.C. Bateman ✉, M. Szynekiewicz, S.K. Roberts, E. Springate, A.D. Ward

Target Fabrication

This report details the target delivery of the Target Fabrication group for High Power Laser (HPL) experiments at the Central Laser Facility over the period spanning April 2023–March 2024, as well as showing historic target supply trends for reference. The Target Fabrication group provides a multitude of target components, technologies and characterisation services crucial to the success of the HPL programme. Following the shutdown of the Vulcan target areas in October 2023 in preparation for the Vulcan 20-20 upgrade, the group is offering “Vulcan Dark Period” support and is tasked with the manufacture of targets for Vulcan-aligned experiments conducted at other facilities.

Over the 2023/24 operating period, the Target Fabrication group provided targets for 12 experimental campaigns—five based on the Gemini laser, three on Vulcan TAW and one on Vulcan TAP at the CLF, along with two Vulcan Dark Period experiments at ZEUS-Michigan and ELI-NP, and one External Access campaign at Orion, AWE.

The vast majority of targets that the group manufactures are solid targets, although multi-component gas cell targets are regularly delivered. With the EPAC facility being commissioned in 2025, ultimately requiring 1–10 Hz target solutions, a liquid targetry system is in development giving the ability to create sub-micron films of deionized water as a high repetition rate target or plasma mirror solution. As such, the Target Fabrication group will be equipped to deliver targets comprising solid, liquid or gaseous media.

A solid target comprises virtually any material (metals, polymers and ceramics), coated to nanometrically precise thicknesses in a range of geometries and characterised to micron-scale precision to ensure they fall within tight tolerances. There is generally a difference between the type of target requested for Vulcan and those for Gemini experiments. Vulcan targets are typically more complex (for example single target assemblies on posts) with a focus on precision-assembly 3D microstructures and mass-limited targets. Gemini targets are typically less complex and more mass-manufacturable to accommodate the higher repetition rate of the laser. Typical Gemini targets include multi-layer or ultra-thin foils on arrays or tape substrates.

Supported Experiments

The 12 experimental campaigns supported over this operating period, along with a summary of the main target types requested, are shown in Table 2. Gemini TA2 experiments are not covered in the scope of this report. It is also worth noting that there is often significant variation in target numbers across each campaign; gas jet experiments for example may only request a few tens of targets such as alignment wires or filter packs whereas other experiments may request thousands of array or tape-based targets.

Table 2: Experimental campaigns supported by the Target Fabrication group and the types of targets requested over the 2023/24 operating period.

Experiment	Area	Main target types
0523 Kettle (22210012)	Gemini TA3	Multi-layer tapes, filter packs
0823 Jaroszynski (22210025)	Gemini TA3	Gas jet, alignment
1023 Doria (22210024)	Gemini TA3	Ultra-thin foil—arrays
0224 Sarri (23210006)	Gemini TA3	Gas jet, alignment
0324 Najmudin (23210013)	Gemini TA3	Gas cells
0523 McKenna (22210005)	Vulcan TAP	Ultra-thin foils—single posts
0523 Oliver (22210011)	Vulcan TAW	Thick foils—single posts, 3D microstructures, alignment
0623 Woolsey (22210003)	Vulcan TAW	Thick foils—single posts, filter packs
0623 Keenan	External: AWE	Thick foils—single posts, gas cells
0823 Fuchs (22210006)	Vulcan TAW	Thick foils—single posts
0224 Lancaster	Vulcan Dark Period: Michigan	Thick foils—arrays
1123 Ahmed	Vulcan Dark Period: ELI-NP	Ultra-thin foil—arrays

Target Complexity and Classification

Targets are classified as Class 1, Class 2 and Class 3, depending on their level of complexity or the level of research and planning required for their manufacture. While the definitions can be somewhat subjective, they are generally defined as follows:

- Class 1: require fewer specialist resources to manufacture. Materials are typically procured ‘off-the-shelf’ and minimal specialist equipment is required for assembly. Typical targets include several-micron-thick foils or alignment wires glued to posts.
- Class 2: require the use of specialist manufacturing equipment and knowledge, which would be a very involved process for a non-Target Fabrication specialist to replicate. Examples include multi-nanometre thin-films and multilayer coatings.
- Class 3: require long-term R&D projects to establish and perfect, often referred to as “high-specification targets”. Such targets include complex 3D assemblies, MEMS-components, low-density foams and multi-step/ etched tape targets. If the complexity of a Class 3 target derives from the development of an initial process or building/procuring specialist apparatus, then it may be downgraded from a Class 3 for subsequent experiments (such as multi-layer tape targets).

It is important to note that for the scope of this report there is a distinction between a “target” and a “component”. A component is any single item that is fabricated and issued for experimental delivery from the laboratory, which can include components with multiple individual targets on it. Thus, an array is a single component, which typically holds 25 targets. Similarly, a spool of tape is considered a single component, which contains many hundreds of targets per spool.

Target Supply

Over the 12 experiments supported over the 2023/24 operating period, a total of 7887 targets were issued.

79.8% (6291) of these targets were supplied to Vulcan-based experiments, and the remaining 20.2% (1596) were supplied to Gemini. Although Gemini is a higher repetition rate laser and typically commands larger target quantities compared to Vulcan, there are two reasons leading to this year's supply inversion:

- During this operating period there were a high number of gas jet/refillable gas cell shots on Gemini, which are not tracked for the scope of this report.
- Of the 6291 targets supplied to Vulcan-based experiments, 1241 targets were supplied to Vulcan TAW and TAP—the remaining 5050 were supplied to Dark Period supporting facilities, which were able to shoot array-based targets.

Figures 6 and 7 below shows the complexity breakdown of targets delivered to both Gemini and Vulcan-based experiments over the 2023/24 operating period.

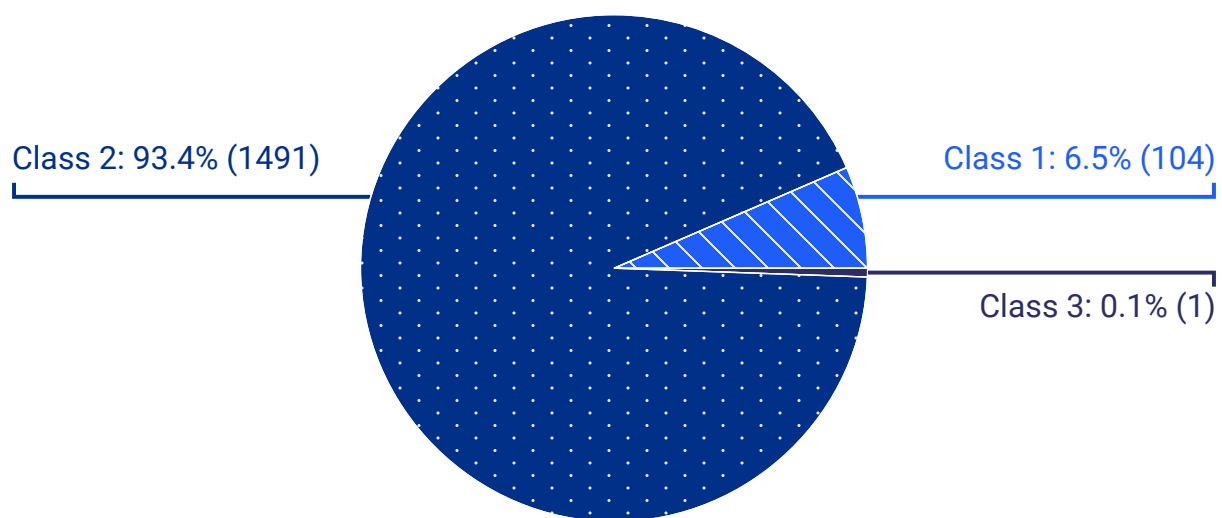


Figure 6: Target complexity breakdown (Class 1, 2 and 3 targets) delivered to Gemini experiments in 2023/24.

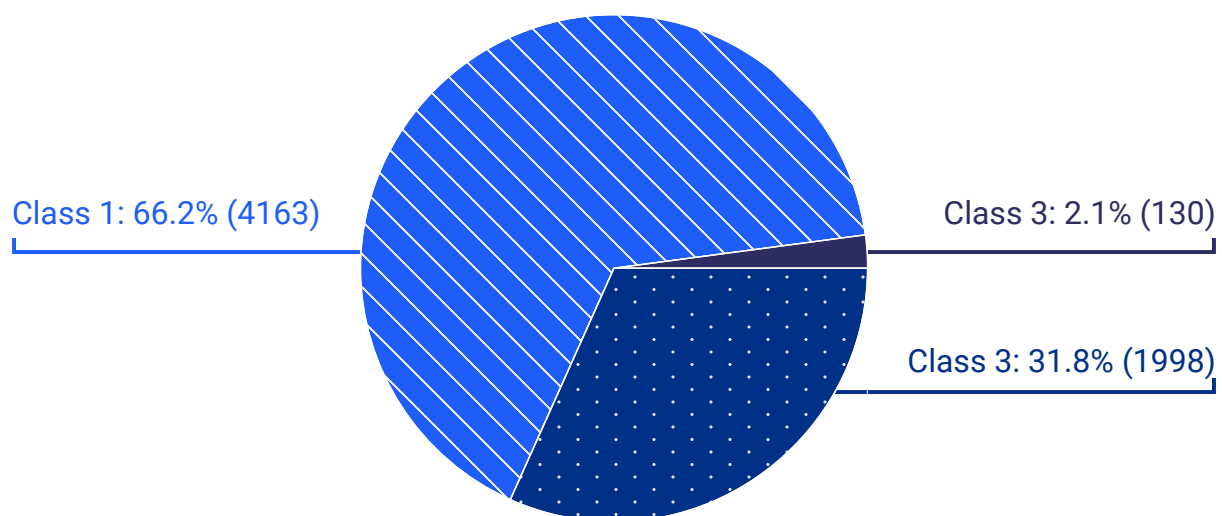


Figure 7: Target complexity breakdown (Class 1, 2 and 3 targets) delivered to Vulcan-based experiments in 2023/24.

Comparing Figures 6 and 7 shows that while Vulcan experiments generally requested a much higher percentage of simpler Class 1 targets, it also commanded a much higher (130 vs 1) quantity of the highest complexity of targets. This is due to the fact that as Vulcan operates on a lower repetition rate, and typically with only a few targets mounted in a single pumpdown cycle, precise alignment is crucial and thus a larger proportion of alignment (i.e. Class 1 targets) are necessary.

Gemini experiment requirements over the operating period comprised mainly of multi-layer tapes or ultra-thin foil arrays, and thus the vast majority of target requests are classified as Class 2 complexity. The fact that a much larger quantity of targets (i.e. in tape or array form) can be installed in a single pumpdown cycle means that a lower proportion of alignment targets are required.

Table 3: A detailed breakdown of target types supplied to each facility over the reporting period.

Target Type	Gemini	Vulcan-based
Alignment	16	156
Thick foils	88	4007
Ultra-thin foils	571	1993
Multi-layer foils	920	5
3D micro-structures	1	130
Foams	0	0
MEMS/Mass limited	0	0
Total	1596	6291

Target Supply Trends

Over the last 13 years (over which detailed target records have been tracked), there has been a steady, year-over-year increase on the number of targets requested. With the exception of 2021/22, which had no Gemini TA3 solid target experiments, there has been a significant increase in target supply over the last five years—especially evident between 2022 and 2024. This is driven by the development of both tape targetry technology and also the TAAS automated assembly robotic system^[2] within Target Fabrication, enabling much larger quantities of targets to be manufactured.

Figure 8 shows the total targets supplied in each operating period since 2011-2012.

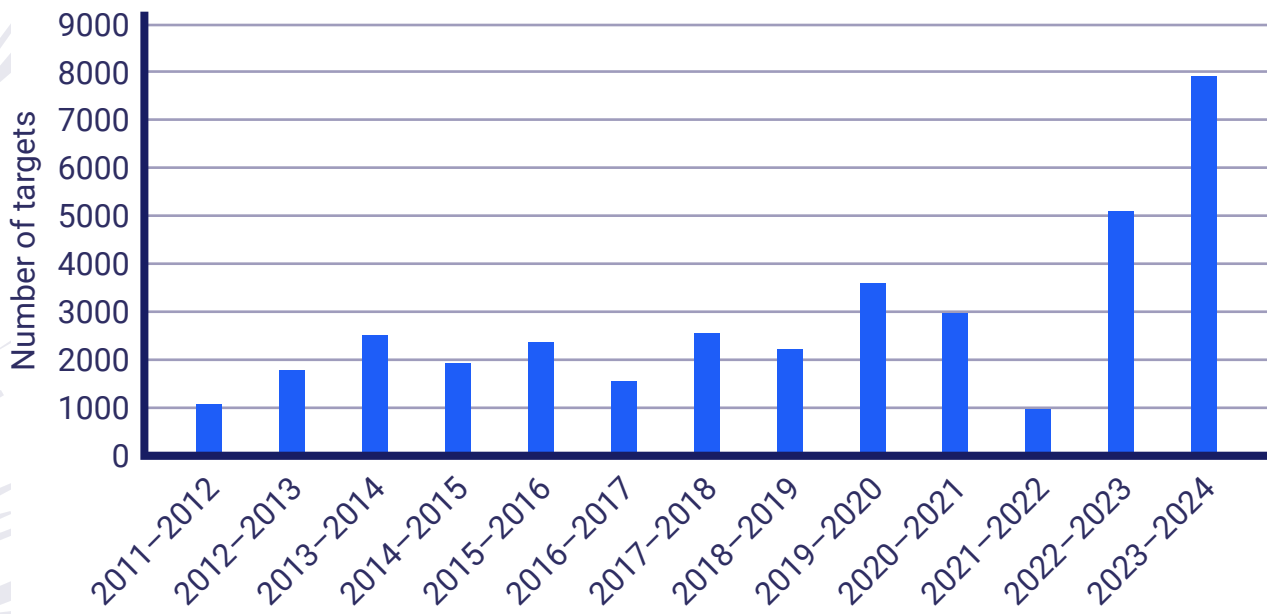


Figure 8: Total number of targets supplied to CLF HPL experiments over each operating period since 2011.

The number of targets supplied in a given year is dependent on experimental proposals, however, and depending on the target types necessary for each experiment this gives rise to fairly significant variability in target numbers year-on-year (e.g. gas jet vs arrays). The sharp supply increase over the last two years is expected to continue to rise, due to the commissioning of EPAC. As this is an applications-based facility, with 10 Hz repetition rate, it is likely that within the next few years solid target requests will be into the tens of thousands.

Quality Assurance

All materials, thin-film coatings, assembly components and characterisation for targets that are issued for HPL experiments are tracked wherever possible. This ensures there is traceability for any target defects if an anomalous result from the dataset following interaction is discovered. Although not currently certified to the ISO9001 QA standard, many of its processes are followed.

Some of the metrics that are tracked are target returns and modifications. This shows how many targets are: a) issued although not requested officially during the planning cycle of the experiment; b) modified during the course of an experiment; and c) returned during/after the experiment due to being out of specification or unable to be shot.

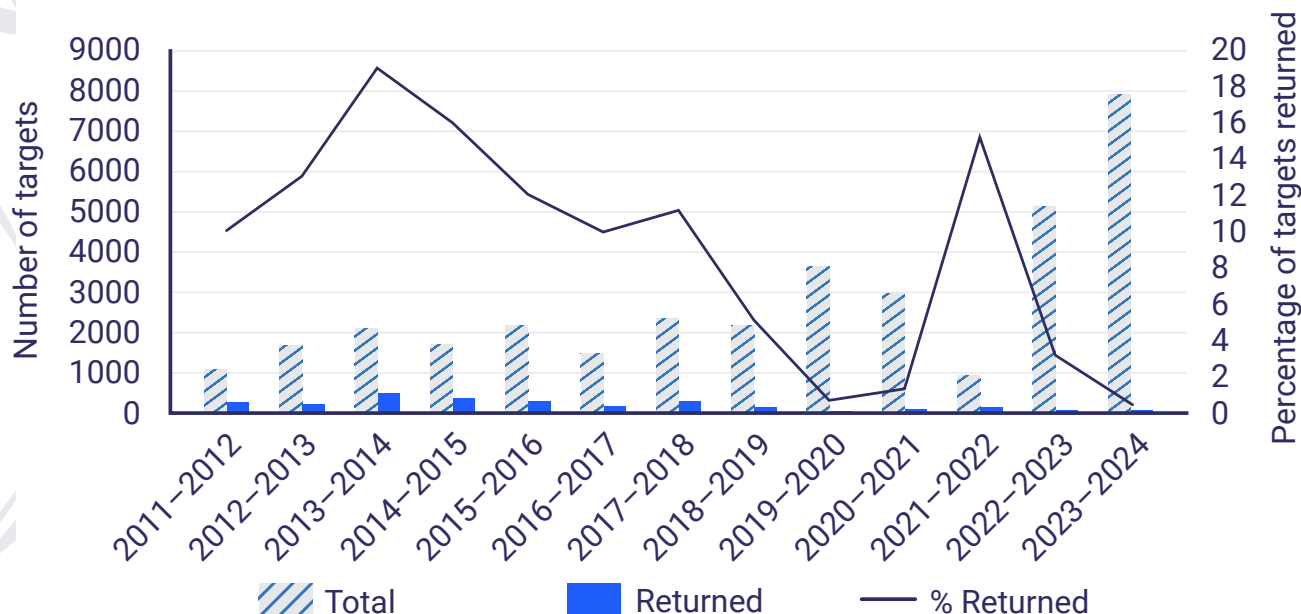


Figure 9: Total issued targets compared to the targets returned unshot or out of specification.

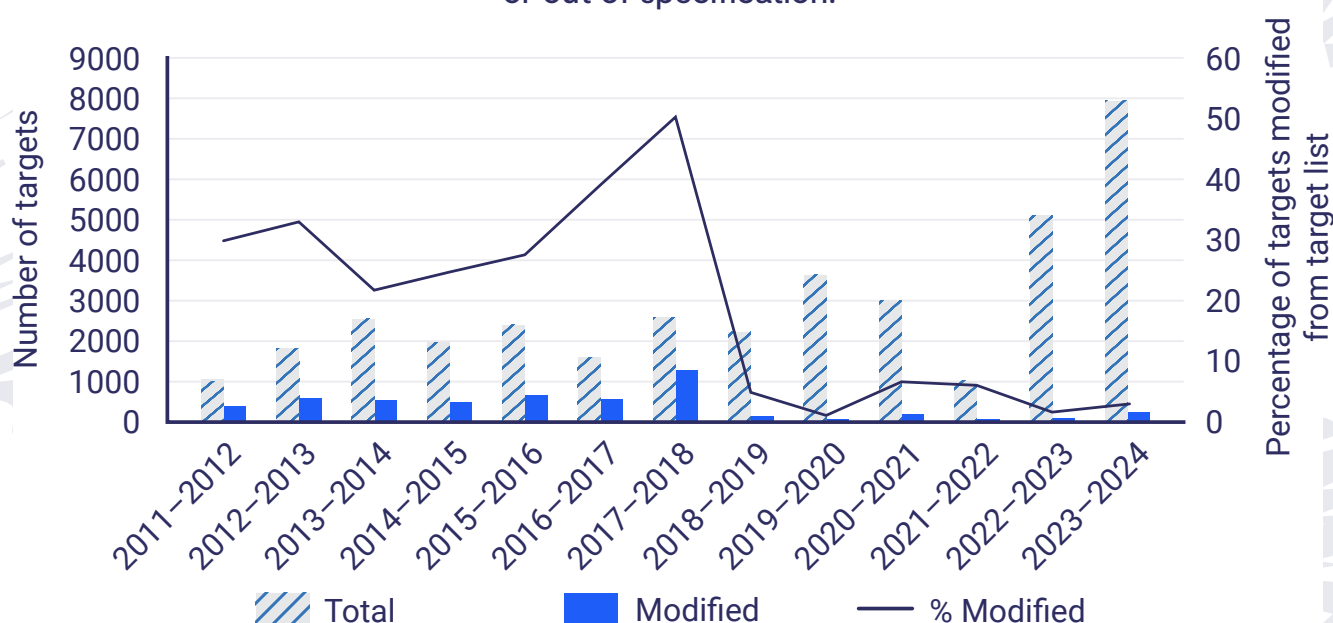


Figure 10: Total issued targets vs those that deviated from their signed-off specification in the planning cycle of the experiment.

As can be seen in Figure 9, the percentage of returned targets has significantly fallen over the last year—the primary reason for this is that a large proportion of the year's targets were issued to off-site experiments to support the Vulcan Dark Period, making target return very difficult or impossible in the scope of a limited time experiment. Further, due to the time-expense of manufacture of tape targets, and the fact that a single spool of tape contains several hundred targets, these are often not returned, somewhat skewing this metric.

Figure 10 shows the number of targets that did not match the specification that was signed off during the experimental planning cycle. Target requests are typically signed off 6–8 weeks prior to the beginning of the experiment, but Target Fabrication try to accommodate day-to-day changes in target design as the scientific aims of the experiment evolve. This is a significant benefit of having an in-house target fabrication capability. The decrease in modified target numbers is for a similar reason to that for target returns; as target requests become either more complex or there is an increase in shot numbers, sign-off has to be more absolute.

Future Targetry Supply

In collaboration with Queen's University Belfast and SLAC, the Target Fabrication group is developing a liquid targetry system capable of injecting nanometre-thick sheets of de-ionised water in vacuo, for both future Gemini experiments as well as a plasma mirror and potential ion acceleration source for EPAC EA2. The first experiment using this system is scheduled for July 2025.

The group continues to develop ultra-stable tape drive systems^[3] as well improving the method for fabrication of multi-layered complex tape targets on spools. A Reel-to-Reel system, allowing a two order of magnitude increase in tape target manufacture, is due for commissioning in 2025 and will integrate the Target Fabrication group's extensive knowledge and in-house technologies to further advance its capability in this field for EPAC delivery.

External Contracts

In the reporting period 2023/24, the operations of Scitech Precision Limited (SPL), the target fabrication commercial spin out, supported the user community on external facilities and continued to expand its capabilities in high repetition rate target manufacture with the delivery of tape drive systems to high power laser facilities around the world. The expansion of the user community across Europe and in the US drove sales of targets to a wider array of customers.

A total of 33 (slightly down from 36 in 2022/23) institutions engaged with SPL over this period for 113 individual contracts (down from 115 last year). However, the turnover increased to a record value of £407k, which is a 35% increase and represents a change in focus of the business from small value contracts to larger value national laboratory lab support, particularly in the US. In the reporting period, SPL delivered contracts where it utilised the wide range of capabilities that are available on the RAL campus, including the combination of single point diamond turning and micro-assembly to deliver highly complex targets as well as the delivery of complete targetry systems to complement its capabilities in individual target supply. This work is underpinned by the licensing agreements SPL has with STFC to market and sell the tape drive technology, delivering royalties into the CLF and to its inventors.

Acknowledgements

The Target Fabrication group would like to thank Dr Charlotte Palmer and Peter Parsons (Queen's University Belfast), as well as Griffin Glenn and Daniel DePonte (SLAC) for their continued collaborative efforts in the design of the CLF's liquid targetry capability.

References:

1. S. Astbury, C. Spindloe & M. Tolley "Target Fabrication Operational Statistics April 2022–2023", CLF Annual Report 2022–2023
2. J. Fields, P. Ariyathilaka, S. Astbury, C. Spindloe & M. Tolley "Current developments in the Target Array Assembly System", CLF Annual Report 2022–2023
3. W. Robins, S. Astbury, C. Spindloe & M. Tolley "Advances in Tape Target Technologies towards 1Hz Operation for EPAC and other High Repetition Rate Facilities", CLF Annual Report 2021–2022

Authors: S. Astbury ✉, C. Spindloe and M.K. Tolley

Vulcan

Vulcan has completed its final experimental period (April to September 2023) ahead of the Vulcan 20-20 upgrade, with 37 full experimental weeks allocated between target areas West (TAW) and Petawatt (TAP). Overall, the laser statistics show an operational standard consistent with that achieved last year, with an overall reliability percentage of 92%.

The experiments dependent on the long pulses continued to present less than 5% rms values, resulting in a reliability of 99% for the M Oliver experiment. The short pulse beamlines had a lower than expected reliability for the Woolsey experiment, due to alignment sensitivity issues. On all other experiments, reliability was above the 92% baseline.

Table 5 (next page) shows the operational schedule and statistics for 2023/24. Information on the number of shots, energy-on-target success rate and availability hours is also provided in the table. Numbers in parentheses indicate the total number of full energy laser shots delivered to target, followed by the number of these that failed and the percentage of successful shots. The second set of numbers are the availability of the laser to target areas during normal operating hours and including outside hours operations.

The total number of full disc amplifier shots that were fired to target this year was 860. Table 4 shows how this figure compares with that for the four previous years. 69 shots failed to meet user requirements. The overall shot success rate to target for the year is 92%, compared to 84%, 80%, 88% and 92% in the previous four years.

Table 4: Shot totals and proportion of failed shots for the past five years.

Year	Total number of shots	Number of failed shots	Reliability
2019–2020	653	102	84%
2020–2021	325	64	80%
2021–2022	604	73	88%
2022–2023	601	51	92%
2023–2024	860	69	92%

Table 5: Experimental schedule for the period April to September 2023.

Period	TAW	TAP
6 March – 15 April	C Armstrong Direct Laser Acceleration of Electrons to Superponderomotive Energies (Shots 72, Failed 4, Reliability 94.4%) (Availability 83.8%, w extra hours 91.3%) (5 + 1 weeks) 22110016	N/A
13 March – 15 April	N/A	M Borghesi Ultra-high dose rate effects in cellular response to proton irradiation (Shots 122, Failed 9, Reliability 92.6%) (Availability 75.9%, w extra hours 88.0%) (5 weeks) 22210020
1 May – 3 June	M Oliver Direct Imaging of the Inelastic Response of Silicon to Shock Compression (Shots 102, Failed 1, Reliability 99.0%) (Availability 89.4%, w extra hours 97.8%) (5 weeks) 22210011	P McKenna Non-linear Compton scattering from intense laser pulse interactions with near-critical-density plasma (Shots 88, Failed 4, Reliability 95.5%) (Availability 90.6%, w extra hours 99.0%) (5 weeks) 22210005
26 June – 29 July	N Woolsey Characterisation of stimulated Raman sidescattering and its competition with backscattering in the context of Direct Drive Laser Fusion (Shots 141, Failed 28, Reliability 80.1%) (Availability 90.3%, w extra hours 109.0%) (5 weeks) 22210003	N/A
3 July – 13 August	N/A	Commercial Beam Time (Shots 208, Failed 15, Reliability 92.8%) (Availability 88.8%, w extra hours 94.4%) (6 weeks) 23510000
21 August – 23 September	J Fuchs Investigating particle acceleration dynamics in interpenetrating magnetized collisionless super-critical shocks (Shots 125, Failed 8, Reliability 93.6%) (Availability 97.6%, w extra hours 107.2%) (5 weeks) 22210006	N/A

Figure 11 shows the reliability of the Vulcan laser to all target areas over the past five years. The shot reliability in 2023/24 to TAW was 91.8%, down 1.2% from the previous year. The shot reliability to TAP was 93.6%, up 7.6% from 86% in 2022/23.

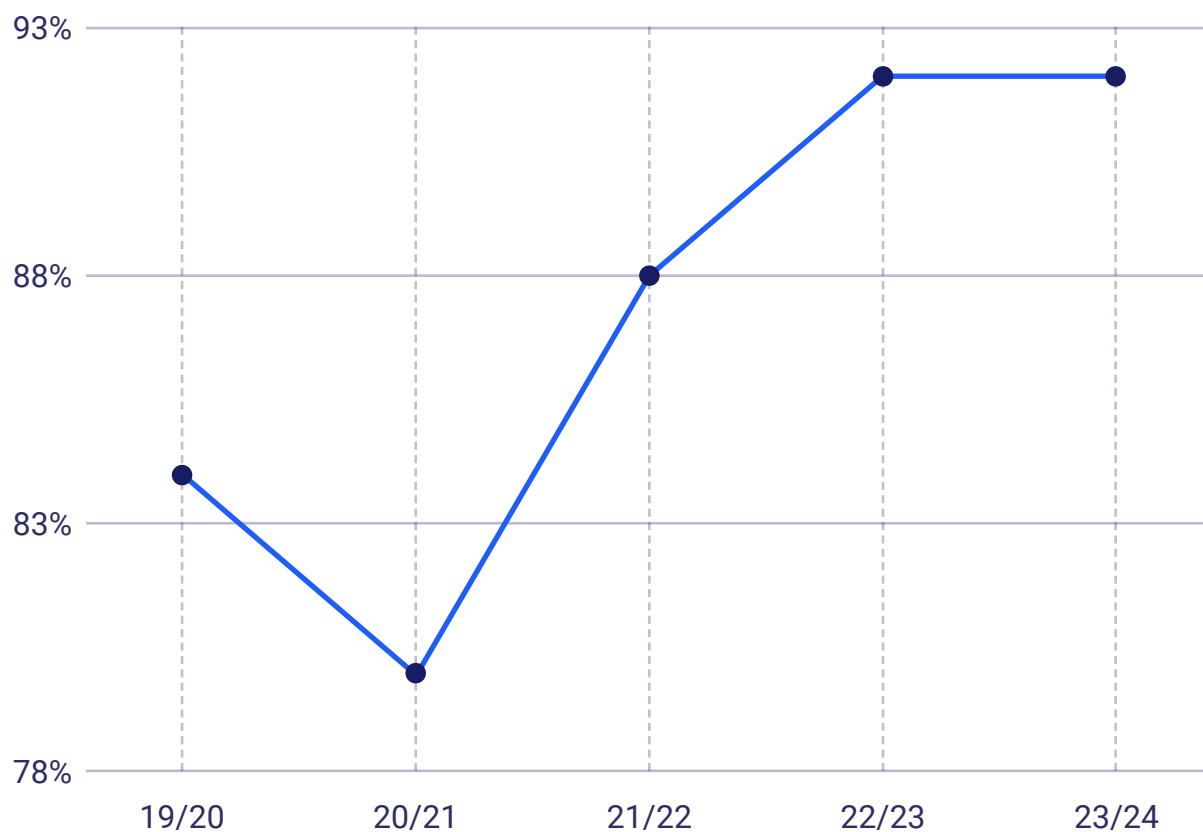


Figure 11: All areas shot reliability for each year 2019 to 2023.

Availability was affected by a single event for Woolsey and commercial access campaigns that took two days out of the operational campaigns.

Availability was reduced by problems with the high voltage part of the system, in rod or disk amplifier elements. Throughout the year, there were 11 failures on elements on the disk amplification chain/capacitor bank, and two on the rod amplification chain. Each time there was a problem with these elements, it took between three hours and one-and-a-half days to resolve.

There is a requirement (originally instigated for the EPSRC FAA) that the laser system be available from 09:00 to 17:00 hours, Monday to Thursday, and from 09:00 to 16:00 hours on Fridays, during the five-week periods of experimental data collection (a total of 195 hours over the five-week experimental period). The laser has mainly met the startup target of 9:00 am, but it has been common practice to operate the laser well beyond the standard contracted finish time on several days during the week. In addition, the introduction of early start times on some experiments continues to lead to improvements in availability.

On average, Vulcan has been available for each experiment to target areas for 88% of the time during contracted hours, compared with 95.7% for the previous year. The overall availability to all target areas was over 98%, compared with 113.2% in 2022/23, with an average reliability of 92.6%.

Publications

Journal Papers

Artemis

C Sayers, G Cerullo, Y Zhang, C Sanders, R Chapman, A Wyatt, G Chatterjee, E Springate, D Wolverson, E Da Como, E Carpane

Exploring the charge density wave phase of 1T-TaSe₂: Mott or charge-transfer gap?
PHYSICAL REVIEW LETTERS, 130, 156401 (2023)

CALTA

M De Vido, G Quinn, D Clarke, L McHugh, P Mason, J Spear, JM Smith, M Divoky, J Pilar, O Denk, TJ Butcher, C Edwards, T Mocek, JL Collier

Demonstration of stable, long-term operation of a nanosecond pulsed DPSSL at 10 J, 100 Hz
OPTICS EXPRESS, 32, 11907 (2024)

S Banerjee, J Spear

Enhancement of compressive stresses by application of shaped temporal pulses in confinement layer free nanosecond laser shock peening
OPTICS & LASER TECHNOLOGY, 175, 110790 (2024)

P Mason, H Barrett, S Banerjee, T Butcher, J Collier

Generation of joule-level green bursts of nanosecond pulses from a DPSSL amplifier
OPTICS EXPRESS, 31, 19510 (2023)

M De Vido, PJ Phillips, D Meissner, S Meissner, G Quinn, S Banerjee, M Divoky, PD Mason

High energy, high pulse rate laser operation using crystalline adhesive-free bonded Yb:YAG slabs
OPTICS EXPRESS, 31, 28101 (2023)

D Clarke, J Phillips, M Divoky, J Pilar, P Navratil, M Hanus, P Severova, O Denk, T Paliesek, M Smrz, P Mason, T Butcher, C Edwards, J Collier, T Mocek

Improved stability second harmonic conversion of a diode-pumped Yb:YAG laser at the 0.5 kW level
OPTICS LETTERS, 48, 6320 (2023)

M Divoky, J Phillips, J Pilar, M Hanus, P Navratil, O Denk, T Paliesek, P Severova, D Clarke, M Smrz, T Butcher, C Edwards, J Collier, T Mocek

Kilowatt-class high-energy frequency conversion to 95 J at 10 Hz at 515 nm
HIGH POWER LASER SCIENCE AND ENGINEERING, 11, e65 (2023)

EPAC

J Phillips, J Smith, P Mason, M De Vido, T Butcher, C Hernandez-Gomez, J Collier, A Wojtusiak

Extreme photonics applications centre: high energy DPSSL pump for a 10 Hz PW-level laser
PROCEEDINGS OF SPIE, 12577, 1257707 (2023)

CD Armstrong, GG Scott, S Richards, JK Patel, K Fedorov, RJ Gray, K Welsby, PP Rajeev

X-ray detector requirements for laser-plasma accelerators

FRONTIERS IN PHYSICS, 11, 1286442 (2023)

Gemini

S Feister, K Cassou, S Dann, A Döpp, P Gauron, AJ Gonsalves, A Joglekar, V Marshall, O Neveu, H Schlenvoigt, MJV Streeter, CAJ Palmer

Control systems and data management for high-power laser facilities

HIGH POWER LASER SCIENCE AND ENGINEERING, 11, e56 (2023)

A Doherty, S Fourmaux, A Astolfo, R Ziesche, J Wood, O Finlay, W Stolpe, D Batey, I Manke, F Légaré, M Boone, D Symes, Z Najmudin, M Endrizzi, A Olivo, S Cipiccia

Femtosecond multimodal imaging with a laser-driven X-ray source

COMMUNICATIONS PHYSICS, 6, 288 (2023)

J Jonnerby, A von Boetticher, J Holloway, L Corner, A Picksley, AJ Ross, RJ Shalloo, C Thornton, N Bourgeois, R Walczak, SM Hooker

Measurement of the decay of laser-driven linear plasma wakefields

PHYSICAL REVIEW E, 108, 055211 (2023)

K Pöder, J Wood, N Lopes, J Cole, S Alatabi, M Backhouse, P Foster, A Hughes, C Kamperidis, O Kononenko, S Mangles, C Palmer, D Rusby, A Sahai, G Sarri, D Symes, J Warwick, Z Najmudin

Multi-GeV electron acceleration in wakefields strongly driven by oversized laser spots

PHYSICAL REVIEW LETTERS, 132, 195001 (2024)

B John, K Middleman, OB Malyshev, X Gu, DR Symes, DR Emerson

Numerical investigation of transmission probability characteristics in the first low-density region of a laser wakefield accelerator

MICROFLUIDICS AND NANOFUIDICS, 27, 52 (2023)

AJ Ross, J Chappell, JJ van de Wetering, J Cowley, E Archer, N Bourgeois, L Corner, DR Emerson, L Feder, XJ Gu, O Jakobsson, H Jones, A Picksley, L Reid, W Wang, R Walczak, SM Hooker

Resonant excitation of plasma waves in a plasma channel

PHYSICAL REVIEW RESEARCH, 6, L022001 (2024)

Plasma Physics

AR Bell, M Sherlock

The fast VFP code for solution of the Vlasov-Fokker-Planck equation

PLASMA PHYSICS AND CONTROLLED FUSION, 66, 035014 (2024)

I Turcu, D Margarone, L Giuffrida, A Picciotto, C Spindloe, A Robinson, D Batani
Borane (BmHn), Hydrogen rich, Proton Boron fusion fuel materials for high yield laser-driven Alpha sources

JOURNAL OF INSTRUMENTATION, 19, C03065 (2024)

G Vacalis, G Marocco, J Bamber, R Bingham, G Gregori

Detection of high-frequency gravitational waves using high-energy pulsed lasers

CLASSICAL AND QUANTUM GRAVITY, 40, 155006 (2023)

RW Paddock, TS Li, E Kim, JJ Lee, H Martin, RT Ruskov, S Hughes, SJ Rose, CD Murphy, RHH Scott, R Bingham, W Garbett, VV Elisseev, BM Haines, AB Zylstra, EM Campbell, CA Thomas, T Goffrey, TD Arber, R Aboushelbaya, MW Von der Leyen, RHW Wang, AA James, I Ouatu, R Timmis, S Howard, E Atonga, PA Norreys
Energy gain of wetted-foam implosions with auxiliary heating for inertial fusion studies
PLASMA PHYSICS AND CONTROLLED FUSION, 66, 025005 (2023)

D Batani, A Colaïtis, F Consoli, CN Danson, LA Gizzi, JJ Honrubia, T Kühl, S Le Pape, J Miquel, JM Perlado, RHH Scott, M Tatarakis, V Tikhonchuk, L Volpe
Future for Inertial Fusion Energy in Europe: A roadmap
HIGH POWER LASER SCIENCE AND ENGINEERING, 11, e83 (2023)

S Krishnamurthy, S Chintalwad, APL Robinson, RMGM Trines, B Ramakrishna
Observation of proton modulations in laser-plasma interaction
PLASMA PHYSICS AND CONTROLLED FUSION, 65, 085020 (2023)

APL Robinson
Reduction of fast ion drag in the presence of 'hollow' non-Maxwellian electron distributions
PLASMA PHYSICS AND CONTROLLED FUSION, 66, 035017- (2024)

A Mondal, R Sabui, S Tata, RMGM Trines, SV Rahul, F Li, S Sarkar, W Trickey, RY Kumar, D Rajak, J Pasley, Z Sheng, J Jha, M Anand, R Gopal, APL Robinson, M Krishnamurthy
Shaped liquid drops generate MeV temperature electron beams with millijoule class laser
COMMUNICATIONS PHYSICS, 7, 85 (2024)

RY Kumar, R Sabui, R Gopal, F Li, S Sarkar, W Trickey, M Anand, J Pasley, Z Sheng, RMGM Trines, RHH Scott, APL Robinson, V Sharma, M Krishnamurthy
Tailored mesoscopic plasma accelerates electrons exploiting parametric instability
NEW JOURNAL OF PHYSICS, 26, 033027 (2024)

Vulcan

D Bailie, S White, R Irwin, C Hyland, R Warwick, B Kettle, N Breslin, SN Bland, DJ Chapman, SPD Mangles, RA Baggot, ER Tubman, D Riley
K-Edge Structure in Shock-Compressed Chlorinated Parylene
ATOMS, 11, 135 (2023)

P Martin, H Ahmed, D Doria, M Cerchez, F Hanton, D Gwynne, A Alejo, J Fernandez-Tobias, J Green, A Macchi, D Maclellan, P McKenna, J Ruiz, M Swantusch, O Willi, S Zhai, M Borghesi, S Kar
Narrow-band acceleration of gold ions to GeV energies from ultra-thin foils
COMMUNICATIONS PHYSICS, 7, 3 (2024)

W Yao, M Nakatsutsumi, S Buffechoux, P Antici, M Borghesi, A Ciardi, SN Chen, E d'Humières, L Gremillet, R Heathcote, V Horný, P McKenna, MN Quinn, L Romagnani, R Royle, G Sarri, Y Sentoku, H Schlenvoigt, T Toncian, O Tresca, L Vassura, O Willi, J Fuchs
Optimizing laser coupling, matter heating, and particle acceleration from solids using multiplexed ultraintense lasers
MATTER AND RADIATION AT EXTREMES, 9, 047202 (2024)

Target Fabrication

I Turcu, D Margarone, L Giuffrida, A Picciotto, C Spindloe, A Robinson, D Batani
Borane (BmHn), Hydrogen rich, Proton Boron fusion fuel materials for high yield laser-driven Alpha sources

JOURNAL OF INSTRUMENTATION, 19, C03065 (2024)

M King, A Higginson, C McGuffey, R Wilson, G Schaumann, T Hodge, JB Ohland, S Gales, MP Hill, SF Pitt, C Spindloe, CN Danson, MS Wei, FN Beg, M Roth, D Neely, RJ Gray, P McKenna

Geometry effects on energy selective focusing of laser-driven protons with open and closed hemisphere-cone targets

PLASMA PHYSICS AND CONTROLLED FUSION, 66, 015001 (2023)

Ultra

AEJ Hoffman, W Temmerman, E Campbell, AA Damin, I Lezcano-Gonzalez, AM Beale, S Bordiga, J Hofkens, V Van Speybroeck

A critical assessment on calculating vibrational spectra in nanostructured materials

JOURNAL OF CHEMICAL THEORY AND COMPUTATION, 20, 513-531 (2023)

AJ Auty, PA Scattergood, T Keane, T Cheng, G Wu, H Carson, J Shipp, A Sadler, T Roseveare, IV Sazanovich, AJHM Meijer, D Chekulaev, PIP Elliot, M Towrie, JA Weinstein

A stronger acceptor decreases the rates of charge transfer: ultrafast dynamics and on/off switching of charge separation in organometallic donor-bridge-acceptor systems

CHEMICAL SCIENCE, 14, 11417-11428 (2023)

N Thirö, G Chatterjee, Y Pertot, O Albert, G Karras, Y Zhang, AS Wyatt, M Towrie, E Springate, GM Greetham, N Forget

A versatile high-average-power ultrafast infrared driver tailored for high-harmonic generation and vibrational spectroscopy

SCIENTIFIC REPORTS, 13, 18874 (2023)

NT Hunt

Biomolecular infrared spectroscopy: making time for dynamics

CHEMICAL SCIENCE, 15, 414-430 (2024)

PM Donaldson, GM Greetham, CT Middleton, BM Luther, MT Zanni, P Hamm, AT Krummel

Breaking barriers in ultrafast spectroscopy and imaging using 100 kHz amplified Yb-laser systems

ACCOUNTS OF CHEMICAL RESEARCH, 56, 2062-2071 (2023)

W Whitaker, IV Sazanovich, Y Kwon, W Jeon, MS Kwon, AJ Orr-Ewing

Characterization of the reversible intersystem crossing dynamics of organic photocatalysts using transient absorption spectroscopy and time-resolved fluorescence spectroscopy

JOURNAL OF PHYSICAL CHEMISTRY A, 127, 10775-10788 (2023)

PM Keane, C Zehe, FE Poynton, SA Bright, S Estayalo-Adrián, SJ Devereux, PM Donaldson, IV Sazanovich, M Towrie, SW Botchway, CJ Cardin, DC Williams, T Gunnlaugsson, C Long, JM Kelly, SJ Quinn
Correction: Time-resolved infra-red studies of photo-excited porphyrins in the presence of nucleic acids and in HeLa tumour cells: insights into binding site and electron transfer dynamics
PHYSICAL CHEMISTRY CHEMICAL PHYSICS, 25, 23316-23317 (2023)

S Maiti, LDA Siebbeles
Developments and challenges involving triplet transfer across organic/inorganic heterojunctions for singlet fission and photon upconversion
JOURNAL OF PHYSICAL CHEMISTRY LETTERS, 14, 11168-11176 (2023)

Y He, JT Collado, JN Iuliano, HA Woroniecka, CR Hall, AA Gil, SP Laptanok, GM Greetham, B Illarionov, A Bacher, M Fischer, JB French, A Lukacs, SR Meech, PJ Tonge
Elucidating the signal transduction mechanism of the blue-light-regulated photoreceptor YtvA: From photoactivation to downstream regulation
ACS CHEMICAL BIOLOGY, 19, 696-706 (2024)

M Stitch, D Avagliano, D Graczyk, IP Clark, L González, M Towrie, SJ Quinn
Good vibrations report on the DNA quadruplex binding of an excited state amplified Ruthenium Polypyridyl IR probe
JOURNAL OF THE AMERICAN CHEMICAL SOCIETY, 145, 21344-21360 (2023)

G Bressan, IA Heisler, GM Greetham, A Edmeades, SR Meech
Half-broadband two-dimensional electronic spectroscopy with active noise reduction
OPTICS EXPRESS, 31, 42687 (2023)

AP Hawkins, AE Edmeades, CDM Hutchison, M Towrie, RF Howe, GM Greetham, PM Donaldson
Laser induced temperature-jump time resolved IR spectroscopy of zeolites
CHEMICAL SCIENCE, 15, 3453-3465 (2024)

DJ Shaw, LC Waters, SL Strong, MED Schulze, GM Greetham, M Towrie, AW Parker, CE Prosser, AJ Henry, ADG Lawson, MD Carr, RJ Taylor, NT Hunt, FW Muskett
Modulation of IL-17 backbone dynamics reduces receptor affinity and reveals a new inhibitory mechanism
CHEMICAL SCIENCE, 14, 7524-7536 (2023)

A Karunakaran, KJ Francis, C Bowen, RJ Ball, Y Zhao, L Wang, NB McKeown, M Carta, PJ Fletcher, R Castaing, MA Isaacs, LJ Hardwick, G Cabello, IV Sazanovich, F Marken
Nanophase-photocatalysis: Loading, storing, and release of H₂O₂ using graphitic carbon nitride
CHEMICAL COMMUNICATIONS, 59, 7423-7426 (2023)

SH Rutherford, CDM Hutchison, GM Greetham, AW Parker, A Nordon, MJ Baker, NT Hunt
Optical screening and classification of drug binding to proteins in human blood serum
ANALYTICAL CHEMISTRY, 95, 17037-17045 (2023)

AM Gardner, G Neri, B Siritanaratkul, H Jang, KH Saeed, PM Donaldson, AJ Cowan
Potential dependent reorientation controlling activity of a molecular electrocatalyst
JOURNAL OF THE AMERICAN CHEMICAL SOCIETY, 146, 7130-7134 (2024)

- G Cabello, IV Sazanovich, I Siachos, M Bilton, BL Mehdi, AR Neale, LJ Hardwick
Simultaneous surface-enhanced Raman scattering with a Kerr gate for fluorescence suppression
 JOURNAL OF PHYSICAL CHEMISTRY LETTERS, 15, 608-615 (2024)
- J Tolentino Collado, E Bodis, J Pasitka, M Szucs, Z Fekete, N Kis-Bicskei, E Telek, K Pozsonyi, SM Kapetanaki, G Greetham, PJ Tonge, SR Meech, A Lukacs
Single amino acid mutation decouples photochemistry of the BLUF domain from the enzymatic function of OaPAC and drives the enzyme to a switched-on state
 JOURNAL OF MOLECULAR BIOLOGY, 436, 168312 (2024)
- E Plackett, C Robertson, A De Matos Loja, H McGhee, G Karras, IV Sazanovich, RA Ingle, MJ Paterson, RS Minns
Structural dynamics around a hydrogen bond: Investigating the effect of hydrogen bond strengths on the excited state dynamics of carboxylic acid dimers
 THE JOURNAL OF CHEMICAL PHYSICS, 160, 124311 (2024)
- PM Donaldson
The 2D-IR spectrum of hydrogen-bonded silanol groups in pyrogenic silica
 THE JOURNAL OF CHEMICAL PHYSICS, 160, 104204 (2024)
- JB Eastwood, TJ Burden, LA Hammarback, C Horbaczewskyj, TFN Tanner, IP Clark, G Greetham, M Towrie, IJS Fairlamb, JM Lynam
The importance of understanding (pre)catalyst activation in versatile C-H bond functionalisations catalysed by $[\text{Mn}_2(\text{CO})_{10}]$
 CHEMICAL SCIENCE, 15, 9183-9191 (2024)
- IS Camacho, E Wall, IV Sazanovich, E Gozzard, M Towrie, NT Hunt, S Hay, AR Jones
Tuning of B_{12} photochemistry in the CarH photoreceptor to avoid radical photoproducts
 CHEMICAL COMMUNICATIONS, 59, 13014-13017 (2023)
- B Procacci, SLD Wrathall, AL Farmer, DJ Shaw, GM Greetham, AW Parker, Y Rippers, M Horch, JM Lynam, NT Hunt
Understanding the $[\text{NiFe}]$ hydrogenase active site environment through ultrafast infrared and 2D-IR spectroscopy of the subsite analogue $\text{K}[\text{CpFe}(\text{CO})(\text{CN})_2]$ in polar and protic solvents
 JOURNAL OF PHYSICAL CHEMISTRY B, 128, 1461-1472 (2024)
- E Nicolaidou, AW Parker, IV Sazanovich, M Towrie, SC Hayes
Unraveling excited state dynamics of a single-stranded DNA-assembled conjugated polyelectrolyte
 JOURNAL OF PHYSICAL CHEMISTRY LETTERS, 14, 9794-9803 (2023)
- NA Lau, D Ghosh, S Bourne-Worster, R Kumar, WA Whitaker, J Heitland, JA Davies, G Karras, IP Clark, GM Greetham, GA Worth, AJ Orr-Ewing, HH Fielding
Unraveling the ultrafast photochemical dynamics of nitrobenzene in aqueous solution
 JOURNAL OF THE AMERICAN CHEMICAL SOCIETY, 146, 10407-10417 (2024)
- IJS Fairlamb, JM Lynam
Unveiling mechanistic complexity in manganese-catalyzed C-H bond functionalization using IR spectroscopy over 16 orders of magnitude in time
 ACCOUNTS OF CHEMICAL RESEARCH, 57, 919-932 (2024)

Octopus

EM Fletcher, BC Bateman, SW Botchway, AD Ward, IA Sparkes

Applying optical tweezers with TIRF microscopy to quantify physical interactions between organelles in the plant endomembrane system

CURRENT PROTOCOLS, 3 (2023)

SH Jones, MD King, AR Rennie, AD Ward, RA Campbell, AV Hughes

Aqueous radical initiated oxidation of an organic monolayer at the air–water interface as a proxy for thin films on atmospheric aerosol studied with neutron reflectometry

JOURNAL OF PHYSICAL CHEMISTRY A, 127, 8922-8934 (2023)

C Qiu, Y Odarchenko, Q Meng, H Dong, IL Gonzalez, M Panchal, P Olalde-Velasco, F Maccherozzi, L Zanetti-Domingues, ML Martin-Fernandez, AM Beale

Compositional evolution of individual CoNPs on Co/TiO₂ during CO and syngas treatment resolved through soft XAS/X-PEEM

ACS CATALYSIS, 13, 15956-15966 (2023)

RM Lees, B Pichler, AM Packer

Contribution of optical resolution to the spatial precision of two-photon optogenetic photostimulation in vivo

NEUROPHOTONICS, 11, 015006 (2024)

RS Iyer, SR Needham, I Galdadas, BM Davis, SK Roberts, RCH Man,

LC Zanetti-Domingues, DT Clarke, GO Fruhwirth, PJ Parker, DJ Rolfe, FL Gervasio, ML Martin-Fernandez

Drug-resistant EGFR mutations promote lung cancer by stabilizing interfaces in ligand-free kinase-active EGFR oligomers

NATURE COMMUNICATIONS, 15, 2130 (2024)

A Kobiela, L Hovhannisyan, P Jurkowska, JB de la Serna, A Bogucka, M Deptuía, AA Paul, K Panek, E Czechowska, M Rychiówski, A Królicka, J Zieliński, S Gabrielsson, M Pikuía, M Trzeciak, GS Ogg, D Gutowska-Owsiak

Excess filaggrin in keratinocytes is removed by extracellular vesicles to prevent premature death and this mechanism can be hijacked by *Staphylococcus aureus* in a TLR2-dependent fashion

JOURNAL OF EXTRACELLULAR VESICLES, 12, 12335 (2023)

BM Davis, SR Needham, C Tynan, S Roberts, E Garcia-Gonzalez, M Martin-Fernandez, DJ Rolfe

FLImP-assisted MINFLUX overcomes molecular localization errors to reveal the structure of heterogeneous membrane protein systems

BIOPHYSICAL JOURNAL, 123, 434a (2024)

A Milsom, AM Squires, AD Ward, C Pfrang

Molecular self-organization in surfactant atmospheric aerosol proxies

ACCOUNTS OF CHEMICAL RESEARCH, 56, 2555-2568 (2023)

JM Rowland, TL van der Plas, M Loidolt, RM Lees, J Keeling, J Dehning, T Akam, V Priesemann, AM Packer

Propagation of activity through the cortical hierarchy and perception are determined by neural variability

NATURE NEUROSCIENCE, 26, 1584-1594 (2023)

AM Mackenzie, HE Smith, RR Mould, JD Bell, AV Nunn, SW Botchway

Rooting out ultraweak photon emission a-mung bean sprouts

JOURNAL OF PHOTOCHEMISTRY AND PHOTOBIOLOGY, 19, 100224 (2024)

HE Smith, AM Mackenzie, C Seddon, R Mould, I Kalampouka, P Malakar, SR Needham, K Beis, JD Bell, A Nunn, SW Botchway

The use of NADH anisotropy to investigate mitochondrial cristae alignment

SCIENTIFIC REPORTS, 14, 5980 (2024)

RR Mould, AM Mackenzie, I Kalampouka, AVW Nunn, EL Thomas, JD Bell, SW Botchway

Ultra weak photon emission – a brief review

FRONTIERS IN PHYSIOLOGY, 15, 1348915 (2024)

B Zhang, KD Richards, BE Jones, AR Collins, R Sanders, SR Needham, P Qian, A Mahadevegowda, C Ducati, S Botchway, RC Evans

Ultra-small air-stable triplet-triplet annihilation upconversion nanoparticles for anti-stokes time-resolved imaging

ANGEWANDTE CHEMIE INTERNATIONAL EDITION, 62, e202308602 (2023)

DL Jones, MB Andrews, SW Botchway, A Ward, JR Lloyd, LS Natrajan

An investigation into the role of c-type cytochromes and extracellular flavins in the bioreduction of uranyl(VI) by *Shewanella oneidensis* using fluorescence spectroscopy and microscopy

ENVIRONMENTAL RADIOCHEMICAL ANALYSIS ed. N. Evans, Royal Society of Chemistry, vol. 357, ch. 15, pp. 158-174 (2023)

V Kriechbaumer, SW Botchway

Immunoprecipitation and FRET-FLIM to determine metabolons on the plant ER

METHODS IN MOLECULAR BIOLOGY, 2772, pp.169-177 (2024)

C Pain, V Kriechbaumer, A Candeo

Observing ER dynamics over long timescales using Light Sheet Fluorescence Microscopy

METHODS IN MOLECULAR BIOLOGY, 2772, pp. 323-335 (2024)

C Pain, C Tynan, SW Botchway, V Kriechbaumer

Variable-angle epifluorescence microscopy for single-particle tracking in the plant ER

METHODS IN MOLECULAR BIOLOGY, 2772, pp. 273-283 (2024)

Individual Contributions and Collaborative Science

O Alexander, JCT Barnard, EW Larsen, T Avni, S Jarosch, C Ferchaud, A Gregory, S Parker, G Galinis, A Tofful, D Garratt, MR Matthews, JP Marangos

Observation of recollision-based high-harmonic generation in liquid isopropanol and the role of electron scattering

PHYSICAL REVIEW RESEARCH, 5, 043030 (2023)

G Gregori, G Marocco, S Sarkar, R Bingham, C Wang

Measuring Unruh radiation from accelerated electrons

EUROPEAN PHYSICAL JOURNAL C: PARTICLES AND FIELDS, 84, 475 (2024)

G Vacalis, A Higuchi, R Bingham, G Gregori
Classical Larmor formula through the Unruh effect for uniformly accelerated electrons

PHYSICAL REVIEW D, 109, 024044 (2024)

MJ Green, H Ge, SE Flower, C Pourzand, SW Botchway, H Wang, N Kuganathan, G Kociok-Kohn, M Li, S Xu, TD James, SI Pascu

Fluorescent naphthalimide boronates as theranostics: structural investigations, confocal fluorescence and multiphoton fluorescence lifetime imaging microscopy in living cells

RSC CHEMICAL BIOLOGY, 4, 108-1095 (2023)

R Waite, CT Adams, DR Chisholm, CHC Sims, JG Hughes, E Dias, EA White, K Welsby, SW Botchway, A Whiting, GJ Sharples, CA Ambler

The antibacterial activity of a photoactivatable diarylacetylene against Gram-positive bacteria

FRONTIERS IN MICROBIOLOGY, 14, 1243818 (2023)

SC Gillespie, M van der Laan, D Poonia, S Maiti, S Kinge, LDA Siebbeles, P Schall
Optical signatures of charge- and energy transfer in TMDC/TMDC and TMDC/perovskite heterostructures

2D MATERIALS, 11, 022005 (2024)

S Mosca, Q Lin, R Stokes, T Bharucha, B Gangadharan, R Clarke, LG Fernandez, M Deats, J Walsby-Tickle, BY Arman, SR Chunekar, KD Patil, S Gairola, K Van Assche, S Dunachie, HA Merchant, R Kuwana, A Maes, J McCullagh, C Caillet, N Zitzmann, PN Newton, P Matousek

Innovative method for rapid detection of falsified COVID-19 vaccines through unopened vials using handheld Spatially Offset Raman Spectroscopy (SORS)

VACCINE, 41, 6960-6968 (2023)

M Dooley, J Luckett, MR Alexander, P Matousek, H Dehghani, AM Ghaemmaghani, I Notingher

Optimization of diffuse Raman spectroscopy for in-vivo quantification of foreign body response in a small animal model

BIOMEDICAL OPTICS EXPRESS, 14, 6592 (2023)

T Bharucha, B Gangadharan, R Clarke, LG Fernandez, BY Arman, J Walsby-Tickle, M Deats, S Mosca, Q Lin, R Stokes, S Dunachie, HA Merchant, A Dubot-Pères, C Caillet, J McCullagh, P Matousek, N Zitzmann, PN Newton

Repurposing rapid diagnostic tests to detect falsified vaccines in supply chains

VACCINE, 42, 1506-1511 (2024)

B Gardner, J Haskell, P Matousek, N Stone

Guided principal component analysis (GPCA): a simple method for improving detection of a known analyte

ANALYST, 149, 205-211 (2023)

A Botteon, M Vermeulen, L Cristina, S Bruni, P Matousek, C Miliani, M Realini, L Angelova, C Conti

Advanced microspatially offset Raman Spectroscopy for noninvasive imaging of concealed texts and figures using Raman signal, fluorescence emission, and overall spectral intensity

ANALYTICAL CHEMISTRY, 96, 4535-4543 (2024)

GP Robertson, S Mosca, C Castillo-Blas, FA Son, OK Farha, DA Keen, S Anzellini, TD Bennett

Survival of zirconium-based metal–organic framework crystallinity at extreme pressures

INORGANIC CHEMISTRY, 62, 10092-10099 (2023)

S Šušnjar, F Martelli, S Mosca, SK Venkata Sekar, J Swartling, N Reistad, A Farina, A Pifferi

Two-layer reconstruction of Raman spectra in diffusive media based on an analytical model in the time domain

OPTICS EXPRESS, 31, 40573 (2023)

CW Patrick, Y Gao, P Gupta, AL Thompson, AW Parker, HL Anderson

Masked alkynes for synthesis of threaded carbon chains

NATURE CHEMISTRY, 16, 193-200 (2023)

AM Taylor, JH Matthews, AR Bell

UHECR echoes from the Council of Giants

MONTHLY NOTICES OF THE ROYAL ASTRONOMICAL SOCIETY, 524, 631-642 (2023)

A Grubišić-Čabo, M Michiardi, CE Sanders, M Bianchi, D Curcio, D Phuyal, MH Berntsen, Q Guo, M Dendzik

In situ exfoliation method of large-area 2D materials

ADVANCED SCIENCE, 10, 2301243 (2023)

D Curcio, CE Sanders, A Chikina, HE Lund, M Bianchi, V Granata, M Cannavacciuolo, G Cuono, C Autieri, F Forte, G Avallone, A Romano, M Cuoco, P Dudin, J Avila, C Polley, T Balasubramanian, R Fittipaldi, A Vecchione, P Hofmann

Current-driven insulator-to-metal transition without Mott breakdown in Ca_2RuO_4

PHYSICAL REVIEW B, 108, L161105 (2023)

AL Soenarjo, Z Lan, IV Sazanovich, YS Chan, M Ringholm, A Jha, DR Klug

The transition from unfolded to folded g-quadruplex dna analyzed and interpreted by two-dimensional infrared spectroscopy

JOURNAL OF THE AMERICAN CHEMICAL SOCIETY, 145, 19622-19632 (2023)

G Zeraouli, DA Mariscal, R Hollinger, SZ Anaraki, EN Folsom, E Grace, D Rusby, MP Hill, GJ Williams, GG Scott, B Sullivan, S Wang, J King, KK Swanson, RA Simpson, BZ Djordjevic, S Andrews, R Costa, B Cauble, F Albert, JJ Rocca, T Ma

Flexible tape-drive target system for secondary high-intensity laser-driven sources

REVIEW OF SCIENTIFIC INSTRUMENTS, 94, 123306 (2023)

H Abu-Shawareb et al.

Achievement of target gain larger than unity in an inertial fusion experiment

PHYSICAL REVIEW LETTERS, 132, 065102 (2024)

MJ Rosenberg, AA Solodov, JF Myatt, S Hironaka, J Sivajeyan, RK Follett, T Filkins, AV Maximov, C Ren, S Cao, P Michel, MS Wei, JP Palastro, RHH Scott, K Glize, SP Regan

Effect of overlapping laser beams and density scale length in laser-plasma instability experiments on OMEGA EP

PHYSICS OF PLASMAS, 30, 042710 (2023)

JF Ong, P Ghenuche, ICE Turcu, A Pukhov, KA Tanaka

Ultra-high-pressure generation in the relativistic transparency regime in laser-irradiated nanowire arrays

PHYSICAL REVIEW E, 107, 065208 (2023)

P Svensson, T Campbell, F Graziani, Z Moldabekov, N Lyu, VS Batista, S Richardson, SM Vinko, G Gregori

Development of a new quantum trajectory molecular dynamics framework

PHILOSOPHICAL TRANSACTIONS OF THE ROYAL SOCIETY A: MATHEMATICAL PHYSICAL AND ENGINEERING SCIENCES, 381, 20220325 (2023)

RY Engel, O Alexander, K Atak, U Bovensiepen, J Buck, R Carley, M Cascella, V Chardonnet, GS Chiuzbaian, C David, F Döring, A Eschenlohr, N Gerasimova, Fd Groot, LL Guyader, OS Humphries, M Izquierdo, E Jal, A Kubec, T Laarmann, C Lambert, J Lüning, JP Marangos, L Mercadier, G Mercurio, PS Miedema, K Ollefs, B Pfau, B Rösner, K Rossnagel, N Rothenbach, A Scherz, J Schlappa, M Scholz, JO Schunck, K Setoodehnia, C Stamm, S Techert, SM Vinko, H Wende, AA Yaroslavtsev, Z Yin, M Beye

Electron population dynamics in resonant non-linear x-ray absorption in nickel at a free-electron laser

STRUCTURAL DYNAMICS, 10, 054501 (2023)

T Gawne, T Campbell, A Forte, P Hollebon, G Perez-Callejo, OS Humphries, O Karnbach, MF Kasim, TR Preston, HJ Lee, A Miscampbell, QY van den Berg, B Nagler, S Ren, RB Royle, JS Wark, SM Vinko

Investigating mechanisms of state localization in highly ionized dense plasmas

PHYSICAL REVIEW E, 108, 035210 (2023)

J Krása, T Burian, V Hájková, J Chalupský, Š Jelínek, K Frantálová, M Krupka, Z Kuglerová, SK Singh, V Vozda, L Vyšín, M Šmíd, P Perez-Martin, M Kühlman, J Pintor, J Cikhardt, M Dreimann, D Eckermann, F Rosenthal, SM Vinko, A Forte, T Gawne, T Campbell, S Ren, Y Shi, T Hutchinson, O Humphries, T Preston, M Makita, M Nakatsutsumi, X Pan, A Köhler, M Harmand, S Toleikis, K Falk, L Juha

Ion emission from warm dense matter produced by irradiation with a soft x-ray free-electron laser

MATTER AND RADIATION AT EXTREMES, 9, 016602 (2024)

T Gawne, SM Vinko, JS Wark

Quantifying ionization in hot dense plasmas

PHYSICAL REVIEW E, 109, L023201 (2024)

P Jimenéz-Calvo, Y Naciri, A Sobolewska, M Isaacs, Y Zhang, A Leforestier, J Degrouard, S Rouzière, C Goldmann, D Vantelon, S Hettler, NJ Zaluzec, R Arenal, P Launois, MN Ghazzal, E Paineau

Ti-modified imogolite nanotubes as promising photocatalyst 1D nanostructures for H₂ production

SMALL METHODS, 8, 2301369 (2023)

Laser Science and Development

S Buck, D Reid, M Galimberti

Automated control and stabilization of ultrabroadband laser pulse angular dispersion

APPLIED OPTICS, 63, 1613 (2024)

J Morse, W Carter, P Oliveira, M Galimberti

Automated long-term stability of a high-energy laser

OPTICS, 4, 595-601 (2023)

P Oliveira, M Galletti, C Suci, M Galimberti

Maximum operational fluence limits for temporally shaped nanosecond long pulses

APPLIED SCIENCES, 14, 4211 (2024)

Theses

Artemis

Abma, G

Isomer-resolved spectroscopy and imaging of biomolecules

Radboud University (2024)

Majchrzak, P

Manipulating electronic structures of quantum materials at extreme time- and length-scales

Aarhus University (2023)

Gemini

Hughes, A

Models of X-rays and electron beams from laser wakefield accelerators

Imperial College London (2024)

Ross, A

Resonant excitation of plasma wakefields in long plasma channels

University of Oxford (2023)

Los, E

Applications of Bayesian inference to radiation reaction experiments

Imperial College London (2023)

Xu, N

Development of high repetition rate intense laser driver and laser driven particle sources

Imperial College London (2023)

Vulcan

Charlwood, M

Photoionised plasmas in the laboratory

Queen's University Belfast (2024)

Dollier, E

Advancing laser-driven ion acceleration: optimising with machine learning and investigating sources of instability

University of Strathclyde (2024)

Goodman, J

Optimisation of proton acceleration and synchrotron radiation in ultraintense laser-solid interactions

University of Strathclyde (2024)

McCallum S

Methods for dosimetric measurement and characterisation of laser-driven ion beams

Queen's University Belfast (2023)

McMurray, A

Irradiation of 3D cell models at ultra-high dose rates

Queen's University Belfast (2023)

Hume, E

Investigation of ultra-intense laser interactions with long scale length pre-plasmas and nanowire targets via escaped electrons

University of York (2023)

Paddock, R

A study of foam targets for direct-drive inertial confinement fusion

University of Oxford (2023)

Ultra

O'Neill, J

A photophysical and time-resolved investigation into Porphyrin and BODIPY dyes as photosensitisers towards Solar Fuel Generation and Antimicrobial Activity

Dublin City University (2024)

Kearney, L

Synthesis and photophysics of novel molecular photo- and electrocatalysts for CO₂ valorisation and hydrogen generation: advancing sustainable solutions to climate change

Dublin City University (2024)

Pagano, K

Molecular-structure dependent electron-phonon coupling in organic semiconductors

Imperial College London (2024)

Royle, C

The ultrafast dynamics of platinum-based complexes

University of Sheffield (2024)

Cerpentier, F

The use of spectroscopic, electrochemical and spectroelectrochemical techniques in the development of improved photocatalysts for the production of solar fuels

Dublin City University (2023)

Eastwood, J

A time-resolved infrared spectroscopy led mechanistic study into the reactivity of Manganese Carbonyl complexes: with a focus on routes of precatalyst activation relating to application in C-H bond functionalisation reactions

University of York (2023)

Burden, T

An investigation into the application and mechanisms of Manganese(I) in C-H functionalisation and organic synthesis

University of York (2023)

Octopus

Lewns, F

Sol to scaffold: Novel hybrid formulations for 3D biofabrication of in vitro tissue models

University of Birmingham (2024)

Noakes, F

New approaches to biological imaging, anticancer therapeutics and pancreatic cancer diagnostics based on Phenazine Cations, related transition metal complexes, and G-coupled protein receptors

University of Sheffield (2024)

Hitchman, C

Complexes that mitigate or mediate fibrosis: Structural and biophysical characterisation of the ERAD checkpoint and the gal-3-fibrosome

University of Leicester (2024)

Chu-Antypas, A

Investigating the interactions of cell surface receptors in brain development

University of Oxford (2023)

Panel Membership and CLF Structure

Octopus and Ultra Facility Access Panel

Reviewers

Professor A. Beale (Panel Chair)

Department of Chemistry
University College London

Dr S. Ameer-Beg

School of Cancer and
Pharmaceutical Sciences
King's College London

Professor S. Charalambous-Hayes

Department of Chemistry
University of Cyprus

Dr A. Cowan

Department of Chemistry
University of Liverpool

Dr E. Gibson

School of Natural and Environmental
Sciences
University of Newcastle

Dr J. Hohlbein

Department of Agrotechnology
and Food Sciences
Wageningen University

Professor M. King

Department of Earth Sciences
Royal Holloway, University of London

Dr. V. Kriechbaumer

Department of Biological
and Medical Sciences
Oxford Brookes University

Professor J. Lynam

Department of Chemistry
University of York

Professor G. McConnell

Centre for Biophotonics
University of Strathclyde

Professor H. Müller-Werkmeister

Institute of Chemistry
—Physical Chemistry
University of Potsdam

Professor T. Oliver

School of Chemistry
University of Bristol

Professor R. Owens

Nuffield Department of Medicine
University of Oxford
and Rosalind Franklin Institute

Professor L. Schermelleh

Department of Biochemistry
University of Oxford

Professor L. Spagnolo

School of Molecular Biosciences
University of Glasgow

Research Council Representatives

C. Miles

BBSRC

A. Chapman

EPSRC

A. Staines

MRC

L. Bettington

NERC

A. Wilcox

STFC

Science and Technology Facilities Council Representatives

Dr D. T. Clarke (Head of Laser for Science Facility)
Central Laser Facility
Science and Technology Facilities Council

Prof J.L Collier (Director)
Central Laser Facility
Science and Technology Facilities Council

Dr G.M. Greetham (Ultra Group Leader)
Central Laser Facility
Science and Technology Facilities Council

Dr M. Martin-Fernandez (Octopus Group Leader)
Central Laser Facility
Science and Technology Facilities Council

Dr E. Gozzard
ISIS and CLF User Office
Science and Technology Facilities Council

Dr S.R. Needham (Panel Secretary)
Central Laser Facility
Science and Technology Facilities Council

Artemis Facility Access Panel

Reviewers

Professor P. King (Panel Chair)
University of St Andrews, UK

Professor J. Tisch
Imperial College, London

Dr J. Stähler
Fritz Haber Institute, Berlin, Germany

Professor V. Stavros
University of Warwick, UK

Dr C. Cacho
Diamond Light Source, Harwell, Didcot, UK

Professor C. Vallance
University of Oxford

Dr O. Johannsen
University of Edinburgh

Science and Technology Facilities Council Representatives

Dr E. Springate (Artemis Group Leader)
Central Laser Facility
Science and Technology Facilities Council

Dr D.T Clarke (Head of Laser for Science Facility)
Central Laser Facility
Science and Technology Facilities Council

Dr C.E. Sanders (Panel Secretary)
Central Laser Facility
Science and Technology Facilities Council

Dr E. Gozzard
ISIS Neutron and Muon Source
Science and Technology Facilities Council

Gemini, Vulcan and Orion Facility Access Panel

Reviewers

Professor N. Woolsey (Panel Chair)

York Plasma Institute
University of York

Professor B. Hidding

Department of Physics
University of Strathclyde

Professor B. Dromey

Department of Pure and Applied Physics
Queen's University of Belfast

Professor T. Arber

Department of Physics
University of Warwick

Professor G. Gregori

Clarendon Laboratory
University of Oxford

Professor C. Ridgers

York Plasma Institute
University of York

Dr S. Mangles

Blackett Laboratory
Imperial College London

Dr A. Klisnick

Institut des Sciences Moléculaires
d'Orsay
Université Paris-Saclay

Dr J. Pasley

York Plasma Institute
University of York

Dr B. Cros

Laboratory of Gas Physics and Plasmas
Université Paris-Sud

Research Council Representatives

Mr C. Danson

AWE

Mr E. Gumbrell

AWE

Mr S. Pitt

AWE

Science and Technology Facilities Council Representatives

Professor J.L. Collier (Director)

Central Laser Facility
Science and Technology Facilities Council

Ms C. Hernandez-Gomez (Associate Director, Head of High Power Laser Programme)

Central Laser Facility
Science and Technology Facilities Council

Dr M. Galimberti (Vulcan Laser)

Central Laser Facility
Science and Technology Facilities Council

Dr P. Oliveria (Vulcan Laser)

Central Laser Facility
Science and Technology Facilities Council

Mr R.J. Clarke (Experimental Science Group Leader)

Central Laser Facility
Science and Technology Facilities Council

Professor R. Pattathil (Gemini Group Leader)

Central Laser Facility
Science and Technology Facilities Council

Dr D. Symes (Gemini Target Area Section Leader)

Central Laser Facility
Science and Technology Facilities Council

Mr S.J. Hawkes (Gemini Operations Manager)

Central Laser Facility
Science and Technology Facilities Council

Dr N. Bourgeois (Gemini Target Area)

Central Laser Facility
Science and Technology Facilities Council

Mr C. Spindloe (Target Fabrication)

Central Laser Facility
Science and Technology Facilities Council

Dr D. Carroll (Panel Secretary)

Central Laser Facility
Science and Technology Facilities Council

Dr E. Gozzard

ISIS Neutron and Muon Source
Science and Technology Facilities Council

Central Laser Facility Structure



Director
Professor John Collier



Lasers for Science Division
Dr Dave Clarke



CALTA Division
Dr Thomas Butcher



High Power Lasers Division
Ms Cristina Hernandez-Gomez
Associate Director



Engineering and Technology Division
Mr Steve Blake



Ultra
Dr Greg Greetham



Octopus
Prof. Marisa Martin-Fernandez



Artemis
Dr Emma Springate



Gemini
Prof. Rajeev Pattathil
Head, Novel Accelerators and EPIC



Experimental Science
Mr Rob Clarke



Target Fabrication
Mr Chris Spindloe



Mechanical
Mr Steve Hook



Electrical
Mr Kenny Rodgers



Vulcan
Dr Marco Galimberti



Plasma Physics
Dr Alex Robinson

Author Index

Initials	Surname	Institution	Page
J.	Aaron	Advanced Imaging Center, HHMI Janelia Research Campus, Ashburn, Virginia, USA	79
H.	Ahmed	Central Laser Facility, STFC Rutherford Appleton Laboratory, Harwell Campus, Didcot, UK	37, 65
S.	Al-Atabi	John Adams Institute for Accelerator Science and Department of Physics, University of Oxford, UK	38
E.A.	Anderson	Chemistry Research Laboratory, Department of Chemistry, University of Oxford, UK	71
D.	Angal-Kalinin	ASTeC, STFC Daresbury Laboratory and Cockcroft Institute, Sci-Tech Daresbury, Warrington, UK	51
A.F.	Antoine	Center for Ultrafast Optical Science, University of Michigan, USA	37
L.	Antonelli	First Light Fusion, Kidlington, UK	38
E.	Archer	John Adams Institute for Accelerator Science and Department of Physics, University of Oxford, UK	32
P.	Ariyathilaka	Central Laser Facility, STFC Rutherford Appleton Laboratory, Harwell Campus, Didcot, UK	60, 61
C.	Armstrong	Central Laser Facility, STFC Rutherford Appleton Laboratory, Harwell Campus, Didcot, UK	65
C.	Arran	York Plasma Institute, University of York, UK	38
S.	Arrowsmith	Chemistry Research Laboratory, Department of Chemistry, University of Oxford, UK	71
S.	Astbury	Central Laser Facility, STFC Rutherford Appleton Laboratory, Harwell Campus, Didcot, UK	60, 96
S.	Aswartham	Leibniz IFW Dresden, Germany	68
Z.	Athawes-Phelps	Central Laser Facility, STFC Rutherford Appleton Laboratory, Harwell Campus, Didcot, UK	54, 55, 66
T.	Audet	School of Mathematics and Physics, Queen's University Belfast, UK	37
M.	Babzien	Accelerator Test Facility, Brookhaven National Laboratory, New York, USA	39

Initials	Surname	Institution	Page
M.P.	Backhouse	John Adams Institute for Accelerator Science and Department of Physics, University of Oxford, UK	28, 29, 30, 31, 34
A.R.	Bainbridge	ASTeC, STFC Daresbury Laboratory and Cockcroft Institute, Sci-Tech Daresbury, Warrington, UK	51, 52
C.	Baird	Central Laser Facility, STFC Rutherford Appleton Laboratory, Harwell Campus, Didcot, UK	65
M.D.	Balcazar	Center for Ultrafast Optical Science, University of Michigan, USA	37
S.	Banerjee	Central Laser Facility, STFC Rutherford Appleton Laboratory, Harwell Campus, Didcot, UK	12, 42, 48
B.C.	Bateman	Central Laser Facility, STFC Rutherford Appleton Laboratory, Harwell Campus, Didcot, UK	94
A.M.	Beale	Department of Chemistry, University College London, UK; Research Complex at Harwell, Didcot, UK	72, 80
K.	Beis	Department of Life Sciences, imperial College London, UK; Research Complex at Harwell, Didcot, UK	73
J.D.	Bell	School of Life Sciences, Research Centre for Optimal Health, University of Westminster, London, UK	73, 75
C.C.M.	Bernitzky	Department of Physics, Freie Universität Berlin, Germany	88
Y.	Biddick	Chemistry Research Laboratory, Department of Chemistry, University of Oxford, UK	71
R.	Bingham	Central Laser Facility, STFC Rutherford Appleton Laboratory, Harwell Campus, Didcot, UK; Department of Physics, SUPA, University of Strathclyde, Glasgow, UK	64
J.A.	Birrell	School of Life Sciences, University of Essex, Colchester, UK	88
D.	Bloemers	Central Laser Facility, STFC Rutherford Appleton Laboratory, Harwell Campus, Didcot, UK	28, 30
P.	Blum	Deutsches Elektronen-Synchrotron DESY, Hamburg, Germany	29, 30, 31, 34

Initials	Surname	Institution	Page
M.	Borghesi	School of Mathematics and Physics, Queen's University of Belfast, UK	65
S.	Borisenko	Leibniz IFW Dresden, Germany; Würzburg-Dresden Cluster of Excellence ct.qmat, Germany	68
S.W.	Botchway	Central Laser Facility, STFC Rutherford Appleton Laboratory, Harwell Campus, Didcot, UK	35, 73, 74, 75
N.	Bourgeois	Central Laser Facility, STFC Rutherford Appleton Laboratory, Harwell Campus, Didcot, UK	28, 29, 30, 31, 32, 33, 34, 51, 52, 56
S.	Bourne-Worster	Department of Chemistry, University College London, UK	86
P.	Bradford	Central Laser Facility, STFC Rutherford Appleton Laboratory, Harwell Campus, Didcot, UK	38
E.	Brambrink	HiBEF at the European XFEL, Schenefeld, Germany	48
I.	Brown	School of Biosciences, University of Kent, Canterbury, UK	79
B.	Büchner	Leibniz IFW Dresden, Germany; Würzburg-Dresden Cluster of Excellence ct.qmat, Germany	68
S.	Buck	Central Laser Facility, STFC Rutherford Appleton Laboratory, Harwell Campus, Didcot, UK	44
S.	Buffechoux	LULI-CNRS, CEA, Sorbonne Université, Ecole Polytechnique, Institut Polytechnique de Paris, France	40
T.J.	Burden	Department of Chemistry, University of York, UK	90
T.J.	Butcher	Central Laser Facility, STFC Rutherford Appleton Laboratory, Harwell Campus, Didcot, UK	41, 43, 44, 45, 46, 47, 48, 50
A.A.	Butler	Chemistry Research Laboratory, Department of Chemistry, University of Oxford, UK	71
S.D.	Cafiso	HZDR at the European XFEL, Schenefeld, Germany	48
L.	Calvin	School of Mathematics and Physics, Queen's University Belfast, UK	35, 37

Initials	Surname	Institution	Page
I.S.	Camacho	Biometrology, Chemical and Biological Sciences, National Physical Laboratory, Teddington, UK	87
E.	Campbell	Cardiff Catalysis Institute, School of Chemistry, Cardiff University, UK	80
J.	Carderelli	Center for Ultrafast Optical Science, University of Michigan, USA	37
D.	Carroll	Central Laser Facility, STFC Rutherford Appleton Laboratory, Harwell Campus, Didcot, UK	65
G.	Casati	John Adams Institute for Accelerator Science and Department of Physics, University of Oxford, UK	39
K.	Cassou	Université Paris-Saclay, CNRS/IN2P3, France	57
N.	Cavanagh	School of Mathematics and Physics, Queen's University Belfast, UK	37
O.	Cavanagh	School of Mathematics and Physics, Queen's University of Belfast, UK	65
R.T.	Chapman	Central Laser Facility, STFC Rutherford Appleton Laboratory, Harwell Campus, Didcot, UK	69, 70, 71
S.E.J.	Chapman	Central Laser Facility, STFC Rutherford Appleton Laboratory, Harwell Campus, Didcot, UK	103
J.	Chappell	John Adams Institute for Accelerator Science and Department of Physics, University of Oxford, UK	32
P.	Chaudary	National Physical Laboratory, Middlesex, UK	35
O.	Cheklov	Central Laser Facility, STFC Rutherford Appleton Laboratory, Harwell Campus, Didcot, UK	45, 53
S.	Chen	"Horia Hulubei" National Institute for Physics and Nuclear Engineering, Bucharest-Magurele, Romania	40
T.-L.	Chew	Advanced Imaging Center, HHMI Janelia Research Campus, Ashburn, Virginia, USA	79
G.	Christian	John Adams Institute for Accelerator Science and Department of Physics, University of Oxford, UK	34
A.	Ciardi	Sorbonne Université, Observatoire de Paris, Université PSL, Paris, France	40
I.P.	Clark	Central Laser Facility, STFC Rutherford Appleton Laboratory, Harwell Campus, Didcot, UK	86, 90

Initials	Surname	Institution	Page
D.L.	Clarke	Central Laser Facility, STFC Rutherford Appleton Laboratory, Harwell Campus, Didcot, UK	41, 43, 47, 49
D.T.	Clarke	Central Laser Facility, STFC Rutherford Appleton Laboratory, Harwell Campus, Didcot, UK	76
R.J.	Clarke	Central Laser Facility, STFC Rutherford Appleton Laboratory, Harwell Campus, Didcot, UK	65
C.	Cobo	John Adams Institute for Accelerator Science and Department of Physics, University of Oxford, UK	28, 29, 30, 31, 34
C.	Colgan	John Adams Institute for Accelerator Science and Department of Physics, University of Oxford, UK	37
J.L.	Collier	Central Laser Facility, STFC Rutherford Appleton Laboratory, Harwell Campus, Didcot, UK	41, 43, 44, 45, 47, 48, 50
A.R.	Collins	Department of Materials Science and Metallurgy, University of Cambridge, UK	74
M.J.	Cook	Central Laser Facility, STFC Rutherford Appleton Laboratory, Harwell Campus, Didcot, UK	65
L.	Corner	Cockcroft Institute of Accelerator Science, University of Liverpool, UK	33
A.J.	Cowan	Department of Chemistry and Stephenson Institute for Renewable Energy, University of Liverpool, UK	81
T.	Cowan	HZDR at the European XFEL, Schenefeld, Germany	48
J.	Cowley	John Adams Institute for Accelerator Science and Department of Physics, University of Oxford, UK	32
G.	Cristoforetti	Intense Laser Irradiation Laboratory, INO-CNR, Pisa, Italy	67
J.	Crone	ASTeC, STFC Daresbury Laboratory and Cockcroft Institute, Sci-Tech Daresbury, Warrington, UK	51, 52
B.F.E.	Curchod	Department of Chemistry, University of Bristol, UK	91
E.	d'Humières	University of Bordeaux, Centre Lasers Intenses et Applications, CNRS, CEA, Talence, France	40
S.J.D.	Dann	Central Laser Facility, STFC Rutherford Appleton Laboratory, Harwell Campus, Didcot, UK	28, 30, 57

Initials	Surname	Institution	Page
J.A.	Davies	Department of Chemistry, University College London, UK	86
B.M.	Davis	Central Laser Facility, STFC Rutherford Appleton Laboratory, Harwell Campus, Didcot, UK	76
T.	de Faria Pinto	Central Laser Facility, STFC Rutherford Appleton Laboratory, Harwell Campus, Didcot, UK	44, 45, 53
M.	De Vido	Central Laser Facility, STFC Rutherford Appleton Laboratory, Harwell Campus, Didcot, UK	42, 43, 49, 50
A.	Dearling	John Adams Institute for Accelerator Science and Department of Physics, University of Oxford, UK	38
O.	Denk	HiLASE Centre, Institute of Physics of the Czech Academy of Sciences, Dolní Břežany, Czech Republic	43, 47
M.	Divoky	HiLASE Centre, Institute of Physics of the Czech Academy of Sciences, Dolní Břežany, Czech Republic	41, 42, 43, 47
C.	Dobson	Central Laser Facility, STFC Rutherford Appleton Laboratory, Harwell Campus, Didcot, UK	41, 61
P.M.	Donaldson	Central Laser Facility, STFC Rutherford Appleton Laboratory, Harwell Campus, Didcot, UK	63, 81, 84, 82, 85, 88
H.	Dong	Department of Chemistry, University College London, UK; Research Complex at Harwell, Didcot, UK	72
Y.F.	Dong	Beijing National Laboratory for Condensed Matter Physics, Institute of Physics, Chinese Academy of Sciences, China	67
A.	Döpp	Ludwig–Maximilians–Universität München, Germany	57
Á.	dos Santos	Department of Oncology and Metabolism, University of Sheffield, UK	79
N.P.	Dover	John Adams Institute for Accelerator Science and Department of Physics, University of Oxford, UK	39
S.	Dragomir	Central Laser Facility, STFC Rutherford Appleton Laboratory, Harwell Campus, Didcot, UK	62
M.	Du	Department of Materials Science and Engineering, University of Sheffield, UK	79

Initials	Surname	Institution	Page
C.	Ducati	Department of Materials Science and Metallurgy, University of Cambridge, UK; The Faraday Institution, Harwell Science and Innovation Campus, Didcot, UK	74
T.	Dzelainis	Central Laser Facility, STFC Rutherford Appleton Laboratory, Harwell Campus, Didcot, UK	55
J.B.	Eastwood	Department of Chemistry, University of York, UK	90
C.B.	Edwards	Central Laser Facility, STFC Rutherford Appleton Laboratory, Harwell Campus, Didcot, UK	41, 43, 47, 48
H.	Edwards	Engineering Division, Central Laser Facility, STFC Rutherford Appleton Laboratory, Harwell Campus, Didcot, UK	60
P.J.I.	Ellis	School of Biosciences, University of Kent, Canterbury, UK	79
D.R.	Emerson	Scientific Computing Department, STFC Daresbury Laboratory, Warrington, UK	32
O.C.	Ettlinger	John Adams Institute for Accelerator Science and Department of Physics, University of Oxford, UK	38, 39
R.C.	Evans	Department of Materials Science and Metallurgy, University of Cambridge, UK	74
I.J.S.	Fairlamb	Department of Chemistry, University of York, UK	90
L.	Feder	John Adams Institute for Accelerator Science and Department of Physics, University of Oxford, UK	32
K.	Fedorov	Central Laser Facility, STFC Rutherford Appleton Laboratory, Harwell Campus, Didcot, UK	55
C.	Fegan	School of Mathematics and Physics, Queen's University of Belfast, UK	65
S.	Feister	California State University Channel Islands, USA	57
H.H.	Fielding	Department of Chemistry, University College London, UK	86
J.	Fields	Central Laser Facility, STFC Rutherford Appleton Laboratory, Harwell Campus, Didcot, UK	60
O.J.	Finlay	Central Laser Facility, STFC Rutherford Appleton Laboratory, Harwell Campus, Didcot, UK	35, 54, 55, 66
B.	Fisher	York Plasma Institute, University of York, UK	67

Initials	Surname	Institution	Page
F.	Forgat	Department of Oncology and Metabolism, University of Sheffield, UK	79
G.O.	Fruhworth	Comprehensive Cancer Centre, School of Cancer and Pharmaceutical Sciences, King's College London, UK	76
J.	Fuchs	LULI-CNRS, CEA, Sorbonne Université, Ecole Polytechnique, Institut Polytechnique de Paris, France	40
C.	Gajo	Department of Chemistry, University of Bristol, UK	91
M.	Galimberti	Central Laser Facility, STFC Rutherford Appleton Laboratory, Harwell Campus, Didcot, UK	44
A.M.	Gardner	Department of Chemistry and Stephenson Institute for Renewable Energy, University of Liverpool, UK; Early Career Laser Laboratory, University of Liverpool, UK	81
P.	Gauron	Université Paris-Saclay, CNRS/IN2P3, France	57
E.	Gerstmayr	School of Mathematics and Physics, Queen's University Belfast, UK	28, 29, 30, 31, 34, 35
F.L.	Gervasio	School of Pharmaceutical Sciences, University of Geneva, Switzerland; ISPSO, University of Geneva, Switzerland; Chemistry Department, University College London, UK; Swiss Institute of Bioinformatics, University of Geneva, Switzerland	76
D.	Ghosh	School of Chemistry, University of Bristol, UK	86
L.	Gizzi	Intense Laser Irradiation Laboratory, INO-CNR, Pisa, Italy	67
I.	Gladadas	School of Pharmaceutical Sciences, University of Geneva, Switzerland; ISPSO, University of Geneva, Switzerland	76
K.	Glize	Central Laser Facility, STFC Rutherford Appleton Laboratory, Harwell Campus, Didcot, UK	38
K.	Glize	Key Laboratory for Laser Plasmas (MoE) and School of Physics and Astronomy, & Collaborative Innovation Center of IFSA, Shanghai Jiao Tong University, China	67
A.J.	Gonsalves	BELLA Center, Lawrence Berkeley National Laboratory, California, USA	57

Initials	Surname	Institution	Page
J.S.	Green	Central Laser Facility, STFC Rutherford Appleton Laboratory, Harwell Campus, Didcot, UK	65
G.M.	Greetham	Central Laser Facility, STFC Rutherford Appleton Laboratory, Harwell Campus, Didcot, UK	63, 82, 85, 86, 88, 90, 91
L.	Gremillet	CEA/DAM/DIF, Arpajon, France	40
X.J.	Gu	Scientific Computing Department, STFC Daresbury Laboratory, Warrington, UK	32
T.	Hall	Central Laser Facility, STFC Rutherford Appleton Laboratory, Harwell Campus, Didcot, UK	65
P.	Hamm	Department of Chemistry, University of Zurich, Switzerland	85
L.A.	Hammarback	Department of Chemistry, University of York, UK	90
M.	Hanus	HiLASE Centre, Institute of Physics of the Czech Academy of Sciences, Dolní Břežany, Czech Republic	41, 47
R.	Harding	Central Laser Facility, STFC Rutherford Appleton Laboratory, Harwell Campus, Didcot, UK	48
Y.	Hari-Gupta	School of Biosciences, University of Kent, Canterbury, UK	79
M.	Harman	Central Laser Facility, STFC Rutherford Appleton Laboratory, Harwell Campus, Didcot, UK	45
M.	Harris	Central Laser Facility, STFC Rutherford Appleton Laboratory, Harwell Campus, Didcot, UK	61
S.	Hawkes	Central Laser Facility, STFC Rutherford Appleton Laboratory, Harwell Campus, Didcot, UK	28, 30, 44, 45, 53, 92
O.A.	Hawkins	Department of Chemistry, University of Bristol, UK	91
S.	Hay	Department of Chemistry and Manchester Institute of Biotechnology, The University of Manchester, UK	87
D.	Heathcote	Chemistry Research Laboratory, Department of Chemistry, University of Oxford, UK	71
R.	Heathcote	Central Laser Facility, STFC Rutherford Appleton Laboratory, Harwell Campus, Didcot, UK	40, 44, 45

Initials	Surname	Institution	Page
J.	Heitland	Department of Chemistry, University College London, UK	86
C.	Hernandez-Gomez	Central Laser Facility, STFC Rutherford Appleton Laboratory, Harwell Campus, Didcot, UK	44, 45, 46, 48, 50
G.S.	Hicks	Magdrive, Harwell Campus, Didcot, UK	38
J.	Hills	John Adams Institute for Accelerator Science and Department of Physics, University of Oxford, UK	28, 29, 30, 31, 34
H.	Hoepfner	HZDR at the European XFEL, Schenefeld, Germany	48
P.	Hofmann	Department of Physics and Astronomy, Aarhus University, Denmark	68
J.	Holloway	John Adams Institute for Accelerator Science and Department of Physics, University of Oxford, UK	33
S.M.	Hooker	John Adams Institute for Accelerator Science and Department of Physics, University of Oxford, UK	32, 33
C.	Horbaczewski	Department of Chemistry, University of York, UK	90
M.	Horch	Department of Physics, Freie Universität Berlin, Germany	88
D.A.	Horke	Institute for Molecules and Materials, Radboud University, Nijmegen, The Netherlands	70
V.	Horný	LULI-CNRS, CEA, Sorbonne Université, Ecole Polytechnique, Institut Polytechnique de Paris, France	40
K.	Howland	School of Biosciences, University of Kent, Canterbury, UK	79
E.	Hume	Intense Laser Irradiation Laboratory, INO-CNR, Pisa, Italy	67
N.T.	Hunt	Department of Chemistry and Biomedical research Institute, University of York, UK	87, 89
P.	Hunyor	RAL Space, STFC Rutherford Appleton Laboratory, Harwell Campus, Didcot, UK	60
R.A.	Ingle	Department of Chemistry, University College London, UK	70
S.	Irving	Central Laser Facility, STFC Rutherford Appleton Laboratory, Harwell Campus, Didcot, UK	61

Initials	Surname	Institution	Page
R.S.	Iyer	Central Laser Facility, STFC Rutherford Appleton Laboratory, Harwell Campus, Didcot, UK	76
O.	Jakobsson	John Adams Institute for Accelerator Science and Department of Physics, University of Oxford, UK	32
H.	Jang	Department of Chemistry and Stephenson Institute for Renewable Energy, University of Liverpool, UK	81
A.	Joglekar	Department of Nuclear Engineering and Radiological Sciences, University of Michigan, USA; Ergodic LLC, San Francisco, USA	57
A.R.	Jones	Biometrology, Chemical and Biological Sciences, National Physical Laboratory, Teddington, UK	87
B.E.	Jones	Department of Materials Science and Metallurgy, University of Cambridge, UK; Diamond Light Source, Harwell Science and Innovation Campus, Didcot, UK	74
J.F.	Jones	Department of Chemistry, University of Bristol, UK	91
J.K.	Jones	ASTeC, STFC Daresbury Laboratory and Cockcroft Institute, Sci-Tech Daresbury, Warrington, UK	51, 52
J.	Jonnerby	John Adams Institute for Accelerator Science and Department of Physics, University of Oxford, UK	33
C.J.C.	Jordan	Department of Chemistry, University of Bristol, UK	91
I.	Kalampouka	School of Life Sciences, Research Centre for Optimal Health, University of Westminster, London, UK	73
S.	Kar	School of Mathematics and Physics, Queen's University of Belfast, UK	65
G.	Karras	Central Laser Facility, STFC Rutherford Appleton Laboratory, Harwell Campus, Didcot, UK	86, 91
L.	Kennedy	John Adams Institute for Accelerator Science and Department of Physics, University of Oxford, UK	28, 29, 30, 31, 34
B.	Kettle	John Adams Institute for Accelerator Science and Department of Physics, University of Oxford, UK	36, 37
M.	Khan	York Plasma Institute, University of York, UK	38, 67
M.	King	Department of Physics, SUPA, University of Strathclyde, Glasgow, UK; The Cockcroft Institute, Sci-Tech Daresbury, Warrington, UK	64

Initials	Surname	Institution	Page
R.J.	Kingham	Blackett Laboratory, Imperial College London, UK	38
A.	Kirrandar	Chemistry Research Laboratory, Department of Chemistry, University of Oxford, UK	71
S.	Klein	Nuclear Engineering & Radiological Sciences, University of Michigan, USA	61
K.	Knoefel	HZDR at the European XFEL, Schenefeld, Germany	48
P.	Koester	Intense Laser Irradiation Laboratory, INO-CNR, Pisa, Italy	67
I.	Kovalchuk	Leibniz IFW Dresden, Germany; Kyiv Academic University, Ukraine	68
A.T.	Krummel	Department of Chemistry, Colorado State University, USA	85
A.	Kuibarov	Leibniz IFW Dresden, Germany	68
R.	Kumar	Department of Chemistry, University College London, UK	86
M.	Kurttila	Biometrology, Chemical and Biological Sciences, National Physical Laboratory, Teddington, UK	87
D.	Lambert	Department of Oncology and Metabolism, University of Sheffield, UK	79
N.A.	Lau	Department of Chemistry, University College London, UK	86
O.	Lenz	Department of Chemistry, Technische Universität Berlin, Germany	88
I.	Lezcano Gonzalez	Department of Chemistry, University College London, UK; Research Complex at Harwell, Didcot, UK	72, 80
W.	Li	Accelerator Test Facility, Brookhaven National Laboratory, New York, USA	39
Y.	Li	Central Laser Facility, STFC Rutherford Appleton Laboratory, Harwell Campus, Didcot, UK	58
L.	Liu	School of Optoelectronic Engineering, Xidian University, Xi'an, China	58
Z.	Liu	Chemistry Research Laboratory, Department of Chemistry, University of Oxford, UK	71

Initials	Surname	Institution	Page
N.	Lopes	Instituto de Plasmas e Fusão Nuclear, Instituto Superior Tecnico, Universidade de Lisboa, Portugal	28, 29, 30, 31, 34
E.E.	Los	John Adams Institute for Accelerator Science and Department of Physics, University of Oxford, UK	28, 29, 30, 31, 34, 37
R.	Luo	John Adams Institute for Accelerator Science and Department of Physics, University of Oxford, UK	28, 29, 30, 31, 34
B.M.	Luther	Department of Chemistry, Colorado State University, USA	85
J.M.	Lynam	Department of Chemistry, University of York, UK	90
M.	M. Borghesi	School of Mathematics and Physics, Queen's University Belfast, UK	40
Y.	Ma	Center for Ultrafast Optical Science, University of Michigan, USA	37
F.	Maccherozzi	Diamond Light Source, Harwell Science and Innovation Campus, Didcot, UK	72
A.M.	Mackenzie	Central Laser Facility, STFC Rutherford Appleton Laboratory, Harwell Campus, Didcot, UK	73, 75
N.M	Madugula	Central Laser Facility, STFC Rutherford Appleton Laboratory, Harwell Campus, Didcot, UK	71
H.	Maguire	School of Mathematics and Physics, Queen's University Belfast, UK	35
A.	Mahadevegowda	Department of Materials Science and Metallurgy, University of Cambridge, UK; The Faraday Institution, Harwell Science and Innovation Campus, Didcot, UK	74
S.	Maiti	Central Laser Facility, STFC Rutherford Appleton Laboratory, Harwell Campus, Didcot, UK	82
P.	Majchrzak	Department of Physics and Astronomy, Aarhus University, Denmark	68
P.	Malakar	Central Laser Facility, STFC Rutherford Appleton Laboratory, Harwell Campus, Didcot, UK	62, 63, 73, 82, 91
R.C.H.	Man	Comprehensive Cancer Centre, School of Cancer and Pharmaceutical Sciences, King's College London, UK	76

Initials	Surname	Institution	Page
S.P.D.	Mangles	John Adams Institute for Accelerator Science and Department of Physics, University of Oxford, UK	36, 37
V.	Marshall	Central Laser Facility, STFC Rutherford Appleton Laboratory, Harwell Campus, Didcot, UK	56, 57
P.	Martin	School of Mathematics and Physics, Queen's University of Belfast, UK	65
M.L.	Martin-Fernandez	Central Laser Facility, STFC Rutherford Appleton Laboratory, Harwell Campus, Didcot, UK	72, 76, 79
P.D.	Mason	Central Laser Facility, STFC Rutherford Appleton Laboratory, Harwell Campus, Didcot, UK	41, 42, 43, 44, 45, 46, 48, 50
M.	Masruri	HZDR at the European XFEL, Schenefeld, Germany	48
C.A.	McAnespie	School of Mathematics and Physics, Queen's University Belfast, UK	35, 66
H.	McArthur	School of Biosciences, University of Kent, Canterbury, UK	79
A.	McCay	School of Mathematics and Physics, Queen's University of Belfast, UK	65
C.	McDonnell	Patrick G. Johnston Centre for Cancer Research, Queen's University Belfast, UK	35
H.G.	McGhee	Department of Chemistry, University College London, UK	70
L.	McHugh	Central Laser Facility, STFC Rutherford Appleton Laboratory, Harwell Campus, Didcot, UK	43, 46
P.	McKenna	Department of Physics, SUPA, University of Strathclyde, UK; The Cockcroft Institute, Sci-Tech Daresbury, Warrington, UK	40, 64
S.J.	McMahon	Patrick G. Johnston Centre for Cancer Research, Queen's University Belfast, UK	35
D.	Meissner	Onyx Optics Inc., Dublin, California, USA	42
S.	Meissner	Onyx Optics Inc., Dublin, California, USA	42
Q.	Meng	School of Chemical Engineering and Light Industry, Guangdong University of Technology, China	72
J.	Merrick	Chemistry Research Laboratory, Department of Chemistry, University of Oxford, UK	71

Initials	Surname	Institution	Page
C.T.	Middleton	PhaseTech Spectroscopy Inc., Madison, Wisconsin, USA	85
A.	Milsom	School of Geography, Earth and Environmental Sciences, University of Birmingham, UK	78
R.S.	Minns	School of Chemistry and Chemical Engineering, University of Southampton, UK	69, 70
T.	Mocek	HiLASE Centre, Institute of Physics of the Czech Academy of Sciences, Dolní Břežany, Czech Republic	41, 43, 47
D.	Molloy	School of Mathematics and Physics, Queen's University of Belfast, UK	65
J.	Morse	Central Laser Facility, STFC Rutherford Appleton Laboratory, Harwell Campus, Didcot, UK	103
R.R.	Mould	School of Life Sciences, Research Centre for Optimal Health, University of Westminster, London, UK	73, 75
B.D.	Muratori	ASTeC, STFC Daresbury Laboratory and Cockcroft Institute, Sci-Tech Daresbury, Warrington, UK	51, 52
Z.	Najmudin	John Adams Institute for Accelerator Science and Department of Physics, University of Oxford, UK	28, 29, 30, 31, 34, 37, 38, 39
M.	Nakatsutsumi	LULI-CNRS, CEA, Sorbonne Université, Ecole Polytechnique, Institut Polytechnique de Paris, France	40
P.	Navratil	HiLASE Centre, Institute of Physics of the Czech Academy of Sciences, Dolní Břežany, Czech Republic	41, 47
S.R.	Needham	Central Laser Facility, STFC Rutherford Appleton Laboratory, Harwell Campus, Didcot, UK	35, 73, 74, 76
G.	Neri	Department of Chemistry and Stephenson Institute for Renewable Energy, University of Liverpool, UK	81
O.	Neveu	Université Paris-Saclay, CNRS/IN2P3, France	57
P.	Nilson	Laboratory for Laser Energetics (LLE), University of Rochester, New York, USA	61
M.	Notley	Central Laser Facility, STFC Rutherford Appleton Laboratory, Harwell Campus, Didcot, UK	38

Initials	Surname	Institution	Page
J.F.P.	Nunes	Diamond Light Source, Harwell Science and Innovation Campus, Didcot, UK	71
A.V.	Nunn	School of Life Sciences, Research Centre for Optimal Health, University of Westminster, London, UK; The Guy Foundation, Chedington, Dorset, UK	73, 75
Y.	Odarchenko	Department of Chemistry, University College London, UK; Research Complex at Harwell, Didcot, UK	72
P.	Olalde-Velasco	Diamond Light Source, Harwell Science and Innovation Campus, Didcot, UK	72
P.	Oliveira	Central Laser Facility, STFC Rutherford Appleton Laboratory, Harwell Campus, Didcot, UK	103
T.A.A.	Oliver	Department of Chemistry, University of Bristol, UK	91
A.J.	Orr-Ewing	School of Chemistry, University of Bristol, UK	86
H.L.	Owen	ASTeC, STFC Daresbury Laboratory and Cockcroft Institute, Sci-Tech Daresbury, Warrington, UK	51, 52
P.	P. Antici	INRS-EMT, Varennes, Quebec, Canada	40
T.H.	Pacey	ASTeC, STFC Daresbury Laboratory and Cockcroft Institute, Sci-Tech Daresbury, Warrington, UK	51, 52
T.	Paliesek	HiLASE Centre, Institute of Physics of the Czech Academy of Sciences, Dolní Břežany, Czech Republic	41, 47
C.A.J.	Palmer	School of Mathematics and Physics, Queen's University Belfast, UK	39, 57
M.	Panchal	Department of Chemistry, University College London, UK; Research Complex at Harwell, Didcot, UK	72
P.J.	Parker	Protein Phosphorylation Laboratory, The Francis Crick Institute, London, UK; School of Cancer and Pharmaceutical Sciences, Guy's Campus, King's College London, UK	76
M.A.	Parkes	Department of Chemistry, University College London, UK	69, 70
R.	Pattathil	Central Laser Facility, STFC Rutherford Appleton Laboratory, Harwell Campus, Didcot, UK	44

Initials	Surname	Institution	Page
C.	Pfrang	School of Geography, Earth and Environmental Sciences, University of Birmingham, UK; Department of Meteorology, University of Reading, UK	78
P.J.	Phillips	Central Laser Facility, STFC Rutherford Appleton Laboratory, Harwell Campus, Didcot, UK	41, 42, 44, 45, 46, 47, 48, 50
A.	Picksley	John Adams Institute for Accelerator Science and Department of Physics, University of Oxford, UK	32, 33
K.	Pidlisna	School of Biosciences, University of Kent, Canterbury, UK	79
J.	Pilar	HiLASE Centre, Institute of Physics of the Czech Academy of Sciences, Dolní Břežany, Czech Republic	41, 43, 47
C.	Pizzey	Central Laser Facility, STFC Rutherford Appleton Laboratory, Harwell Campus, Didcot, UK	12
I.	Pogorelsky	Accelerator Test Facility, Brookhaven National Laboratory, New York, USA	39
M.	Polyanskiy	Accelerator Test Facility, Brookhaven National Laboratory, New York, USA	39
K.M.	Prise	Patrick G. Johnston Centre for Cancer Research, Queen's University Belfast, UK	35
A.L.B.	Pyne	Department of Materials Science and Engineering, University of Sheffield, UK	79
P.	Qian	Materials and Structural Analysis, Thermo Fisher Scientific, Eindhoven, The Netherlands	74
C.	Qiu	Department of Chemistry, University College London, UK; Research Complex at Harwell, Didcot, UK	72
H.	Qiu	Central Laser Facility, STFC Rutherford Appleton Laboratory, Harwell Campus, Didcot, UK	59
G.	Quinn	Central Laser Facility, STFC Rutherford Appleton Laboratory, Harwell Campus, Didcot, UK	42, 43, 49
M.	Quinn	SUPA, Department of Physics, University of Strathclyde, UK	40
P.P.	Rajeev	Central Laser Facility, STFC Rutherford Appleton Laboratory, Harwell Campus, Didcot, UK	37

Initials	Surname	Institution	Page
C.	Rankine	Department of Chemistry, University of York, York, UK	71
W.O.	Razmus	School of Chemistry and Chemical Engineering, University of Southampton, UK	69
M.P.	Read	First Light Fusion, Kidlington, UK	38
K.D.	Richards	Department of Materials Science and Metallurgy, University of Cambridge, UK	74
C.P.	Ridgers	York Plasma Institute, University of York, UK	38
S.K.	Roberts	Central Laser Facility, STFC Rutherford Appleton Laboratory, Harwell Campus, Didcot, UK	58, 59, 76, 94
P.A.	Robertson	School of Chemistry, University of Nottingham, UK; Chemistry Research Laboratory, Department of Chemistry, University of Oxford, UK	71
J.	Robinson	Scitech Precision Limited, Rutherford Appleton Laboratory, Harwell Campus, Didcot, UK	61
M.S.	Robinson	European XFEL, Hamburg, Germany	71
P.	Rodríguez Maciá	School of Chemistry, University of Leicester, UK	88
D.J.	Rolfe	Central Laser Facility, STFC Rutherford Appleton Laboratory, Harwell Campus, Didcot, UK	76
D.E.	Rollins	Department of Materials Science and Engineering, University of Sheffield, UK	79
L.	Romagnani	LULI-CNRS, CEA, Sorbonne Université, Ecole Polytechnique, Institut Polytechnique de Paris, France	40
S.J.	Rose	John Adams Institute for Accelerator Science and Department of Physics, University of Oxford, UK	36
A.J.	Ross	John Adams Institute for Accelerator Science and Department of Physics, University of Oxford, UK	32, 33
R.	Royle	Department of Physics, University of Nevada, USA	40
K.H.	Saaed	Department of Chemistry and Stephenson Institute for Renewable Energy, University of Liverpool, UK	81
C.	Sanders	Central Laser Facility, STFC Rutherford Appleton Laboratory, Harwell Campus, Didcot, UK	68
R.	Sanders	Central Laser Facility, STFC Rutherford Appleton Laboratory, Harwell Campus, Didcot, UK	74

Initials	Surname	Institution	Page
R.	Sarasola	Engineering Division, Central Laser Facility, STFC Rutherford Appleton Laboratory, Harwell Campus, Didcot, UK	60
J.	Sarma	School of Mathematics and Physics, Queen's University Belfast, UK	28, 29, 30, 31, 34, 35
G.	Sarri	School of Mathematics and Physics, Queen's University Belfast, UK	29, 34, 35, 37, 40
I.V.	Sazanovich	Central Laser Facility, Research Complex at Harwell, STFC Rutherford Appleton Laboratory, Harwell, Didcot, UK	63, 80, 82, 87, 88
G.	Schettino	National Physical Laboratory, Middlesex, UK	35
H.-P.	Schlenvoigt	Helmholtz-Zentrum Dresden–Rossendorf, Germany	57
H.-P.	Schlenvoigt	LULI-CNRS, CEA, Sorbonne Université, Ecole Polytechnique, Institut Polytechnique de Paris, France	40
H.	Schmitz	Central Laser Facility, STFC Rutherford Appleton Laboratory, Harwell Campus, Didcot, UK	45, 64
J.	Schnell	Nuclear Engineering & Radiological Sciences, University of Michigan, USA	61
J.	Schoknecht	Department of Chemistry, Technische Universität Berlin, Germany	88
C.	Seddon	(Department of Life Sciences, Imperial College London, UK; Research Complex at Harwell, Didcot, UK	73
Y.	Sentoku	Institute of Laser Engineering, Osaka University, Japan	40
P.	Severova	HiLASE Centre, Institute of Physics of the Czech Academy of Sciences, Dolní Břežany, Czech Republic	41, 47
R.J.	Shalloo	John Adams Institute for Accelerator Science and Department of Physics, University of Oxford, UK	33
R.J.	Shalloo	Deutsches Elektronen-Synchrotron DESY, Hamburg, Germany	29, 34
D.	Shchepanovska	Department of Chemistry, University of Bristol, UK	91

Initials	Surname	Institution	Page
B.J.A.	Shepherd	ASTeC, STFC Daresbury Laboratory and Cockcroft Institute, Sci-Tech Daresbury, Warrington, UK	51
A.	Shepperd	Central Laser Facility, STFC Rutherford Appleton Laboratory, Harwell Campus, Didcot, UK	48
G.	Shipunov	Leibniz IFW Dresden, Germany	68
J-P.	Shwinkendorf	HZDR at the European XFEL, Schenefeld, Germany	48
B.	Siritanaratkul	Department of Chemistry and Stephenson Institute for Renewable Energy, University of Liverpool, UK	81
H.E.	Smith	Central Laser Facility, STFC Rutherford Appleton Laboratory, Harwell Campus, Didcot, UK	73, 75
J.M.	Smith	Central Laser Facility, STFC Rutherford Appleton Laboratory, Harwell Campus, Didcot, UK	43, 48, 50
M.	Smrz	HiLASE Centre, Institute of Physics of the Czech Academy of Sciences, Dolní Břežany, Czech Republic	41, 47
J.L.	Spear	Central Laser Facility, STFC Rutherford Appleton Laboratory, Harwell Campus, Didcot, UK	43, 48
C.	Spindloe	Central Laser Facility, STFC Rutherford Appleton Laboratory, Harwell Campus, Didcot, UK; Scitech Precision Limited, Rutherford Appleton Laboratory, Harwell Campus, Didcot, UK	60, 61, 96
E.	Springate	Central Laser Facility, STFC Rutherford Appleton Laboratory, Harwell Campus, Didcot, UK	68, 69, 70, 71, 94
A.M.	Squires	Department of Chemistry, University of Bath, UK	78
G.	Stenning	ISI Neutron and Muon Source, STFC Rutherford Appleton Laboratory, Harwell Campus, Didcot, UK	60
A.	Stranger	School of Biosciences, University of Kent, Canterbury, UK	79
M.J.V.	Streeter	Centre for Light-Matter Interactions, School of Mathematics and Physics, Queen's University Belfast, UK	37, 57, 66
N.H.	Stuart	Central Laser Facility, STFC Rutherford Appleton Laboratory, Harwell Campus, Didcot, UK	44
O.	Suvorov	Leibniz IFW Dresden, Germany	68

Initials	Surname	Institution	Page
D.R.	Symes	Central Laser Facility, STFC Rutherford Appleton Laboratory, Harwell Campus, Didcot, UK	37, 51, 52, 54, 55
M.	Szynkiewicz	Central Laser Facility, STFC Rutherford Appleton Laboratory, Harwell Campus, Didcot, UK	94
M.C.	Tang	Central Laser Facility, STFC Rutherford Appleton Laboratory, Harwell Campus, Didcot, UK	59
Y.	Tang	Central Laser Facility, STFC Rutherford Appleton Laboratory, Harwell Campus, Didcot, UK	45, 53
T.F.N.	Tanner	Department of Chemistry, University of York, UK	90
A.	Thomas	Central Laser Facility, STFC Rutherford Appleton Laboratory, Harwell Campus, Didcot, UK	28, 30
A.G.R.	Thomas	Center for Ultrafast Optical Science, University of Michigan, USA	37
H.J.	Thompson	School of Chemistry and Chemical Engineering, University of Southampton, UK	69, 70
J.O.F.	Thompson	Central Laser Facility, STFC Rutherford Appleton Laboratory, Harwell Campus, Didcot, UK	69, 70, 71
C.	Thornton	Central Laser Facility, STFC Rutherford Appleton Laboratory, Harwell Campus, Didcot, UK	33
M.K.	Tolley	Central Laser Facility, STFC Rutherford Appleton Laboratory, Harwell Campus, Didcot, UK	60, 96
S.	Tomlinson	Central Laser Facility, STFC Rutherford Appleton Laboratory, Harwell Campus, Didcot, UK	44, 45
M.	Toncian	HZDR at the European XFEL, Schenefeld, Germany	48
T.	Toncian	Institut für Laser und Plasmaphysik, Heinrich Heine Universität Düsseldorf, Germany	40
T.	Toncian	HZDR at the European XFEL, Schenefeld, Germany	48
C.P.	Toseland	Department of Oncology and Metabolism, University of Sheffield, UK	79
H.	Towrie	Central Laser Facility, STFC Rutherford Appleton Laboratory, Harwell Campus, Didcot, UK	14
M.	Towrie	Central Laser Facility, STFC Rutherford Appleton Laboratory, Harwell Campus, Didcot, UK	63, 80, 82, 90

Initials	Surname	Institution	Page
O.	Tresca	SUPA, Department of Physics, University of Strathclyde, UK	40
R.	Trines	Central Laser Facility, STFC Rutherford Appleton Laboratory, Harwell Campus, Didcot, UK	64
D.M.	Vaithyanathan	Department of Physics, Freie Universität Berlin, Germany	88
C.	Vallance	Chemistry Research Laboratory, Department of Chemistry, University of Oxford, UK	71
L.	Vassura	LULI-CNRS, CEA, Sorbonne Université, Ecole Polytechnique, Institut Polytechnique de Paris, France	40
A.	von Boetticher	John Adams Institute for Accelerator Science and Department of Physics, University of Oxford, UK	33
R.	Walczak	John Adams Institute for Accelerator Science and Department of Physics, University of Oxford, UK; Somerville College, University of Oxford, UK	32
R.	Walczak	John Adams Institute for Accelerator Science and Department of Physics, University of Oxford, UK	33
E.	Wall	Department of Chemistry and Manchester Institute of Biotechnology, The University of Manchester, UK	87
C.A.	Walsh	Lawrence Livermore National Laboratory, California, USA	38
L.	Wang	Central Laser Facility, STFC Rutherford Appleton Laboratory, Harwell Campus, Didcot, UK	58, 59, 79
W.	Wang	John Adams Institute for Accelerator Science and Department of Physics, University of Oxford, UK	32
Y.Y	Wang	York Plasma Institute, University of York, UK	67
A.D.	Ward	Central Laser Facility, STFC Rutherford Appleton Laboratory, Harwell Campus, Didcot, UK	78, 94
M.J.	Watson	Johnson Matthey Technology Centre, Billingham, UK	80
R.A.	Watts	John Adams Institute for Accelerator Science and Department of Physics, University of Oxford, UK	36
W.A.	Whitaker	School of Chemistry, University of Bristol, UK	86

Initials	Surname	Institution	Page
O.	Willi	Institut für Laser und Plasmaphysik, Heinrich Heine Universität Düsseldorf, Germany	40
A.	Wojtusiak	Central Laser Facility, STFC Rutherford Appleton Laboratory, Harwell Campus, Didcot, UK	44, 45, 50
N.C.	Woolsey	York Plasma Institute, University of York, UK	38, 67
G.A.	Worth	Department of Chemistry, University College London, UK	86
A.S.	Wyatt	Central Laser Facility, STFC Rutherford Appleton Laboratory, Harwell Campus, Didcot, UK	70
D.	Wyatt	Central Laser Facility, STFC Rutherford Appleton Laboratory, Harwell Campus, Didcot, UK	61
N.	Xu	John Adams Institute for Accelerator Science and Department of Physics, University of Oxford, UK	39
W.	Yao	LULI-CNRS, CEA, Sorbonne Université, Ecole Polytechnique, Institut Polytechnique de Paris, France	40
A.	Yaresko	Max-Planck-Institute for Solid State Research, Stuttgart, Germany	68
S.	Yong Zi Ru	School of Biosciences, University of Kent, Canterbury, UK	79
X.H.	Yuan	Key Laboratory for Laser Plasmas (MoE) and School of Physics and Astronomy, & Collaborative Innovation Center of IFSA, Shanghai Jiao Tong University, China	67
S.	Zaehler	Focused Energy GmbH, Darmstadt, Germany	67
L.C.	Zanetti-Domingues	Central Laser Facility, STFC Rutherford Appleton Laboratory, Harwell Campus, Didcot, UK	72, 76
M.T.	Zanni	Department of Chemistry, University of Wisconsin, USA	85
T.	Zata	Central Laser Facility, STFC Rutherford Appleton Laboratory, Harwell Campus, Didcot, UK	48
B.	Zhang	Department of Materials Science and Metallurgy, University of Cambridge, UK; CAS Key Laboratory of Design and Assembly of Functional Nano-structures and Fujian Provincial Key Laboratory of Nanomaterials, Fujian Institute of Research on the Structure of Matter, Chinese Academy of Sciences, China	74

Initials	Surname	Institution	Page
J.	Zhang	Key Laboratory for Laser Plasmas (MoE) and School of Physics and Astronomy, & Collaborative Innovation Center of IFSA, Shanghai Jiao Tong University, China	67
Y.	Zhang	Central Laser Facility, STFC Rutherford Appleton Laboratory, Harwell Campus, Didcot, UK	68, 69, 70, 71
Y.H.	Zhang	Beijing National Laboratory for Condensed Matter Physics, Institute of Physics, Chinese Academy of Sciences, China	67
X.	Zhao	Key Laboratory for Laser Plasmas (MoE) and School of Physics and Astronomy, & Collaborative Innovation Center of IFSA, Shanghai Jiao Tong University, China	67



Science and
Technology
Facilities Council

Central Laser Facility